

REAL-TIME MAXIMUM POWER TRACKING AND ROBUST LOAD MATCHING OF A STAND-ALONE PHOTOVOLTAIC SYSTEM

A Dissertation

Presented to

The Faculty of the Graduate School
Tennessee Technological University

by

Mohammad Saad Alam

In Partial Fulfillment

of the Requirements for the Degree

DOCTOR OF PHILOSOPHY

Engineering

May 2009

UMI Number: 3355191

INFORMATION TO USERS

The quality of this reproduction is dependent upon the quality of the copy submitted. Broken or indistinct print, colored or poor quality illustrations and photographs, print bleed-through, substandard margins, and improper alignment can adversely affect reproduction.

In the unlikely event that the author did not send a complete manuscript and there are missing pages, these will be noted. Also, if unauthorized copyright material had to be removed, a note will indicate the deletion.

UMI[®]

UMI Microform 3355191
Copyright 2009 by ProQuest LLC
All rights reserved. This microform edition is protected against
unauthorized copying under Title 17, United States Code.

ProQuest LLC
789 East Eisenhower Parkway
P.O. Box 1346
Ann Arbor, MI 48106-1346


CERTIFICATE OF APPROVAL OF DISSERTATION

**REAL-TIME MAXIMUM POWER TRACKING AND ROBUST LOAD
MATCHING OF A STAND-ALONE PHOTOVOLTAIC SYSTEM**


by

Mohammad Saad Alam

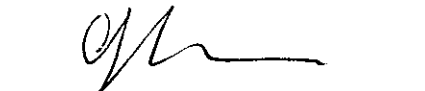
Graduate Advisory Committee:


Ali T. Alouani, Chairperson

29-04-09
Date


Charles Carnal

29-Apr-2009
Date


Ghader Radman

29-04-09
Date


S Venkat Raman
Venkat Subramanian

29-Apr-09
Date


Michael Allen

April 30, 2009
Date

Approved for the Faculty:


Francis Otuonye
Associate Vice President for
Research and Graduate Studies

5/6/09
Date

Copyright © Mohammad Saad Alam, 2009

All rights reserved

AN ABSTRACT OF A DISSERTATION

REAL-TIME MAXIMUM POWER TRACKING AND ROBUST LOAD MATCHING OF A STAND-ALONE PHOTOVOLTAIC SYSTEM

Mohammad Saad Alam

Doctor of Philosophy in Engineering

This work deals with modeling and maximum power tracking of a stand-alone photovoltaic (PV) power generator.

In the modeling part of the research, a dynamic model of a solar cell has been developed, simulated, and validated using experimental data. Effects of parameter variations have been accounted for in the dynamic model. It was found that the actual real-time maximum power that a PV can produce is significantly different from the average power provided by the manufacturer. Preliminary experimental testing showed that one can extract as much as 23.35% more power from the PV than what is suggested by the manufacturer.

For real-time maximum power transfer, a control strategy that combines the use of a DC/DC boost converter, fuzzy logic control, and a modified queen bee genetic algorithm has been developed. Preliminary simulations show the promise of the approach.

It is believed that this research will lead to improvement in the efficiency of solar cells using real-time modeling and controls.

ACKNOWLEDGEMENTS

It is firstly due to the grace of the Almighty, Allah s.w.t. & secondly, the good wishes of my mother & elders that I have been able to complete my PhD.

I owe my most sincere gratitude & thanks to my advisor Dr. Ali Tahar Alouani, for his valuable guidance, constructive suggestions, healthy criticism, continuous patience & sincere supervision throughout the course of my research, provided the much-needed continuity.

I am also grateful to Dr. Charles Carnal, Dr. Ghadir Radman, Dr. Venkat Subramanian, and Dr. Michael Allen for their time and effort for being on my advisory committee. Special appreciation goes to Dr. Allen for his assistance in the analysis of Design of Experiment.

I am also thankful to Mr. Conard F. Murray, R& D Engineer, ECE Department, TTU, and Mr. Wael Deabes, PhD candidate, ECE Deptt., TTU, for their help in the experimental setup and execution process.

I am forever indebted to Dr. Mohammad F. Azeem, Associate Professor, Department of Electrical Engineering, A.M.U., Aligarh, India, for his precious suggestions & useful cooperation, though after testing my zeal properly.

Thanks are due to Electric Ship program (funded by Office of Naval Research) at Mississippi State University, Center of Energy System Research, ECE Department, and Graduate School at Tennessee Technological University (TTU) for the financial support during my PhD.

Finally, thanks to my family members, teachers, friends, and colleagues for their warm support and patience during the research and writing of this thesis and throughout my career path. This includes all my professors and friends at Aligarh Muslim University, U.P. India, Illinois Institute of Technology, IL, Mississippi State University, MS, Tennessee Tech University, TN, and work colleagues and managers, at Cummins Inc., Chrysler LLC, and Mercedes-Benz Hybrid LLC who encouraged my work and made valuable suggestions; their friendship is unforgettable.

DEDICATION

To my mother, my wife,

My sister, my mother-in-law

&

My grandmother(s)

TABLE OF CONTENTS

	Page
LIST OF FIGURES	ix
LIST OF TABLES	xii
 Chapter	
1. Introduction.....	1
1.1 Global Energy Demand.....	1
1.2 Role of Photovoltaic Systems in the Emerging Need of Alternative Technologies	5
1.3 Motivation and Contribution of the Research.....	6
1.4 Organization of the Dissertation	9
References.....	11
 2. Photovoltaic Fundamentals.....	 12
2.1 Background.....	12
2.2 Solar Cell Fundamentals.....	14
2.2.1 Semiconductors.....	14
2.2.2 PN Junction.....	15
2.2.3 Photoconduction	16
2.2.4 PV Cell.....	17
2.2.5 PV Module and Array.....	18
2.3 PV System Components	19
2.3.1 Central PV Power Station System	19
2.3.2 Distributed PV Power Generation System.....	19
2.3.2.1 Stand-alone PV Power Generation System.....	19
2.3.2.2 Grid Interactive PV Power Generation System	20
2.3.2.3 Hybrid PV Power Generation System	21
2.4 Solar Cell Characteristics.....	22
2.4.1. Equivalent Electrical Circuit.....	24
2.4.2 Open Circuit Voltage and Short Circuit Current	25
2.4.3 I-V and P-V Curves	26
2.4.4 Performance Factors	27
2.4.4.1 Solar Irradiance.....	27
2.4.4.2 Temperature	27
2.4.4.3 Sun angle and Sun Tracking.....	29
2.4.4.4 Other Factors.....	31
2.4.5. Maximizing the Performance.....	32
2.4.5.1 Efficiency and Energy Losses.....	32
2.4.5.2 Operation at Peak Power.....	33
2.4.5.2.1 Maximum Power Point Tracking.....	33
2.4.5.2.2 Electrical Load Matching.....	34
References.....	35

3. Photovoltaic: Modeling	36
3.1 Existing PV Models	36
3.1.1 Literature Survey	36
3.1.1.1 Static Model of PV	37
3.1.2 Development of a Static Model of PV in MATLAB/ Simulink	44
3.1.3 Limitations of Static Model	47
3.2 Modeling and Simulation.....	48
3.2.1 Development of a Dynamic Model of PV in MATLAB/ Simulink.....	48
3.2.2 Comparison of Static and Dynamic PV Models	54
3.2.3 Limitations of Dynamic Model.....	59
3.2.4 Solar cell parameter calculation.....	60
3.2.5 Simulation, Results, and Analysis	68
3.3 Experimental Validation	71
3.3.1 Hardware Setup.....	71
3.3.2 Data Collection	72
3.4 Design of Experiment (DoE)	75
3.4.1 Model Validation and Analysis	76
References.....	82
4. Load matching Control of Stand-alone PV Systems at Maximum Power Point Transfer.....	85
4.1 Maximum Power Point Tracking (MPPT).....	85
4.1.1 Literature Survey	85
4.1.1.1 Existing MPPT Strategies and their Limitations	86
4.1.1.2 Existing Control Strategies and their Limitations.....	90
4.1.2. Control Strategy for Optimizing the Load Matching for Stand-alone PV	95
4.2 Fuzzy Logic Control	97
4.2.1. Fuzzy Knowledge-Based Control (FKBC).....	98
4.2.1.1 Fuzzification Module	98
4.2.1.2 Knowledge Base	100
4.2.1.2.1 Database.....	100
4.2.1.2.2 Rule Base	100
4.2.1.3 Inference Engine	103
4.2.1.4 Defuzzification Module	105
4.2.2 Tuning of Scaling Factors through Applied Genetic Algorithm	107
4.2.2.1 Overview of Genetic Algorithm	110
4.2.2.2 Modified Queen Bee Evolution	112
4.2.2.3 Weighted Base Crossover Operator.....	113
4.3 Modeling and Simulation.....	115
4.3.1 FKBC Design Parameters	116
4.3.2 Modeling and Simulation of AGABFLC.....	122
4.3.2.1 Initialization and Learning.....	122
4.3.3 Simulation Results and Discussion.....	125
4.3.3.1 AGABFLC Simulation Results.....	128
4.4 Strategy for a Potential Hardware Development of AGABFLC	134
References.....	135

5. Conclusions, Recommendations, and Further Scope of Research.....	139
5.1 Conclusions.....	139
5.2 Recommendations and Further scope of Research.....	140
5.2.1 Modeling and Simulation of Photovoltaic (PV) Systems.....	140
5.2.2 Design of Experiment.....	141
5.2.3 Modeling and Simulation of Control and Model Validation.....	141
5.2.4 Design and Development of Hardware for Control System.....	141
APPENDICES	
Appendix A Nomenclature.....	142
Appendix B MATLAB/Simulink, Lab VIEW Models (PV).....	143
Appendix C Specifications of the Instruments Used in the Experiment.....	146
Appendix D Report on the Design of Experiment.....	151
Appendix E Experimental Data.....	158
Appendix F Solution of Transcendental equation.....	171
Appendix G Fuzzy logic Control Fundamentals.....	180
Appendix H DC-DC converter.....	185
Appendix I MATLAB/Simulink Model (AGABFLC).....	189
VITA.....	190

LIST OF FIGURES

	Page
Figure 1.1 Global Energy Consumption	1
Figure 1.2 Energy Consumption by Fuel Type, 2005	2
Figure 1.3 Electricity Demands 1980-2025	3
Figure 1.4 Electricity Production Capacities 1980-2025	3
Figure 1.5 The world and U.S. Net Electricity Generation by Type in 2005	5
Figure 1.6 Distribution of Solar Energy	6
Figure 2.1 Free Electron Hole Flow through a Semiconductor	15
Figure 2.2 Free Electron Hole Flow through a Semiconductor	16
Figure 2.3 X- Section of a Typical PV Cell.....	17
Figure 2.4 PV Cell, Module, and Array.....	18
Figure 2.5 A typical Stand-Alone PV Power Generation System	20
Figure 2.6 A typical Grid Interactive PV Power Generation System	21
Figure 2.7 Illuminated PN Junction.....	22
Figure 2.8 Characteristic of an Illuminated and Non-Illuminated p-n Junction.....	23
Figure 2.9 Equivalent Circuit of (a) Five and (b) Four Parameter Photovoltaic Cell.....	25
Figure 2.10 I-V Characteristic, Maximum Power Point, P-V Characteristic of a Typical PV Cell.....	26
Figure 2.11.a Effect of Variation of Temperature on the PV Characteristic	28
Figure 2.11.b Effect of Variation of Irradiance on the PV Characteristic	29
Figure 2.12 Kelly Cosine Curve for a PV Cell from $\theta = 0^\circ$ to $\theta = 90^\circ$	30
Figure 2.13 Load Matching with Resistive Load.....	33
Figure 3.1 Equivalent Circuit of PV Cell.....	38
Figure 3.2 V-I Characteristics for Different Values of Irradiance Considering $T_c=25^\circ \text{C}$	45
Figure 3.3 Output Power Vs Output Voltage Characteristics for Different Values of Irradiance Considering $T=25^\circ \text{C}$	45
Figure 3.4 V-I Characteristics for Different Values of Temperature with $G_T=800 \text{ W/m}^2$	46
Figure 3.5 Output Power Vs Output Voltage Characteristics for Different Values of Temperature Considering $G_T= 1000 \text{ W/m}^2$	47
Figure 3.6 Daily Irradiance Over a Period of One Month from the Data.....	51
Figure 3.7 Daily Temperature Over a Period of One Month from the Data.....	52
Figure 3.8 Variation of Solar Irradiance Over the Day	52
Figure 3.9 Pattern of Cell Temperature and Ambient Temperature in a Day.....	53
Figure 3.10 Profile of the Maximum Power Obtained through Static Model	54
Figure 3.11 Profile of the Maximum Power Obtained through Static Model during 9 AM-6 PM.....	55
Figure 3.12 Profile of the Maximum Power Obtained through Dynamic Model.....	55
Figure 3.13 Profile of the Maximum Power Obtained through Dynamic Model during 10 AM – 5 PM	56
Figure 3.14 Angle of Incidence and Refraction in Media with Refractive Indices n_1 and n_2	60

Figure 3.15 Implementation Strategy of the Dynamic PV Model	68
Figure 3.16 Variation of Maximum Power Over the Whole Day.....	70
Figure 3.17 Variation of Maximum Power from 9:30 AM to 5:30 PM	71
Figure 3.18 Experimental Setup-Solar Panels	72
Figure 3.19 Experimental Setup-Data Collection.....	73
Figure 3.20 Experimental Setup for Model Validation	74
Figure 3.21 Scatter Plot of Predicted Vs. Experimental Maximum Power Values	77
Figure 3.22 Normal Quantile-Quantile Plot of Sample Quantities Vs the Theoretical Quantities	78
Figure 3.22 Scatter Plot of the residuals Vs. the Predicted Wattage	79
Figure 3.23 Scatter Plot of Predicted Vs. Experimental Wattage Values-I.....	80
Figure 3.24 Scatter Plot of Predicted Vs. Experimental Wattage Values-II.....	80
Figure 3.25 Scatter Plot of Predicted Vs. Experimental Wattage Values-III	81
Figure 4.1 Block Diagram of Control Strategy.....	96
Figure 4.2 Block Diagram of Fuzzy Logic Controller.....	99
Figure 4.3.a Membership Functions of the Variables.....	101
Figure 4.3.b Membership Functions of the Variables.....	102
Figure 4.4 Center of Gravity Defuzzifier.....	106
Figure 4.5 A Graphical Representation of the Center-of-Sums Defuzzification Method	106
Figure 4.6 GA-Based Adaptive Fuzzy Logic Control Scheme.....	109
Figure 4.7 Crossover in String.....	110
Figure 4.8 Flowchart of Genetic Algorithm	111
Figure 4.9 Schematic Diagram of Splitting of Pools Generation by Generation in Modified Queen Bee Evolution	112
Figure 4.10 Schematic Representation of Weight Base Uniform Crossover.....	114
Figure 4.11 Schematic Diagram of a DC-DC boost converter with switch S closed	117
Figure 4.12 Gaussian Membership Function for Inputs e^* & ce^*	119
Figure 4.13 Triangular Membership Functions for Output dc^*	120
Figure 4.14 Surface of the Fuzzy Membership Function	120
Figure 4.15 GA-Based Learning Patterns for K_e , K_{ce} , and K_{dc}	124
Figure 4.16 Pattern of the PV Panel Current and Actual Load Current with Fixed Load in a Day	126
Figure 4.17 Pattern of the PV Panel Current and Actual Load Current With Variable Load in a Day.....	126
Figure 4.18 Ref. Load Voltage, Pattern of the PV Array Voltage, and the DC/DC Boost Converter Voltage for Fixed Load in a Day	127
Figure 4.19 Ref. Load Voltage, Pattern of the PV Array Voltage, and the DC/DC Boost Converter Voltage for Variable Load in a Day.....	127
Figure 4.20 Pattern of First Input of FLC Error Voltage with Fixed Voltage in a Day	128
Figure 4.21 Pattern of First Input of FLC Error Voltage with Variable Voltage in a Day.....	129
Figure 4.22 Pattern of Second Input of FLC Change in Error Voltage for Variable Load in a Day	129
Figure 4.23 Pattern of the Duty Cycle with Fixed Load in a Day	130
Figure 4.24 Pattern of the Duty Cycle for Variable Load in a Day	130
Figure 4.25 Patterns of the RMMP and with Fixed R_{load} in a Day	131
Figure 4.26 Pattern of the RMMP and Variable R_{load} in a Day	131

Figure 4.27 Patterns of the MPPT Model Power and Power Harvested by the Load from PV Array with Fixed Load in a Day	132
Figure 4.28 Pattern of the MPPT Model Power and Power Harvested by the Variable Load from PV Array in a Day.....	133
Figure 4.29 Strategy for the Hardware Development of the Controller	134
Figure B.1 Simulink Model of PV Cell (Static Model)	143
Figure B.2 Simulink Model of PV Cell (Dynamic Model)	143
Figure B.3 Simulink Model of PV Cell with Parametric Estimation	144
Figure B.4 Data Collection through DAQ	144
Figure B.5 Lab View Model of PV Module	145
Figure F.1 Convergence of $x_{n+1} = \theta'(x_n)$	175
Figure F.2 Newton Raphson Method	179
Figure G.1 Graphical Representation of Crisp and Fuzzy Set.....	181
Figure G.2 Typical Shapes of Membership Functions:	182
Figure H.1 Schematic Diagram of a DC-DC Boost Converter with Switch S Open.....	185
Figure H.2 Pattern of the Variations of Different Variables of DC-DC Converter in a Duty Cycle	186
Figure H.3 Schematic Diagram of a DC-DC Boost Converter with switch S Closed.....	187
Figure I.1 Simulink Model of the PV System with AGABFL Controller	189

LIST OF TABLES

	Page
Table 2.1 Mathematical and Kelly Cosine Curve of a PV cell output current	30
Table 3.1 Values of parameters in Static model	44
Table 3.2 Variable Data and the maximum power obtained	57
Table 3.3 Uses of PV systems (percent of survey respondents)	58
Table 3.4 Improved PV dynamic model after including parametric variation	69
Table 3.5 List of equipments used in the experiment	74
Table 3.6 Standard Regression plots and Verification actions	76
Table 4.1 Major Characteristics of MPPT Techniques	90
Table 4.2 Rule Base	102
Table 4.3 Rules for WCO	113
Table 4.4 Rule-base for FKBC	121
Table 4.5 Values of GA Parameters	123
Table 4.6 Values of Tuned AGABFLC Parameters	124

CHAPTER 1

INTRODUCTION

Energy is extremely important to humans in today's world. We rely on energy to the point that our lives will be entirely interrupted if energy became unavailable. Energy is used to power our homes with light and daily use appliances; our cars, planes, and trains for transportation; our computers for education, product development, business records; and so many other things which we take for granted.

1.1 Global Energy Demand

Within the next twenty years, the world energy consumption is anticipated to increase by roughly 44% [1.1]. This prediction is based on the statistics in Figure 1.1 which show the worldwide trend of energy demand for the past 35 years and its projection based on the previous growth pattern.

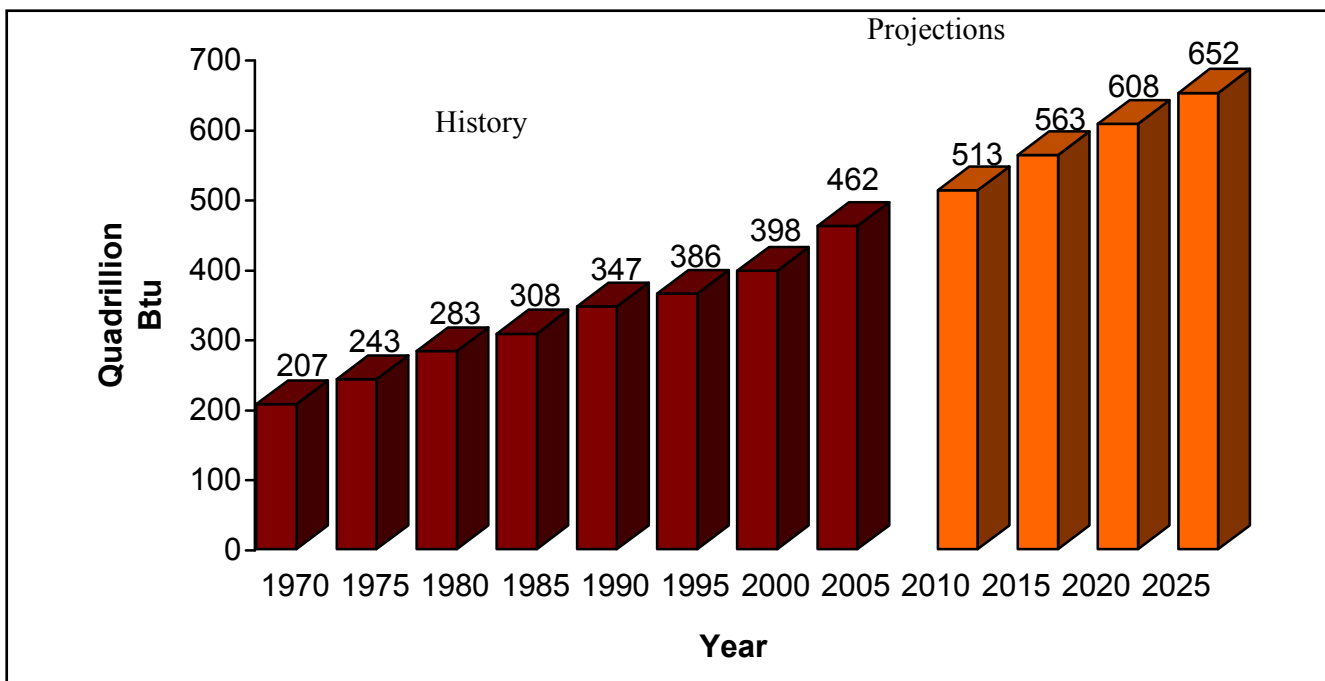


Figure 1.1 Global Energy Consumption [1.1-1.3]

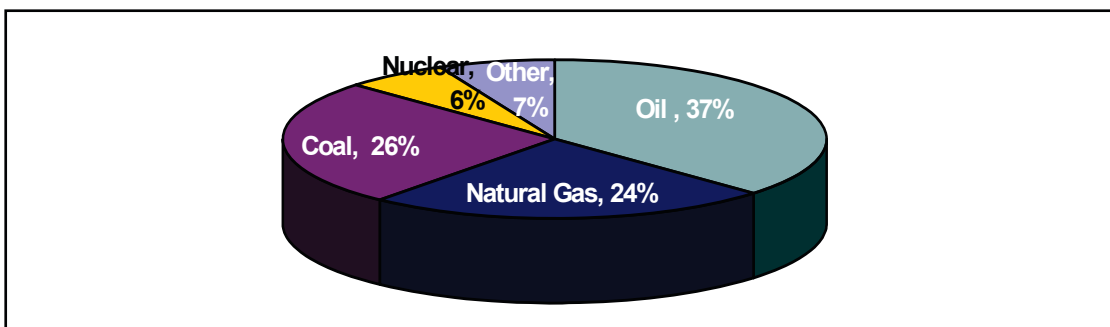


Figure 1.2 Energy Consumption by Fuel Type, 2005 [1.1 -1.3]

Figure 1.2 illustrates the global energy consumption by fuel type in 2005. It is apparent from the figure that fossil fuels offer a major component of the total energy used (approximately 87% in 2005). Future economic growth of the world largely relies on the ability to meet this escalating energy demand.

It is well-known that fossil fuels are unequally concentrated in areas around the world, which may cause future tensions between countries if their economy is exceedingly reliant on these scarce resources. Furthermore, producing and consuming electrical energy by using the present day technologies has caused substantial damage to the ozone and the environment of many areas around the world. As a result, it is an important task for humanity to discover a way to create the required amount of energy while using the most efficient sources.

The use of electricity is expected to increase by nearly 50% in the next twenty years [1.1-1.3], as shown in Figure 1.3. The figure also shows that the U.S. is responsible for the consumption of almost 25% of the total global electricity demand, and is expected to grow approximately 44% by the year 2025 [1.1-1.3]. Also, the electrical requirements set by the newly evolving economies of China and India are increasing even more rapidly.

In order to obtain the required electrical demands of the future, a widespread extension of production power is essential. Global production power is anticipated to expand from 3,872 GW (gigawatts) in 2005 to about 5,500 GW in 2025 (Figure 1.4) with an average yearly growth rate of 2.2% [1.1-1.4].

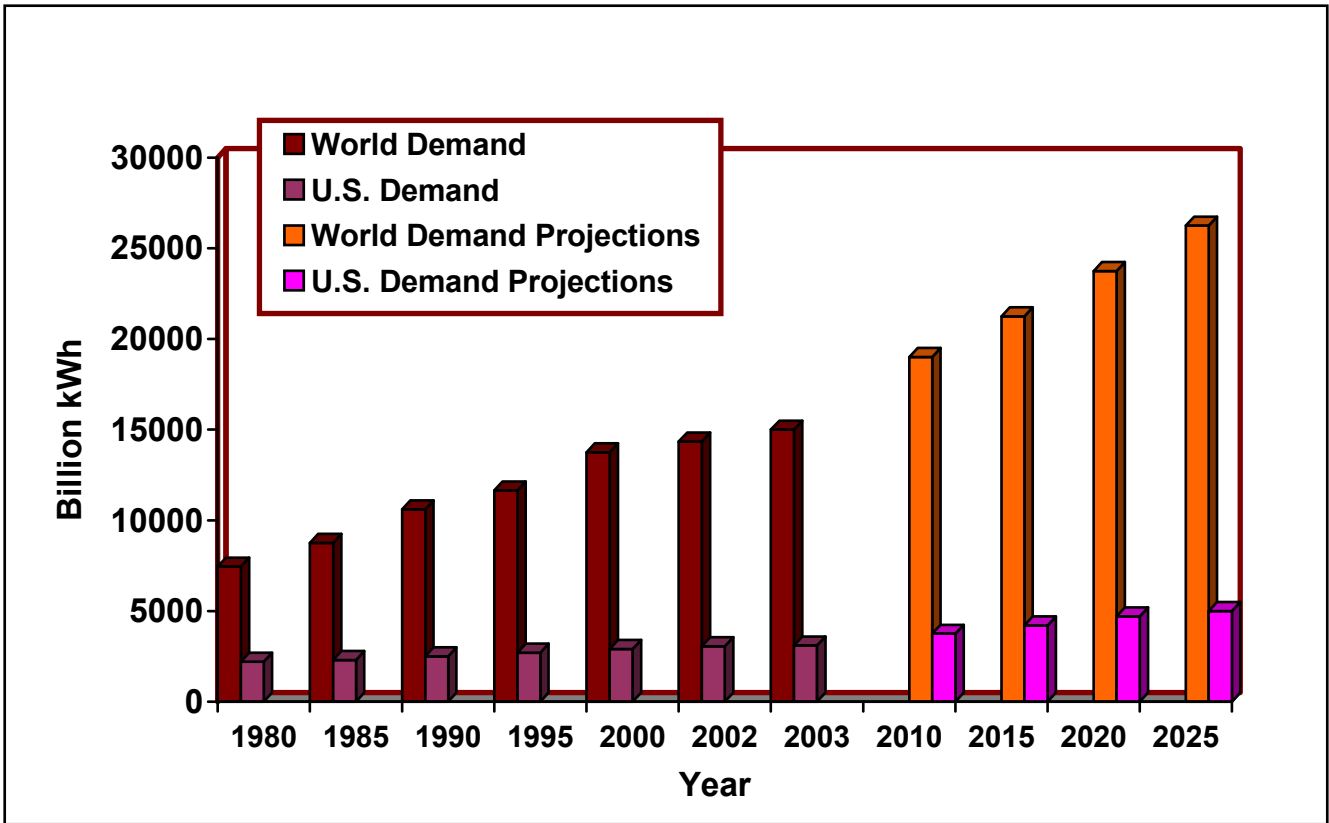


Figure 1.3 Electricity Demands 1980-2025 [1.1-1.3]

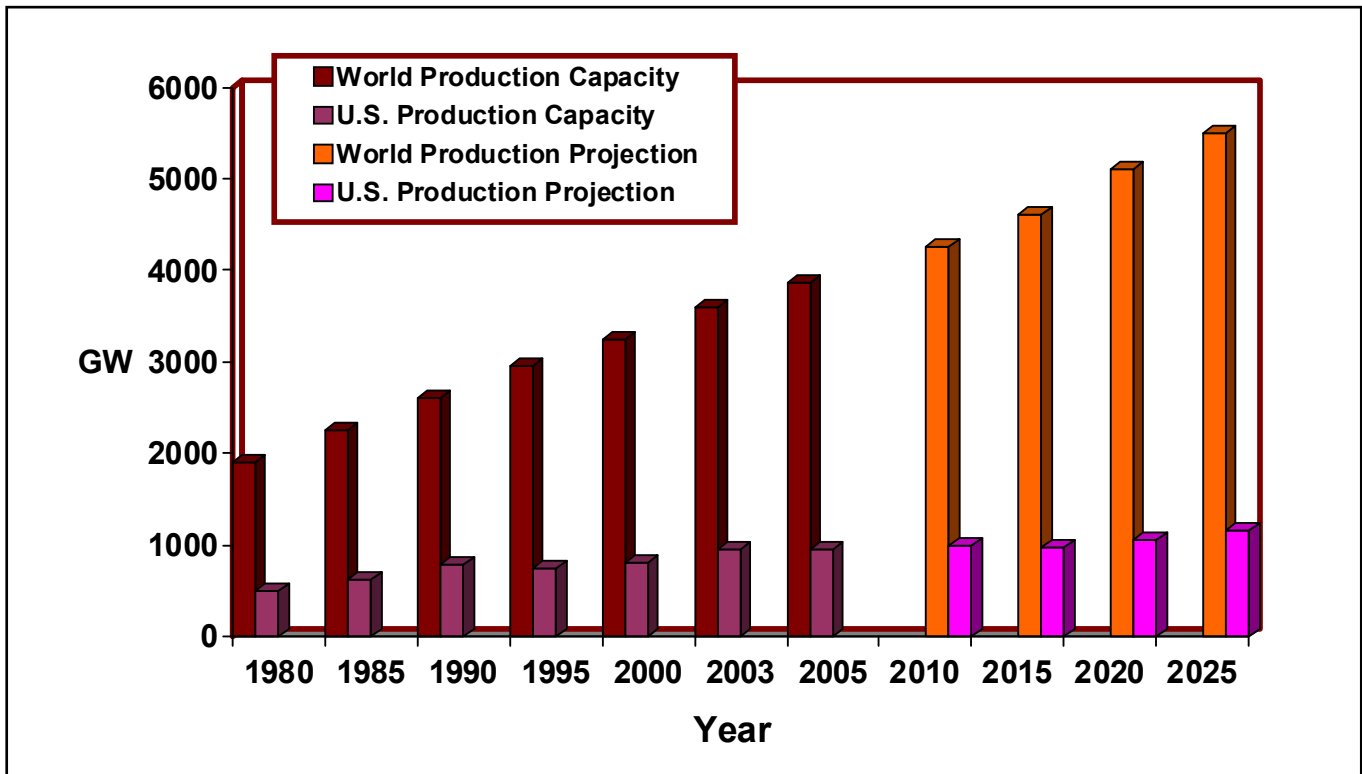


Figure 1.4 Electricity Production Capacities 1980-2025 [1.1-1.4]

The U.S.'s electricity generating capacity has been increasing steadily; however, not at the same high pace as the world's generating capacity. Therefore, the percentage ratio from the U.S. on the world scale is expected to decrease from 25% in 2005 to approximately 20% by the year 2025 (Figure 1.4) as indicated by the estimated projections by Energy Information Administration (EIA). Even so, the electricity generation capacity of the U.S. is anticipated to rise by approximately 20% between the year 2005 and 2025 [1.1]. When contrasting Figure 1.3 with Figure 1.4, it is apparent that the U.S. production capacity is increasing at a slower pace than the electricity consumption rate. If this trend continues, the U.S. will soon have to start importing its electric power to meet its needs.

Several types of energy sources allow for the production of electricity. Power can be produced through traditional thermal power plants (by means of fossil fuels or nuclear energy), hydropower stations, and additional various power generating units (photovoltaic arrays, wind turbine generators, biomass power plants, fuel cells, geothermal power stations, etc.). Nuclear energy and fossil fuels such as coal, oil, and natural gasses are all nonrenewable, limited resources. Alternatively, power can also be generated by unlimited, self-renovating resources such as wind and solar energy, which would allow future energy demand to be continually upheld. Figure 1.5 illustrates the U.S.'s net electricity production by type in 2005 and compares it to the world's production. It is apparent from the figure that over 80% of world's electricity production is still being supplied by conventional thermal power plants and nuclear power plants [1.1-1.4]. Excluding hydroelectric power, the amount of electricity produced from other renewable sources is insignificant.

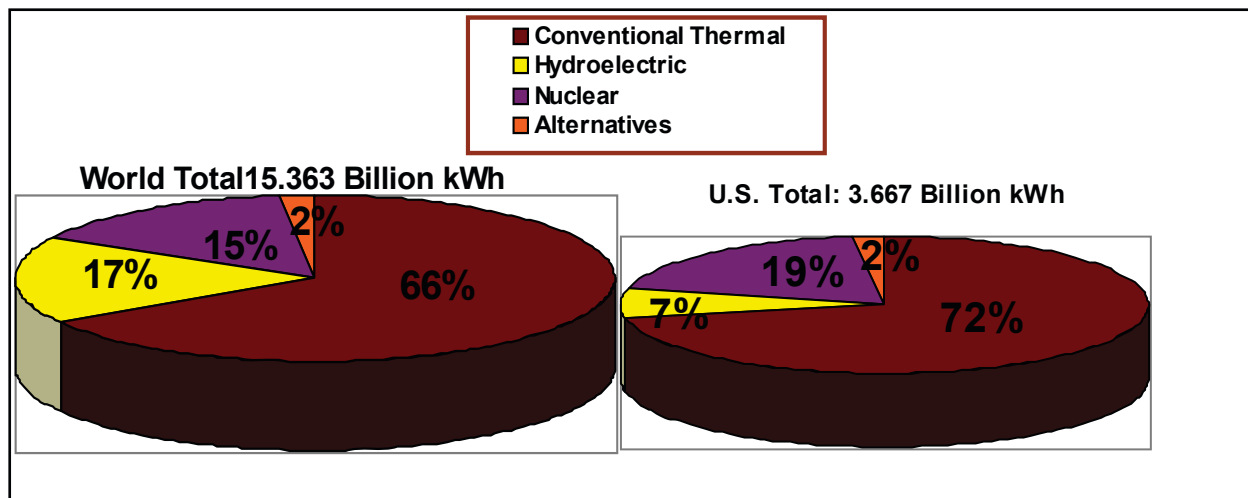


Figure 1.5 The world and US Net Electricity Generation by Type in 2005 [1.1, 1.4]

1.2 Role of Photovoltaic Systems in the Emerging Need of Alternative Technologies

As can be seen in Figure 1.6, solar energy is the source for many of the natural aspects of our daily life. For example, energy from the sun is what naturally powers the weather, including the temperature which in turn causes the water cycle and wind. Also, the sun is needed to give energy to every living thing. First, plants generate energy from the sun's rays through the process of photosynthesis. Then the energy is passed from the plant (in a lesser quantity) to any animal which eats the plant and then to any animal which eats that animal and so on. Many other examples of the use of solar energy can also be seen in Figure 1.6.

This brings us to the importance of capturing and processing solar energy and using it to meet our needs of artificial energy which have resulted from inventions of technology. Though we have other means of artificial energy, such as oil and coal, solar energy is the most natural energy source. Solar energy is free and limitless. Also, the consumption of solar energy does not harm humans, animals, or the natural environment of the earth. Furthermore, solar energy does not have any limits such as wind power does, because unlike wind, solar radiation can be found in every location of the

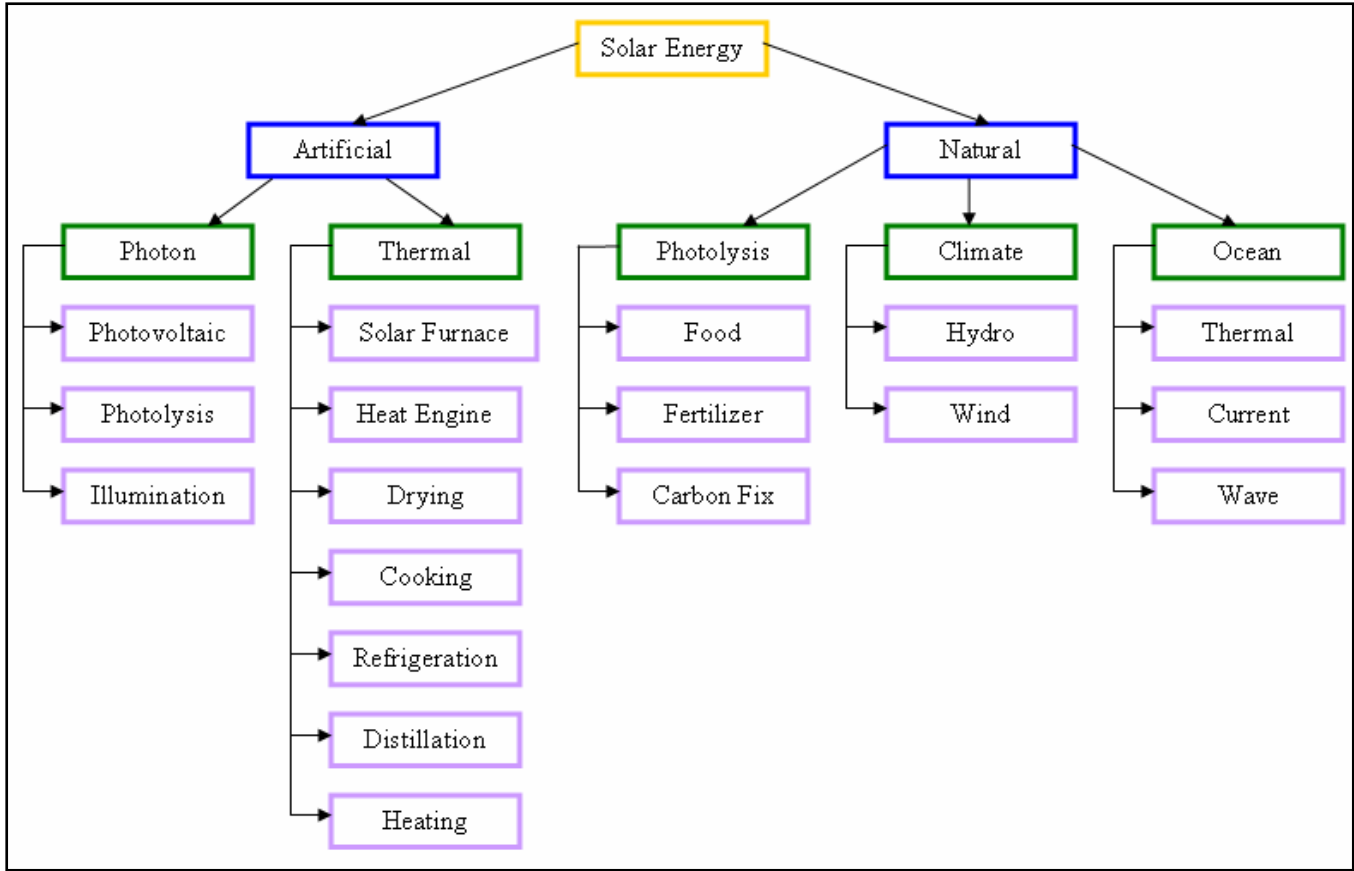


Figure 1.6 Distribution of Solar Energy [1.5]

world. For these reasons, it is important to make use of this exemplary source of energy to meet our increasing demands.

1.3 Motivation and Contribution of the Research

Harnessing the power from natural resources in general and in particular from solar power is a well established and progressive research area. Since the 1960's, various researchers have done numerous inventions, innovations, and researches on the power generation through sun light using photovoltaic devices. However, there is still a huge potential in this research area in terms of globalization, commercialization, system efficiency, and cost per unit of power. Although many

scholars are addressing these issues and many state of the art technologies do exist, solar power still has not been commercialized and utilized in replacement of conventional non-renewable power generation technologies.

The main hurdle in harnessing solar power is the efficiency of solar cells. Furthermore, the available output power is not accurately tracked because of the way solar cells are currently being modeled using assumptions such as temperature cell, T_C , and irradiance, G_T , are fixed. The reality is that T_C and G_T varies significantly from morning to afternoon. Also, the parameters of the cell do change with uncertain changes in weather conditions and ambient temperature. To obtain an optimal controller performance, the model of the system should be well determined with consideration of all the possible variations and parameters. The basic two variables that are required and must be considered on site and on a real-time basis to obtain maximum and efficient instantaneous solar power are the solar irradiance and the temperature. In commercial PV cells these two variables are averaged over standard weather condition to estimate the power output capacity of the PV panel.

Various maximum power point tracking (MPPT) techniques have been proposed in the past to obtain maximum power but again because of the estimated prediction of the weather condition, the promised maximum output power that would make a big difference in the current efficiency of the commercial solar cells has not been achieved. A review of 91 MPPT techniques is summarized in [1.7]. In [1.8] a predictive neural network model of PV is formulated and a governor control scheme is proposed for a hybrid PV, battery, diesel power generation system. As mentioned in the training data, the time interval of the data collection is 5 minutes which accounts for less than 10 hours for 186 data points. However, for stand-alone PV applications, the data points should vary over several days with different weather conditions to take into account all the different performance scenarios of the PV module in different weather conditions.

Also, parameters like heat loss coefficient, thermal capacitance, transmittance and absorptance coefficient are assumed to have constant values, such as heat loss coefficient U_L which is assumed to have an approximate value of 0.9 in most of the models of PV cells [1.9-1.12]. However, that is not true in most cases as heat loss coefficient varies over a wide range depending upon the properties of materials and weather conditions [1.9-1.12].

Due to the above mentioned limitations, there is an inexistence of efficient controlling technologies: a major reason of the significantly low efficiency of these systems. Most times, systems are designed for standard conditions and variation in those conditions due to changing weather and parametric variations lead to inefficient performance because of the inability to handle and control the rapid dynamic conditions optimally [1.12-1.22].

To address these issues, a dynamic model is developed considering the variability of irradiance and ambient temperature on a real-time basis using the data acquisition system and an R^2 value of 0.997 is obtained for 370 data points over the period of 20 days. These days consists of all bright, cloudy, rainy and normal days. Also, the obtained values are validated with hardware set up with an accuracy of 0.1 – 3.9%.

This model will now be used in conjunction with a dc-dc boost converter and an applied genetic algorithm-based fuzzy logic controller as governor control to obtain the optimum suitable load management on a real-time basis. The loads are connected in series through Breakers (in simulation) and can be connected with MOSFET(s) in hardware setup for real-time switching and tapping of the load through Fuzzy logic Control for harnessing the instantaneous maximum output power.

1.4 Organization of the Dissertation

The ongoing Chapter 1 is entitled “Introduction.” In the beginning, importance, need, and future global scenario of the energy production through conventional and alternative technologies are addressed. Further, the role of Photovoltaic in the emerging need of alternative technologies is covered in brief. With this background, the reason and motivation of the research is detailed, followed by the significance and contribution of this study.

In Chapter 2, entitled “Photovoltaic Fundamentals,” solar cell fundamentals are reviewed followed by an overview of the components of a Photovoltaic system. Further, the solar cell characteristics are analyzed in detail.

Chapter 3 is entitled “Photovoltaic Modeling.” After the literature survey of modeling techniques and review of mathematical and electrical model of photovoltaic, a steady state and a dynamic Simulink® model are developed and compared. Based on the investigation of the parameter variations, the parametric calculation is also incorporated in the Simulink model and the results are discussed. Afterwards, this MATLAB®/Simulink model is inculcated in the LabVIEW environment to validate the model with the Hardware setup. The experiment is being performed over a span of three weeks and the model is validated through design of experiment. There are five appendices for Chapter 3. Appendix A includes the Nomenclature. Appendix B consists of the Simulink and LabVIEW models. Appendix C covers the specifications of the hardware and instruments being used during the experiment. Appendix D is a report on the design of experiment which explains the statistical calculations and analysis for the validation of the model. Appendix E has the experimental results. Appendix F describes the concept of the solution of transcendental equations followed by the description of Newton –Raphson method for the solution of the characteristic equation of PV which is a transcendental equation.

In Chapter 4, entitled “Optimal Load matching of Stand –alone PV Systems at Maximum Power Point,” the PV model that was developed and validated previously is implemented in conjunction with a dc-dc boost converter and an applied genetic algorithm-based fuzzy logic controller as governor control in the MATLAB/Simulink environment to obtain the suitable load management on a real-time basis. There are three appendices for Chapter 4. Appendix G covers the fundamentals and basics of fuzzy logic control. Appendix H covers a brief theory and modeling of a DC-DC buck boost converter. Appendix I consists of Simulink model of the control scheme.

Chapter 5 is entitled “Conclusion, Recommendations, and Scope for Further Research.” After the explanation of the results obtained through modeling, design, experimental validation of the model, and the development of load matching through applied genetic algorithm-based fuzzy logic based control at maximum power point, recommendations for future work are provided.

REFERENCES

- [1.1] International Energy Outlook 2005, Energy Information Administration (EIA), <http://www.eia.doe.gov/iea.12/08/2008>.
- [1.2] International Energy Annual 2003, EIA, <http://www.eia.doe.gov/iea.12/08/2008>.
- [1.3] System for the Analysis of Global Energy Markets 2005, EIA, <http://www.eia.doe.gov/iea.12/08/2008>.
- [1.4] Annual Energy Outlook 2006 (Early Release), EIA, <http://www.eia.doe.gov/.12/08/2008>.
- [1.5] O. Ulleberg, "Stand-alone power system for the future: Optimal design, Operation and Control of the Solar-Hydrogen System," PhD Dissertation, NUST, Norway, 1998.
- [1.6] A.Mellit, S.A.Kalogiru, "Artificial Intelligence Techniques for Photovoltaic Applications: A review," *Journal of Progress and Energy and Combustion Science*, Vol. 34, pp: 574-632, 2008.
- [1.7] T. Esum, P. L. Chapman, "Comparison of Photovoltaic Array Maximum Power Point Tracking Techniques," *IEEE Transactions on Energy Conversion*, Vol. 22, No. 2 pp: 439-449, June 2007.
- [1.8] A.A. Al-Alawi, S.M. Al-Alawi, S.M.Islam, "Predictive control of an integrated PV-diesel water and power supply system using an artificial neural network," *Journal of Renewable Energy*, Vol 32, pp: 1426-1439, 2007.
- [1.9] T.U. Townsend, A Method for Estimating the Long-Term Performance of Direct-Coupled Photovoltaic Systems, MS thesis, University Of Wisconsin – Madison, 1989.
- [1.10] T. Townsend, et al., "A New Performance Index for PV System Analysis," 24th IEEE PVSC, Dec. 1994.
- [1.11] Y.Huang et al., "A Z source Inverter for the residential photovoltaic systems," *International Power Electronic Conference*, 2005.
- [1.12] S. A. Papathanassiou, N. G. Boulaxis, "Power limitations and energy yield evaluation for wind farms operating in island systems," *J. of Renewable Energy*, Vol. 31, 2006, pp: 457-479.
- [1.13] S. Alpay, L. Bilir, S. Ozdemir, B. Ozerdem, "Wind speed time series characterization by Hilbert transform," *Int. J. Energy Res*, 2006, Vol. 30 pp: 359-364.
- [1.14] M. Chinchilla, S. Arnalte, J.C. Burgos, J.L. Rodríguez, "Power limits of grid-connected modern wind energy systems," *J. of Renewable Energy*, Vol. 31, 2005, pp: 1455-1470.
- [1.15] U. V. Paatero, P. D. Lund, "Effects of large-scale photovoltaic power integration on electricity distribution networks," *J. of Renewable Energy*, Vol. 32, 2007, pp: 216-234.
- [1.16] W. Swiegers and J.H.R. Enslin, "An integrated maximum power point tracker for photovoltaic panels," *proceeding of IEEE International Symposium on Industrial Electronics*, Vol.1 pp: 40-44,1998.
- [1.17] Y.H.Lim and D.C. Hamill, "Simple maximum power point tracker for photovoltaic arrays," *IEEE Power Electronics Letters*, 36(11), pp: 997-999, May 2000.
- [1.18] Y-Ch. Kuo et al., "Novel maxium power point racking controller for photovoltaic energy conversion system," *IEEE Transactions on Industrial Electronics*, 48(3), pp: 594-601, June 2001.
- [1.19] S. Jain, V. Aggarwal, "A new algorithm for rapid tracking of approximate power point in photovoltaic systems," *IEEE Power Electronics Letters*, 2(1), pp: 16-19, March 2004.
- [1.20] J.A. Jiang, T.L. Huang, Y.T. Hsiao, and C.H. Chen, "Maximum Power Tracking for Photovoltaic Power System," *Journal of Science and Engineering*, 8(2):147-153, 2005.
- [1.21] M.A.S. Masoum, H. Dehbonei, and E.F. Fuchs, "Theoretical and experimental analyses of photovoltaic systems with voltage and current-based maximum power-point tracking," *IEEE Trans. Energy Conversion*, 17(4):514-522, Dec. 2002.
- [1.22] F. Harashima, H. Inaba, N. Takashima, "Microprocessors-controlled SIT inverter for solar energy system," *IEEE Trans. on Industrial Electronics*, Vol. IE-34, No.1, 1987.

CHAPTER 2

PHOTOVOLTAIC FUNDAMENTALS

2.1 Background

The term “photovoltaic” is derived from two Greek words: phos meaning “light,” and voltaic meaning “electrical.” In turn, voltaic is named after the Italian physicist Volta, which is the same origin of the measurement “volts” [2.1]. “Photovoltaic” has been used in English vocabulary since 1849 [2.1]; however, the PV effect was first announced by Bequerel in 1839 and commercial use of this form of power production did not come until much later during the mid-1950’s [2.2]. The cost of PV power production has been much too high to effectively compete with the other forms of conventional power sources. However, the concern of cost is becoming less of a problem as we have seen a dramatic drop in price from \$100/kWh in 1962 [2.3] to as little as \$0.30/kWh in 2008 [2.24].

Photovoltaic (PV) energy conversion is the process of converting light energy directly into electric energy. PV power is generated only when specific conditions are met, including proper absorption of solar radiation, creation of movable electron/hole pairs, collection of charges, and connection of oppositely charged contacts. Conceptually, a solar cell is an electrical current source, driven by a flux of radiation. There are other light sources available which can also produce photovoltaic electricity [2.5]; however, only solar radiation-based PV cells are analyzed in this dissertation.

In a PV panel, semiconductors account for nearly 60% of overall expenses. Commercially available PV’s are generally only 10-20% efficient, producing energy in normal sunlight at the rate of 1-2 kWh per sq. m each day. On average, complete solar radiation of 1 kW per sq. meter will generate a potential difference of approximately 0.5 V and a current density of 200 A per sq. m. of

cell area. Therefore, a standard industrial cell of 100 sq cm area will generate approximately 2 A of current. The cell has a typical life span of little more than twenty years [2.5]. Also, because the system is stationery, it can be left in isolated locations without maintenance [2.4]. There are many advantages of using PV systems over other common power sources. Some of these benefits include [2.4]:

- i. These systems have long life spans with a duration of 20+ years.
- ii. Solar PV systems perform in nearly any weather condition and have an immediate response to solar radiation.
- iii. Solar PV systems are dependable, modular, sturdy, and require little maintenance.
- iv. PV systems operate silently.

Some disadvantages of the PV system are: [2.4]:

- i. PV systems have high initial cost and a large investment is required for the setup.
- ii. As this is a weather-dependent device, energy storage in the form of batteries is required as backup and the battery cost further increases the installation cost.
- iii. The power output is not constant as it depends on the weather conditions.
- iv. The overall efficiency of the system is lower than the other power generating technologies.
- v. The performance of the PV system deteriorates over time due to aging factor of the semiconductor material. Furthermore, the performance of all the solar cells in a module does not remain the same with the passing age, which also results in increased losses and decreased efficiency.
- vi. There are also losses due to the reflection from the active surface of the PV module which prevents the photons to penetrate into the semiconducting material. At the time of production, the surface of the PV module is treated with a special anti-reflecting material to have a

pyramidal or textured structure. This treated layer vanishes with time. Therefore, aging plays a vital role in the performance of the PV module as well.

2.2 Solar Cell Fundamentals

2.2.1 Semiconductors:

Silicon (Si) is one of the best semiconductors because it has four valence electrons, allowing it to powerfully bind with surrounding atoms by forming a covalent bond [2.5]. Though silicon is expensive, it is widely available, making it the best material for use as a semiconductor.

At an ideal temperature of zero, a semiconductor is able to work as a supreme insulator as there are no charge carriers obtainable for transmission of current. When the temperature increases, a Si atom releases an electron from the valence orbit and thus creates a vacancy or hole in the valence orbit. An electron hole pair is formed during this process. These electron hole pairs can also be formed by means of photonic radiations. A Si crystal at room temperature will have the following conditions at any given point in time [2.5]:

- i. A number of forming free electron-holes
- ii. A recombination of free electron-holes
- iii. A number of isolated electrons and holes remain until recombination.

In a Si atom there are equal numbers of electrons and holes. Such a semiconductor is known as an intrinsic semi conductor. On applying a potential across a semiconductor, electron-hole pairs that are being formed because of thermal agitation begin to flow in the direction of opposite polarity and these charge carriers create a current in the semiconductor. This phenomenon is portrayed in Figure 2.1. Conductivity of the Si semiconductors is increased through the doping process by adding

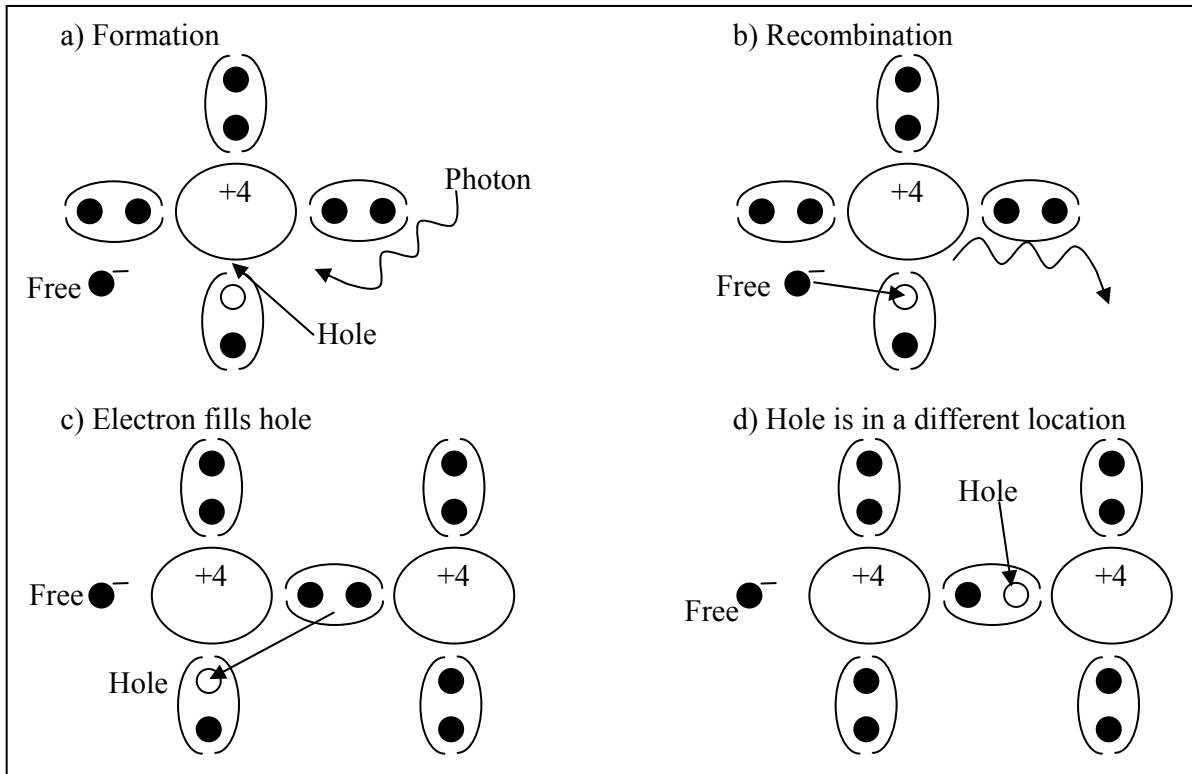


Figure 2.1 Free Electron-Hole Flow Through a Semi Conductor [2.11]

impurity atoms to intrinsic Si atoms resulting in n type or p type silicon depending upon the majority of free electrons or free holes, respectively. The different electrical properties of the semiconductors are obtained by regulating the level of doping. In fact, the doping level is inversely proportional to the resistance of semiconductor [2.6-2.7].

2.2.2 PN Junction

When a junction between a p type and n type semiconductor material is formed, holes and electrons diffuse from a higher concentration to a lower concentration surface separated by the junction. The remaining charge particles that are left after the recombination of holes and electrons accumulate in the form of a layer along the junction and are known as depletion layer. The holes form the positively charged layer while electrons form the negatively charged layer which results in

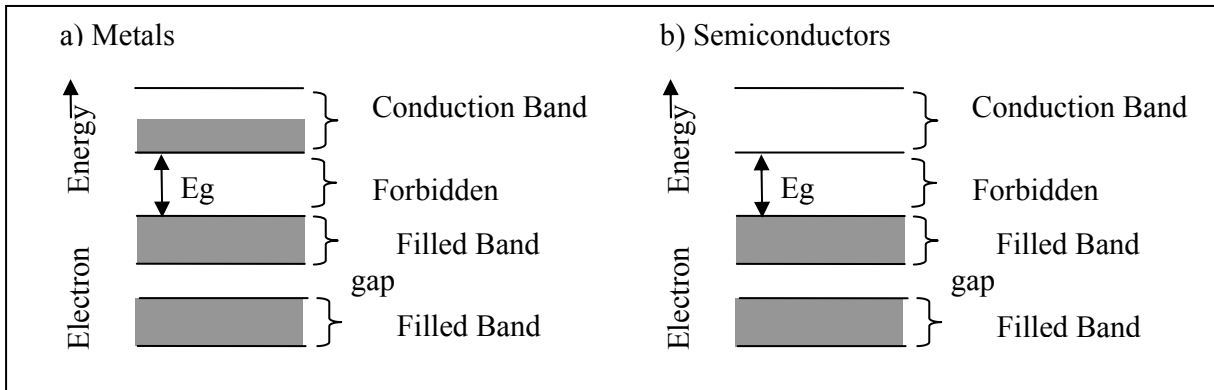


Figure 2.2 Free Electron Hole Flow through a Semi Conductor [2.11]

an electrostatic potential along the junction which causes an electric field in the depletion region. This voltage difference produces an energy barrier that further hinders the combination of an electron hole pair from the opposite side of the junction and thus stops the flow of charge. This energy barrier is known as potential energy hill, energy gap or barrier voltage. Figure 2.2 portrays energy bands for a junction prior to and following the establishment of a depletion layer.

2.2.3 Photoconduction

The energy, E , in a photon is given by

$$E = h\nu = \frac{hc}{\lambda} \quad (\text{joules}) \quad \text{or} \quad E = \frac{1.24}{\lambda} \quad (\text{ev}) \quad (2.1)$$

where

h : Planck's constant ($h = 6.63 \times 10^{-34}$ joules-sec),

c : Speed of light (2.988×10^8 m / s),

ν : Frequency of photons (Hz),

λ : Wavelength of photons (m or μm),

1 eV: 1.6×10^{-19} joules.

To generate an electron hole pair through a light ray or beam of photons, the energy of the photons must overcome the semiconductor energy band gap, E_g [2.5]. Due to the existing electric field around the junction, the generated electron hole pair will be attracted to the p and n sides, respectively. These additional charges will develop a potential difference which will result in a flow of current if the load is connected across the terminal.

2.2.4 PV Cell

A photovoltaic cell consists of an exclusive p-n junction semiconductor diode where the position of the junction is near to the surface [2.6]. The typical configuration of a PV cell is n-on-p with p type silicon at the bottom of a thickness of 100 to 350 microns and a diffused thin layer of n type silicon at the top [2.5]. The current produced by the incident photons are collected through an Ohmic contact connected with the metallic grid on the top of the junction and forms the negative terminal of the solar cell. The bottom surface is also connected through a metallic Ohmic contact over the entire surface and forms the positive terminal of the cell. As shown in Figure 2.3, anti-reflecting coating is done on the top layer and reflective surface at the bottom layer of the PV cell to enhance the photo conduction process.

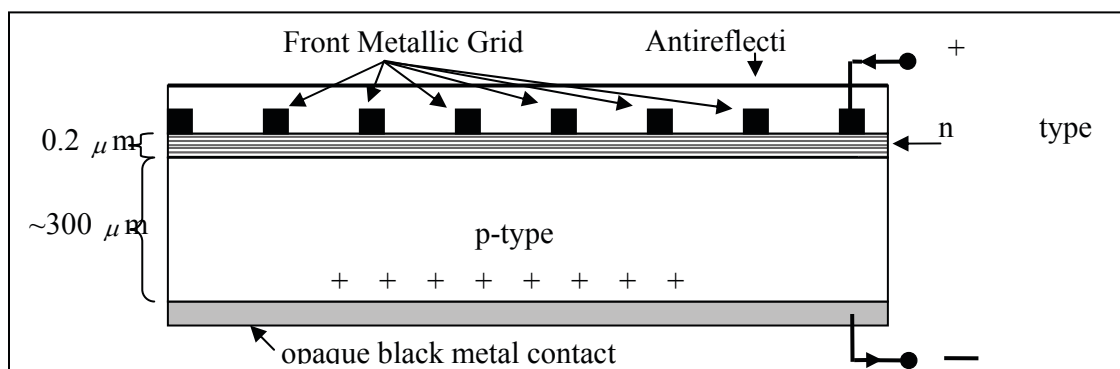


Figure 2.3 X- Section of a Typical PV Cell [2.5, 2.7]

2.2.5 PV Module and Array

A PV cell is the building block of a PV system. Because of its output limitations of 0.5 – 0.6 V and size limitation of a few square centimeters, typically 36-40 such cells are connected in series or parallel circuits on a panel and are known as a PV module[2.6]. A number of such PV panels are connected in series or parallel combination to form an array in order to provide the required wattage. An outline of a PV cell, module and an array is shown in Figure 2.4. A PV array is manufactured in various fabrication stages. A laboratory cell is first modified into a production cell which serves as the building block of a production module. Several production modules are combined to obtain an operating array. Based on the power requirement and climatic conditions, an operating PV system is established through the combination of various PV arrays along with different electrical and power electronic devices.

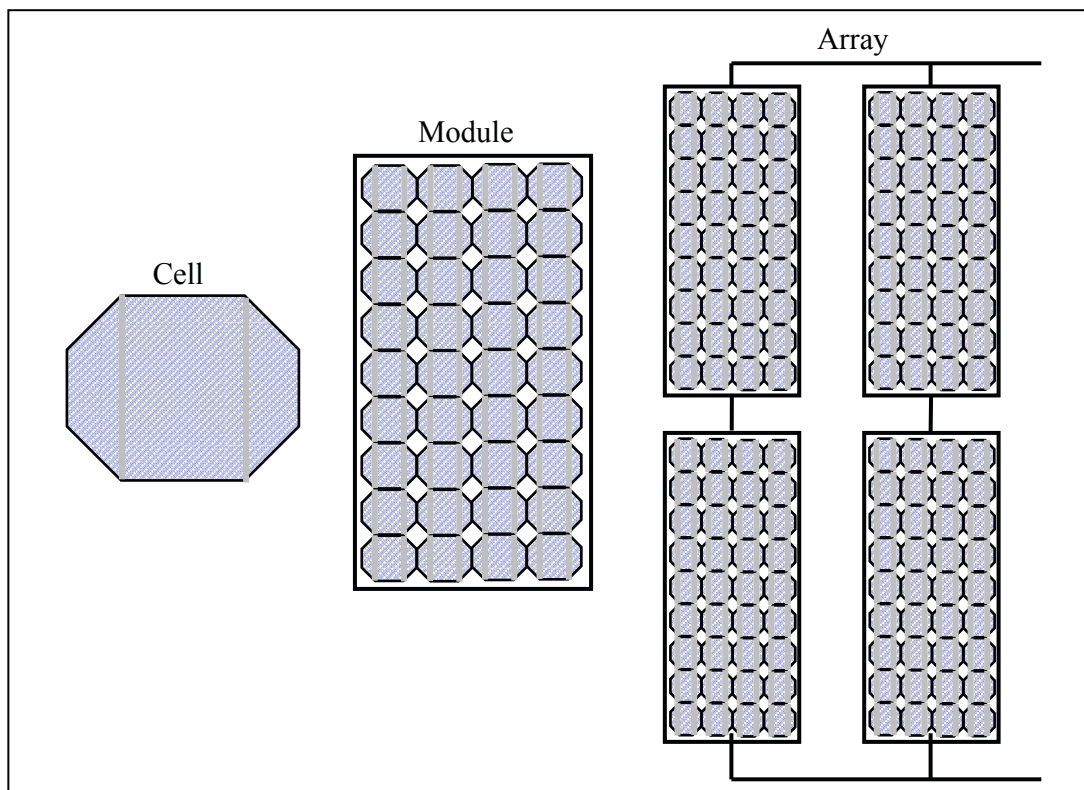


Figure 2.4 PV Cell, Module, and Array

2.3 PV System Components

PV Systems are broadly classified into central power station and distributed power generation systems.

2.3.1 Central PV Power Station System

Central PV power station systems are installed in a few MW capacities and are connected to a grid to provide peak power loads during the day time. The experimental setups has been demonstrated in European and North American alternative power markets up to a range of 6 MW [2.5-2.10] but the initial installation cost is a major hindrance in the commercialization of the concept.

2.3.2 Distributed PV Power Generation Systems

Distributed Generation Systems are more viable for alternative power generation technologies in terms of implementation and economical power output on a relatively small scale. Distributed PV power generation systems can further be classified as stand-alone PV systems, grid interactive PV systems, and hybrid PV systems.

2.3.2.1 Stand-alone PV power generation system. Stand-alone systems are onsite power generation systems and are economical for remote areas which are not connected to a grid. They are quite popular in rural areas and for residential or small scale specific load requirements. During the daytime, the power is generated from the PV arrays and the excess power is stored in the battery banks for the nighttime. Figure 2.5 shows the main components of a stand-alone PV

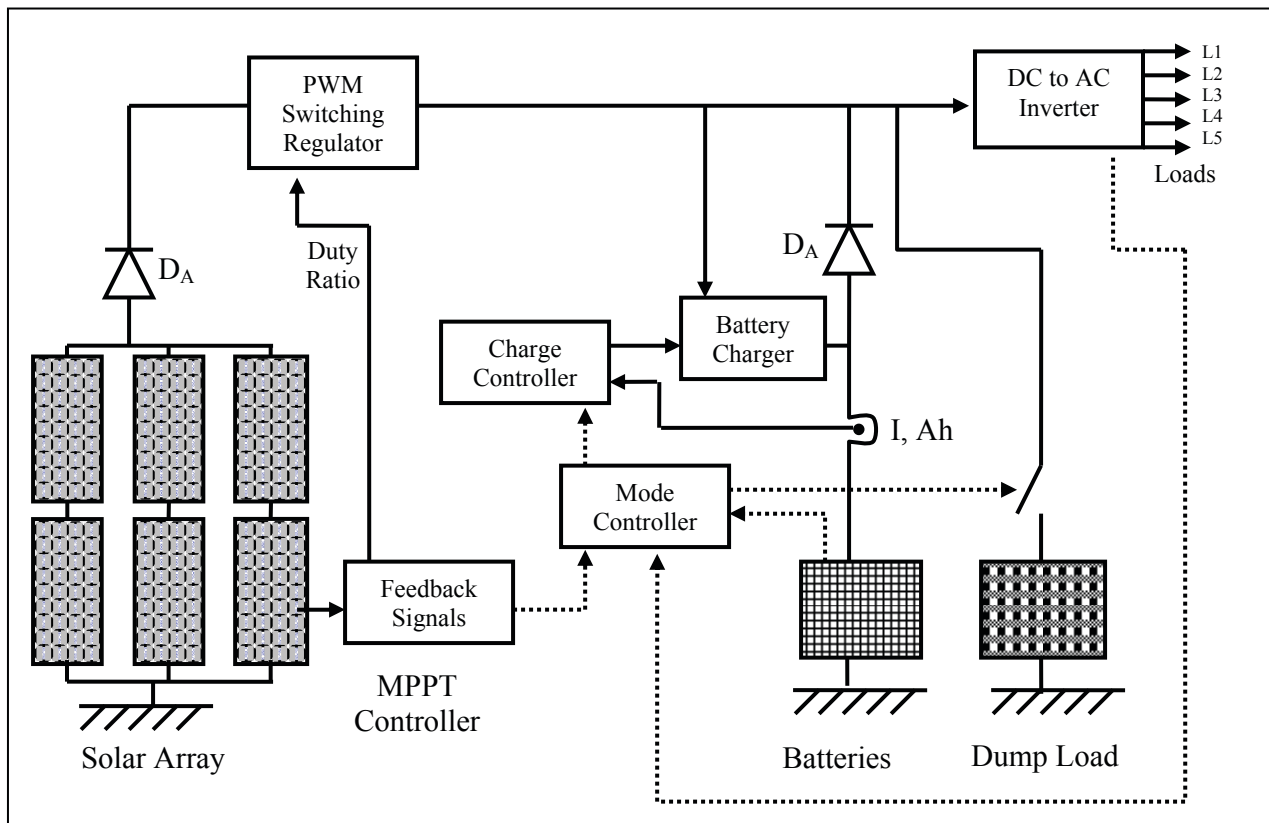


Figure 2.5 A Typical Stand-Alone PV Power Generation System [2.5]

power generation systems. The DC output is fed to the DC/AC inverter and then the converted AC Power is fed to the load. In this figure, Diode D_B is used to prevent the battery from overcharging and diode D_A is used to prevent batteries from discharging through PV arrays during the nighttime. The battery charge controller monitors the charging and discharging of the battery bank. Dump loads are used to extract the excess power in case the battery banks are fully charged.

2.3.2.2 Grid interactive PV power generation system. This can be considered as a special case of stand-alone PV power generation system where the load buses are connected to the grid through a bi-directional metering system. There is no battery storage in grid interactive power systems. The power generated from the PV arrays is fed to the grid through a

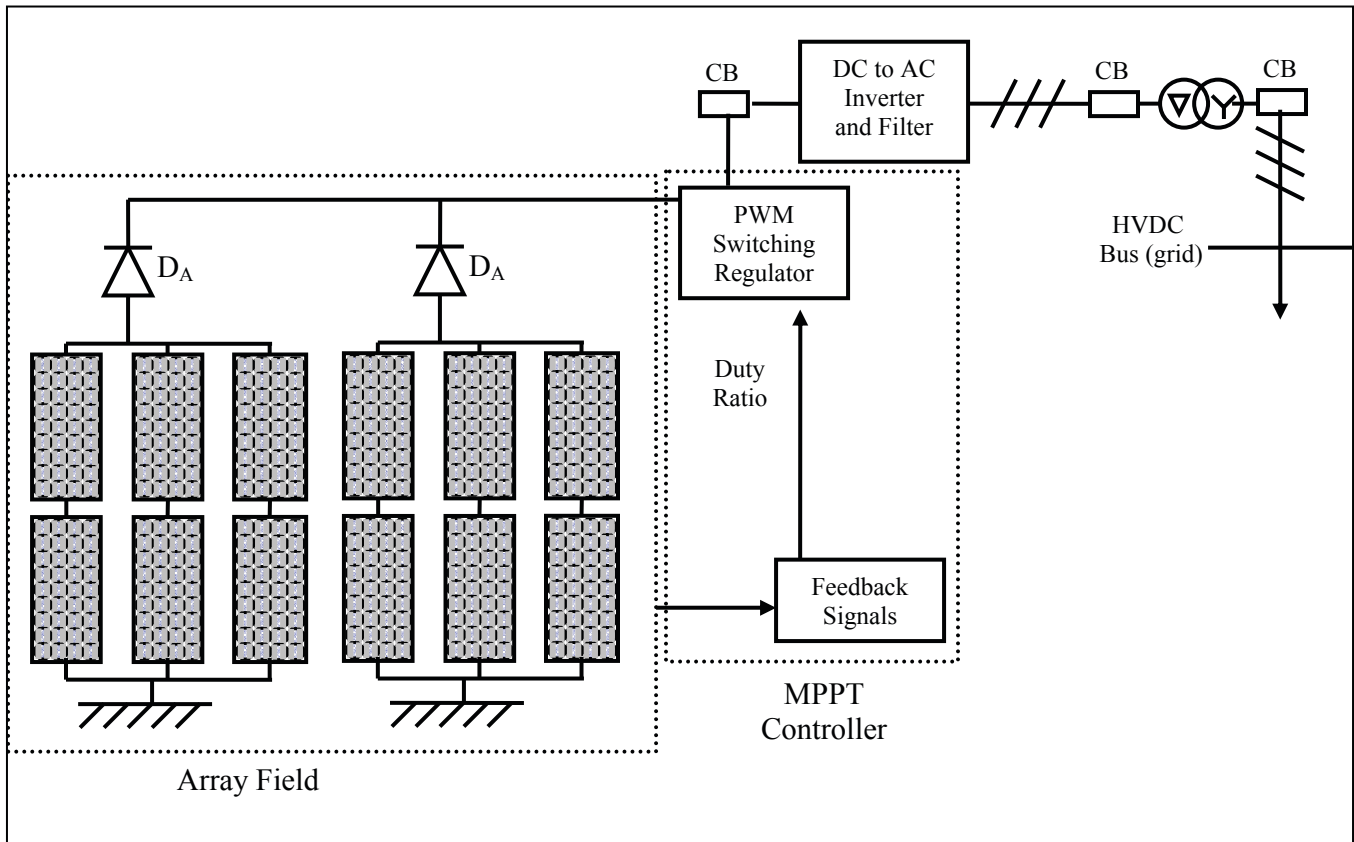


Figure 2.6 A Typical Grid Interactive PV Power Generation System [2.5]

synchronized power mechanism if it is in excess to the local load requirement. The DC power is converted to AC power through an inverter for feeding into the grid after the filtration of harmonics and adjustment of voltage level. In the scenario of power requirement at the local level in case of insufficient power generation from the PV arrays, the power is fed from the grid to meet the load requirement. Figure 2.6 shows the main components of a grid interactive PV power generation system.

2.3.2.3 Hybrid PV generation systems. To optimally utilize the available energy sources, at some locations it is economical to integrate various power generation sources. The PV power generation system is extensively used in conjunction with diesel generators, wind turbines and Combined Heat and Power Plants (CHP) for the optimal utilization of the available

power sources at numerous locations [2.11 – 2.18]. A hybrid control scheme is required to manage the performance of individual power sources efficiently.

2.4 Solar Cell Characteristics

PV power is generated when solar radiation is absorbed by an upper layer of dissimilar semiconducting material such that some electrons jump to a higher energy band, thereby creating mobile electron/hole pairs which results in flow of current. Direct current (DC) current can be obtained if the oppositely charged layers are connected to an external circuit. This effect has been portrayed in Figure 2.7.

To study the electrical characteristic of a PV cell and to develop an equivalent circuit, it is necessary to understand the physical configuration of the PV cell and the ongoing phenomenon in a cell. In an actual cell, there are manufacturing imperfections or inherent material properties which

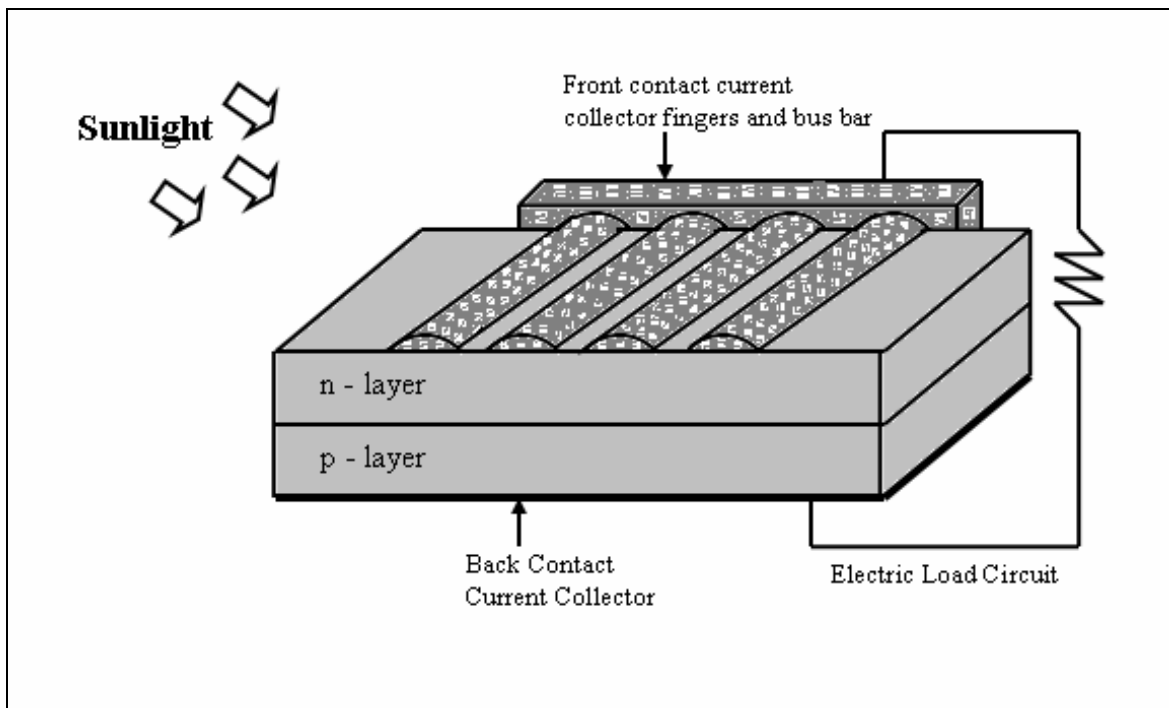


Figure 2.7 Illuminated PN Junction [2.19]

introduce resistances and other limitations which result in the decrement of output efficiency of the cell.

The well-known characteristic of an ordinary silicon PN junction are highlighted in Figure 2.8. Mathematically the current-voltage relationship is given by Shockley diode equation

$$I_d = I_s [\exp(V_d / V_T) - 1] \quad (2.2)$$

where

I_d : diode current,

I_s : reverse saturation current,

V_d : p-n junction / diode voltage

V_T : voltage equivalent of temperature; at room temperature (20 °C), its approximate value is 26mV.

$$V_T = \frac{KT}{q} \quad (2.3)$$

where

K: Boltzmann's constant (= 1.3806×10^{-23} J/k = 8.6174×10^{-5} eV/ K),

T: temperature in °K and

q: charge of an electron (= 1.60218×10^{-19} C)

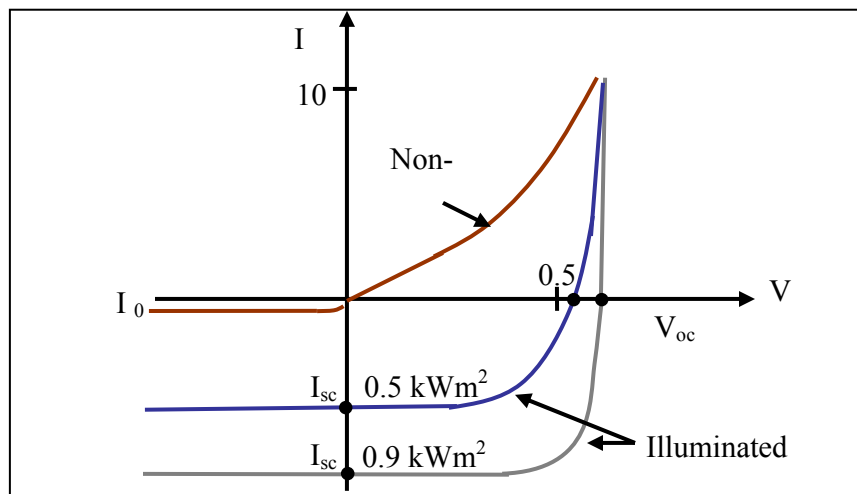


Figure 2.8 Characteristic of an Illuminated and Non-Illuminated p-n Junction [2.5]

When the p-n junction is illuminated, the characteristic gets modified in shape and shifts downwards as a photon-generated component is added with reverse leakage current as shown in Figure 2.8. The out put current generated from the p-n junction, I_o will be the Current due to incident photons, I_λ minus the current through diode. In such a scenario, above diode equation 2.2 becomes

$$I_o = I_\lambda - I_s[\exp(V_d / V_T) - 1] \quad (2.4)$$

where

I_o : p-n junction output current;

I_λ : Photon current; depends on insulation and wavelength of photons.

2.4.1 Equivalent Electrical Circuit

The modified diode equation is obtained for an ideal diode in Equation 2.4 under the assumption that the values of the series R_s and shunt resistances R_{sh} are zero. However, the typical value R_s for a square inch of silicon cell is 0.05 to 0.1 ohms and of R_{sh} is 200 to 300 ohms [2.6]. R_s , also known as internal resistance, varies with the impurities, junction depth, and resistance of the contacts. The value of R_{sh} varies inversely with the leakage current to the ground. The value of series resistance plays a vital role in determining the efficiency of the PV module. A slight increase in the value of series resistance results in a significant drop of the efficiency [2.5]. The equivalent circuits for an ideal and practical diode are shown in Figure 2.9. Thus, modifying equation 2.4, the load current I_o for a practical diode will be

$$I_o = I_\lambda - I_s[\exp(V / V_T) - 1] - (V + IR_s) / R_{sh} \quad (2.5)$$

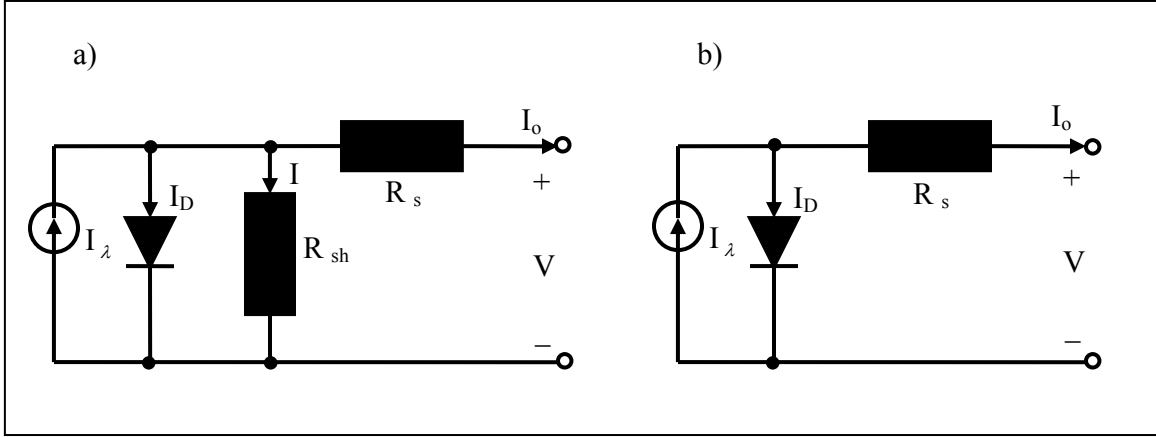


Figure 2.9 Equivalent Circuit of a) Five and b) Four Parameter Photovoltaic Cell [2.11]

2.4.2 Open Circuit Voltage and Short Circuit Current

Open circuit voltage V_{oc} and short circuit current I_{sc} are the two main specifications given by a manufacturer for a Photovoltaic module. The short circuit current is obtained by measuring the terminal current by short circuiting the output terminal of the PV module. During short circuit condition, no current flows through the diode as $V_d = 0$ and the all the circuit current flows through the short circuited terminals will be the current from the light source and hence the magnitude of light source current I_λ will be equal to short circuit current I_{sc} . The short circuit under this condition is given by

$$I_{sc} = I_o + I_s [\exp(V/V_T) - 1] \quad (2.6)$$

Under open circuit voltage condition, the maximum photo voltage is obtained through a PV module.

Assuming load current I_o is equal to zero in Equation 2.6, open circuit voltage will be given by

$$V_{oc} = V_T * \ln \{(I_{sc} / I_s) + 1\} \quad (2.7)$$

2.4.3. I-V and P-V Curves

I-V characteristics of a PV module represent its electrical characteristics. As shown in Figure 2.10 the boundary points of an I-V curve are short circuit current and open circuit voltage. To operate the PV module at the highest possible efficiency, it is required to obtain the maximum power point P_m which can be calculated by drawing a hyperbolic tangent to the I-V curve. The corresponding values of voltage V_m and current I_m are unique values for a given set of weather conditions subject to proper load matching. The power output P of the PV module is the product of the output voltage and current. A P-V curve is also shown in Figure 2.10. It can be noted that the maximum power point in the P-V curve corresponds to the maximum power point or the knee point of the I-V characteristic.

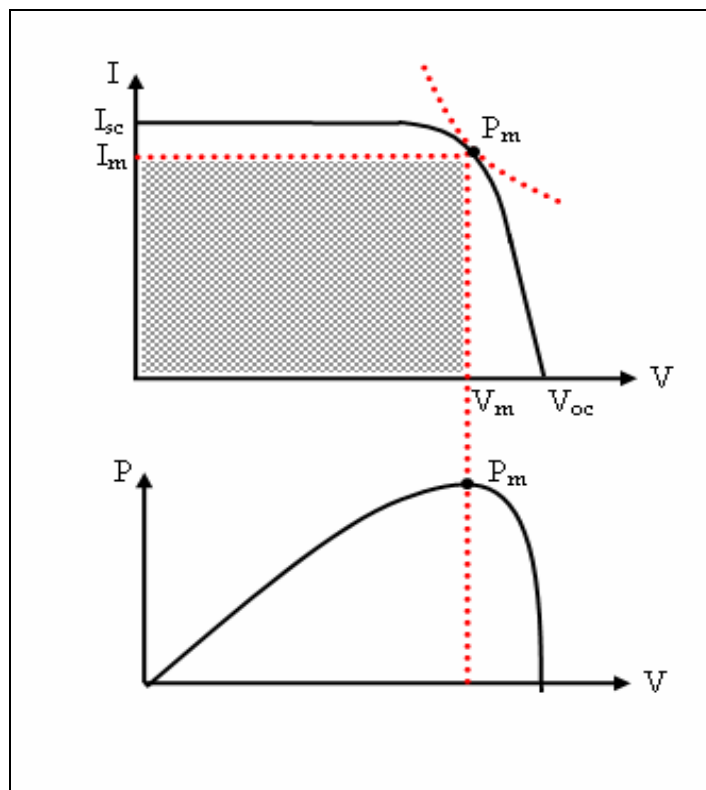


Figure 2.10 I-V Characteristic, Maximum Power Point, P-V Characteristic of a Typical PV Cell [2.5]

It can also be noted that if a rectangle of maximum possible area is inscribed in the I-V characteristic of the PV module, the top right corner of the rectangle will coincide with the maximum power point of the I-V curve. This phenomenon is being used to define fill factor FF, a measure of PV module performance. Fill factor is defined in [2.5]. Fill factor has value of 1 for an ideal diode

$$FF = \frac{V_m I_m}{V_{oc} I_{sc}} \quad (2.8)$$

2.4.4 Performance Factors

The major factors that affect the performance of a PV module are

- i. Solar Irradiance,
- ii. Ambient temperature,
- ii. Load matching,
- iii. Sun angle and Sun tracking,
- iv. Other factors such as shading, clouds, rain, snow, wind etc.

2.4.4.1 Solar irradiance. The magnitude of the generated photovoltaic current is directly proportional to the intensity of the available solar radiation. As can be seen in Figures 2.11 a and b, there is marginal drop in the output current with decreasing value of solar intensity which results in minimizing the maximum power. It can also be observed that the overall variation in the open circuit voltage as compared to short circuit current is relatively small.

2.4.4.2 Temperature. Variation in temperature affects both the short circuit current as well as the open circuit voltage of a PV module. As shown in Figure 2.11a, with decreasing temperature, the value of short circuit current decreases while the value of open circuit voltage increases.

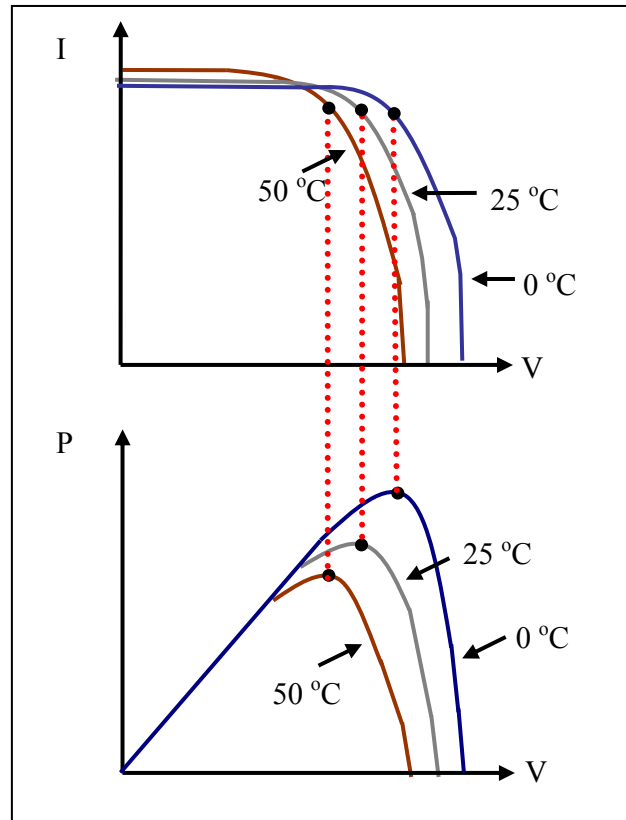


Figure 2.11.a Effect of Variation of Temperature on the PV Characteristic [2.5]

The average value of solar irradiance and cell temperature are among the major performance conditions of a PV module given by a manufacturer. In practice, the solar irradiance is specified as 1000 w/m^2 and a temperature value of $25 \text{ }^\circ\text{C}$. The other specifications, such as maximum power, short circuit current, and open circuit voltage are also calculated and specified at the above mentioned values of solar irradiance and temperature. The amount of solar irradiance incident on the effective PV module area is used to determine the current output efficiency of a particular PV module. As shown in Figure 2.11b, with decreasing irradiance, the short circuit current decreases with slight variation in the open circuit voltage.

Due to varying irradiance and temperature, the specified output power by the manufacturer is always different than the obtained maximum output power. It has been found through experiment (Appendix D) that even the averaged values of irradiance and temperature over a 12 hour duration

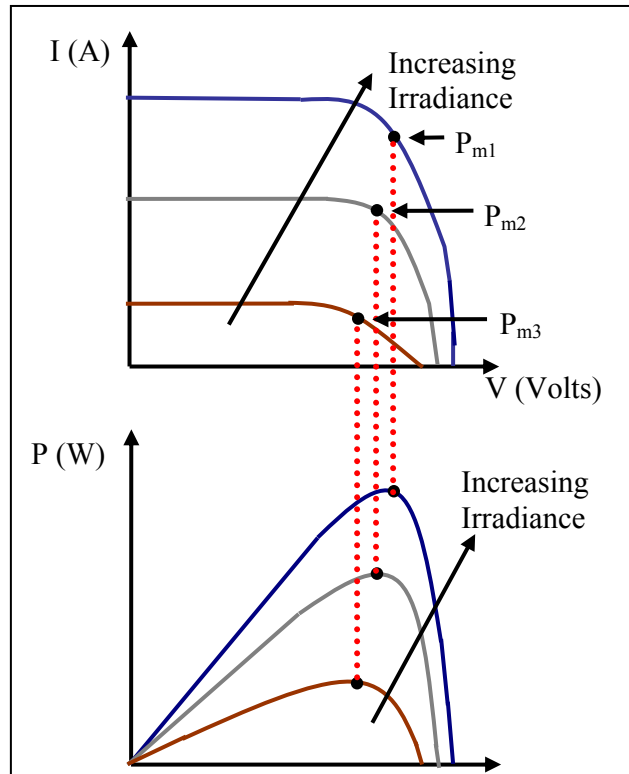


Figure 2.11.b Effect of Variation of Irradiance on the PV Characteristic [2.5]

will result in different values of maximum output power than the aggregate of hourly obtained maximum output power values.

2.4.4.3 Sun angle and sun tracking. Ideally, the sunrays should be normal to the PV panel. Practically, it is achievable through sun tracking devices, though some error does occur due to mechanical limitations of tracking motors. Considering the PV output current as I_n at the ideal conditions, then the practically achievable PV output current I is calculated as [2.6], where θ is the angle between the normal and the sun line.

$$I = I_n \cos \theta \quad (2.9)$$

This cosine law is valid from $\theta = 0^\circ$ to $\theta \sim 50^\circ$. Above approximately 50° , the electrical output does not obey this cosine function and practically there is no generation of power above

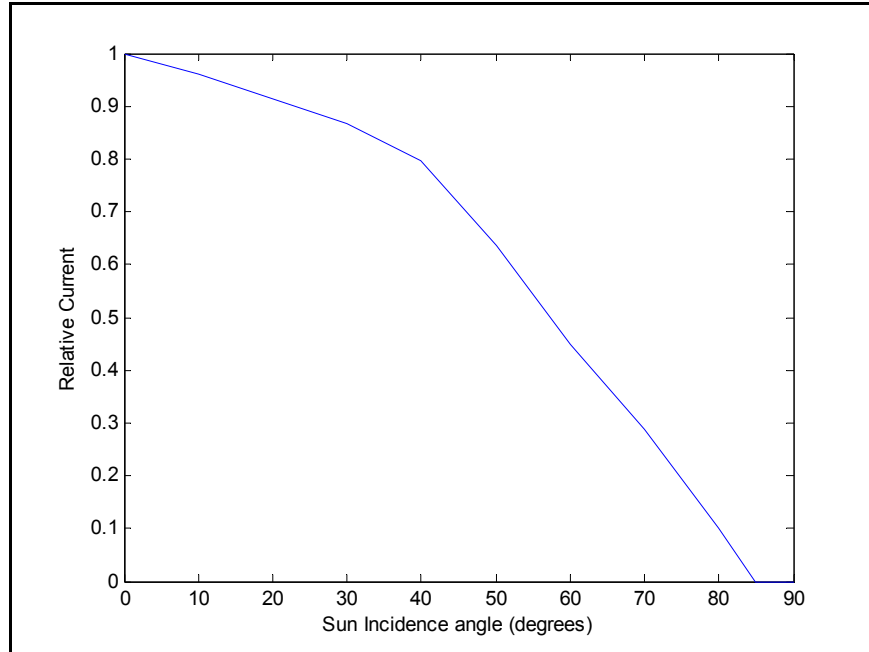


Figure 2.12 Kelly Cosine Curve for a PV Cell from $\theta = 0^\circ$ to $\theta = 90^\circ$ [2.6]

$\theta \sim 85^\circ$. The actual power- angle curve for a PV cell is known as Kelly Cosine [2.6] as drawn in Figure 2.12.

Table 2.1 shows the difference in the Mathematical and cosine values of the output current of a silicon cell.

The output power of the PV module can be enhanced by implementing the sun tracking system [2.11]. This tracking increases the amount of incident energy on the effective area of the PV

Table 2.1 Mathematical and Kelly Cosine Curve of a PV Cell Output Current [2.6]

Sun Angle (degrees)	Mathematical Cosine Value	Kelly Cosine Value
30	0.866	0.866
50	0.643	0.635
60	0.5	0.45
80	0.174	0.1
85	0.087	0

module. The path of the sunflower movement from sunrise to sunset is the basis in designing the tracking path of these devices. There are two types of sun tracking devices available in the market:

- i. One-axis tracker [2.11]. This type of tracker tracks the sun from east to west, from sunrise to sunset.
- ii. Two-axis tracker [2.11]. This type of tracker not only tracks the sun from east to west, from sunrise to sunset, but also follows the position of season from north to south to correspond to the season of the year. Therefore, the efficiency of the two-axis tracker is more than the one-axis tracking system.

An approximate 40% increase in energy yield has been observed through the tracking systems-based PV modules when compared to fixed PV modules. Contrary to this the tracking systems results in the increased installation, operation, and maintenance costs. An economic analysis is required to decide the tracking implementation based on the overall gain.

The PV module is designed for rough weather conditions and is quite rugged. The sun trackers use a DC motor for the movement process. These DC motors and the whole tracking system are not prone to drastic changes in weather condition and could result in frequent maintenance expenses.

2.4.4.4 Other factors. Shading or partial shading of a PV module could happen through clouds, a building, a tree, etc. Shadowing of a cell results in losing the photo voltage and this cell in a module will increase local resistive losses, thus, hindering the performance of the whole PV module. The current losses are not in proportion to the effected shadowed area; however, shadowing on a larger area could result in the abruption of the operation.

As the effects of solar irradiance and ambient temperature were discussed earlier, ideally a PV module should give maximum efficiency on a bright cool day. From design of experiment (Appendix D) it has been observed on a statistical basis that the increment in irradiance comes with

an increment in temperature too. The other climatic factors that have to be taken into account in the electrical design of a PV module are clouds, rain, wind, and snow. PV module does generate power on a cloudy day but its performance is reduced because of the lack of irradiance. Rain does not directly affect the performance, but the clouds before the rain create hindrance in the operation of a PV module. A positive effect of the rain is that it wipes off the dust from the front of the panel which later improves the photoconduction process.

Wind provides a natural cooling to the PV module. In practice 1m/s value of wind is assumed in the calculation. As far as snow is concerned, because of the angular placement of the PV modules, snow usually does not collect on the module surface. The snow also does not affect the PV module mechanically, as its robust design is able to withstand impact from objects as big as a golf ball [2.6].

2.4.5 Maximizing the Performance

To maximize the performance of any device, it is obvious that the losses must be limited. In the case of a PV module, besides limiting the losses, maximum power point is also tracked by proper electrical load matching. This is achieved by different maximum power point tracking (MPPT) methodologies (explained in detail in Chapter 4), but as mentioned earlier, the installation, operation and maintenance of these devices are expensive.

2.4.5.1 Efficiency and energy losses. The conversion efficiency η of a solar cell is the ratio of electrical power output to incident solar power.

$$\eta = \frac{\text{Solar output power}}{\text{Incident solar power}} \quad (2.9)$$

There are various loss mechanisms in a PV module. Commercially available PV modules have an average efficiency of 10%-15% [2.19-2.22]. Some losses are due to inherent physical

properties of the materials such as the flow of electron is obstructed by grain boundaries in polycrystalline silicon which reduce the power output [2.19-2.22]. It is nearly impossible to rectify them by external means. Also, the entire spectrum of photons in the solar radiation is usually not utilized to the maximum. Those photons whose energy band gap is lower than the energy band gap of silicon (1.1 eV) do not contribute in the generation of photo current. In addition, the photons with a higher energy band gap lose their energy as heat which results in thermal losses. There are also thermal losses due to the physical nature of silicon material. These thermal losses result into parametric variation which should be taken into consideration when assessing the realistic performance of the PV module [2.16, 2.22- 2.23].

2.4.5.2 Operation at peak power. The PV modules have a unique characteristic of operating at the maximum power point, subject to proper load matching. This maximum power point is unique for a particular ambient temperature and solar irradiance as shown in Figure 2.11.

2.4.5.2.1 Maximum power point tracking. The maximum power point varies over the whole day with the variation of the sun irradiance and weather conditions. In order to track it exactly, an appropriate value of load has to be matched. A literature survey of the existing MPPT techniques is provided in Chapter 4.

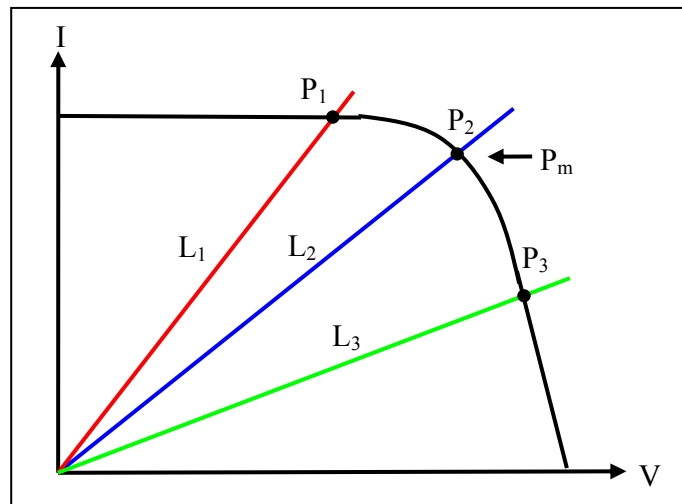


Figure 2.13 Load Matching with Resistive Load [2.5]

2.4.5.2.2 Electrical load matching. The operating point for a PV module is the intersection of the source and the load line in the I-V curve. Recalling Figure 2.11 and drawing the operating point for different resistive loads on the I-V curve as shown in Figure 2.13. The maximum power point is P_2 for the middle value of resistance.

So, a proper load matching is necessary for operating the PV module at its maximum power point in order to achieve its maximum possible efficiency.

REFERENCES

- [2.1] A. Smee, "Elements of Electro-Biology, or The Voltaic Mechanism of Man; of Electro-Pathology, Especially of the Nervous System," Longman, Brown, Green, and Longmans. London:1849.
- [2.2] G. J. Shushnar et al., "Balance of System costs for a 5 MW photovoltaic generating station," IEEE Trans. Power Apparatus System, vol. PAS-104, no.8, pp:2006-2011, 1985.
- [2.3] J.G.Vera, "Operations for rural electrifications in Mexico," IEEE Trans. On Energy Conversion, vol.7, no.3, pp :426-433, 1992.
- [2.4] R.Kumar, J.E.Bigger, "Photovoltaic Systems," proceedings of the IEEE, vol. 81, np.3, pp: 365-377, 1993.
- [2.5] B.H. Khan, Non- conventional energy technologies, McGrawHill Publications, 2005.
- [2.6] M. R. Patel, Wind and Solar Power Systems, CRC Press LLC, 1999.
- [2.7] J.A. Duffie, W.A. Beckman , Solar Engineering of Thermal Processes; John Wiley & Sons Inc. 1991.
- [2.8] C. Palaniappan et al., Renewable Energy Technologies, Narosa Publishing House.
- [2.9] G. N. Tiwari, Solar energy, Narosa Publishing House, 2002.
- [2.10] T. Bhattacharya, Terrestrial solar photovoltaics, Narosa Publishing House, 1998.
- [2.11] R. A. Messenger and J. Ventre, Photovoltaic systems engineering, CRC Press 2000.
- [2.12] T. Markvart, Ed., Solar Electricity, John Wiley & Sons, U.K. 1994.
- [2.13] "Stand-alone Photovoltaic Systems: A Handbook of Recommended Design Practices," Sandia National Laboratories, NM, 1995.
- [2.14] V. Paatero, P. D. Lund, "Effects of large-scale photovoltaic power integration on electricity distribution networks," J. of Renewable Energy, Vol. 32, 2007, pp: 216–234.
- [2.15] M. Bosanac, B. Sørensen, I. Katic, H. Sørensen, B. Nielsen, J. Badran, "Photovoltaic/Thermal Solar Collectors and Their Potential in Denmark," EFP Report, May 2003.
- [2.16] J. S. Coventry, "A solar concentrating photovoltaic / thermal collector," Australian National University, June 2004.
- [2.17] Alberto Fernandez-Infantes, Javier Contreras, Jose L. Bernal-Agustin, "Design of grid connected PV systems considering electrical, economical and environmental aspects: A practical case," J. of Renewable Energy Vol. 31 , pp:2042–2062, 2006.
- [2.18] M.A. Green, "Prospects for photovoltaic efficiency enhancement using low-dimensional structures," proceedings of Nanotechnology, Vol 11, Issue 4 pp: 401-405 ,2000.
- [2.19] T.U. Townsend, A Method for Estimating the Long-Term Performance of Direct-Coupled Photovoltaic Systems, MS thesis, University Of Wisconsin – Madison, 1989.
- [2.20] T. Townsend, et al., "A New Performance Index for PV System Analysis," 24th IEEE PVSC, Dec. 1994.
- [2.21] Ø. Ulleberg ,S. O. MØRNER, "TRNSYS simulation models for solar-hydrogen systems, " Solar Energy, Vol. 59, No. 4-6, pp. 271-279, 1997.
- [2.22] F.A. Farret , M.G. Simões, Integration of Alternative Sources of Energy, John Wiley & Sons, Inc., 2006.
- [2.23] I. Mahderekal, "Thermal Analysis of a Concentrating Photovoltaic Receiver," Howard R. Hughes College of Engineering, May 2004.
- [2.24] Phtotovoltaic Industry Statstics: Cost, "<http://www.solarbuzz.com/StatsCosts.htm>," accessed on 12/31/2008.

CHAPTER 3

PHOTOVOLTAIC MODELING

3.1 Existing PV Models

3.1.1. Literature Survey

The literature in the field of photovoltaic in general, and in particular, the modeling aspects, is very rich [3.1- 3.45]. During the last few decades, numerous researchers have addressed the issues of design and modeling of PV systems from different angles which have led the PV research and development to a feasible power generation technology. On the commercial basis, however, PV technology is still in progressive stage as compared to the conventional power-generating technologies in terms of cost and efficiency. To facilitate the commercialization of PV systems as a competitive power-generating technology, focused and specialized research is still required on both the aspects of modeling and design. In this chapter various researches on the modeling of PV systems and associated applications are reported in brief followed by a detailed review of the modeling aspects of a typical PV module. The detailed literature surveys on modeling aspects, from as early as the 1950's to as recent as 2008, can be viewed in [3.1, 3.2, 3.16, 3.23, 3.41].

The literature on modeling of photovoltaic module is very rich and is still in progress [3.1- 3.5, 3.7, 3.8, 3.13, 3.16, 3.22, 3.23, 3.28, 3.31, 3.41, 3.33, 3.37, 3.38, etc.] In [3.16], over 180 predictive modeling approaches of metrological data are reviewed and the performances of conventional and Artificial Intelligence techniques are compared. The development in research in this direction is definitely leading towards the overall improvement of the PV system, but there always exists a certain amount of error when the natural phenomena are being modeled or predicted. For the most part, modeling and prediction techniques [3.2, 3.5, 3.8, 3.16, 3.22, 3.33, 3.37, and 3.38]

consider the metrological data of the past to model and predict the performance in the future. However, on experimental basis it has been proven that there exists a significant amount of error between the predicted and the real-time data [Section 3.3 and 3.4].

PV system is a highly nonlinear system as the system of equations of the equivalent circuits is represented by transcendental equations (Equations 3.1- 3.12). A detailed explanation is given below in section 3.1.1.1. Various researchers have incorporated these nonlinearities in their models through conventional as well as artificial intelligence modeling techniques to enhance the performance of the PV system. A detail of these modeling methodologies is available in literatures [3.1, 3.2, 3.16, 3.23, 3.41]. These researches set forth a progressive approach towards the modeling aspects of PV systems but are limited to assumed standard climatic and weather conditions. For practical purposes, it is required not only to consider the real-time variation of the weather conditions but also to take into account the parametric variation in the PV system due to the changing weather condition for obtaining the best possible efficient performance [section 3.2.4].

3.1.1.1 Static model of PV. The basic criteria for modeling a photovoltaic device are its electrical characteristics, i.e. the current and voltage-current relationship of a PV cell for varying weather conditions [3.1]. The basic model available in literature is one diode model which is based on the finding of various researchers [1-10]. The equivalent circuit of one diode model is shown in Figure 3.1 from which Equations 3.1-3.4 can be developed. The details of the applicability and methodology of this model are explained in [3.3, 3.8].

The output load current will be

$$I_0 = I_\lambda - I_d - I_P \quad (3.1)$$

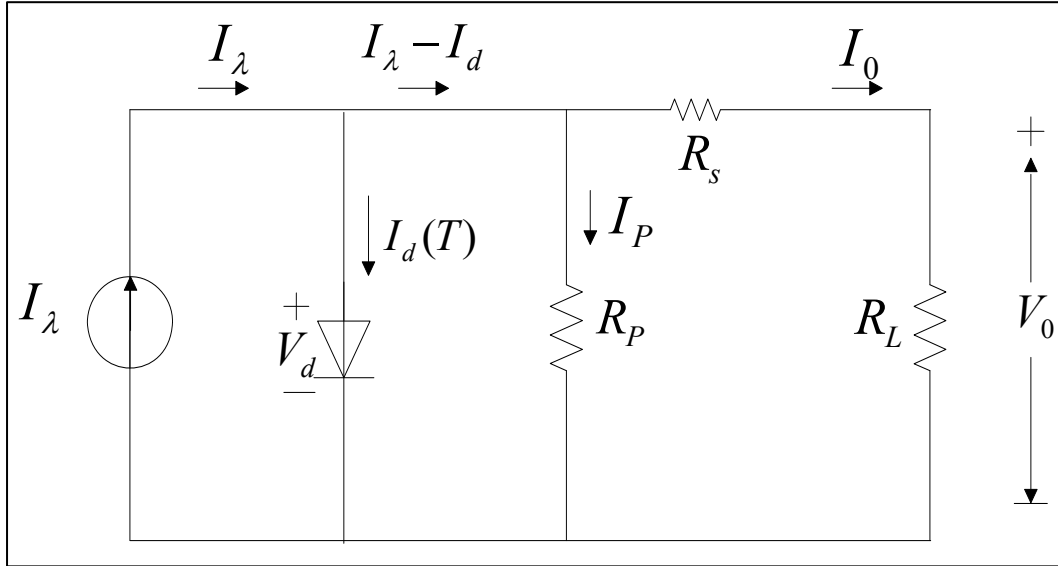


Figure 3.1 Equivalent Circuit of PV Cell [3.1]

The Shockley diode current is given by the classical expression as given in Equation 2.2 [3.3]

$$I_d = I_s [e^{qV_d/\eta kT} - 1] \quad (3.2)$$

So, for obtaining output current Equation 3.1 can be rewritten as [3.3]:

$$I_0 = I_\lambda - I_s [e^{qV_d/\eta kT} - 1] - \frac{V_d}{R_p} \quad (3.3)$$

where

V_d : Diode voltage and can be expressed as [3.3]

$$V_d = I_0(R_s + R_L) = V_0 \left(1 + \frac{R_s}{R_L} \right) \quad (3.4)$$

The equivalent electrical circuit drawn in Figure 3.1 is widely used in the literature for the modeling of photovoltaic cells. This model can be used for the modeling of a PV module and an array, depending on the number of cells connected in series in a module and the number of modules connected in series or parallel in an array.

The output power of the PV device will be the product of the output current and the output voltage which are dependent on the series, parallel and load resistances, and the currents and voltages across them. The values of these currents and voltages are dependent on the solar irradiance and the ambient temperature [3.1- 3.10].

$$P = V_o * I_o \quad (3.5)$$

Examining and recombining Equations 3.1 – 3.5, the relationship between the output voltage V_o and the load current I_o can be expressed as

$$I_o = I_\lambda - I_s \left[e^{\frac{V_o + I_o R_s}{\alpha}} - 1 \right] \quad (3.6)$$

where

I_λ : Photon current; depends on insulation and wavelength of photons;

I_s : Reverse saturated current of the diode;

I_d : Temperature-dependent diode current;

I_p : PV cell leakage current;

I_o : PV cell output current;

V_o : Output Voltage;

V_T : Equivalent voltage to the Junction temperature; $V_T = kT / q = T / 11$;

V_d : Voltage across the diode (V_d);

k : Boltzman constant: $k = 1.38047 \times 10^{-23}$;

q : Electron charge; $q = 1.60210 \times 10^{-19}$;

α : curve fitting parameter;

R_s : Series resistance;

R_p : Shunt resistance;

R_L : Load resistance.

This model is referred as a four parameter model in the literature [3.1, 3.3, 3.7, 3.8, 3.10].

The four parameters are

- i α : curve fitting parameter;
- ii I_λ : Photon current; depends on insulation and wavelength of photons;
- iii I_o : PV cell output current;
- iv R_s : Series resistance.

These parameters are needed for establishing the Voltage- Current relationship of the PV model. In [3.8] a detailed method for the calculation of these four parameters is described. Three of the four possible scenarios can be calculated from the data provided by the manufacturer. The manufacturer usually provides the value of V and I_o at open circuit, short circuit, and maximum power point at reference conditions [3.1]. The reference conditions consider in this thesis are $T_a=25$ °C and $G_T= 1000$ watts/m². The fourth scenario can be analyzed from the calculation of temperature coefficients at open circuit voltage $\mu_{V,oc}$ and at short circuit current $\mu_{I,sc}$ [3.2]. The value of

temperature coefficients at open circuit voltage and short circuit current can be achieved by measurement at reference solar irradiance through Equations 3.7 and 3.8, respectively.

$$\mu_{V,oc} = \frac{\Delta V_{oc}}{\Delta T} = \frac{V_{oc,T_2} - V_{oc,T_1}}{T_2 - T_1} \quad (3.7)$$

$$\mu_{I,sc} = \frac{\Delta I_{sc}}{\Delta T} = \frac{I_{sc,T_2} - I_{sc,T_1}}{T_2 - T_1} \quad (3.8)$$

where

V_{oc} : open circuit voltage (V);

$\mu_{V,oc}$: Temperature coefficients at open circuit voltage (V/°C);

I_{sc} : Short circuit current (Amp);

$\mu_{I,sc}$: Temperature coefficient of the short-circuit current (Amp/°C);

T_1, T_2 : Two temperatures centered around the reference temperature.

I_{λ} , I_s , and α will be function of temperature if series resistance R_s in the circuitry of Figure 3.1 is assumed as independent of temperature [3.1-3.2]. In [3.2] is proved mathematically as well as experimentally that Equations 3.9, 3.11-3.12 are valid estimations for most of the PV modules.

i. α : *curve fitting parameter*:

The curve fitting parameter, light current and saturation current expressed in [3.1] as

$$\alpha = \frac{T_{cref} + 273}{T_c + 273} \alpha_{ref} \quad (3.9)$$

$$\alpha_{ref} = \frac{2V_{mp,ref} - V_{oc,ref}}{\frac{I_{sc,ref}}{I_{sc,ref} - I_{mp,ref}} + \ln\left(1 - \frac{I_{mp,ref}}{I_{sc,ref}}\right)} \quad (3.10)$$

where

α_{ref} : The value of α at the reference condition; (1000W/m² and 25 °C);

$V_{mp,ref}$: maximum power point voltage at the reference condition (V);

$I_{mp,ref}$: maximum power point current at the reference condition (A);

$I_{sc,ref}$: short circuit current at the reference condition (A).

ii. Light Current I_{λ} [3.1]

$$I_{\lambda} = \frac{G_T}{G_{T,ref}} \left[I_{\lambda,ref} + \mu_{I,sc} (T_c - T_{c,ref}) \right] \quad (3.11)$$

where

G_T : irradiance (W/m²);

$G_{T,ref}$: reference irradiance (1000 W/m²);

$I_{\lambda,ref}$: Light current at the reference condition (1000W/m² and 25 °C);

T_c : PV cell temperature (°C);

$T_{c,ref}$: reference temperature (25 °C);

$\mu_{I,sc}$: Temperature coefficient of the short-circuit current (A/°C);

Both $I_{\lambda,ref}$ and $\mu_{I,sc}$ can be obtained from manufacturer data sheet [3.2].

iii. *Saturation Current* I_s is calculated at the reference condition as [3.1- 3.3]:

$$I_s = I_{s,ref} \left(\frac{T_{cref} + 273}{T_c + 273} \right)^3 * e^{\left[\frac{E_g N_s}{q \alpha_{ref}} \left(1 - \frac{T_{cref} + 273}{T_c + 273} \right) \right]} \quad (3.12)$$

where

E_g : Band gap of the material (1.17 eV for Si materials);

N_s : number of cells in series of a PV module;

q : charge of an electron ($1.60217733 \times 10^{-19}$ C);

$I_{s,ref}$: Saturation current at the reference condition (A); (1000W/m^2 and 25°C).

$I_{s,ref}$: Can be calculated as [3.1-3.2]

$$I_{s,ref} = I_{\lambda,ref} * e^{\left[\frac{V_{oc,ref}}{\alpha_{ref}} \right]} \quad (3.13)$$

where

$V_{oc,ref}$: The open circuit voltage of the PV module at reference condition. The value of $V_{oc,ref}$ is provided by manufacturers.

iv. The value of *Series Resistance* is usually provided by the manufacturer. It has also been estimated as [3.2]:

$$R_s = \frac{\alpha_{ref} * \ln \left(1 - \frac{I_{mp,ref}}{I_{sc,ref}} \right) + V_{oc,ref} - V_{mp,ref}}{I_{mp,ref}} \quad (3.14)$$

3.1.2 Development of a Static Model of PV in MATLAB/ Simulink

Note that the above model is a static model derived under the assumptions of constant PV temperature, constant weather condition, and constant solar irradiance. This static model is a tool to obtain the ideal characteristic of a photovoltaic cell under normal operating temperature and weather conditions (NOCT) which is the temperature in a PV module when ambient temperature T_a is 20 °C, solar irradiance G_T 0.8 kW/m², wind speed 1 m/s, and the manufacturer data given in literature [3.1].

In what follows, the static model is summarized briefly with the results obtained through Simulink model based on static conditions. For the verification of the performance of Simulink model, two different solvers, namely ode45 (dormand-price) and ode23 (Bogacki-Shampine), are used. The PV module considered here for the study and analysis consists of 153 cells in series and has the following manufacturer parameters [3.1]. Temperature of the cell is considered as 25 °C for varying irradiance case and irradiance as 1000 w/m² for varying temperature case. The reference temperature and irradiance are taken as 25 °C and 1000 w/m². The manufacturer data for the parametric values are: the open circuit voltage coefficient as -0.3318; reference saturation current as 2.664 A, reference maximum current as 2.448 A, reference maximum voltage as 70.731 V. The results obtained through Simulink model are shown in Figures 3.2- 3.5.

Table 3.1 Values of Parameters in Static Model

Number of PV Cells	153
Temperature of the Cell	25 °C
Solar Irradiance	1000 w/m ²
Open Circuit Voltage Coefficient	-0.3318
Reference Saturation Current	2.664 A
Reference Maximum Current	2.448 A
Reference Maximum Voltage	70.731 V

Figure 3.2 and Figure 3.3 show the output voltage vs. output current (V-I) and output power vs. output voltage (P-V) characteristics, respectively, for fixed cell temperature and varying irradiance.

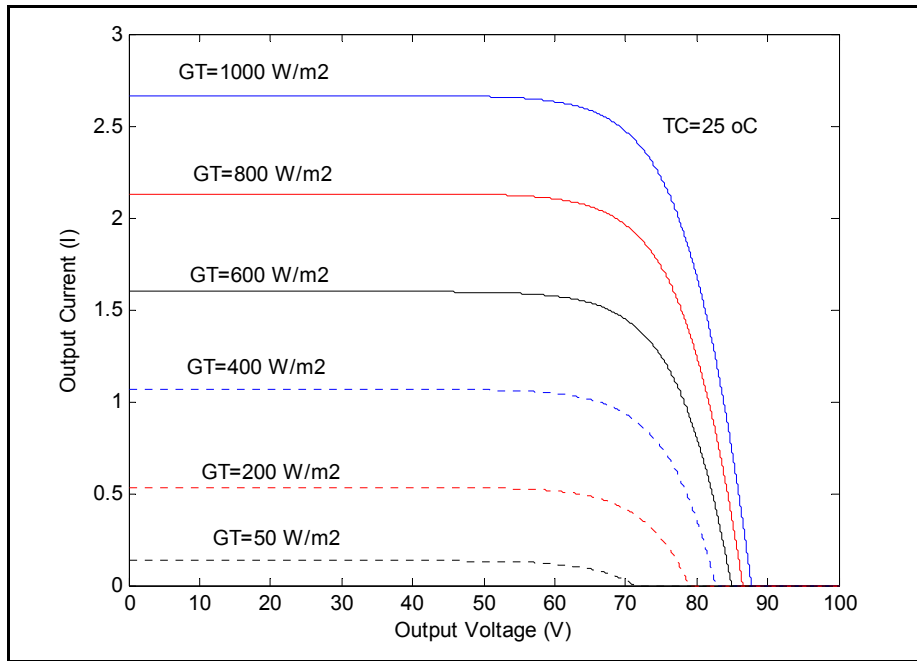


Figure 3.2 V-I Characteristics for Different Values of Irradiance Considering $T_c=25^{\circ}\text{C}$

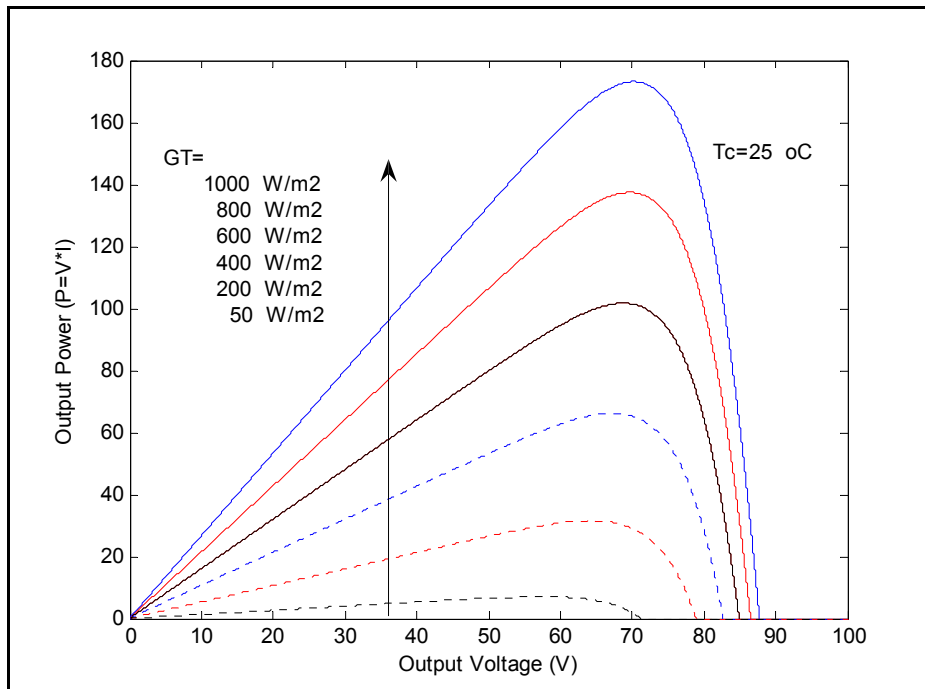


Figure 3.3 Output Power Vs Output Voltage Characteristics for Different Values of Irradiance Considering $T=25^{\circ}\text{C}$

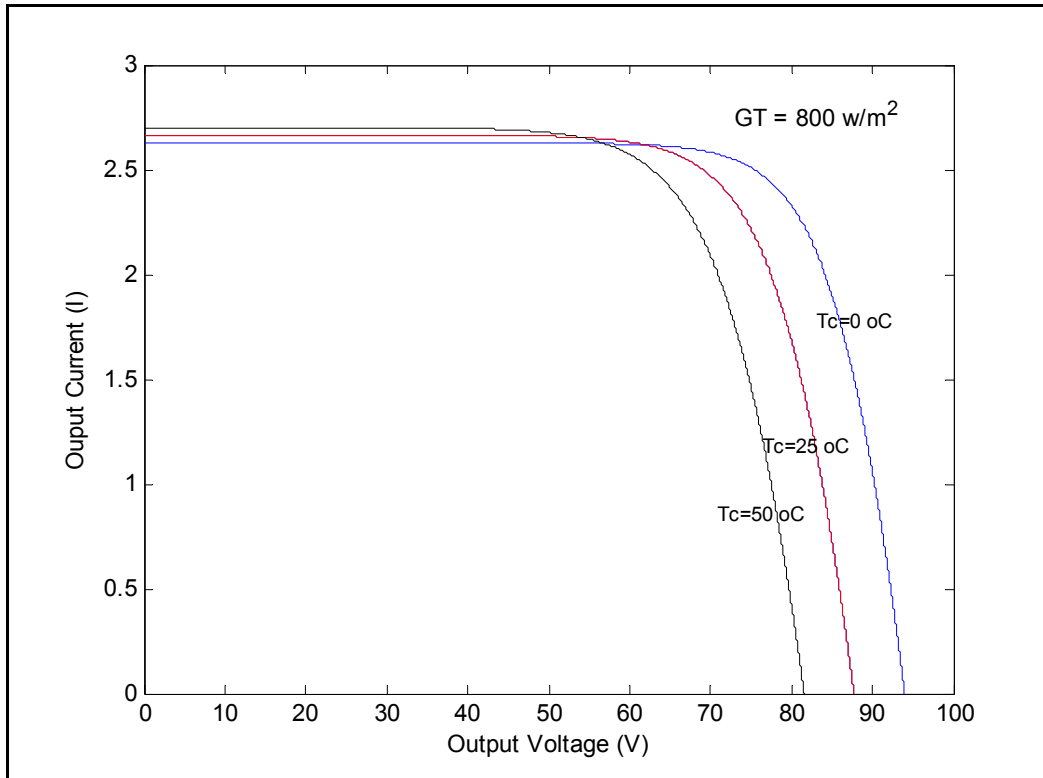


Figure 3.4 V-I Characteristics for Different Values of Temperature with $G_T=800 \text{ w/m}^2$

Figure 3.2 and 3.3 shows that with decreasing irradiance there is a negligible change in maximum output voltage and there is a marginal decrement in the output current and the maximum power point decreases.

Figure 3.4 and Figure 3.5 show the output voltage vs. output current (V-I) and output power vs. output voltage (P-V) characteristics, respectively, for fixed irradiance and varying cell temperature.

These figures show that for a fixed irradiance, as the cell temperature decreases, a small decrement in output current occurs with an increment in output voltage and correspondingly the maximum power point also increases.

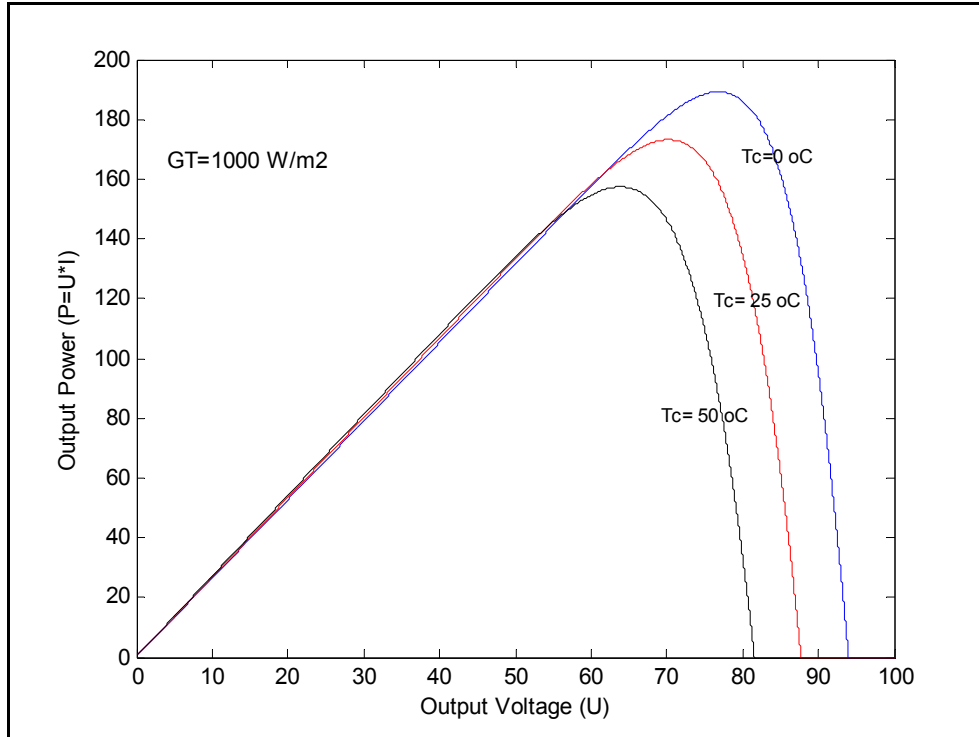


Figure 3.5 Output Power Vs Output Voltage Characteristics for Different Values of Temperature Considering $G_T = 1000 \text{ W/m}^2$

3.1.3 Limitations of Static Model

The dynamic model equation has been mentioned in many researches; however, the researchers [3.1-3.28, 3.30-3.45] and authors [3.3] until recently have considered the static model or the NOCT weather condition as in Equation 3.15 in their models. Due to this assumption, these models are unable to deliver the rated results in changing weather conditions.

In a practical PV system, there are many dynamics involved, such as changing weather conditions results in varying solar irradiance, ambient temperature, wind, shading etc. In just a single day from sunrise to sun et there is a wide variation of solar irradiance and ambient temperature. If these dynamics are taken properly into consideration, efficiency of the system would be increased and will eventually result in more economic power generation. The major driving forces

are the ambient temperature and the solar irradiance G_T which changes with the changing position of the sun, angular placement of the photovoltaic module, and weather conditions.

3.2 Modeling and Simulation

To understand the phenomenon of a Photovoltaic cell, firstly, a static model has been developed through the help of literature, analyzed, and simulated in Simulink. However, this static model has various assumptions and there is a need of analyzing the dynamic aspects of the photovoltaic cell. In a Photovoltaic system, the system behavior changes dynamically with the change in the ambient temperature, solar irradiance, and the weather condition from location to location. It is not possible to predict the system through a static model. A static model provides an idea of the ideal characteristic of a photovoltaic cell under fixed operating temperature and weather conditions. For variation in the weather conditions to be taken into account, it is necessary to develop a dynamic model of the overall system. In the following section, aspects of dynamic modeling are covered, briefly followed by an effort to develop the dynamic model of the photovoltaic cell. The extents to which dynamics that are incorporated in the literature are by averaging the solar irradiance over the daytime with fixed value of temperature [3.8, 3.10].

3.2.1 Development of a Dynamic Model of PV in MATLAB/ Simulink

In real-world scenario, a PV module does not operate under normal operating temperature and weather conditions (NOCT) of fixed temperature and irradiance. This is due to the fact that between sunrise and sunset, the ambient temperature T_a and the solar irradiance G_T varies over a wide range. Also, the intensity of radiations can be different in a region during the same period of time

[3.15]. There could be a variation of 10 to 13 °C in ambient temperature in less than four or five hours on an average day [3.46]. Besides that, cloudy weather also affects the intensity of solar radiations.

Although the PV module or the cell temperature T_c mainly depends on the ambient temperature and irradiance, the operation characteristic of the PV module does affect the cell temperature. In fact, the solar energy is converted into electrical as well as thermal energy from a PV module. The thermal energy is dissolute through convection, conduction, and radiations and this phenomenon varies with the design of the PV module, the angle at which they are installed, speed of the wind, cooling method, etc. Thus, it is obvious that these changes will affect the output voltage and the maximum power supplied by the PVM. One of the objectives of this research is to determine the efficiency of a solar cell when realistic assumptions about ambient temperature and irradiance variations are taken into consideration.

The dynamical behavior of the cell temperature is given by

$$\frac{dT_c}{dt} = \frac{1}{C_t} [\tau\alpha G_T - \eta_c G_T - U_L (T_c - T_a)] \quad (3.16)$$

where

$\tau\alpha$: Transmittance – absorptance product of PV cell;

η_c : Efficiency of the PV cell;

C_t : Overall heat capacity per unit area of the PV cell/ thermal capacitance [J/(°C. m²)];

U_L : Overall heat loss coefficient (W/m²).

The reader is referred to [3.1] about details of the derivation of Equation (3.14). It can be inferred from the above equation that the junction temperature T_c of a photovoltaic module is a function of surrounding temperature T_a , irradiance G_T , transmittance, absorptance of the solar

radiations, design, placement of PV module and convective, conductive and radiative heat losses at the surface of the cell [3.8]. All these variables and parameters have values that vary over a wide range depending upon the atmospheric condition, geographic location, etc. A detailed analysis of the parameters is discussed later in section 3.2.4.

In most of the literature on the modeling of PV cells [3.1, 3.7, 3.13, 3.23, 3.28, 3.31, 3.41, etc.], irradiance has been considered as constant with the variation of temperature. Since the irradiance and ambient temperatures change significantly with changing position of sun and angular placement of the photovoltaic module, it is impractical to consider the irradiance and ambient temperature as constant. To obtain a realistic model of the photovoltaic module and to study its real-time characteristic with the variation of temperature and irradiance, a dynamic model must be developed and analyzed.

A state space model is developed through the dynamic model (Equation 3.16) of the PV cell. Equation 3.16 can be written as

$$\frac{dT_c}{dt} = -b_1 T_c + b_2 T_a + a G_T \quad (3.17)$$

where

$$a = \frac{1}{C_t} [\tau\alpha - \eta_c] \quad (3.18)$$

$$b_2 = -b_1 = \frac{1}{C_t} [U_L] \quad (3.19)$$

Equation (3.17) can be written in state space form as

$$\dot{T}_c = -b_1 * [T_c] + [b_2 \quad a] \begin{bmatrix} T_a \\ G_T \end{bmatrix} \quad (3.18)$$

Comparing with the state space model:

$$\begin{aligned}\dot{X} &= Ax + Bu \\ Y &= Cx + Du\end{aligned}\tag{3.20}$$

where

$$\begin{aligned}A &= -b_1, & B &= [b_2 \quad a_1] \\ C &= 1, & D &= 0\end{aligned}\tag{3.21}$$

Ambient temperature T_a and the Irradiance G_T are the real-time variable inputs to the state space model. The parameters a , b_1 , and b_2 are calculated based on the standard values of the PV cell parameters [3.1, 3.7, 3.8] and the detailed calculation is given in section 3.2.4. The output of the state space model is the dynamic cell temperature which is used to calculate the maximum voltage and maximum current of the PV cell so as to obtain the realistic available maximum power. Solar data have been collected from a weather station [3.46-3.47] and analyzed through a Simulink model in the MATLAB environment on daily and monthly basis. For illustration purpose, data for a typical day of July 2005 [3.46- 3.47] have been considered.

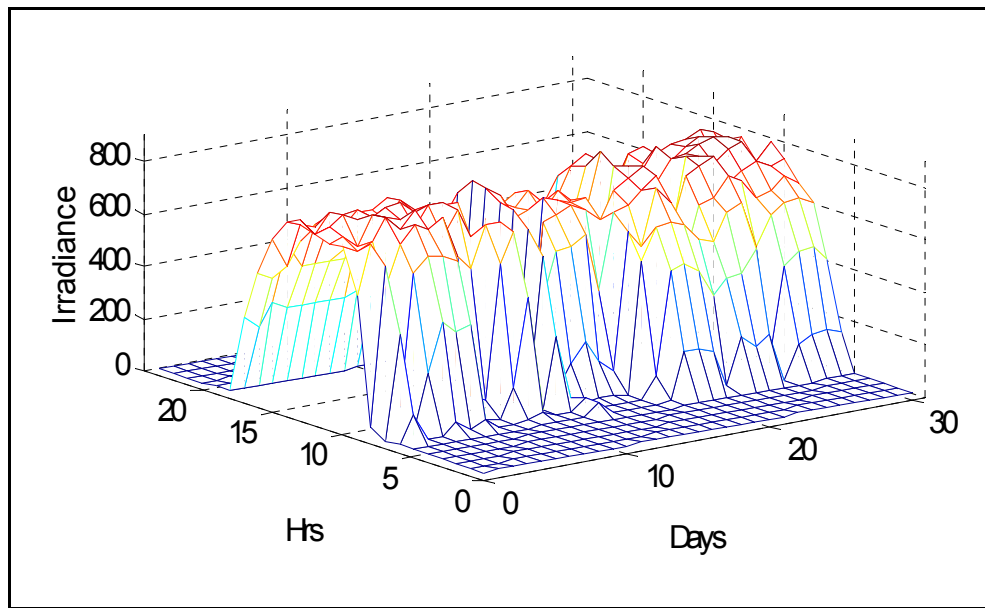


Figure 3.6 Daily Irradiance Over a Period of One Month from the Data

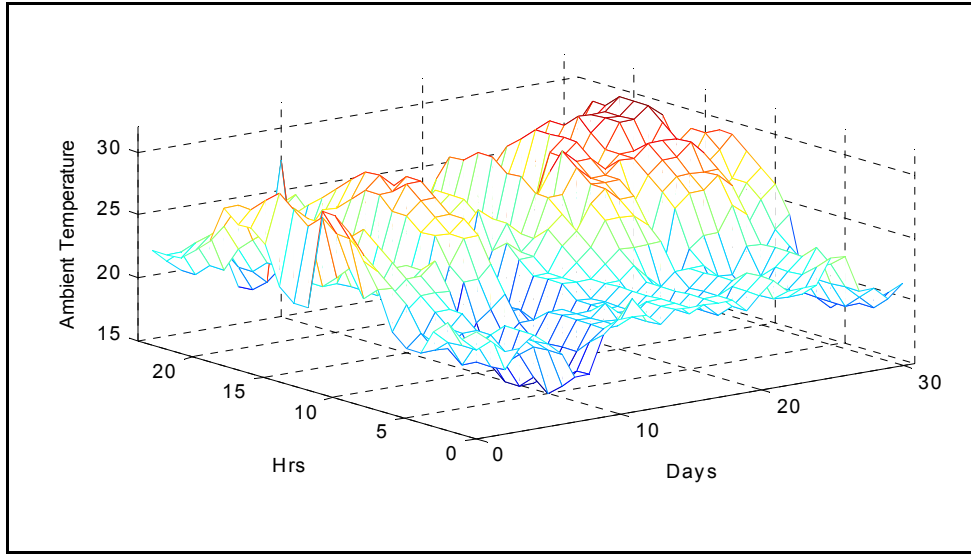


Figure 3.7 Daily Temperature Over a Period of One Month from the Data

The daily variation of solar irradiance and ambient temperature over a period of one month is plotted in Figures 3.6 and 3.7, respectively. The dynamic model developed is applicable to any location on the globe, subject to the availability of the required metrological data.

Figure 3.8 shows the pattern of variation of solar irradiance and Figure 3.9 shows the pattern of cell temperature and ambient temperature for a typical day.

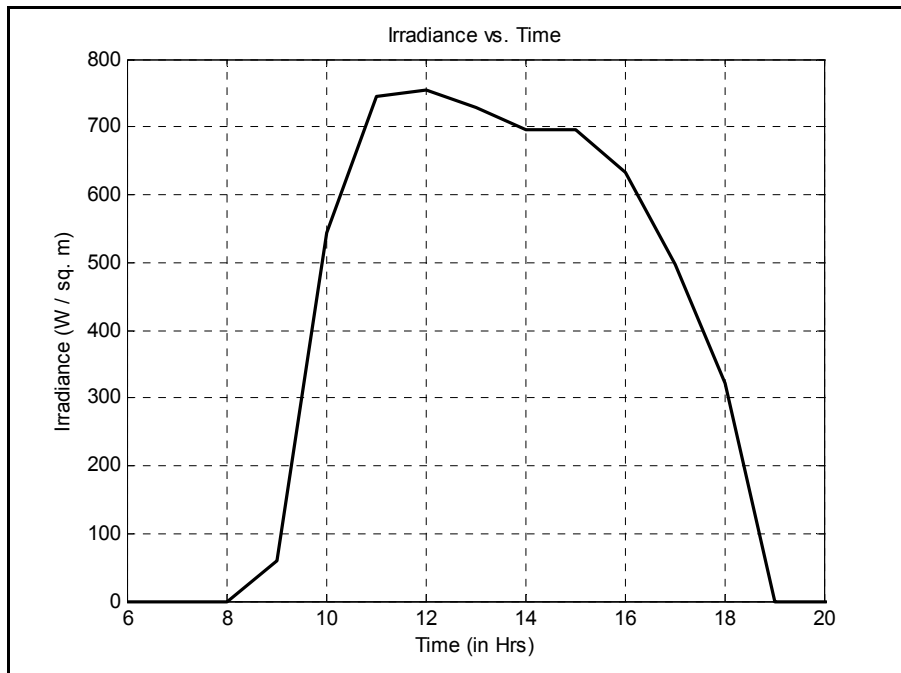


Figure 3.8 Variation of Solar Irradiance Over the Day

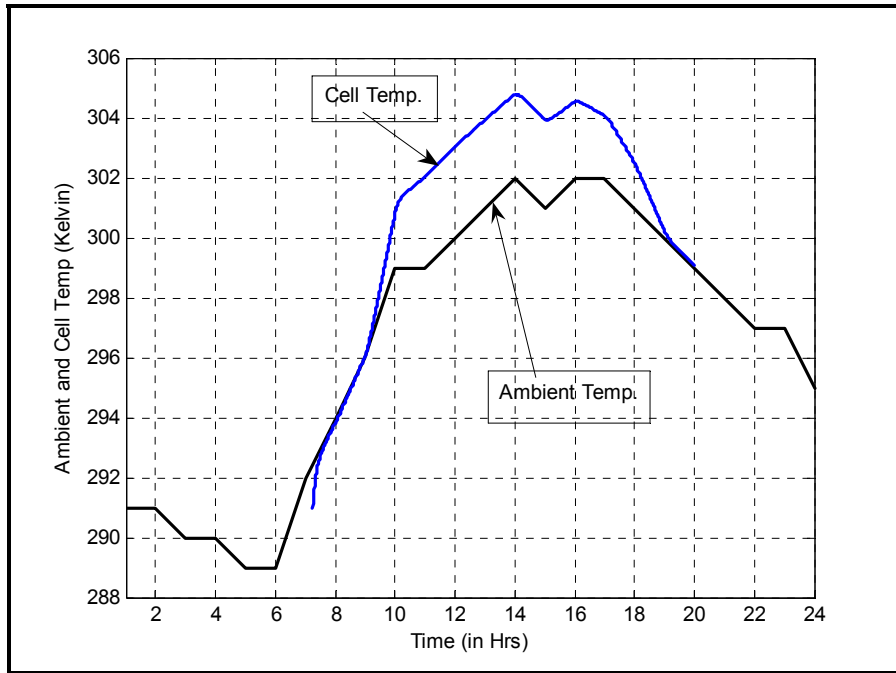


Figure 3.9 Pattern of Cell Temperature and Ambient Temperature in a Day

The pattern of irradiance indicates that sunshine start at 8:00 A.M. and reaches to maximum at 12:00 o'clock noon and sunset took place at 7:00 P.M. Similarly, the pattern of ambient temperature also increases with rise of the sun and reaches to a maximum at 2:00 P.M. and remains there with a little bit variation until 5:00 P.M. and then starts decreasing. The pattern of PV array temperature indicates that the cell temperature remains below the ambient temperature before the sunrise and after sunset irradiance, but as soon as the sunrise starts the PV array the cell temperature starts increasing and remains more than the ambient temperature until sunset. It is because of power harnessing by the PV array, which is due to load current flow through PV array. It can be noticed in Figure 3.8 that as the irradiance increases there is an increase in the difference between cell temperature and ambient temperature. This difference reduces with the decrease in irradiance.

3.2.2 Comparison of Static and Dynamic PV Model

The temperature and Irradiance data obtained from [3.46-3.47] are computed through the dynamic model developed in Simulink and the following results are obtained. Two scenarios are considered, fixed value of irradiance (average of the daily irradiance) with varying ambient temperature and varying solar irradiance and varying ambient temperature. Firstly, the average of the irradiance of the whole day (from sunrise to sunset) has been considered with the varying ambient temperature and later both the variables are considered as per the real-time variation and maximum power obtained has been computed for both the cases on the hourly and daily basis. Figures 3.10 and 3.12 show the profile of the maximum powers obtained on hourly basis for the static and dynamic cases, respectively. The I-V characteristic of the PV module used in this study is shown in Figure 3.2. Figures 3.11 and 3.13 show the maximum power obtained during the period of 10 AM – afternoon when there is abundance of irradiance.

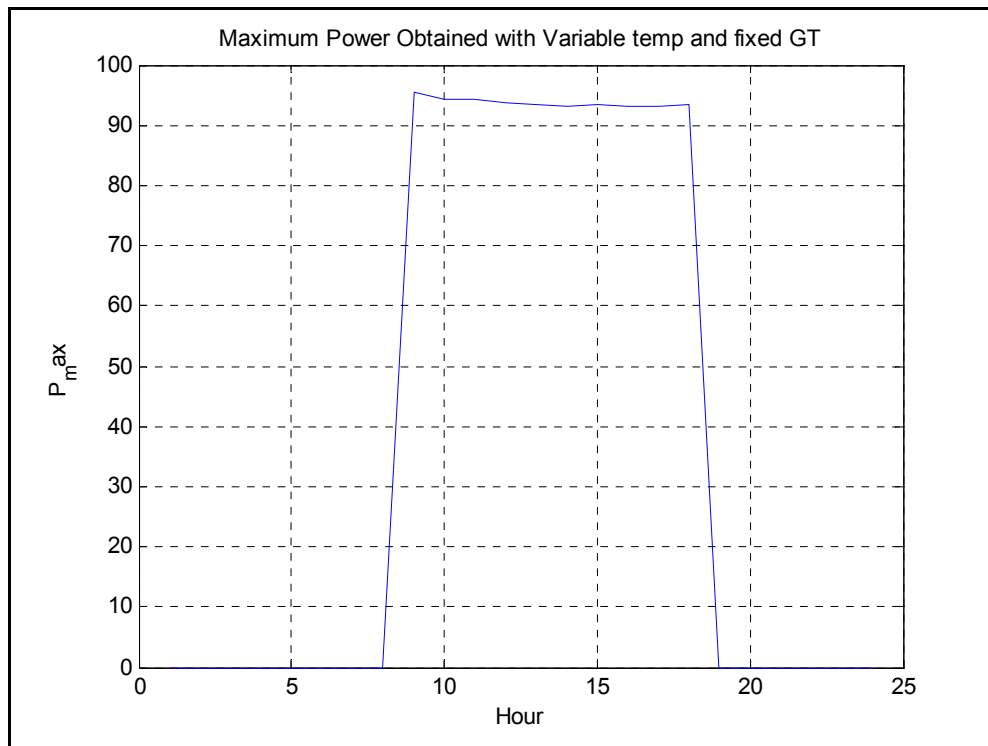


Figure 3.10 Profile of the Maximum Power Obtained Through Static Models

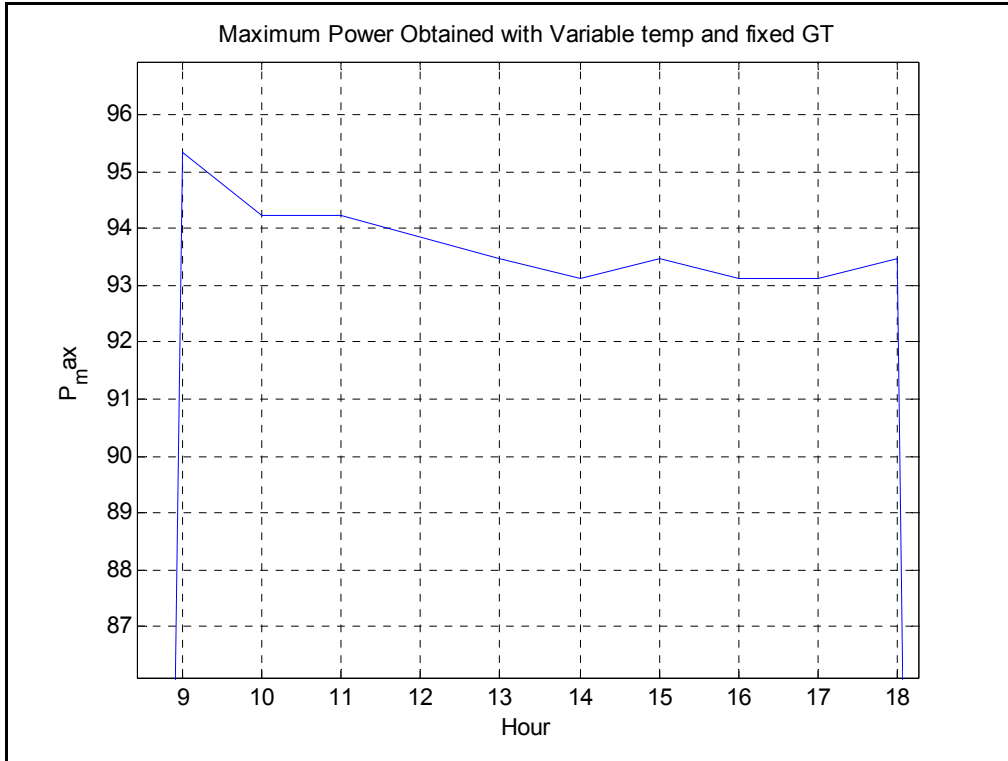


Figure 3.11 Profile of the Maximum Power Obtained Through Static Models During 9 AM- 6 PM

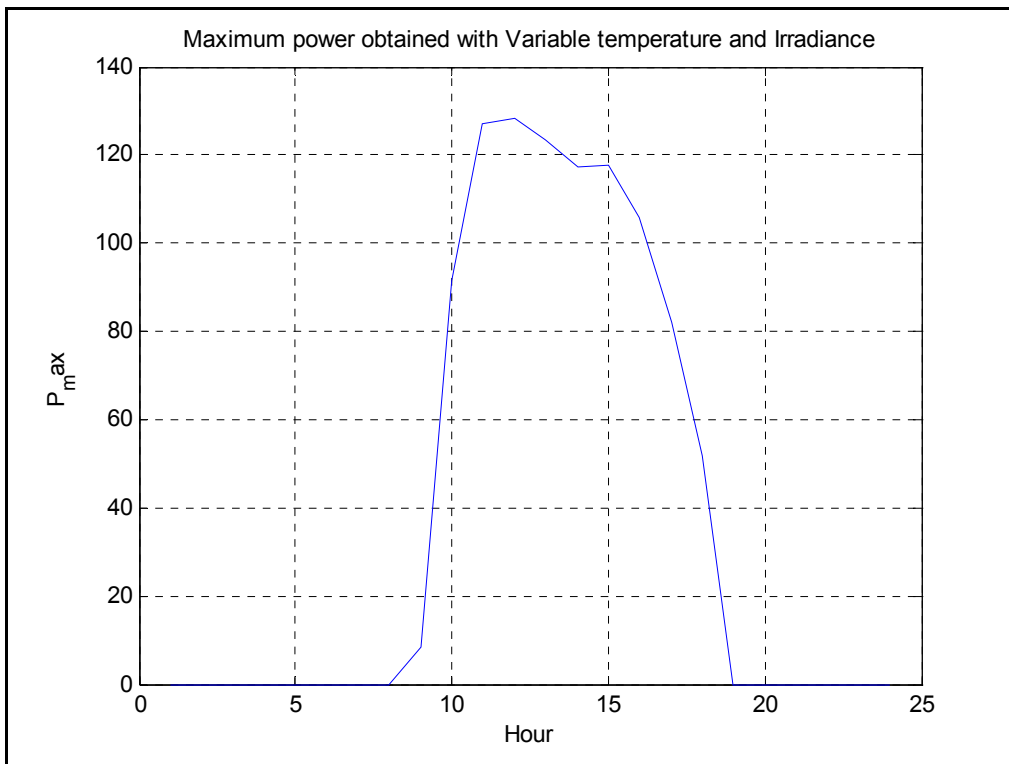


Figure 3.12 Profile of the Maximum Power Obtained Through Dynamic Models

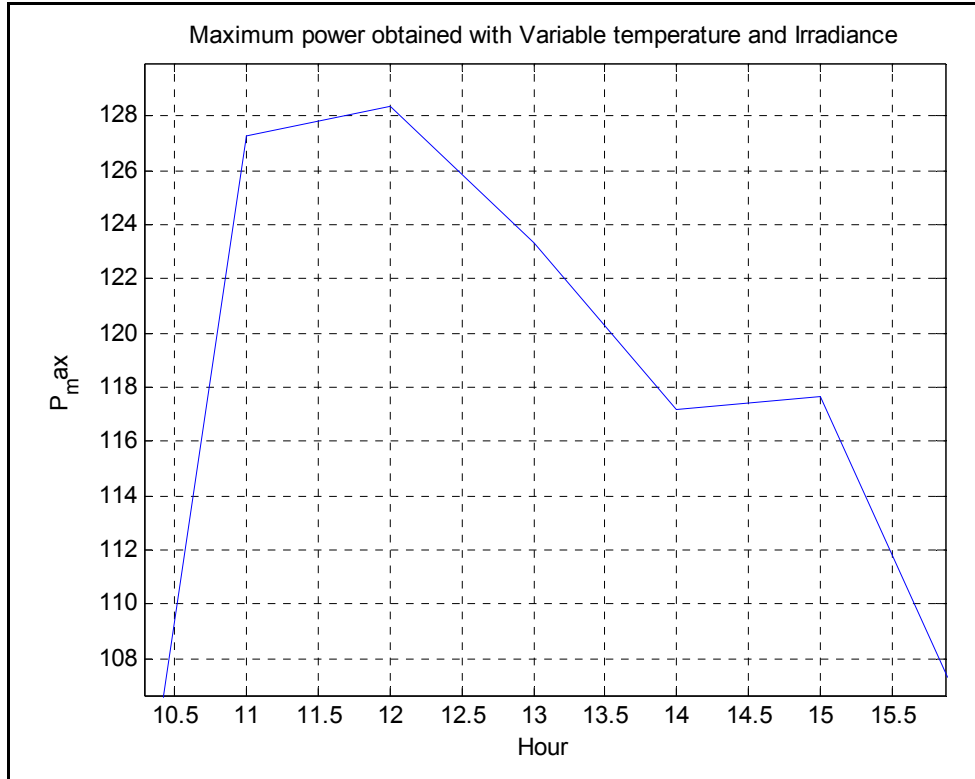


Figure 3.13 Profile of the Maximum Power Obtained Through Dynamic Models during 10 AM- 5 PM

Table 2.1 shows the numerical values of the data and the results obtained. Columns 1 and 2 show the hours of the day and the varying ambient temperature. Columns 3 and 4 show the average value of Irradiance G_T and the maximum power obtained on hourly basis (with fixed G_T), respectively. Columns 5 and 6 comprise of real-time varying irradiance G_T and the maximum power obtained on an hourly basis, respectively. Column 7 shows the difference in the maximum power obtained. Column 8 shows the load mismatch and column 9 shows the wastage of power when the irradiance is more than the assumed average value. It can be further inferred from Table 3.2 that the total daily power obtained through the static case is 937.35 W and through the dynamic model is 953.69 W. Also, the maximum possible bearable load through the static model is 95.33 W while through dynamic model is 128.4 W.

Table 3.2 Variable Data and the Maximum Power Obtained

Hour	Temp.	Fixed GT	P_max	VariableGT	P_max	P_max Difference	Load Mismatch	Wastage
1	18	0	0.00	0	0.00	0.00		
2	18	0	0.00	0	0.00	0.00		
3	17	0	0.00	0	0.00	0.00		
4	17	0	0.00	0	0.00	0.00		
5	16	0	0.00	0	0.00	0.00		
6	16	0	0.00	0	0.00	0.00		
7	18.999	0	0.00	0	0.00	0.00		
8	21	0	0.00	0	0.00	0.00		
9	23	560	95.33	59	8.5108	-86.82	86.82	
10	26.007	560	94.216	545	91.558	-3.77	3.77	
11	26.011	560	94.216	746	127.29	31.96		31.96
12	27.011	560	93.845	755	128.4	33.07		33.07
13	28.011	560	93.475	729	123.31	27.98		27.98
14	29.01	560	93.105	697	117.2	21.87		21.87
15	28.011	560	93.475	697	117.65	22.32		22.32
16	29.009	560	93.105	633	105.93	10.60		10.6
17	29.007	560	93.104	496	81.897	-13.43	13.43	
18	28.005	560	93.475	322	51.94	-43.39	43.39	
19	27	0	0.00	0	0.00	0.00		
20	26	0	0.00	0	0.00	0.00		
21	25	0	0.00	0	0.00	0.00		
22	24	0	0.00	0	0.00	0.00		
23	24	0	0.00	0	0.00	0.00		
24	22	0	0.00	0	0.00	0.00		
Total Power		789.94	937.35		953.69		147.41	147.8
Maximum Possible load			95.3300		128.4005			
Difference in power output		953.69		789.94		163.75		
% Efficiency Increase						20.72%		

So, from the above analysis and the numerical data it is clear that the dynamic model has an edge over the conventional static model. Some of the benefits are:

- i. There is a load mismatch through static model. As seen in column 8, there is a total mismatch of 147.4 W during 4 hrs. In the morning and evening hours the estimated power based on

average value of irradiance is not available through the PV module. Such load mismatching will result in malfunctioning of the machinery on the load side.

- ii. Using the static model, there is waste of 147.8 W of power in a single day for a single module and especially at the peak load demand times of 10 AM – 5 PM which can be obtained through dynamic model by proper load matching.
- iii. The static model can only bare a maximum load of 95 W while the dynamic model can handle a load up to 128 W around noon time.

In the current scenario, PV is one of the well established green power technologies and has been implemented worldwide for grid connection as well as stand-alone applications. For instance the use of PV in stand-alone application can be observed here in Table 3.3 from a survey [3.58].

Table 3.3 Uses of PV Systems (Percent of Survey Respondents) [retabulated from 3.58]

PV pumping (irrigation)		30 %
Livestock watering		9 %
PV pumping (potable water)		35 %
PV water purification		12 %
PV electric fences		16 %
Lighting of poultry /livestock		14 %
Office equipment (computers, etc.)		16 %
Radio or cellular phone communication		42 %
Health centres (refrigeration, lighting, etc.)		44 %
Veterinary service (refrigeration, lighting, etc.)		9 %
Refrigeration (household, retail store, agricultural products, meat, dairy, fish, etc.)		16 %
Lighting, TV, radio, small appliances for commercial services		47 %
Lighting, small power tools for micro-enterprises (repair shop, handicraft)		19 %
Lighting, TV, radio, etc. for household use		81 %
Tourist facilities (lighting, TV, refrigeration of lodges, hotels, etc.)		21 %
Lighting and audiovisuals for schools and other community buildings		37 %
Street lighting		28 %
Others, namely:	Telemonitoring (irrigation)	2 %
	advertising kiosks	5 %
	lighting for fishing	5 %
	portable lanterns	1 %

If just the case of solar water pumps is considered, a mismatch in promised output power and the real output power will result in the failure of the operation of machinery and possibly damage to the winding of the motor because of the wrong estimation of power output. Also, this will affect the irrigation process. In case of transferable medical refrigerators, the load mismatch will not only hamper the performance of the refrigerators but will also ruin the medicines.

In conclusion, a dynamic model with a proper load matching controller can not only give a better performance, but will also play a vital role from the safety point of view by avoiding the efficiency load mismatching in the mornings and evenings.

3.2.3 Limitations of Dynamic Model

Although the dynamic model produced better results but the variation of solar cell parameters viz: overall heat capacity per unit area of the PV cell/ thermal capacitance C_t and overall heat loss coefficient U_L , etc., has not been taken into account. These parameters do not remain constant and vary with the change in cell temperature and affects the output power of the solar panels [3.8]. The effect of parameter variation is minute, if there is less variation in the ambient temperature and considering the parameters as constant will have an error of 2-3% [Table 3.4], as in the case of dynamic model. However, on sunny and warm days it is necessary to take this parametric variation into account for obtaining the precise value of the output voltage and current because of the higher values of temperature which will enhance the thermal effects of the PV cell [3.1, 3.8, Appendix E]. This statement has been proved first through the simulation of PV cell model and then later experimentally. Table 3.4 later shows the difference in the output maximum power of the model with and without the consideration of the parametric variation.

3.2.4 Solar Cell Parameter Calculation

To obtain an idea about the variation of the parameters of the cell temperature given in Equations 3.14- 3.17; the solar cell parameters are studied and analyzed in detail.

$\tau\alpha$: Transmittance absorptance product of PV cell is the dimensionless ratio of absorbed to incident energy and varies with the angle of incidence of the radiations.

For smooth surfaces, Fresnel has derived the expressions mentioned in Equation 3.22 for perpendicular rays and for parallel rays in Equation 3.23, respectively, for the reflection of unpolarized radiation from medium 1 with a refractive index n_1 to medium 2 with refractive index n_2 [3.8] as shown in Figure 3.14.

$$r_{\perp} = \frac{\sin^2(\theta_2 - \theta_1)}{\sin^2(\theta_2 + \theta_1)} \quad (3.22)$$

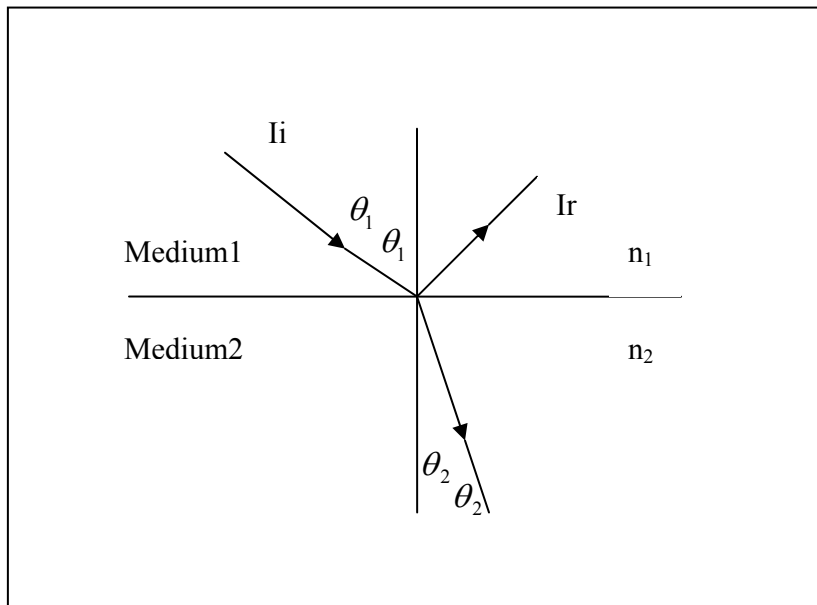


Figure 3.14 Angle of Incidence and Refraction in Media with Refractive Indices n_1 and n_2 [3.8]

$$r_{II} = \frac{\tan^2(\theta_2 - \theta_1)}{\tan^2(\theta_2 + \theta_1)} \quad (3.23)$$

In a PV module, the light rays first hit the glass layer (say medium n_1) and then reflected to the silicon layer of the PV module at angle θ_1 and θ_2 , respectively. From Snell's law they can be related to indices n_1 and n_2 , respectively, as [3.8]

$$\frac{n_1}{n_2} = \frac{\sin \theta_2}{\sin \theta_1} \quad (3.24)$$

So the absorptance τ_r at normal incidence can be calculated through Equation 3.25.

$$\tau_r = \frac{1}{2} \left(\frac{1 - r_{II}}{1 + r_{II}} + \frac{1 - r_{\perp}}{1 + r_{\perp}} \right) \quad (3.25)$$

For a partially transparent plate, the transmittance τ_a can be calculated through Equation 3.26 which is described through Bouguer's law [3.8].

$$\tau_a = \exp\left(-\frac{KL}{\cos \theta_2}\right) \quad (3.26)$$

The total transmittance is thus given by Equation 3.27 for a solar collector with cover materials [3.8].

$$\tau = \tau_a \tau_r \quad (3.27)$$

where

K: proportionality constant: extinction coefficient which is assumed to be constant in a solar spectrum ($K \sim 32\text{m}^{-1}$);

L: Thickness of the cover ($2 \times 10^{-3}\text{m} - 3 \times 10^{-3}\text{m}$);

n_1 and n_2 : are indices of refraction of glass.

The absorptance α of a solar collector can be approximated by Equation 3.28 [3.8].

$$\alpha = 1 - \tau_a \quad (3.28)$$

This product represents the optical property of a cover –absorber (glass –silicon) combination rather than as a product of two properties. Mostly researchers consider this value as 0.9[3.1, 3.8] which is always not correct as a variation over a particular range is observed in the analysis.

ii. η_c : Efficiency of the PV cell is the dimensionless D.C. electric conversion efficiency. It ranges from zero at the short circuit and open circuit points to a typical maximum of about 10 -14% at the maximum power point [3.1, 3.2, 3.8 3.16, 3.23]. However, the efficiency varies in proportion to the maximum power point voltage and current and area of the cell and the irradiance [3.8].

$$\eta_c = \frac{V_{mpp} \times I_{mpp}}{AG_T} \quad (3.29)$$

This is evaluated real-time in the model.

iii. C_t : Overall heat capacity per unit area of the PV cell/ thermal capacitance [J/(°C. m²)] depends upon type of PV module [3.8]. This can be calculated as

$$C_t = \rho L c_p \quad (3.30)$$

where

ρ : Density of the material (kg/m³) ~ 2220 for Silicon;

L : Thickness of the cell ~ 0.01 m;

A : Area of the PV Module;

c_p : Specific heat of the Silicon (J/kg-°C) ~ 745- 800 for 27- 127 °C.

The specific heat can be calculated from the properties of materials chart as [3.57]

$$c_p = \rho A c \frac{dT_c}{dt} \quad (3.31)$$

So, linearly interpolating the value of specific heat for 0 – 50 °C, we have

$$C_t = 1.6 \times 10^4 \text{ J/°C- m}^2$$

iv. U_L : Overall heat loss coefficient (W/m²): U_L is an overall (convective and radiative) loss coefficient, with units of W/m²•C. For simplicity, the loss coefficient is assumed to be constant, which neglects the effect that factors such as wind speed, humidity, and temperature may have on it [3.8]. Although these factors may substantially affect the loss coefficient, their effect on the resulting absolute cell temperature is small [3.1, 3.8]. The detailed analysis is given below.

Overall heat loss coefficients [3.8]:

$$U_L = U_t + U_b + U_e \quad (3.32)$$

Bottom heat loss coefficient is given by

$$U_b = k \frac{1}{L} \quad (3.33)$$

where k and L are insulation thermal conductivity and thickness (k~ 0.045),

So, ($U_b \sim 0.9 \text{ W/m}^2\text{C}$)

Edge heat loss coefficient is given by

$$U_e = k \frac{A_e}{A} \quad (3.34)$$

where

k and A_e are insulation thermal conductivity area of the edge and

A is the area of the collector (k~ 0.045), So, $U_e \sim 0.12 \text{ w/m}^2\text{.C}$.

Top heat loss coefficient is given by [3.8]

$$U_t = \left[\frac{1}{h_{c,p-c} + h_{r,p-c}} + \frac{1}{h_w + h_{r,c-a}} \right]^{-1} \quad (3.35)$$

Convective heat loss from plate to collector [3.8]

$$h_{c,p-c} = N_u \frac{k_1}{L} \quad (3.36)$$

Radiation coefficient from plate to cover [3.8]

$$h_{r,p-c} = \frac{\sigma(T_p^2 + T_c^2)(T_p + T_c)}{\frac{1}{\varepsilon_p} + \frac{1}{\varepsilon_c} - 1} \quad (3.37)$$

Radiation coefficient from the cover to the air is [3.8]

$$h_{r,c-a} = \varepsilon_c \sigma (T_c^2 + T_a^2)(T_c + T_a) \quad (3.38)$$

Wind heat loss coefficient:

$$h_w = 2.8 + 3.0 * V_{wind} \quad (3.39)$$

From Equation 3.36

$$h_{c,p-c} = N_u \frac{k_1}{L}$$

Nussle number is [3.8]

$$N_u = 1 + 1.44 \left[1 - \frac{1708(\sin 1.8\beta)^{1.6}}{R_a \cos \beta} \right]^+ \left[1 - \frac{1708}{R_a \cos \beta} \right]^+ + \left[\left(\frac{R_a \cos \beta}{5830} \right)^{1/3} - 1 \right]^+ \quad (3.40)$$

Reynold's number is given by [3.8]

$$R_a = \frac{g\beta' \Delta T L^3}{\nu \alpha} \quad (3.41)$$

where

Difference in temperature of the cell/ collector surface and temperature of the plate (bottom):

$$\Delta T = (T_p - T_c) \quad (3.42)$$

Volumetric coefficient of expansion (for an ideal gas)

$$\beta' = \frac{1}{T_a} \quad (3.43)$$

So, Reynold's number will be

$$R_a = \frac{gL^3}{\nu\alpha} \left(\frac{\Delta T}{T_a} \right) \quad (3.44)$$

and, Nussle number will be

$$N_u = f\left(\frac{\Delta T}{T_a}, \beta\right) \quad (3.45)$$

So, Radiation coefficient between the plate and the cover will be

$$h_{c,p-c} = \frac{k_1}{L} * f\left(\frac{\Delta T}{T_a}, \beta\right) \quad (3.46)$$

If collector is installed at an angle of 60° ,

then,

$$h_{c,p-c} = \frac{k_1}{L} * f\left(\frac{\Delta T}{T_a}\right) \quad (3.47)$$

Considering [3.1, 3.8]:

g : gravitational constant = 10 m/sec²;

ν : kinematic viscosity $\sim 10^{-5}$;

α : Thermal diffusivity $\sim 10^{-5}$;

ε_p : Plate effective emittance ~ 0.95 ;

ε_c : Collector surface effective emittance. ~ 0.88 ;

L : Plate to cover spacing ~ 25 mm.

For : $0^\circ \leq \text{Cos}\beta \leq 75^\circ$,

For $T_a = 25^\circ\text{C}$,

$T_c = 25^\circ\text{C}$ and

$G_T = 800 \text{ W/m}^2$

The value of U_L is calculated by writing a small code in MATLAB for an idea of the range of values. The range of heat loss coefficient obtained is

$$7.639 \leq U_L \leq 8.468 \quad (3.48)$$

This is in accordance with the literature [3.1, 3.8]. Considering the layer of glass over the Silicon layer, the heat loss coefficient of glass will be calculated as the two resistances in parallel.

Later this analysis is done for instantaneously varying ambient temperature and solar irradiance to incorporate the variation of these parameters on a real-time basis for obtaining realistic maximum power from the solar panels, as shown in Figure 3.13 and Figure B.3.

3.2.5 Simulation, Results and Analysis

Figure 3.15 shows the implementation strategy of the PV model while taking into account parameter variations as well as temperature and irradiance fluctuations. The parameters, namely wind speed, angle of inclination of the PV module, maximum voltage and maximum current along with the ambient temperature, irradiance, and the cell temperature are analyzed, real-time and parametric values are calculated and obtained. These values will be incorporated in the state space model to calculate the coefficients A, B, C, and D of the state space model. These values will be updated real-time to obtain the accurate cell temperature and hence, the true maximum power.

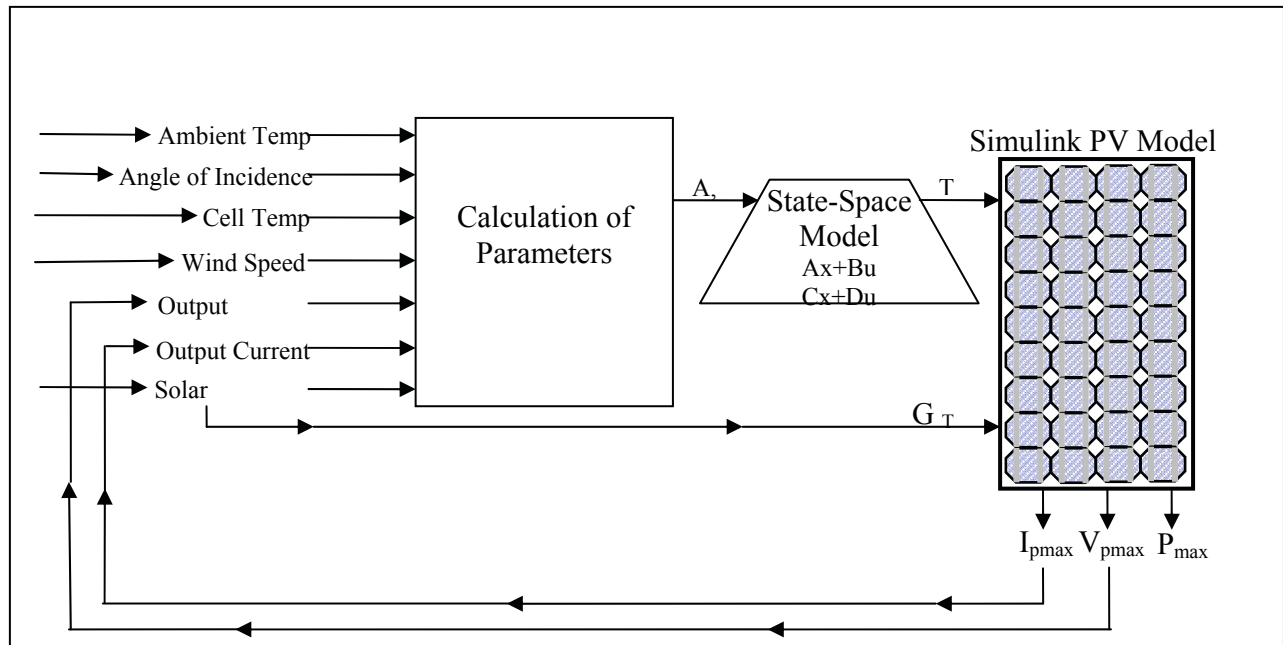


Figure 3.15 Implementation Strategy of the Dynamic PV Model

Table 3.4 Improved PV Dynamic Model After Including Parametric Variation

Hour	Temperature	GT	P_max Dynamic model	P_max parametric estimation	with	P_max Difference
1	18	0	0	0	0	0.00
2	18	0	0	0	0	0.00
3	17	0	0	0	0	0.00
4	17	0	0	0	0	0.00
5	16	0	0	0	0	0.00
6	16	0	0	0	0	0.00
7	18.999	0	0	0	0	0.00
8	21	0	0	0	0	0.00
9	23	59	8.5108	8.52		9.20E-03
10	26.007	545	91.558	93.54		1.98E+00
11	26.011	746	127.29	129.5		2.21E+00
12	27.011	755	128.4	133.76		5.36E+00
13	28.011	729	123.31	125.66		2.35E+00
14	29.01	697	117.2	119.84		2.64E+00
15	28.011	697	117.65	119.96		2.31E+00
16	29.009	633	105.93	108.54		2.61E+00
17	29.007	496	81.897	85.74		3.84E+00
18	28.005	322	51.94	53.73		1.79E+00
19	27	0	0	0		0.00
20	26	0	0	0		0.00
21	25	0	0	0		0.00
22	24	0	0	0		0.00
23	24	0	0	0		0.00
24	22	0	0	0		0.00
Total Power			953.6858	978.79		25.2142
Maximum Possible load			128.4005	133.76		
Difference in power output			25.2			
%Efficiency	increase			2.63%		
% increase in total		Efficiency		23.35%		

The results obtained from the simulation of the Simulink model of PV (Appendix B, Figure B.3) are compared with the results obtained earlier for dynamic model for similar values of varying ambient temperature and solar irradiance.

As can be inferred from the above results, the consideration of parametric variation in the performance of PV module, results in an increment of 2.63 % efficiency. This increment is for a

single day from sunrise to sunset. As a PV module has significantly low efficiency $\sim 10-15\%$, this 2.63% increment will have a significant impact on the overall performance of the PV module. Note that this 2.63% increment in efficiency is top of the 20.72% increment in efficiency from the dynamic PV model. So, the over all gain in the efficiency is 23.35%.

Based on the parametric analysis, the parametric variation has been implemented in the dynamic model and improved results were obtained in terms of true maximum power. There is further improvement in efficiency by 2.62% and a maximum possible load of 134 W can be handled in comparison to 128 W without the variation in the parameter consideration.

Figure 3.16 shows the variation of maximum power over the whole day. Figure 3.17 is obtained by zooming Figure 3.16 to show the variation of maximum power between the peak hours of performance of solar module.

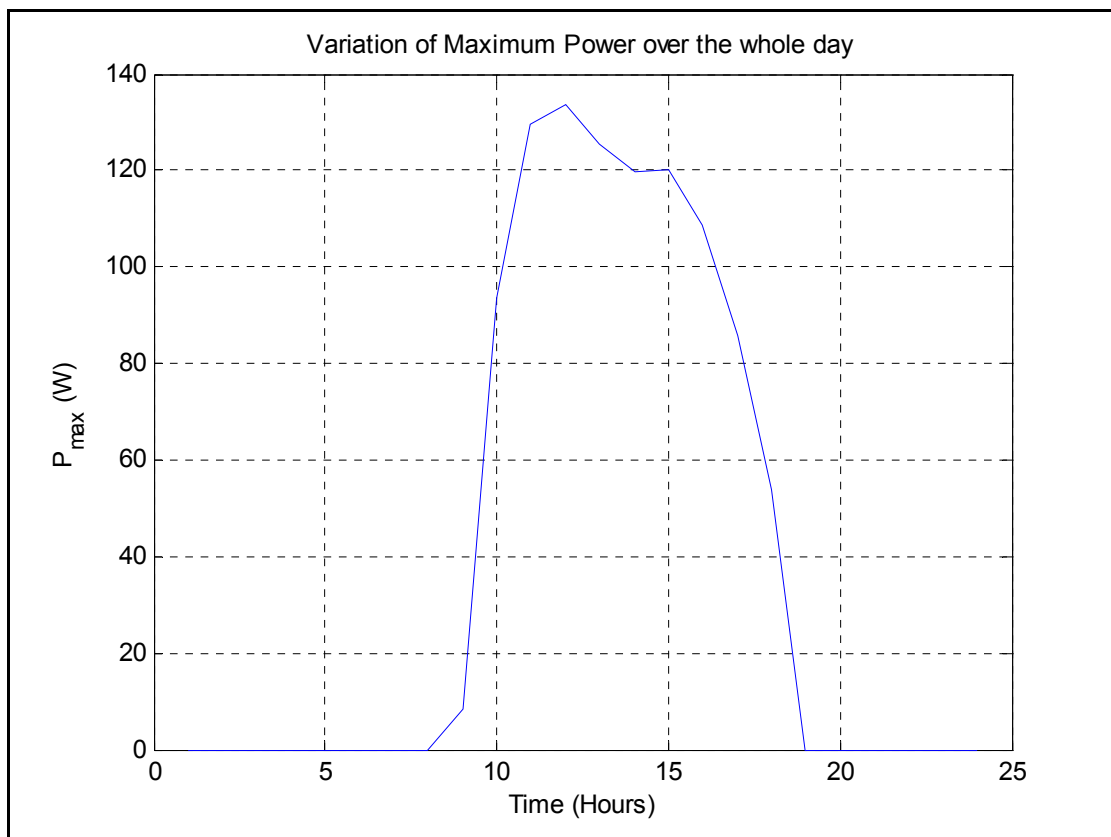


Figure 3.16 Variation of Maximum Power Over the Whole Day

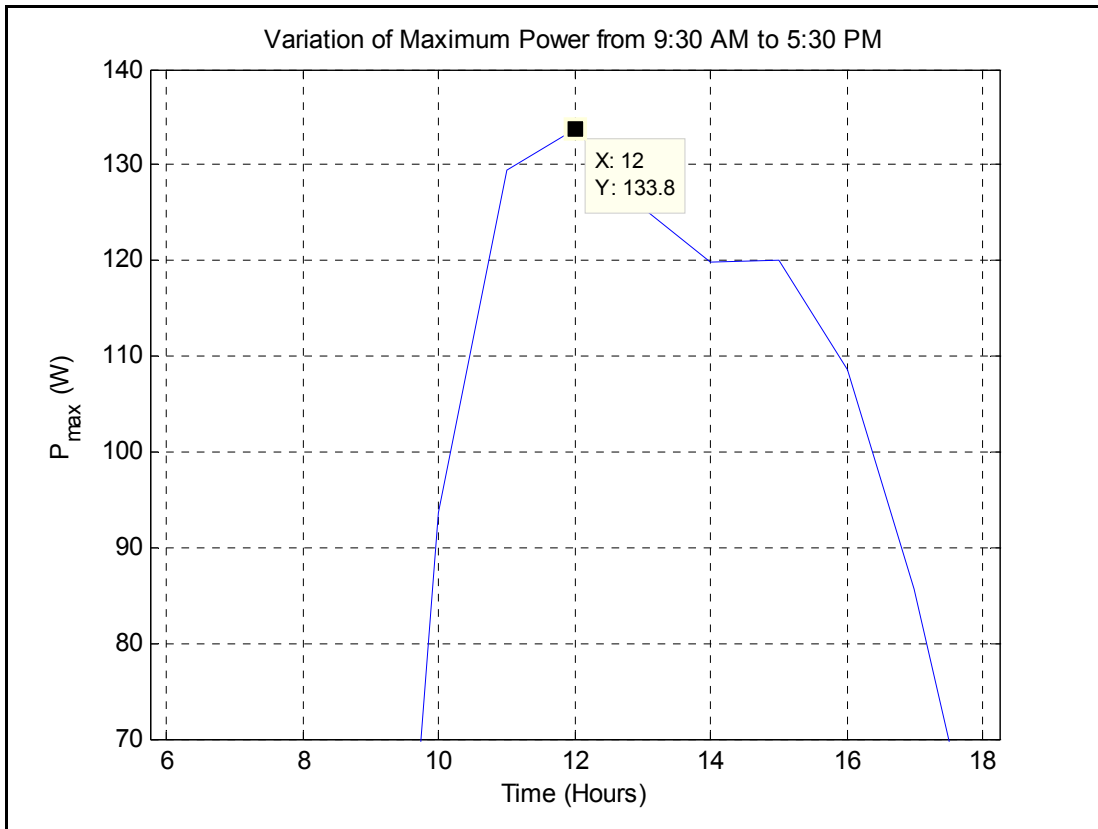


Figure 3.17 Variation of Maximum Power from 9:30 AM to 5:30 PM

It can be seen the maximum value of output power 133.8 W is achieved around noon.

3.3 Experimental Validation

3.3.1 Hardware Setup

To test the accuracy of the developed Simulink PV model, a hardware setup was assembled in order to carry out the experiment. The site of experiment was the rooftop of Prescott Hall of Tennessee Tech University, Cookeville, TN. The testing units were SIEMENS SP75 solar panels. The detailed specifications of all the instruments are given in Appendix C. A wooden frame was built for proper and sturdy angular mounting of the two solar panels as shown in Figure 3.18.

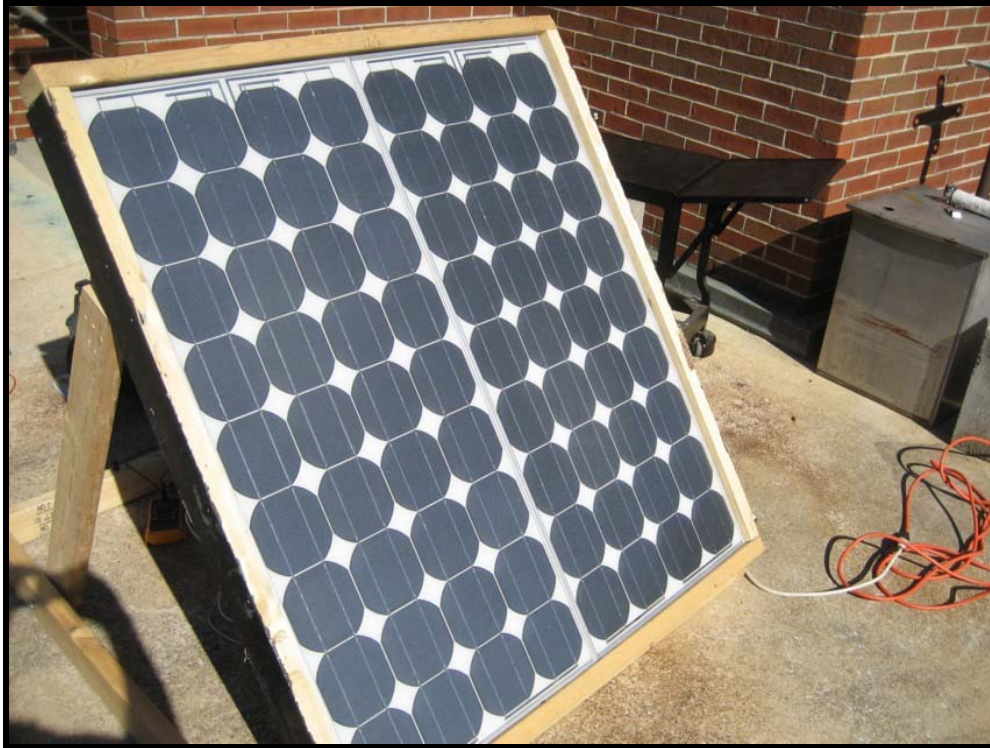


Figure 3.18 Experimental Setup-Solar Panels

3.3.2 Data Collection

The MATLAB/ Simulink model developed earlier was embedded in the LabVIEW environment. The LabVIEW models are shown in Appendix B. The solar irradiance and the ambient temperature data were collected with the help of a dp solar meter 776E and thermocouple [3.50]. The thermocouple was connected to Omega Super MCJ Thermocouple to Analog Connector [3.49]. The real-time solar irradiance and temperature data accessed through these two devices was inputted to the LabVIEW model through NI USB 6008 Data Acquisition System (DAQ) [3.52] as shown in setup in Figure 3.19.

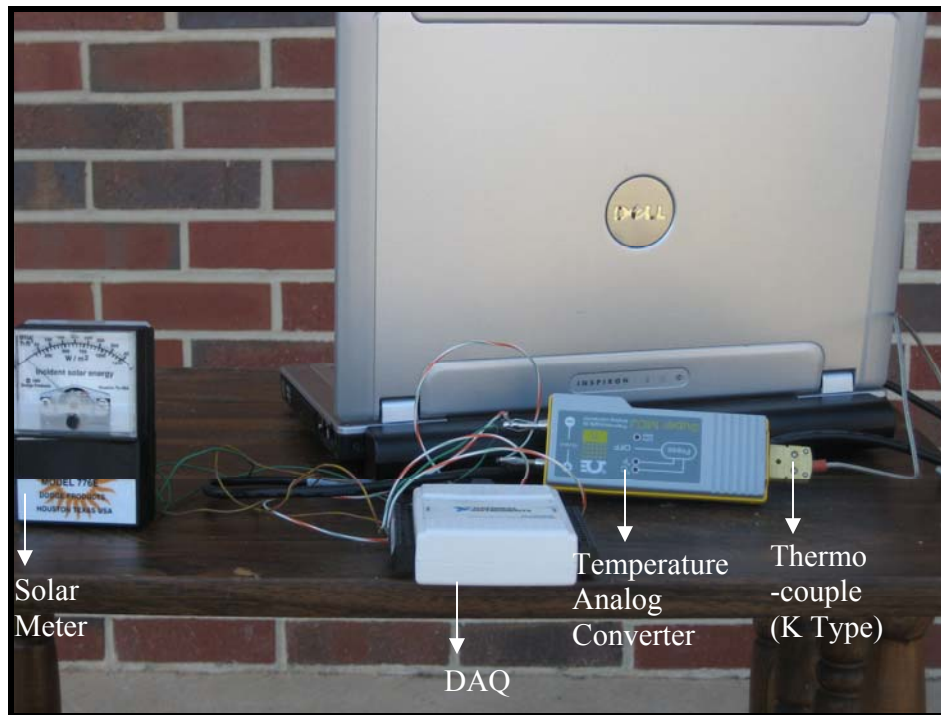


Figure 3.19 Experimental Setup-Data Collection

After acquiring the real-time value of ambient temperature and the irradiance through DAQ system, the model processed these variables and predicts the instantaneous attainable maximum power, the voltage and current at the maximum power, and the corresponding resistive load. This value of resistive load is then programmed into the programmable electronic DC load connected to the solar panels as shown in Figure 3.20. The values of actual (experimental) output current and the actual output voltage are then obtained through the display screen of the DC load. The product of the experimental voltage and current is then compared with the predicted maximum power and the error is calculated. This experimental testing has been carried for a span of 21 days from sun rise to sun set and the data were collected, processed, and results are observed for every 30 minutes. These 21 days consist of bright, cloudy, warm, and cold days with a significant variation of temperature and solar irradiance. The experimental data and the observations are included in Appendix E.

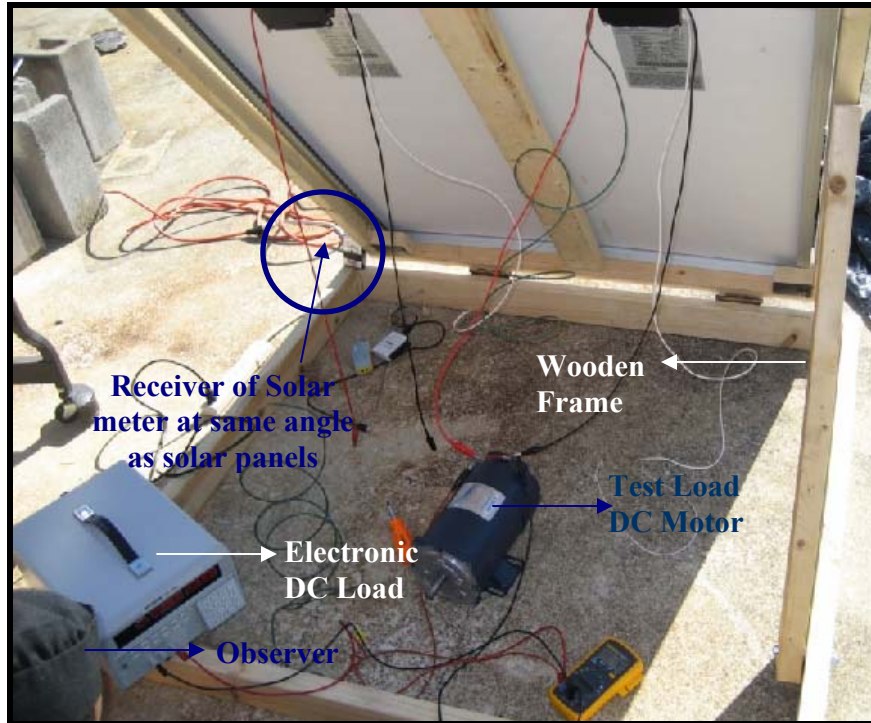


Figure 3.20 Experimental Setup for Model Validation

As can also be noted in Figure 3.20, the angle of placement of solar meter should be in exact angular co-ordinance with that of the angular placement of solar panels for measuring accurate value of solar irradiance.

The results obtained are calculated to observe the error between the predicted and experimentally observed maximum power. The Design of Experiment (DoE) and the model validation and analysis is performed in the next section.

Table 3.5 List of Equipments Used in the Experiment [Appendix C]

1	PV Modules
2	Solar Meter
3	Thermocouple to Analog temp Reader
4	NI USB DAQ
5	Electronic Load
6	Test Load (DC Motor)

3.4 Design of Experiment (DoE)

The basic steps for design for six sigma (DFSS); carrying out a designed experiment for profitable commercial productions are stated in [53] as

A. Before the Experiment

- a. Preliminaries
- b. Identifying response, factors and factor levels
- c. Selecting the design

B. During the Experiment

- d. Collecting the data

C. After the Experiment

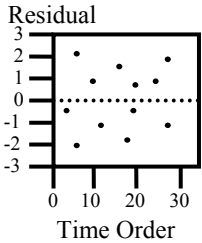
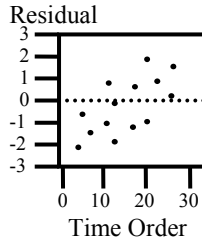
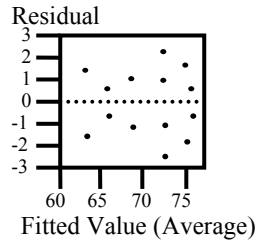
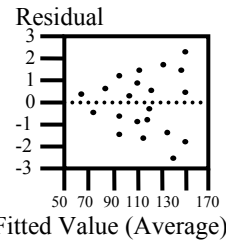
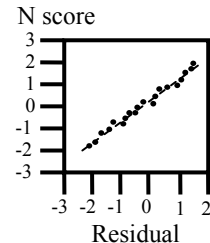
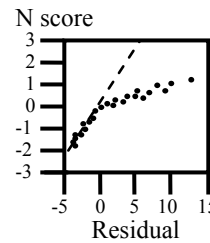
- e. Analyzing the Data
- f. Drawing, verifying, and reporting conclusions
- g. Implementing the recommendations

Part A and Part B have already been completed and reported in the previous sections of this chapter. A brief methodology of the analysis of the data and validation of the model is described in the next few pages and the detailed analysis of the experimental data and validation of the model is reported in Appendix D. A brief theory of the statistical analysis is also covered; details of which can be viewed in [3.53- 3.56].

3.4.1 Model Validation and Analysis

The statistical software package R is used to carry out all the data analysis [3.54-3.55]. Firstly, the data were modeled and the standard error, p-value, and the coefficient of determination R^2 obtained. The p-values and the R^2 value of the response were analyzed to judge the effectiveness of the data by the fitness factor of the regression plot. Next, the stability of the data over time was checked by looking at a time series plot of the residuals. Further diagnostics were run on the model, such as residual and normal probability plots and tests for influential data points (outliers), to check the validity of the model. Recommendations were made then to filter the defected data in order to improve the quality of the model. The nature of the regression plots to be plotted and their characteristics are summarized in Table 3.6.

Table 3.6 Standard Regression Plots and Verification Actions [3.53]

Residual Plots	Good	Bad	Meaning/Actions
1. Time Plots to analyze the stability over time			Any pattern visible over time means another factor, related to time, influences Y. Try to discover it.
2. This plot is a check for constancy; variation does not increase as average increases			This shape means the variation increases as the average of each condition increases a use of square root, log, or inverse transformation on Y is recommended.
3. The Normal Probability Plot of Residuals is a check that residuals are Normal or not.			This shape means residuals are not normal and a transformation on Y is recommended

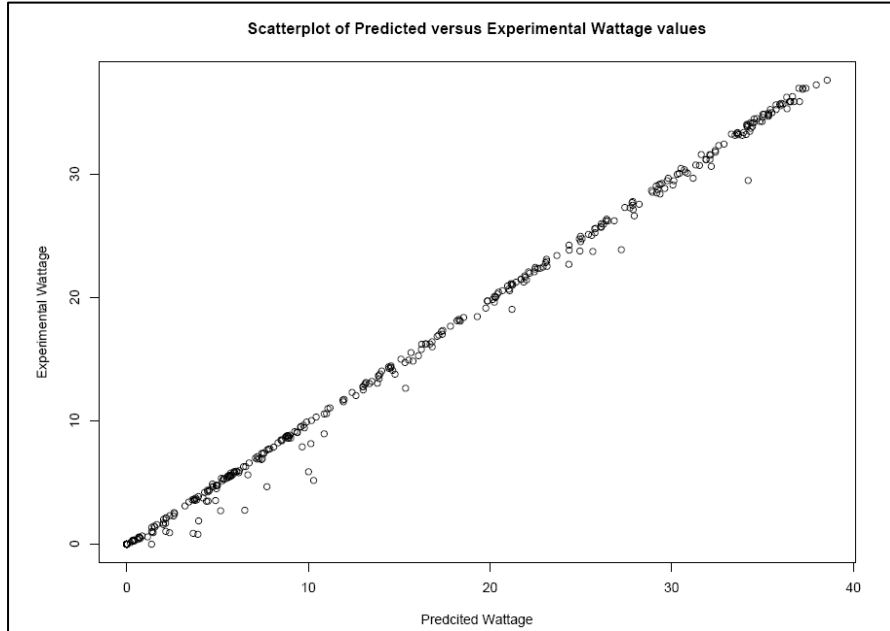


Figure 3.21 Scatter Plot of Predicted Vs. Experimental Maximum Power Values

Figure 3.21 shows the scattered plot of the experimental Wattage obtained from Solar Panels versus Wattage obtained from the PV model (LabView/Simulink model) stated as the predicted data in this analysis.

The standard data model for the regression analysis of the experimental data can be expressed as [3.56] [Appendix D]

$$W_{\text{exp}} = \beta_0 + \beta_1 W_{\text{pred}} + \varepsilon \quad (3.49)$$

where

W_{exp} : Wattage obtained from Solar Panels;

W_{pred} : Wattage obtained from the PV model (LabView/Simulink model);

β_0 : is the intercept (and should be zero unless W_{pred} is a biased);

β_1 : is the slope (and should be 1 unless W_{pred} is not consistent);

ε : is the error of prediction and is assumed to be independent and identically distributed from a normal distribution for each wattage value.

The calculation in R gives the residual standard error: 0.6433 on 368 degrees of freedom and the coefficient of determination R^2 as 0.9972 .This implies that the prediction has 99.72% accuracy [Appendix D].

Afterwards, to validate the model, diagnostics was performed on the data model. The Normal quantile-quantile plot of the residuals is plotted in Figure 3.22 and the scatter plot of the residuals versus the predicted wattage is shown in Figure 3.23.

A deviation from normality of a group of data can be observed in Figure 3.22 as the diagonal line is not followed by the quantile of residuals through out the curve. Also, in Figure 3.21, at least 45-50 data points are under predicted by the model using an influential test on each data point. It was concluded that there is a particular group of data which is causing this effect.

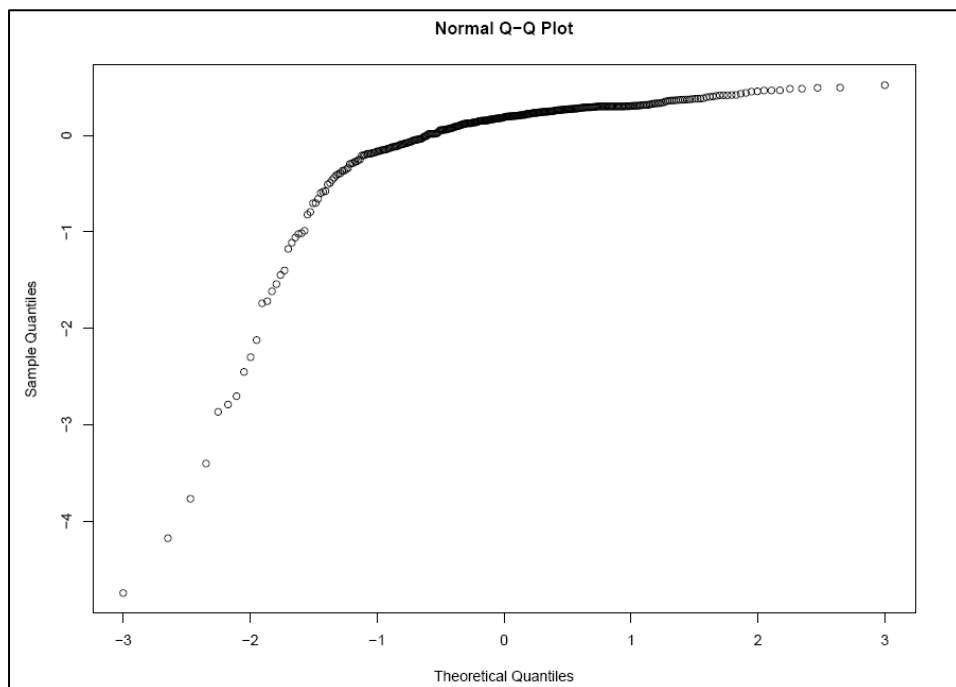


Figure 3.22 Normal Quantile-Quantile Plot of Sample Quantities Vs the Theoretical Quantities

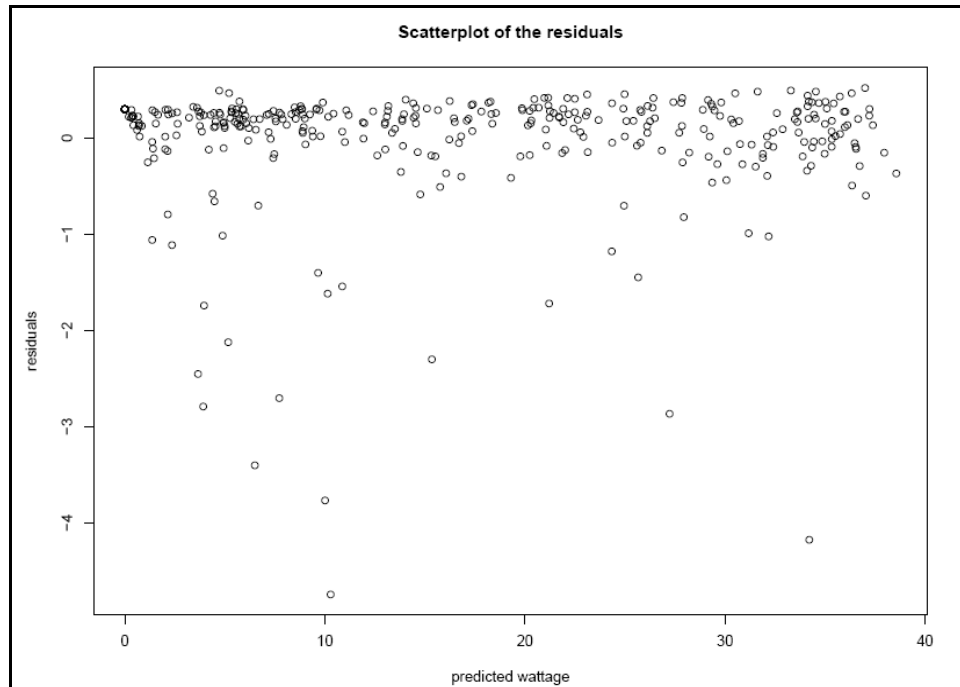


Figure 3.23 Scatter Plot of the Residuals Vs. the Predicted Wattage

After detailed research and plotting of different sets of data, it was inferred that the values of the data at the sunrise and sunset time are influential cases and could be considered outliers. The model is not a good predictor of the output wattage of the solar panels at those two instances but is for the rest of the day. Although the data were collected at every minute of the day, the predicted and experimental wattage values were obtained at every 30 minutes. The values of ambient temperature and the solar irradiance were averaged every 30 minutes to obtain these values and this approximation worked quite well in most of the cases, as there is not much variation of ambient temperature and solar irradiance in a span of 30 minutes. However, upon reconsideration of the experimental data, it has been found that these two variables vary over a significant range during the 30 minutes period of just after sunrise and just before sunset.

Therefore, these data points from every day experimental observations were discarded and the data analysis was performed again and following results are performed. Figure 3.24 shows the scattered plot of the experimental wattage obtained from solar panels versus wattage obtained from the PV model (LabView/Simulink model) stated as the predicted data in this analysis. The

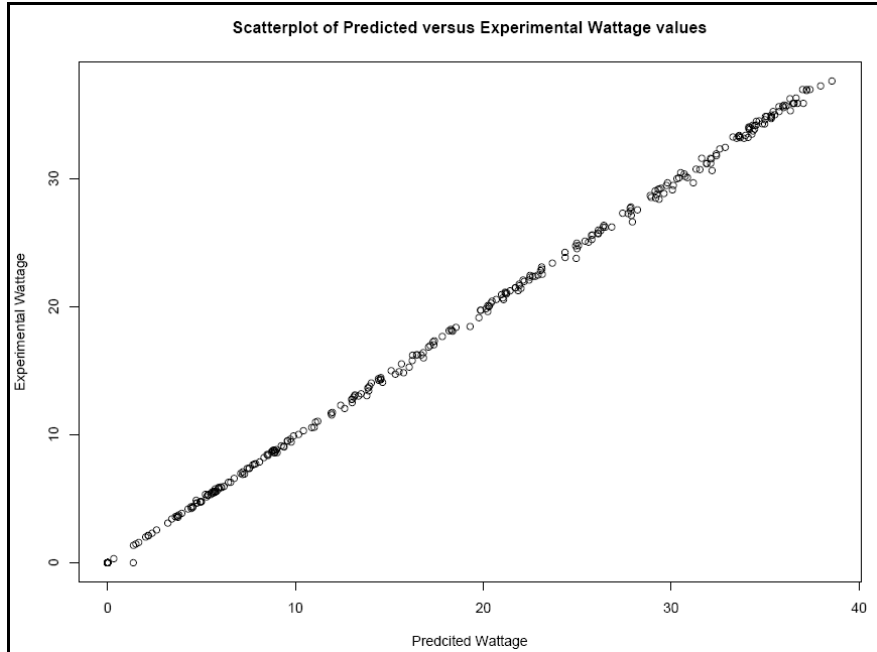


Figure 3.24 Scatter Plot of Predicted Vs. Experimental Wattage Values-I

calculation in R gives the Residual standard error: 0.2384 on 313 degrees of freedom and the coefficient of determination R^2 as 0.9996. This implies that the prediction has 99.96% accuracy [Appendix D].

The Normal quantile-quantile plot of sample quantities versus the theoretical quantities is plotted again in Figure 3.25.

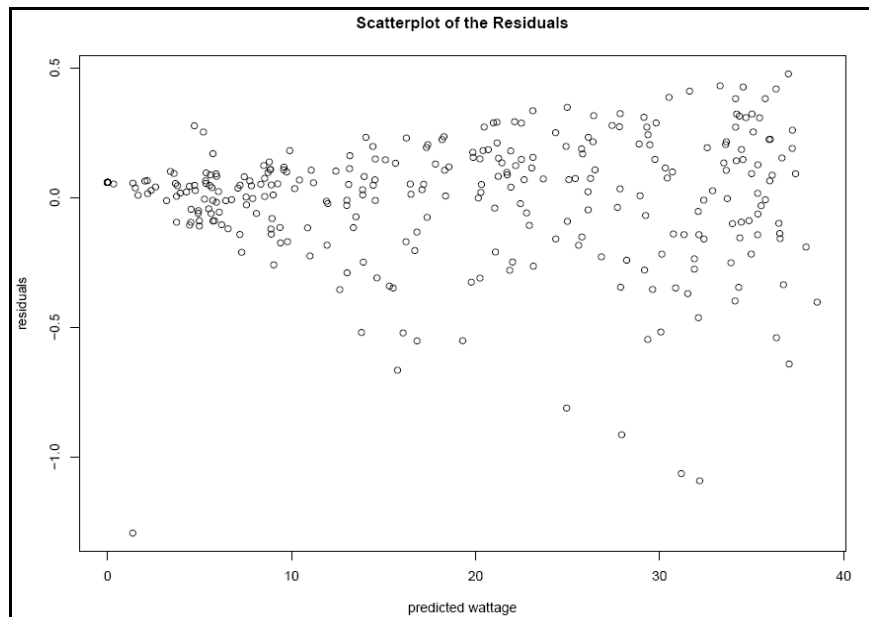


Figure 3.25 Scatter Plot of Predicted Vs. Experimental Wattage Values-II

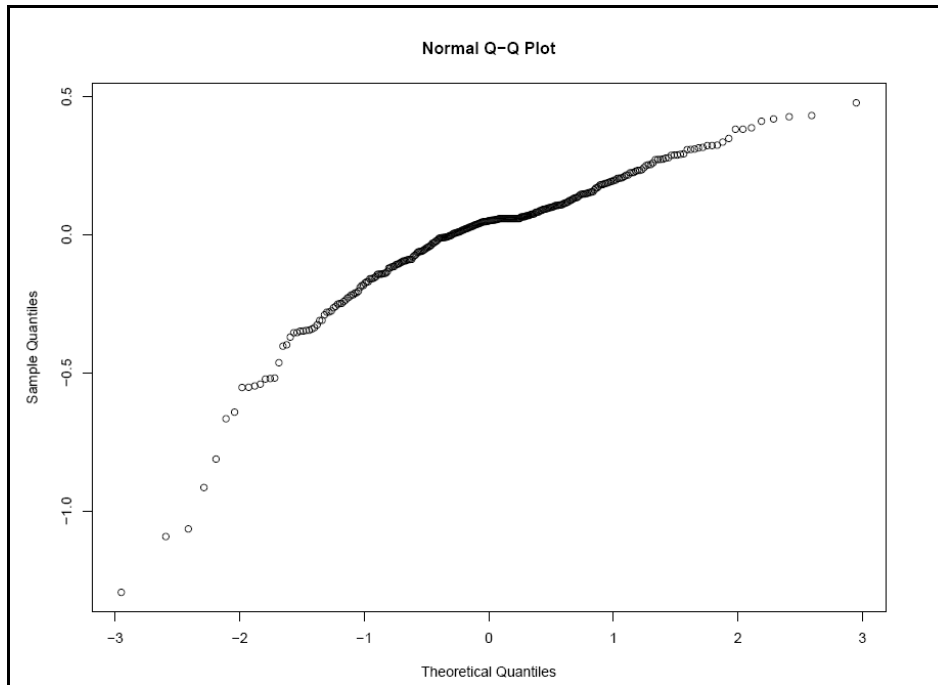


Figure 3.26 Scatter Plot of Predicted Vs. Experimental Wattage Values-III

The scatter plot of the residuals versus the predicted wattage is shown in Figure 3.26. The quantile in Figure 3.26 is far more linear than in Figure 3.23 and hence, an improved result is obtained. Further refinements to the model can be made but with an R^2 value of 99.96%, it was deemed unproductive to the experiment. With the coefficient of determination value of 99.96 % accuracy, this can be inferred that the model is valid and therefore, the experiment is successful [Appendix D].

REFERENCES

- [3.1] Ø. Ulleberg, "Stand-alone Power Systems for the Future: Optimal Design, Operation and Control of Solar Hydrogen System," PhD Dissertation, NUST, Norway, 1998
- [3.2] T.U. Townsend, A Method for Estimating the Long-Term Performance of Direct-Coupled Photovoltaic Systems, MS thesis, University Of Wisconsin – Madison, 1989.
- [3.3] F.A. Ferret, M.G. Simões, Integration of Alternative Sources of Energy, John Wiley & Sons, Inc., 2006.
- [3.4] S. Kaplanis, E. Kaplani, "A model to predict expected mean and stochastic hourly global solar radiation values" J. of Renewable Energy, Vol.32, 2007. pp:1414–1425
- [3.5] T. Townsend, et al., "A New Performance Index for PV System Analysis," 24th IEEE PVSC, Dec. 1994
- [3.6] M. R. Patel, Wind and Solar Power Systems, CRC Press LLC, 1999.
- [3.7] Ø. Ulleberg and S. O. MØRNER, "TRNSYS simulation models for solar-hydrogen systems," Solar Energy, Vol. 59, No. 4-6, pp. 271-279, 1997.
- [3.8] J.A. Duffie, W.A. Beckman, Solar Engineering of Thermal Processes, John Wiley & Sons Inc. 1991.
- [3.9] H. P. Garg and J. Prakash, Solar Energy, Tate McGraw-Hill Pub. Co., 2000
- [3.10] B.H. Khan, Non- conventional energy technologies, McGrawHill Publications, 2005.
- [3.11] J. Tsutsui, Y. Sato, K. Kurokawa, "Modeling the Performance of Several Photovoltaic Modules," Tokyo University of Agriculture and Technology, 2006.
- [3.12] M. Arrouf, S. Ghabrou, "Modeling and Simulation of a Pumping System Fed by Photovoltaic Generator within the MatlabSimulink Programming Environment," University of Batna, 2006.
- [3.13] K. Chao, S. Ho, M. Wang, "Modeling and Fault Diagnosis of a Photovoltaic System," National Chin-Yi University of Technology, 2007.
- [3.14] C. Chiang, T. Chiang, H. Huang, "Modeling a Photovoltaic Power System by CMAC_GBF," 3rd World Conference on Photovoltaic Energy Conversion Osaka, Japan, May 11-18, 2003.
- [3.15] J. F. Randall, J. Jacot, "Is AM1.5 Applicable in Practice? Modeling Eight Photovoltaic Materials with Respect to Light Intensity and Two Spectra," Laboratoire de Production Microtechnique, 2003.
- [3.16] A.Mellit, S.A.Kalogiru, "Artificial Intelligence Techniques for photovoltaic applications: A review," Journal of Progress and Energy and combustion science, Vol. 34, pp574-632, 2008.
- [3.17] I. H. Altas, A. M. Sharaf, "A Photovoltaic Array Simulation Model for Matlab-Simulink GUI Environment," Karadeniz Technical University, 2007.
- [3.18] W. Xiao, W. G. Dunford, A. Capel, "A Novel Modeling Method for Photovoltaic Cells," 2004 35th Annual IEEE Power Electronics Specialists Conference Aachen, Germany, 2004.
- [3.19] S. R. Williams, T. R. Betts, R. Gottschalg, D. G. Infield, N.J.C.M. van der Borg, A. R. Burgers, H. de Moor, W. Warta, G. Friesen, D. Chianese, A. Guerin de Montgareuil, T. Zdanowicz, D. Stellbogen, W. Herrmann, S. Pietruzko, J. Krustok, E. Dunlop, "Evaluating the State of the Art of Photovoltaic Performance Modelling in Europe," Loughborough University,
- [3.20] A. Yilanci, I. Dincer, H. K. Ozturk, "A Review on Solar-Hydrogen/Fuel Cell Hybrid Energy Systems for Stationary Applications," University of Ontario Institute of Technology, 2008.
- [3.21] D. R. Myers, K. Emery, "Terrestrial Solar Spectral Modeling Tools and Applications for Photovoltaic Devices," National Renewable Energy Laboratory, 2002.
- [3.22] M. Wu, E. J. Timpson, S. E. Watkins, "Temperature Consideration in Solar Arrays," University of Missouri-Rolla, 2004.
- [3.23] R. Chenni, M. Makhlof, T. Kerbache, A. Bouzid, "A Deailed Modeling Method for Photovoltaic Cells," Mentouri University Route d' Ain El Bey, 2007.

- [3.24] M. Rashed, A. Elmitwally, S. Kaddah, "New Control Approach for a PV-Diesel Autonomous Power System," Mansoura University, 2007.
- [3.25] K. Whitfield, C. R. Osterwald, "Procedure for Determining the Uncertainty of Photovoltaic Module Outdoor Electrical Performance," NREL, 2001.
- [3.26] Luque A, Hegedus S. Handbook of photovoltaic science and engineering. Wiley-Sons; 2003
- [3.27] J Andrews, A. K. Doddathimmaiah, S. M. Ali, A. Akbarzadeh, "Solar Hydrogen Systems for Remote Area Power Supply From a Triple Bottom Line Perspective," RMIT University
- [3.28] A. Hamidat, B. Benyoucef, "Mathematic Models of Photovoltaic Motor-Pump Systems," Centre for the Development of Renewable Energies, 2007.
- [3.29] C. D. Johnson, "On a 'Science of Modeling' for Dynamic-Systems; Some Fundamental Ideas and Principles," University of Alabama in Huntsville, 2004.
- [3.30] P. L. Zervas, H. Sarimveis, J. A. Palyvos, N.C.G. Markatos, "Prediction of Daily Global Solar Irradiance on Horizontal Surfaces Based on Neural-Network Techniques," National Technical University of Athens, 2007.
- [3.31] R. C. Campbell, "A Circuit-based Photovoltaic Array Model for Power System Studies," IEEE Power Symposium, Page(s):97 - 101 Sept. 30 2007-Oct. 2 2007
- [3.32] H. Gajbert, M. Hall, B. Karlsson, "Optimisation of Reflector and Module Geometries for Stationary, Low-Concentrating, Façade-Integrated Photovoltaic Systems," Lund University, 2007.
- [3.33] C. Li, X. Zhu, G. Cao, S. Sui, M. Hu, "Dynamic Modeling and Sizing optimization of Stand-Alone Photovoltaic Power Systems Using Hybrid Energy Storage Technology," Shanghai Jiao Tong University, 2008.
- [3.34] A. Mellit, S. A. Kalogirou, "Neuro-Fuzzy Based Modeling for Photovoltaic Power Supply System," First International Power and Energy Conference Putrajaya, Malaysia, 2006.
- [3.35] A. Mellit, M. Benghanem, S A. Kaloirou, "Modeling and Simulation of a Stand-Alone Photovoltaic System Using an Adaptive Artificial Neural Network: Proposition for a New Sizing Procedure," University Centre of Medea, 2006.
- [3.36] Y. T. Tan, "A Model of PV Generation Suitable for Stability Analysis," IEEE Transactions on Energy Conversion, Vol. 19 No. 4 pp. 748-755, Dec. 2004.
- [3.37] S. Kaplanis, E. Kaplani, "A Model to Predict Expected Mean and Stochastic Hourly Global Solar Radiation Values," T.E.I. of Petra, 2006.
- [3.38] D. L. King, J. A. Kratochvil, W. E. Boyson, "Measuring Solar Spectral and Angle-of-Incidence Effects on Photovoltaic Modules and Solar Irradiance Sensors," Sandia National Laboratories, 1997.
- [3.39] A.D. Theocharis, A.Menti, J.M. Argitis, T.Zacharias, "Modeling and Simulation of a Single-phase residential photovoltaic system," Power Tech, 2005 IEEE Russia, 27-30 June 2005 pp:1-71 - 7
- [3.40] V. Badescu, "Dynamic Model of a Complex System Including PV Cells, Electric Battery, Electrical Motor and Water Pump," Polytechnic University of Bucharest, 2003.
- [3.41] L. Zhang, Y. F. Bai, "Genetic Algorithm-Trained Radial Basis Function Neural Networks for Modelling Photovoltaic Panels," University of Leeds, 2005.
- [3.42] C. L. Hou, J. Wu, M. Zhang, J.-M. Yang, and J.-P. Li, "Application of adaptive algorithm of solar cell battery charger," in Proc. IEEE Int. Conf. Elect. Utility Deregulation Restruct. Power Technol., 2004, pp. 810–813
- [3.43] .D. Guasch, S. Silvestre, Dynamic Battery Model for Photovoltaic Applications, John Wiley & Sons, Ltd., 2003.
- [3.44] M. Buresch, Photovoltaic Energy Systems. New York: McGraw Hill, 1983.
- [3.45] G. Nofuentes, J. Aguilera, F. J. Munoz, " Tools for the Profitability Analysis of Grid-Connected Photovoltaics," Escuela Politecnica Superior University of Jaen, 2002.
- [3.46] National Solar Radiation Database http://rredc.nrel.gov/solar/old_data/nsrdb/. Accessed on 12/04/2008
- [3.47] NOAA's National Climatic Data Center <ftp.ncdc.noaa.gov> Accessed on 12/12/2008
- [3.48] SIEMENS SP75 PV module manual.
- [3.49] Omega Thermocouple to Analog converter manual

- [3.50] dp Solar meter specifications
- [3.51] Programmable DC Electronic load manual.
- [3.52] National Instruments USB DAQ manual.
- [3.53] Rath, Strong's, "Six Sigma Pocket Guide," Rath and Strong's Management Consultants, MA, USA
- [3.54] Introduction of R software <http://www.gnu.org/software/r/R.html#introduction> accessed on 11/22/2008
- [3.55] Official Introduction to R <http://cran.r-project.org/doc/manuals/R-intro.pdf> accessed on 11/22/2008
- [3.56] J. Neter, M.H.Kutner, C.J. Nachtsheim, W.Wasserman, "Applied Linear Statistical Models," McGrawhill Publ., 2004
- [3.57] F.P. Incropera, D.P. Dewitt, T.L. Bergman, A.S. Lavine, Fundamentals of Heat and Mass Transfer, John Wiley and Sons 2006
- [3.58] FOA Survey, "[http:// www.foa.co.uk](http://www.foa.co.uk)," accessed on 04/05/2008

CHAPTER 4

LOAD MATCHING CONTROL OF STAND –ALONE PV SYSTEM FOR MAXIMUM POWER TRANSFER

4.1. Maximum Power Point Tracking (MPPT)

Maximum Power Point Tracking (MPPT) is a procedure to achieve maximum possible instantaneous power through a PV array. As stated earlier in section 2.5.4.2.1, “the maximum power point varies over the whole day with the variation of weather conditions. In order to track it exactly, an appropriate value of load has to be matched.” A prerequisite to successful load matching is the knowledge of available maximum power real-time.

4.1.1. Literature Survey

Implementing the optimal MPPT technique largely depends on the ease of implementation and suitability and compatibility to the end user's requirements [4.1]. When deciding which MPPT technique is most convenient, one must also consider the number of sensors required. The most common sensors for MPPT application are voltage, current, and temperature sensors. In some cases, it is more suitable to have only one sensor, such as only a voltage sensor, considering that current sensors are costly and rather bulky and also that irradiance sensors are uncommon [4.1]. Therefore, in some instances, it is better to consider an MPPT technique which requires only one sensor and is able to compute other essential values.

Different MPPT techniques have been used for different setups, depending on the task being performed. For example, the task of a PV system used in street lights is only to charge a battery.

Therefore, less sophisticated and inexpensive implementation will suffice. On the other hand, stand-alone photo voltaic power generation systems generally demand prompt convergence to the MPP for optimal matching and safety of the load. As the PV characteristic (Equation 3.6) is a transcendental equation, Newton Raphson method is implemented to obtain the unique solution for the desired convergence of the curve (maximum power point) of Figure 2.10 to obtain the instantaneous MPPT. Mathematically, the value of output current of Equation 3.6 cannot be obtained using common elementary functions because of the transcendental nature of the equation [4.48- 4.49]. Further, justification of the implementation of numerical iterative method is explained in Appendix F, which has provided the basis of the implication of Newton Raphson method for achieving the unique solution of the characteristics equation (Equation 3.6) of a Photovoltaic cell.

4.1.1.1. Existing MPPT strategies and their limitations. Being an essential feature of a PV system, vast literature on MPPT is available and various methods have been proposed, developed, and experimented. In a survey of MPPT techniques published in 2007 [4.1], approximately 19 different methods with different implementation techniques have been proposed in literature. The earliest reported MPPT research work goes back to 1968 with significant amount of research in the last two decades [4.1-4.2].

As stated in the survey and comparison of various MPPT techniques in [4.1] *“these methods vary in complexity, sensors required, convergence speed, cost, and range of effectiveness, implementation hardware and other factors.”* In fact these are the basic criterion for selecting an MPPT technique and are compared in Table 4.1 at the end of this subsection.

Conceptually, an MPPT technique has to locate an instantaneous voltage V_{MPP} and current I_{MPP} automatically at which the PV module should operate to attain maximum power point (MPP) for the instantaneous value of temperature and irradiance. It is possible to have more than one maximum power point (local maxima) during partial shading conditions but on the whole there is only one

correct maximum power point [4.1]. A common draw back in the existing MPPT techniques is that either the temperature or irradiance or both are considered constant or an averaged value is taken into account for the calculation of MPPT. The basic two variables that are required and must be considered on site and on a real-time basis to obtain maximum and efficient instantaneous solar power are the solar irradiance and the temperature. Further, the parameters of solar cells like heat loss coefficient, thermal conductance etc varies with the varying temperature. In commercial PV cells these two variables are averaged over standard weather condition to estimate the power output capacity of the PV panel. Various maximum power point tracking (MPPT) techniques have been proposed in the past to obtain maximum power; but again, because of the estimated prediction of the weather condition, the promised maximum output power that would make a big difference in the current efficiency of the commercial solar cells has not been achieved [4.2-4.45]. The MPPT techniques reported in literature [4.1-4.45] can be categorized as array reconfiguration [4.1], state-based MPPT [4.2], once cycle control (OCC) [4.1], best fixed voltage (BFV) algorithm [4.1] and slide control method [4.1], look up table method [4.2], hill climbing [4.4-4.7], perturb and observe (P&O) method [4.8-4.12], incremental conductance [4.13-4.16], fractional open circuit voltage [4.17-4.20], fractional short circuit current [4.17, 4.19-4.22], ripple correlation control (RCC) [4.1,4.30], load current maximization [4.31-4.33], load voltage maximization [4.31-4.33], linear current control [4.34], dP/dV and dP/dI feed back control [4.35-4.37], current sweep [4.38], DC link capacitor drop control [4.39-4.40], fuzzy logic control [4.41-4.43], and neural network-based control [4.44-4.45]. The detailed mechanism and underlying theory of these methods can be found in [4.1-4.47].

Best fixed voltage (BFV) algorithm is designed based on the annual history of the temperature and irradiance data [4.1]. Based on the collected data the best fixed voltage for the maximum power point is calculated and sets as the operating point of the controller. Erroneous MPP projections always exist because of the dependence on the historical data that is not necessarily periodic and is valid only for a particular geographical location.

Look up Table [4.2] approach is restricted to a specific area and requires that weather conditions remain similar in upcoming years.

MPP is achieved through perturbation of the duty cycle of the dc-dc converter in hill and climbing method [4.4 – 4.7]. Perturb and observe method MPP is achieved through perturbation in the operating voltage of the PV array [4.8-4.12]. Both hill climbing and perturb and observe methods have same basic MPPT technique achieved through different methods. The voltage is increased and decreased around the potential MPP and an increment and decrement in output power is observed and a decision for the subsequent perturbation is decided based on the previous value of obtained maximum power. These methods reported erroneous results and failure under rapidly varying weather conditions [4.1- 4.3].

Fractional open-circuit voltage is based on an approximated linear relationship between the maximum power point voltage and the open circuit voltage ($V_{MPP} \approx V_{OC}$) and fractional short circuit currents is based on an approximated linear relationship between the maximum power point current and short circuit current ($I_{MPP} \approx I_{OC}$) [4.17- 4.22]. Through empirical calculation, a constant of proportionality is usually being calculated and to determine the V_{MPP} and I_{MPP} , respectively. Once the proportionality constant is obtained, open circuit voltage V_{OC} and open circuit current I_{OC} are monitored on a periodical basis by off lining the system from the power supply. This leads to periodical shutdowns and further, as these are approximated relationships, PV array rarely operates on the true MPPT and has proved invalid in partially shaded conditions which resulted in several local maxima [4.1].

Ripple correlation control (RCC) [4.1, 4.30] involves the utilization of the voltage and current ripples due to the switching of dc-dc converter connected to the PV array. At higher switching frequencies RCC reported failure because of the phase shift due to intrinsic capacitance of the PV array [4.1].

The DC link capacitor drop control method does not require the computation of the PV array power [4.1] and was developed specifically for the maximum power point tracking of the PV arrays [4.39] where a dc-dc boost converter is connected in parallel with the load at the output side. To obtain a constant output boost voltage, for a given load, only certain variation is possible in the input voltage of the dc-dc converter which is the output voltage of the dc-dc converter. With varying weather conditions, it is impossible to obtain required input voltage from the PV panel at the maximum power point without varying the load and thus the output performance of dc-link method has reported deterioration in comparison to other MPPT techniques [4.1, 4.39].

A common drawback with most of the MPPT techniques is that they are incapable of handling uncertain weather conditions because of the assumption of averaged solar irradiance and temperature values. Because of this, it is difficult to expect accurate performance through these control technologies. Besides uncertain weather conditions, PV cell parameters are affected by other variables such as heat loss coefficient, transmittance and absorptance product, accumulation of dust, and shading due to cloud and snow cover. Last but not least, aging also affects the performance of a PV cell.

Recently, neural networks were implemented for MPPT [4.44-4.45]. Neural network-based MPPT techniques are well adapted with micro controllers. However, each PV array requires specific neural network training due to its unique characteristics [4.1] which results in additional installation costs. In the past few years, fuzzy logic controllers have been researched and implemented for MMPT of PV arrays because these controllers handle imprecise inputs without state-of-the-art mathematical models [4.41-4.43].

Fuzzy logic controllers are well suited for micro controllers, but their efficiency depends on the vastness and depth of the designer's development of the rule base. Also, most of the fuzzy knowledge-based MPPT techniques were reported to have fixed control parameters [4.1, 4.41-4.43],

Table 4.1 Major Characteristics of MPPT Techniques [Retabulated from 4.1]

MPPT Technique	PV Array Dependent	Analog / Digital	Periodic Tuning	Convergence Speed	Implementation Complexity	Sensed Parameters
Hill-climbing P&O	No	Both	No	Varies	Low	Voltage, Current
IncCond	No	Digital	No	Varies	Medium	Voltage, Current
Fractional V	Yes	Both	Yes	Medium	Low	Voltage
Fractional I	Yes	Both	Yes	Medium	Medium	Current
Fuzzy Logic Control	Yes	Digital	Yes	Fast	High	Varies
Neural Network	Yes	Digital	Yes	Fast	High	Varies
RCC	No	Analog	No	Fast	Low	Voltage, Current
Current Sweep	Yes	Digital	Yes	Slow	High	Voltage, Current
DC Link Control	No	Both	No	Medium	Low	Voltage
Load Current Maximization	No	Analog	No	Fast	Low	Current
Load Voltage Maximization	No	Analog	No	Fast	Low	Voltage
dP/dI Feedback Control	No	Digital	No	Fast	Medium	Current
Linear Current Control	Yes	Digital	Yes	Fast	Medium	Irradiance
State-based MPPT	Yes	Both	Yes	Fast	High	Voltage, Current
OCC MPPT	Yes	Both	Yes	Fast	Medium	Current
BFV	Yes	Both	Yes	N/A	Low	None
Slide Control	No	Digital	No	Fast	Medium	Voltage, Current

which are technically required to be tuned on a real-time basis. A comparison of the above mentioned methods is given in Table 4.1.

4.1.1.2. Existing control strategies and their limitations. The basic criterion of implementing a control method is to extract and apply the valuable information to control a process (plant) so that the overall system has reliable, stable, and efficient operation. The mechanism of a controller can be described as a device which sensed a quantity to adjust the performance of a physical system through estimation, computation, and actuation of the system variables. The overall process of sensing, estimation, computation, and actuation is the fundamental notion of the feedback control. The first step in controlling any physical system

(plant) is to develop the mathematical model for confining the behavior of the system in an observable periphery.

Practically, it is impossible to develop a precise model of any physical system. Various reasons can be justified to this fact, leading from the degree of knowledge of the designer to the inherent uncertainties, complexity of the system, and due to intricate chemical and natural phenomenon occurring within the system. Hence, the developed models are estimated or approximated models, varied in precision due to above mentioned reasons. These estimated models often include unknown or imprecise uncertainties due to non-consideration of parameter variations or inadequate modeling of system dynamics.

Various control design techniques have been developed to address the problem of robust control of uncertain nonlinear dynamical systems [4.50-4.52]. The conventional linear control design techniques assume linearized behavior of uncertain nonlinear dynamical systems and the system transfer function is developed by presuming a norm bound on the uncertainties. H_∞ control method and Linear Quadratic Gaussian with loop transfer recovery (LQG/LTR) approach are one of the two robust linear control techniques [4.53]. However, the robustness of such systems is prominent only in the proximity of operating point of the system. To overcome this shortcoming, nonlinear control design techniques were developed. Lyapunov method of control and Variable Structure Control (VSC) are the two main nonlinear control design methods [4.53]. The stability and robustness in these systems is achieved by certain restriction on the structure of uncertainties known as matching conditions. Thus, various practical systems are excluded whose uncertainties do not meet the criteria of matching conditions. Research works are being carried out to minimize these matching conditions [4.53] and to develop robust nonlinear control methods for uncertain nonlinear dynamical systems.

Distributed generation systems in general and photovoltaic systems in particular are highly nonlinear. Besides, nonlinearity there are numerous uncertainties due to changing weather conditions

which are very difficult to predict. For example the ambient temperature is uncertain and difficult to predict precisely. Also, many parameters like heat loss coefficient, transmittance, absorptance and convective and radiative heat losses at the surface of the cell are assumed to have constant values in the existing models [4.54]. In reality, for instance, U_L , heat loss coefficient has many inherent uncertainties which vary over a wide range depending upon the properties of materials and weather conditions [4.54-4.62]. Due to these uncertainties, in case of stand-alone PV systems, it is very difficult to match the exact load precisely for achieving the instantaneous MPP by using the existing MPPT strategies [4.1-4.48].

When considering the optimality of the overall system i.e. to achieve the optimal load matching at MPP of PV module, the output voltage which is an input to the dc-dc converter is variable and uncertain. The challenge is to generate the accurate duty cycle of the dc –dc converter to obtain the desired boosted output voltage and to optimally match the load at MPPT. Hence, the control method implied to regulate such a system should have following characteristics:

- To minimize the error in the dc-dc output voltage $v(k)$ by appropriate control of the duty cycle $D(k)$.
- To provide a smooth control process near the reference point such that the transients in the controller output i.e. duty cycle should not affect the output of the dc-dc converter.

The control action of a conventional PI controller can be expressed as

$$u = K_p * e + K_I * \int_t edt \quad (4.1)$$

Upon differentiation, the discrete-time based description of the above equation can be described as

$$\Delta u(k) = K_p * \Delta e(k) + K_I * e(k) \quad (4.2)$$

where

u : Controller output;

K_p : Proportionality constant;

K_i : Integral constant;

k : is the k – *th* sampling time;

$e(k)$: Error in the controller input i.e. $e(k) = V_{ref} - V(k)$;

$\Delta e(k)$: Change of error in the controller input i.e. $\Delta e(k) = e(k) - e(k - 1)$;

$\Delta u(k)$: Change of control output $u(k)$ i.e. $\Delta u(k) = u(k) - u(k - 1)$.

The required characteristics of the desired control system mentioned above must have variable gains near the reference point such that a small value of integral constant near V_{ref} and a relatively larger value near the constraint. The conventional PID however, has the major drawback of control chattering; i.e., the controller output is a discontinuous high-frequency switching signal. This makes PID not suitable for this application because of continuous nature of variables and high-frequency switching requirement of dc-dc converter. A practical alternative for various challenging control applications for uncertain nonlinear dynamical systems is Fuzzy Control [4.63]. Fuzzy control offer realistic methods for developing the nonlinear controllers for uncertain nonlinear dynamical systems through the processing of heuristic information. Besides this, a fuzzy logic controller basically interpolates among the consequent of all the rules, according to the firing strength of each rules. Therefore, an FLC can be seen as multiple PID/PI controllers with smooth interpolation capability without chattering phenomena. Fuzzy Control is based on Fuzzy set theory [4.64-4.65] and it treats the complexity and uncertainty of the system by the provision of approximate control solutions. A suitable learning mechanism of the knowledge base and the tuning

of the controller parameters is required to achieve the desired performance on a real-time basis. Learning mechanisms such as genetic algorithm can be implemented to tune the control parameters in such cases.

MPPT techniques when implemented on a PV module results in variable PV output voltage. On the other hand, desired load voltage is achieved through dc-dc converter but in this case, maximum power point tracking is not guaranteed. Practically the strength of one method is a weakness of the other method. To overcome these limitations, both MPPT and dc-dc converter are used for load matching. The novelty of this method is that both the methods of MPPT and control through dc-dc converter are integrated together in order to achieve the advantages of both the methods. Further, because of this merging, the disadvantages of both the methods were wiped off because they were complimentary of each other. MPPT is achieved through the model developed earlier in Chapter 3 and the desired voltage, reference voltage V_{ref} is achieved by the boosted output voltage of the dc-dc converter. The overall supervisory control for load matching and control of duty cycle of the dc-dc converter is achieved through a fuzzy logic controller.

A novel method entitled “Modified queen bee algorithm,” that the author helped develop [4.87] ,which is an applied genetic algorithm method, is also proposed and an algorithm is developed and implemented to tune the parameters of the fuzzy logic controller on a real-time basis.

Further explanation in this context is elaborated in section 4.3. Basics of fuzzy logic control are described briefly in section 4.2. Also, the detail of the control strategy for optimizing the load matching for stand-alone PV through FKBC is discussed in the next section. Tuning of parameters of the FKBC is carried out through Applied Genetic Algorithm in section 4.3.2. A brief overview of the mechanism of the dc-dc converters is outlined in Appendix H.

4.1.2. Control Strategy for Optimizing the Load Matching for Stand-Alone PV

When a solar PV system is deployed for practical applications, the I-V characteristic keeps on changing with insulation and weather conditions. In order to transfer maximum power from the PV at any time, a specific load has to be applied to the PV at that time. Because of the variability of the PV voltage, a dc/dc boost converter, that provides a fixed output voltage by properly adjusting its duty cycle, is generally used to interface the PV and the load. To achieve the MPP for maximum power point extraction from PV array, the MPPT model of PV array, developed in chapter 3, calculates the load that need to be connected to the PV array. This load computed by the MPPT model varies with the cell temperature dynamics, ambient temperature, and irradiance. The load seen by the PV array not only gets affected by the above mentioned factors but also by the duty cycle of the boost converter. The actual load matching condition can be expressed as follows [4.45 – 4.47]

$$R_{load} = R_{MPP} / (1 - D^2) \quad (4.3)$$

where

R_{load} : the actual load resistance connected across the terminal of DC/DC boost converter,

R_{MPP} : the load resistance that should be connected to the PV for maximum power delivery.

This resistance is computed using the maximum power provided by the PV model and the constant output voltage that the DC/DC converter is supposed to maintain. D is the duty cycle for DC/DC boost converter evaluated by the Fuzzy Logic Controller (FLC) for achieving constant rated load output voltage. The Modified Queen Bee-based genetic algorithm played a significant rule in tuning the scaling factors of FKBC [4.87]. It is shown in [4.80] that with the same rule-base FLC has

the ability to optimize the IATE performance index for different application, only one has to tune the scaling factor.

Figure 4.1 represent the scheme for harvesting the MPP power from stand-alone PV array under uncertain environmental conditions.

The inputs to the PV module and the MPPT model are real-time solar irradiance and ambient temperature. During one complete control cycle, the maximum voltage, $V_{MPP,max}$, current $I_{MPP,max}$, and maximum power $P_{MPP,max}$ at MPP of the PV module and the maximum possible load for this maximum power point $Load_{MPP}$ are calculated through MPPT model developed earlier in Chapter 3

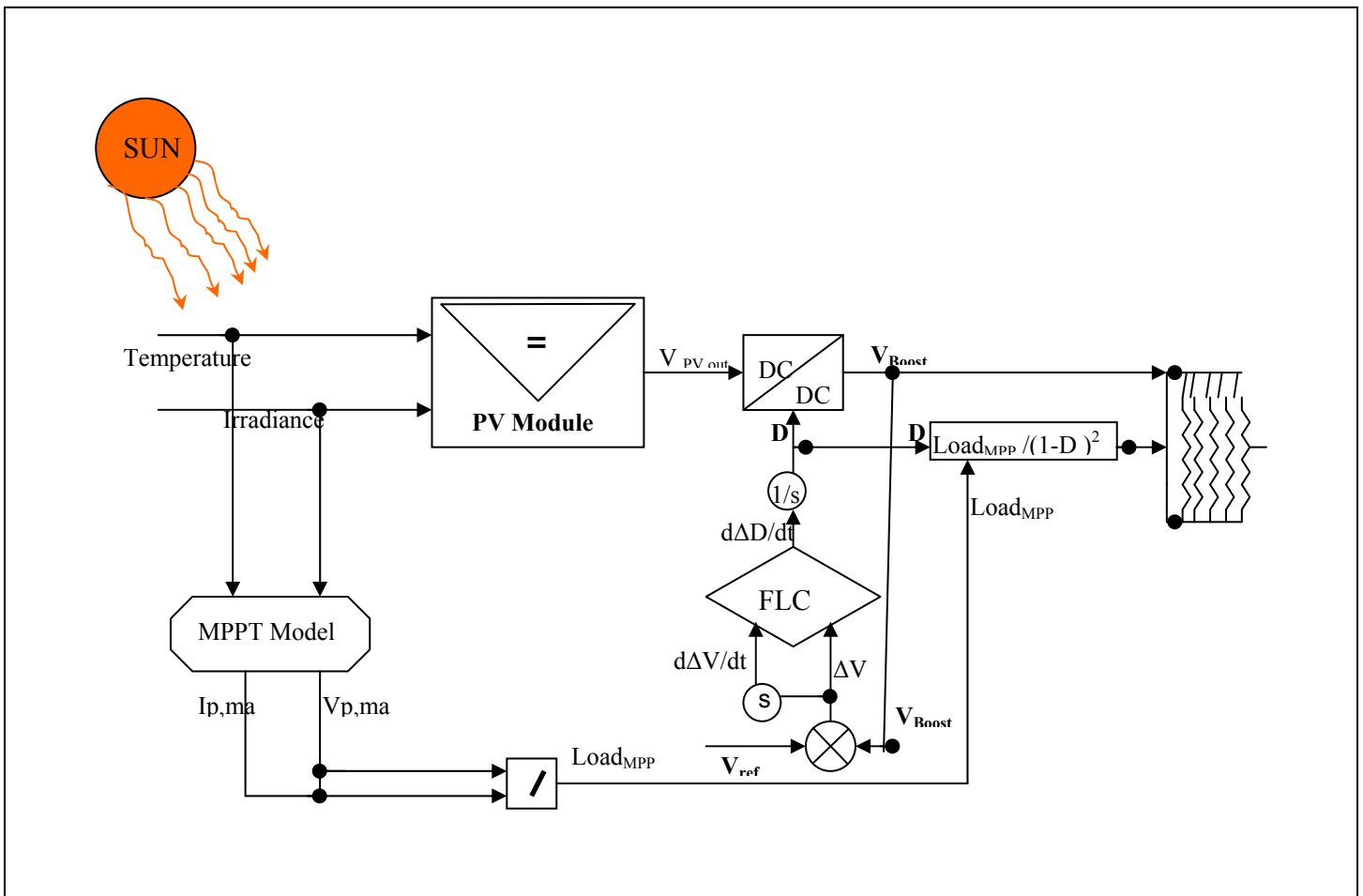


Figure 4. 1 Block Diagram of Control Strategy

(Appendix B). The output voltage of the PV module $V_{PV,out}$ is the input to the dc-dc converter (V_{in}) and D is the control signal; the duty cycle or the duty ratio of the controllable switch of the dc-dc converter. The boost output voltage of the dc-dc converter, V_{Boost} is compared with the reference voltage V_{ref} (assumed as 25 V for simulation purpose but it can be any value). The error in voltage ΔV (inputted as error ‘e’) and change in voltage error $d(\Delta V)/dt$ obtained by comparing the output voltages corresponding to the last two control steps ($\Delta V_k = V_k - V_{k-1}$) are used in determining the membership degree(s) of the change in power variable (inputted as change of error ‘ce’). The error ‘e’ and change in error ‘ce’ are inputted to the fuzzy logic controller, FLC. The output of FLC is the duty cycle ‘dc’ which is used as control signal for switching of the dc-dc converter and for determining the actual load ($Load_{MPP} / (1-D)^2$) as seen by the PV module.

The output power available at the load P_{out} is calculated and compared with the maximum power $P_{MPP,max}$ at MPP. The overall objective is to make the output power at the load level equal to the maximum power provided by the PV model, while maintaining the DC/DC booster voltage at a desired constant level.

4.2 Fuzzy Logic Control

“As the complexity of a system increases, our ability to make precise and yet significant statements about its behavior diminishes until a threshold is reached beyond which precision and significance (or relevance) become almost mutually exclusive characteristics” [4.65].

-Lotfi A. Zadeh

Fuzzy logic control was first introduced by Mamdani [4.63] and is based on Zadeh’s theory of fuzzy sets [4.64-4.65]. Earlier experimentation has revealed that Fuzzy logic control (FLC) produces superior results compared to results yielded from conventional control algorithms in

situations where it is hard to obtain the system model [4.82]. Their design involves using special purpose software products such as Fuzzy logic tool box and SIMULINK [4.88]. Once a development is finalized, the fuzzy algorithm is converted into a computer program or code written in one of the programming languages, such as C, C++, Pascal, FORTRAN, MATLAB, etc. Then the program or the code is imported into the application environment. If the environment is a computer program or a software package, then fuzzy algorithm is embedded. If the environment is digital hardware such as VLSI chips, then fuzzy algorithm is downloaded on digital platforms. If the hardware is an analog device, then the fuzzy algorithm is implemented by circuitry design [4.87].

4.2.1 Fuzzy Knowledge based Control (FKBC)

The basic structure of a fuzzy logic controller consists of fuzzification module (linguistic terms), knowledge base (if-then rules and database), inference engine (decision making logic), and defuzzification module (output interface). The block diagram of a fuzzy logic controller is shown in Figure 4.2.

4.2.1.1 Fuzzification module. Fuzzification module is an interface between the set of crisp values of the current process and the fuzzy inference engine. It could be defined as pointwise mapping from a real valued observed input space to a fuzzy set. The Fuzzification module FM-F1 and FM-F2 performs the following functions [4.66]:

- FM-F1: Perform a scale transformation to have a normalized universe of discourse. When a non-normalized domain is used then there is no need for FM-F1 module.
- FM-F2: Performs the point wise mapping of the crisp values of the current process state variable into fuzzy sets.

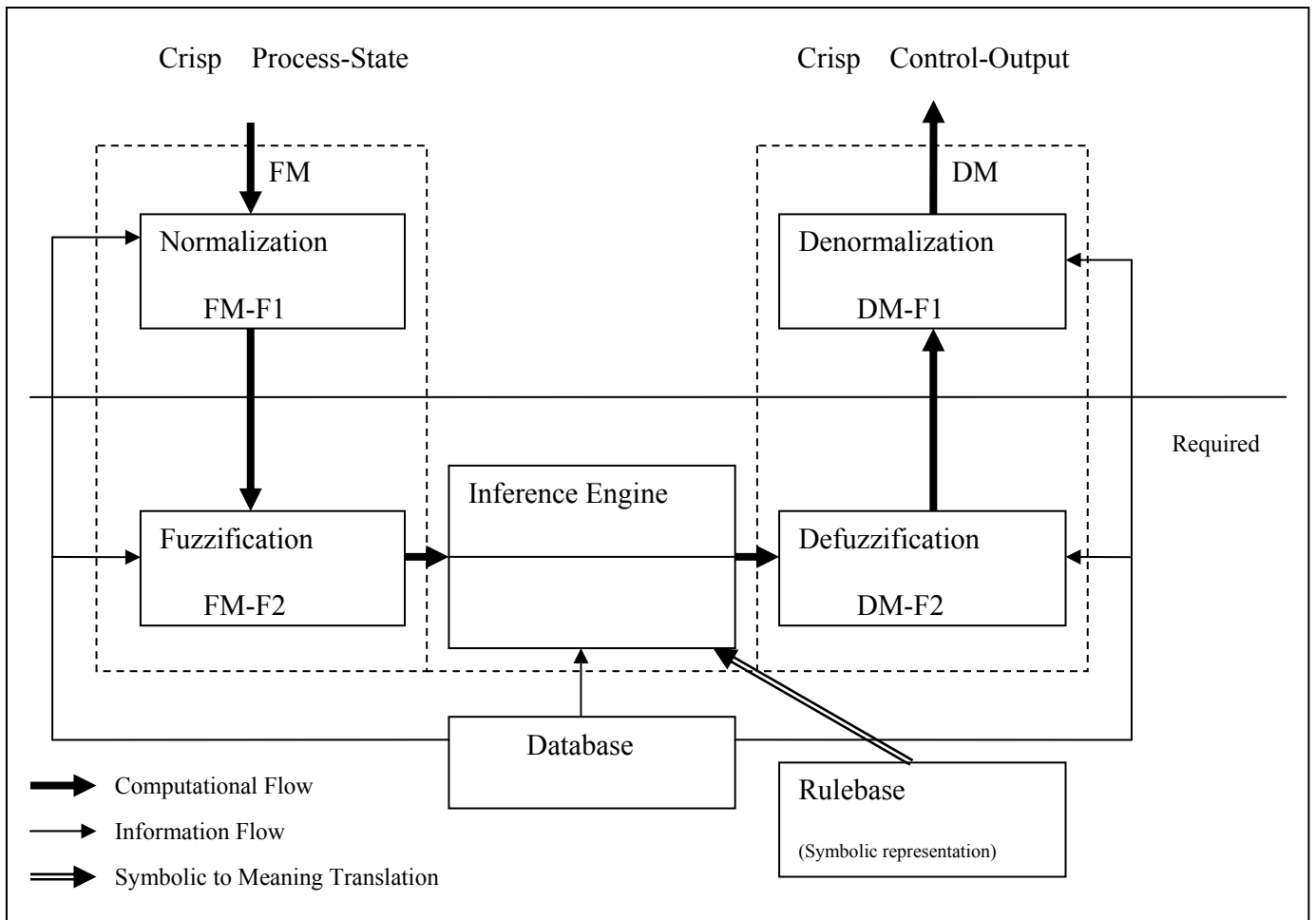


Figure 4.2 Block Diagram of Fuzzy Logic Controller [Redrawn from 4.66]

The design of Fuzzification module or Fuzzification strategy is based on the choice of inference mechanism chosen [4.66]. The inference mechanism can either be composition-based inference or individual rule-based inference (explained in section 4.3.3). There are three major fuzzifiers [4.70] namely Singleton, Triangular, and Gaussian Fuzzifier. Singleton Fuzzifier is mostly used in control applications but Triangular and Gaussian fuzzifiers presents their on training and filtering capabilities. For detailed explanation see [4.66-4.70]. The membership functions of these fuzzifiers can be defined for a real valued point $\mathbf{x}^* \in U \subset R^n$ mapped to a fuzzy set F in U as

- Singleton Fuzzifier:

$$\mu_F(\mathbf{x}) = \begin{cases} 1 & \text{if } \mathbf{x} = \mathbf{x}^* \\ 0 & \text{otherwise} \end{cases} \quad (4.4)$$

- Triangular Fuzzifiers:

$$\mu_F(\mathbf{x}) = \begin{cases} \left(1 - \frac{|\mathbf{x}_1 - \mathbf{x}_1^*|}{b_1}\right) \otimes \dots \otimes \left(1 - \frac{|\mathbf{x}_n - \mathbf{x}_n^*|}{b_n}\right) & \text{if } |\mathbf{x}_i - \mathbf{x}_i^*| \leq b_i, i = 1, 2, 3 \dots n \\ 0 & \text{otherwise} \end{cases} \quad (4.5)$$

- Gaussian Fuzzifiers

$$\mu_F(\mathbf{x}) = e^{-\left(\frac{|\mathbf{x}_1 - \mathbf{x}_1^*|}{a_1}\right)^2} \otimes \dots \otimes e^{-\left(\frac{|\mathbf{x}_n - \mathbf{x}_n^*|}{a_n}\right)^2} \quad (4.6)$$

where a_i and b_i are positive parameters and \otimes is t-norm used as algebraic product.

4.2.1.2. Knowledge base. The knowledge base of FLC consists of database and the rule-base.

4.2.1.2.1 Database. The database has essential information required for the functioning of fuzzification module, rule-base, and defuzzification module. Details include:

- i. Normalization of universe of discourse.
- ii. Fuzzy partition of input and output spaces.
- iii. Choice of membership function of a primary fuzzy set.

4.2.1.2.2 Rule-Base. The rule-base represents the control strategy of the expert (in our case control engineer). A fuzzy rule-base consists of a set of fuzzy IF-THEN rules. [For details see Appendix G]. Features of a rule-base are

- i. Choice of input and output variable.
- ii. Source and derivation of fuzzy control rules.
- iii. Consistency, interactivity and completeness of fuzzy control rules.

Definition [4.70]:

“A set of fuzzy IF-THEN rules is complete if $(\forall) \mathbf{x} \in U, (\exists)$ at least one rule in the fuzzy rule-basis in the form of generalized modus ponens i.e. $\mu_G(y) = \sup_{\mathbf{x} \in U} t|\mu_F(\mathbf{x}) \otimes \mu_{R^i}(\mathbf{x}, y)|$, such that $|\mu_{F^k}(x_i) \neq 0, (\forall) i = 1, 2, \dots, n|$.”

To explain the formation of a rule base, an example of a two input, one output fuzzy controller with $U = U_1 \times U_2 = [0 \ 1] \times [0 \ 1]$ and $V = [0 \ 1]$, is considered. For a controller, the error e between the processing and its reference point is one of the input variables and is partitioned into fuzzy sets: N_I, Z_I , and P_I . Similarly the change in error ce is defined through N_2, Z_2 , and P_2 . The output variable of the FLC u which is the control input to the system (plant) obtained through the fuzzy controller processing of e and ce is represented through NL, NS, Z, PS , and PL . The membership function for the first input variable, error ‘e’ is drawn in Figure 4.3 a.

The membership function for the second input variable, change in error ‘ce’ is drawn in Figure 4.3 b.

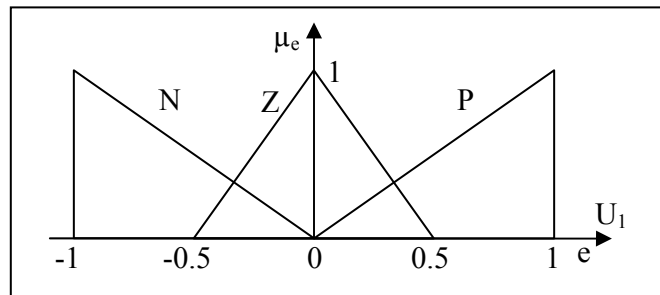


Figure 4.3. a Membership Functions of the Variable e [4.70]

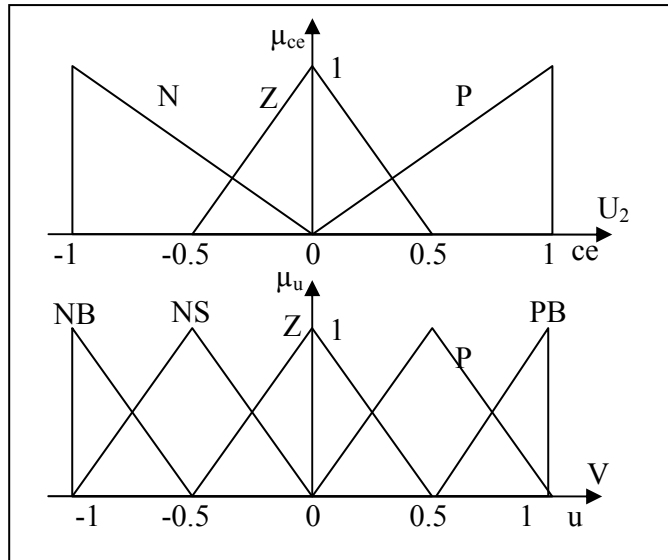


Figure 4.3. b Membership Functions of the Variable ce and du [4.70]

The control action could then be described in linguistic terms through the following fuzzy set of fuzzy IF-THEN rules.

$$\begin{aligned}
 R^1: & \text{ IF } e \text{ is } N \text{ and } ce \text{ is } N, \text{ THEN } u \text{ is } PL \\
 R^2: & \text{ IF } e \text{ is } N \text{ and } ce \text{ is } Z, \text{ THEN } u \text{ is } PS \\
 R^3: & \text{ IF } e \text{ is } N \text{ and } ce \text{ is } P, \text{ THEN } u \text{ is } Z \\
 R^4: & \text{ IF } e \text{ is } Z \text{ and } ce \text{ is } N, \text{ THEN } u \text{ is } Z \\
 R^5: & \text{ IF } e \text{ is } Z \text{ and } ce \text{ is } Z, \text{ THEN } u \text{ is } Z \\
 R^6: & \text{ IF } e \text{ is } Z \text{ and } ce \text{ is } P, \text{ THEN } u \text{ is } Z \\
 R^7: & \text{ IF } e \text{ is } P \text{ and } ce \text{ is } N, \text{ THEN } u \text{ is } Z \\
 R^8: & \text{ IF } e \text{ is } P \text{ and } ce \text{ is } Z, \text{ THEN } u \text{ is } NS \\
 R^9: & \text{ IF } e \text{ is } P \text{ and } ce \text{ is } P, \text{ THEN } u \text{ is } NL
 \end{aligned}
 \tag{4.7}$$

The above rules are tabulated in Table 4.2 as Rule base.

Table 4.2 Rule Base

$\downarrow e$ \xrightarrow{ce}	N	Z	P
N	1. PL	2. PS	3. Z
Z	4. Z	5. Z	6. Z
P	7. Z	8. NS	9. NL

4.2.1.3 Inference engine. A fuzzy inference engine serves as the medium of combining the fuzzy IF-THEN rules from the rule-base into mapping of one fuzzy set F_1 in U_1 to another fuzzy set F_2 in U_2 using fuzzy logic principles. Fuzzy Inference of a set of rules can be performed in two ways: Composition-based inference and Individual rule-based inference.

i.. Composition based inference: In this inference mechanism, the rule-base is represented as a single fuzzy IF-THEN rule by a fuzzy relation over the universal fuzzy sets U and V . There are two combination approaches in the literature for the implication of the set of rules; Mamdani and Gödel combinations [4.66]. Mamdani consider the rules as independent conditional statement. Rules can be combined through union operator where U is any s-norm and this combination is known as Mamdani combination, can be represented as [4.66]

$$\tilde{F}_M = \bigcup_{l=1}^N \tilde{F}_M(k) \quad (4.8)$$

Gödel consider the rules as strongly coupled conditional statement. Rules can be combined through intersection operator where \cap is any t-norm and this combination is known as Gödel combination, can be represented as [4.66]

$$\tilde{F}_G = \bigcap_{l=1}^N \tilde{F}_G(k) \quad (4.9)$$

Due to lack of computational efficiency, the composition-based inference engine is not commonly used in control applications.

ii. Individual-rulebased inference: In this inference mechanism, the output of the inference engine is the combination of the individual output fuzzy sets determined by each fuzzy rule. The brief computational procedure is as follows [4.70]:

a. For the n fuzzy rules, the membership function is determined by

$$\mu_{F_1^k \times F_2^k \times \dots \times F_n^k}(\mathbf{x}_1, \mathbf{x}_2, \dots, \mathbf{x}_n) = \mu_{F_1^k}(\mathbf{x}_1) \otimes \mu_{F_2^k}(\mathbf{x}_2) \otimes \dots \otimes \mu_{F_n^k}(\mathbf{x}_n) \quad (4.10)$$

where

\otimes : represents a t-norm operation

$F_1^k \times F_2^k \times \dots \times F_n^k$: is a fuzzy relation in $U = U_1 \times U_2 \times \dots \times U_n$.

b. Determine $\mu_{F_1^k \times F_2^k \times \dots \times F_n^k}$ according to Mamdani implication or any other implications used in the literature

c. Compute the output fuzzy set G in V for input fuzzy set F in U for each rule according to generalized modus ponens [4.66]. For details see [4.66-4.70].

$$\mu_G(y) = \sup_{\mathbf{x} \in U} \left| \mu_F(\mathbf{x}) \otimes \mu_{R'}(\mathbf{x}, y) \right| \quad (4.11)$$

where

$\mu_{R'}$: Membership functions of individual rule.

d. Thus the inference engine output would be combination of n fuzzy sets (G_1, G_2, \dots, G_n) represented either by union or intersection of each set as [4.66]

$$\mu_G (y) = \mu_{G_1} (y) \oplus \mu_{G_2} (y) \oplus \dots \oplus \mu_{G_n} (y) \quad (4.12)$$

Or it can be represented as

$$\mu_G (y) = \mu_{G_1} (y) \otimes \mu_{G_2} (y) \otimes \dots \otimes \mu_{G_n} (y) \quad (4.13)$$

where \oplus and \otimes represents the operator(s) s - norm and t -norms, respectively.

4.2.1.4 Defuzzification module. Defuzzification module is an interface between the values of fuzzy sets at the output to the physical world of crisp sets. In order to obtain a crisp value, defuzzification performs an output denormalization, which maps the point wise value of control output to its physical domain. Desirable features of a defuzzification method are [4.66]

- i. Continuity
- ii. Disambiguity
- iii. Plausibility
- iv. Algorithmic Complexity
- v. Multiple considerations of rules.

Often used methods of defuzzification are as follows [4.66]:

- i. *Center of gravity / Center of area method (COA):*

COA method defines the defuzzification value of fuzzy set F as its fuzzy centroid.

$$U^* = \frac{\int u F (u) du}{\int_u F (u) du} \quad (4.14)$$

Figure 4.4 shows this method graphically.

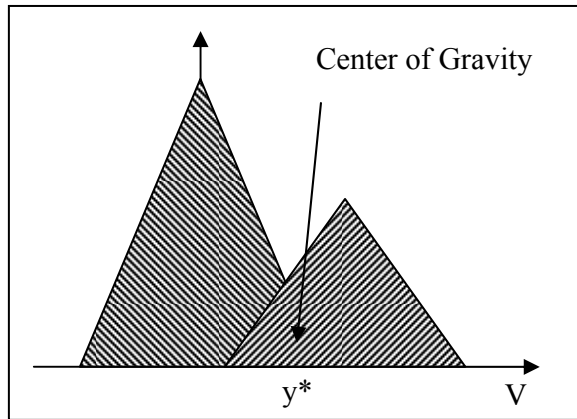


Figure 4. 4 Center of Gravity Defuzzifier [4.66]

ii. *Center of Sums method (COS):*

COS is similar to COA but a faster method with an added feature of multiple consideration of rules. Figure 4.5 shows this method graphically. Center-of-Sums is mathematically given by

$$U^* = \frac{\sum_{i=1}^{\ell} u_i F(u_i)}{\sum_{i=1}^{\ell} F(u_i)} \quad (4.15)$$

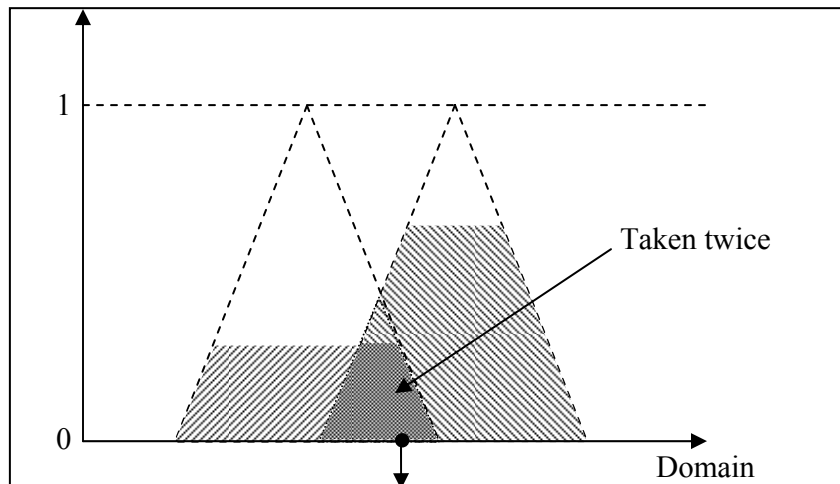


Figure 4. 5 A Graphical Representation of the Center-of-Sums Defuzzification Method [4.66]

iii. *Mean of Maxima method (MOM)*:

MOM method determines the defuzzified value as a mean of all values of universe of discourse having maximal membership grades [4.66].

$$y^* = \frac{1}{q} \sum_{j \in J^*} y_j \quad (4.16)$$

where

J^* is set of elements of y which attain the maximum value of $F(y)$

q is the cardinality of J^* .

4.2.2 Tuning of Scaling Factors through Applied Genetic Algorithm

Unlike classical control systems, involving precise mathematical analysis, Fuzzy logic control (FLC) entails a non-analytic approach [4.66]. Fuzzy control systems require a method of approximate reasoning resembling the process of decision-making performed by human beings. Typically, design of a fuzzy system involves, consulting an expert and formulating the implicit knowledge of the underlying process into a set of linguistic variables and fuzzy rules for complex control systems. The development of fuzzy knowledge base is based on trial and error approach. To surmount these limitations many researches have proposed to combine FLC with other intelligent schemes and no doubt there were many successful attempts also [4.81-4.87]. This research also aims to provide a suitable and efficient technique to enhance the interpretability in Genetic algorithm based fuzzy logic controllers.

Unlike neural network, generic fuzzy systems are unable to learn from data. However; several techniques have been proposed to extract fuzzy rules from training data gathered from

observation of the control strategy [4.75]. The majority of applications in the domain of genetic-Fuzzy systems are concerned with the optimization of fuzzy logic controllers [4.75-4.87]. Genetic algorithms have been used by many researchers [4.77-4.87] who alter membership function in response to the changes of task environment to produce more for fuzzy logic control. The fuzzy logic controller model is developed in Simulink. Figure 4.6 shows the block diagram of a GA-based adaptive fuzzy logic controller.

In this work, FLC is designed with 25 rules. The justification of the choice of number of rules is given in section 4.3.1. The fuzzy systems are implemented in a digital computer domain which involves a simulation environment i.e. SIMULINK. Afterwards FLC is implemented into the dynamic model of PV developed earlier. A computer program is then written for applied Genetic Algorithm to obtain optimal values of FLC parameters in the MATLAB environment. Genetic Algorithms performs an intelligent search for a solution from a very large number of possible solutions. Thus the chances of converging to local minima have been reduced and global optimum can be approached with higher probability. Thus, it has been tried to enhance the performance of FKBC Controller for the proper load matching of PV model for stand-alone application.

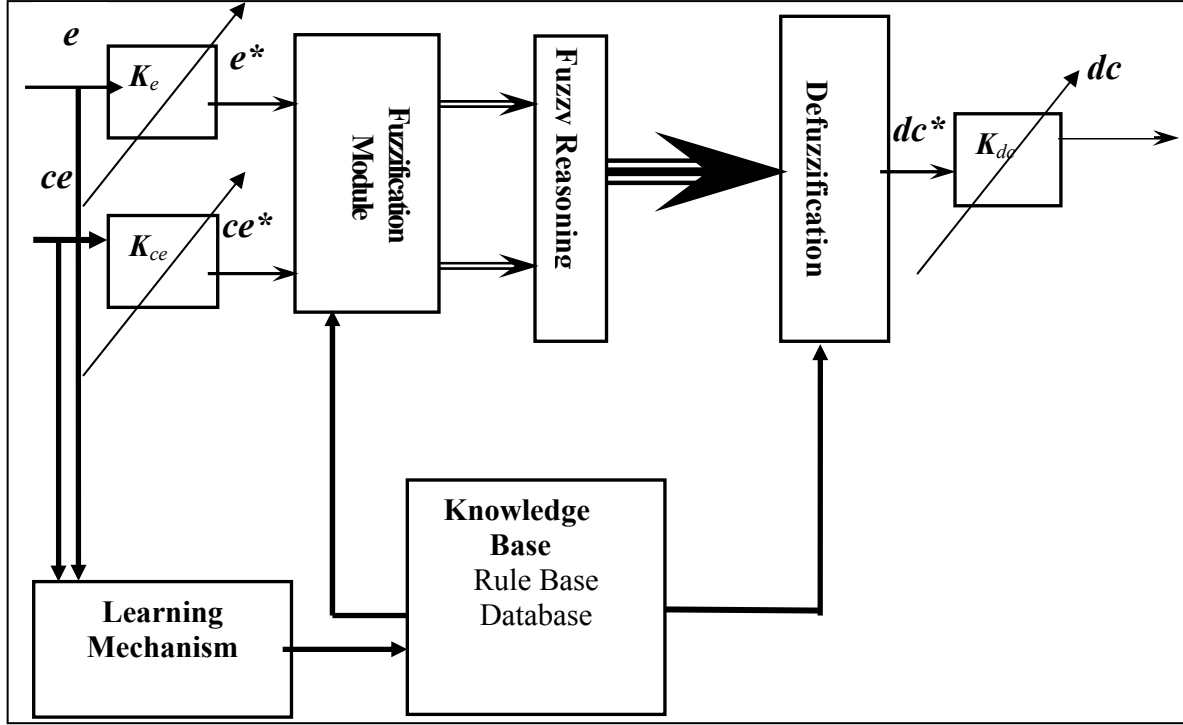


Figure 4. 6 GA Based Adaptive Fuzzy Logic Control Scheme

Various learning mechanism have been applied on different type of tuning application for Fuzzy Knowledge Base Controller (FKBC) exists in the literature. For this research work a modification to the Sung's [4.86] Genetic Algorithm (GA) is applied which has been proposed by the author in [4.87]. The proposed GA utilizes the weighted crossover operator. A fitness function, which guides the evolution process, has been defined as inverse of Integral Absolute Time Error, calculated as [4.87]

$$IATE = \int_0^t |e| dt \quad (4.17)$$

and the fitness of the function will be calculated as [4.87]

$$fitness = \frac{1}{IATE} \quad (4.18)$$

The proposed method is applied, for the tuning of input and output scaling factors of FKBC, for the load matching of the stand-alone PV system on a real-time basis.

4.2.2.1 Overview of genetic algorithm [4.87]. The Genetic Algorithm (GA) is a probabilistic computer driven search and optimization technique modeled after the mechanics of genetic evolution. [4.71-4.79]. GA's exploit objective function to execute random search instead of relying on calculating local derivatives for the search process like classical control optimization methods. GA's are also more likely to arrive at the global optima because they work on a population of points as opposed to conventional optimization techniques, which utilize a point-by-point search approach. Figure 4.7 shows the bit by bit mechanism of a typical GA.

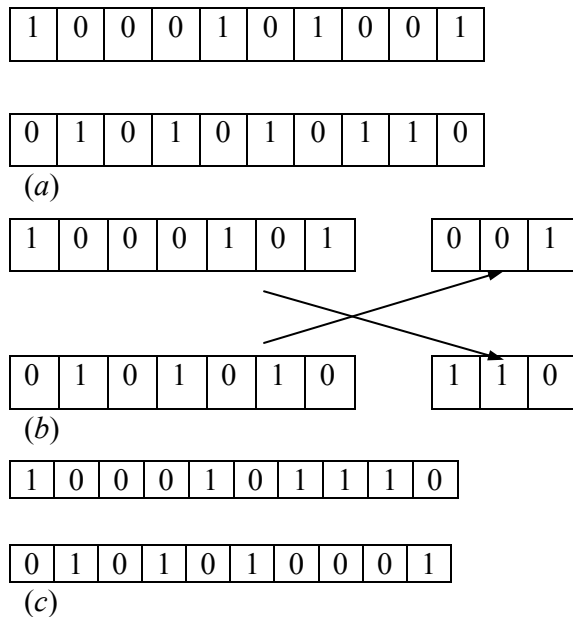


Figure 4.7 [4. 82] Crossover in String

- (a) Two strings are selected at random to be mated.
- (b) A random location in the strings is located (here the location is before the last three bit locations).
- (c) The string portions following the selected location are exchanged.

The three fundamental operators of GA are: reproduction (parent selection), crossover, and mutation. GA's are started with a set of solutions (represented by chromosomes) called population, generated randomly, and the evolutionary process of reproduction, crossover, and mutation are used to generate an entirely new population from the existing population. The reproduction operator selects good chromosomes in the population to form the mating pool. Selection of chromosome for parenthood can range from a totally random process to one that is biased by the chromosome fitness. The modified Queen Bee evolution operators are discussed in Section 4.3.3.2. Crossover operator is

used to exchange genetic materials between the parents with the aim of obtaining better chromosomes. Two parent chromosomes are selected from the mating pool randomly and the crossover rate determines the probability of producing a new chromosome from the parents. A number of crossover operators are discussed in the literature [4.82-4.85]. The crossover operators relevant to the investigations in this research are detailed in Section 4.3.3. The mutation operator is applied next. The mutation operator takes each child chromosome and randomly change some of its genes with a given mutation probability. Flipping a bit in the binary coded GA does mutation. While in non-binary coded GA, mutation involves randomly generating a new character in a specified position. Flowchart in Figure 4.8 gives a pictorial description of the mechanism of genetic algorithm.

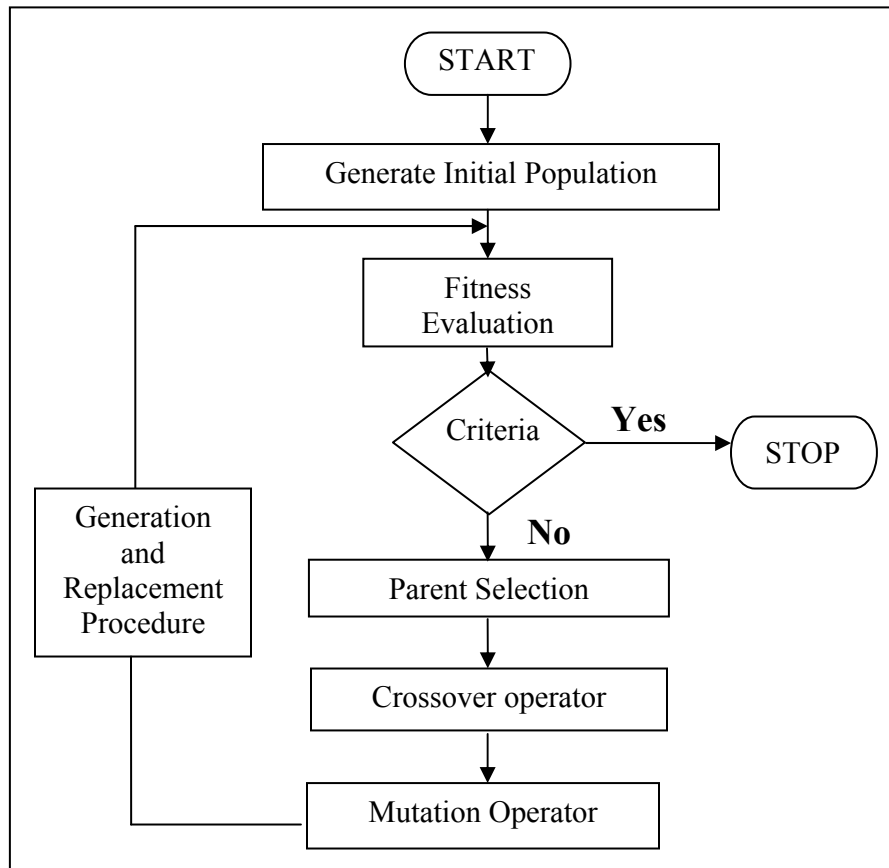


Figure 4. 8 Flowchart of Genetic Algorithm

4.2.2.2 Modified queen bee evolution (parent selection) [4.87]. The queen bee algorithm described in [4.86] is limited to a single pool (honeycomb). I have an advanced concept of modified queen bee algorithm that the bee algorithm should not be restricted to a single pool [4.87]. In nature honeycombs grow around queen bee, and if any queen bee evolves into a honeycomb, she will build another honeycomb by sharing the members from her parent honeycomb. The same concept is applied in proposing the modified queen bee algorithm. The schematic diagram of splitting of pools, generation by generation, with the availability of queen bee for modified bee genetic algorithm is shown in Figure 4.9.

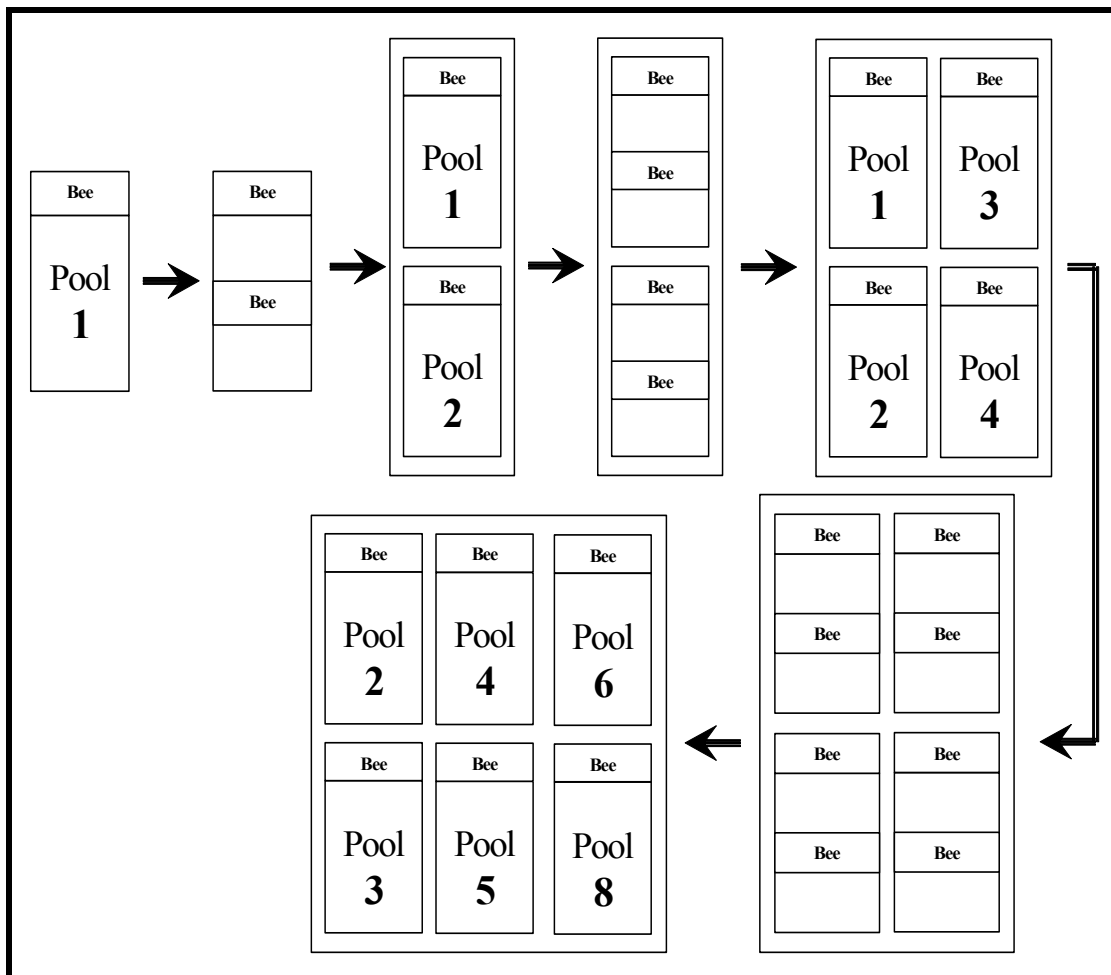


Figure 4. 9 Schematic Diagram of Splitting of Pools Generation by Generation in Modified Queen Bee Evolution [4.87]

Each member (solution) of the pool has to crossover with queen (most fitted solution) of the pool. After splitting the parent pool, due to the birth of queen bee (next most fitted solution), the above-mentioned mating process makes the specified population size of the pool. We identified the new queen in a pool if any solution has the fitness very close (say 98% or above) of the fitness of the mother queen.

4.2.2.3 Weighted base crossover operator [4.87]. The selection of gene in uniform crossover is purely random [4.82]. Each bit is typically crossed with one-half probability and one random value R is being evolved for every gene in the chromosome [4.81]. If R is more than the probability of uniform crossover, the corresponding bit in parent 1 is copied to child 2 and the corresponding bit in parent 2 is copied to child 1, otherwise the corresponding bit in parent 1 is copied to child 1 and the corresponding bit in parent 2 is copied to child 2.

Weighted base crossover operator gene selection is based on the weights assigned to the genes for crossover operation. Weighted base crossover operator enhances GA's performance by guiding it to search for more new state space [4.82]. The uniform crossover is a special case of weighted uniform crossover. In weighted uniform crossover, weights are assigned to each bit/gene in the chromosome according to the similarity of the test patterns in the population. Weighted uniform crossover is then performed, based on some probability which depends on the weights of the parent bits. The rules for Weight based crossover operator [4.87] are shown in Table 4.4

Table 4.3 Rules for WCO [4.87]

OPERATION	Bit/gene Weight of Parent 1	Bit/gene Weight of Parent 2
Same as uniform cross over	0	0
Assign bit of P1 to both C1&C2	0	1
Assign bit of P2 to both C1&C2	1	0
Same as uniform cross over	1	1

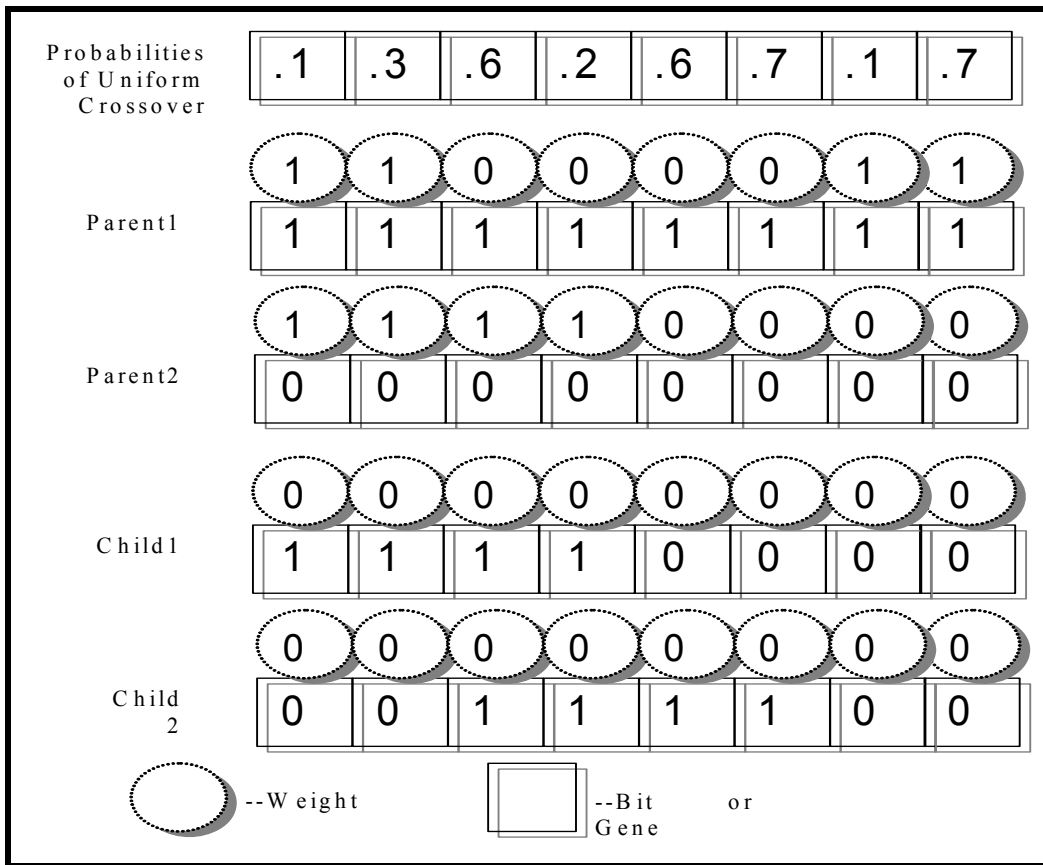


Figure 4.10 Schematic Representation of Weight Base Uniform Crossover [4.87]

For example, two parents P1 and P2 are selected to produce two child chromosomes C1 and C2. Each gene $G_{i,1}$ in parent P1 competes against the corresponding gene $G_{i,2}$ in parent P2. If $W_{i,1}$ is equal to $W_{i,2}$, the bits are crossed with a given probability as in uniform crossover. If $W_{i,1}$ and $W_{i,2}$ are different both the child chromosomes are assigned the value of the lighter bit, i.e., bit with weight 0, as shown in Figure 4.10.

The probability of crossover which varies between 0 and 1 and the values bit for weighted crossover which could be either 0 or 1 are chosen randomly to initialize the process.

The Genetic Algorithm based on modified queen bee evolution described above is compiled in an Algorithm as follows.


```

Algorithm 1:
//t: generation//, //n: population size in a pool//,
//pl: number of pools//, //P: populations//,
//plmax: maximum number of pools//
//ξ: normal mutation rate//,
//pm: normal mutation probability//,
//p'm: strong mutation probability//,
//Iq: a queen bee//, //Im: selected bee//
1  t ← 0: pl(t) ← 1; initialize P{pl(t)}; evaluate P{pl(t)}
2  while 1 (not terminate condition)
3  do
4      t ← t+1
5      while 2 [pl(t)]
6      do 2
7          select P{pl(t)} from P{pl(t-1)(*)}
8          P{pl(t)}=[ Iq{pl(t-1)} , Im{pl(t-1)} ]
9          recombine P{pl(t)}; do crossover; do mutation (*)
10         for i=1 to n
11             if i ≤ (ξ×n)
12                 do mutation with pm
13             else
14                 do mutation with p'm
15             end if
16         end for
17         evaluate P{pl(t)}; search for new_Iq{pl(t)}
18         if ( new_Iq{pl(t)} found )
19             split the pool and new_pl(t) ← pl(t)+1
20         else
21             new_pl(t) ← pl(t)
22         end if
23         if (new_pl(t) > plmax)
24             pl(t) ← plmax (oldest pool deleted)
25         end if
26     end while2
27 end while1

```

4.3 Modeling and Simulation

In order to incorporate the heuristic knowledge of the operation of the PV system to FKBC, knowledge base has to be developed to be used by the inference engine.

4.3.1 FKBC Design Parameters

The Knowledge base of FKBC consists of Rule-based and database. The rule-base for a FKBC can be developed by the observation of error and change of error of the system. Further, these rules have to be associated with the proper membership functions.

The relationship between the duty cycle and the input and output voltage of the dc-dc boost converter is analyzed in Appendix H and obtained in Equation H.10 as

$$V_o = \frac{V_i}{1-D} \quad (4.19)$$

where

V_o : Input voltage of DC-DC converter also termed as V_{Boost} .

V_i : Input voltage of DC-DC converter also termed as $V_{\text{PV,out}}$.

D : Duty cycle of the converter.

From Figure 4.1, these variables at the DC-DC converter can be correlated with the variables at the Controller as

V_{ref} : The reference voltage is the step input to the controller.

V_{Boost} : Transient response of V_{out} .

$D(k)-D(k-1)$: Change in duty cycle is the controller output.

It can be inferred from Equation 4.19 that for smaller values of duty cycle the boost voltage will be larger and as the value of duty cycle increases, the output boost voltage will start decreasing. As mentioned earlier that error 'e' defined as $e(k) = V_{\text{ref}} - V(k)$ and the change of error 'ce' defined as $\Delta e(k) = e(k) - e(k-1)$ are the input to the fuzzy logic controller. The change in the

control output i.e. change in duty cycle ‘dc’ is $\Delta dc(k) = dc(k) - dc(k - 1)$, where k is the $k - th$ sampling time.

A dc-dc boost converter model is developed in Simulink and is embedded into the overall system model as shown in Appendix I. The underlying theory of dc-dc converter modeling is explained in Appendix H. A block diagram of dc-dc boost converter is shown in Figure 4.11.

The error ‘e’ $e(k) = V_{ref} - V_{boost}(k)$ is calculated and change of error ‘ce’ is also computed.

In FKBC, the error e between the processing point and a set point in one of the input variables is partitioned into fuzzy sets: NB, NS, ZE, PS, and PB as shown in Figure 4.12. Similarly the change in error ce is classified as NB, NS, ZE, PS, and PB. The output variable dc of FLC, which is defined as the change in the duty cycle for dc-dc converter, is classified in terms of controller output as NB, NM, NS, ZE, PS, PM, and PB. Five fuzzy set is a good choice between the explosion of fuzzy rules and high descritization [4.78]. The performance of the controller can be further enhanced by using finer fuzzy partitioned sub space. This will result in having more control rules. The number of fuzzy rules increases exponentially with the increment in the number of fuzzy sets. This phenomenon is termed as explosion of rules [4.63]. With a larger number of partitions, the resolution of the controller output will improve. However, this will be achieved at the cost of

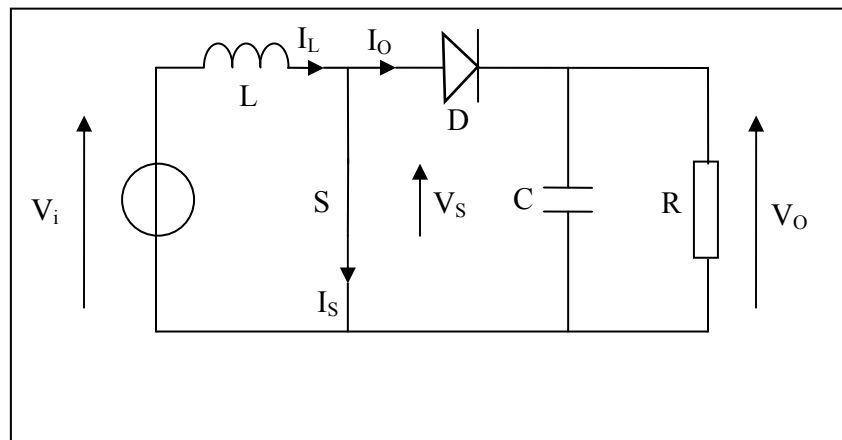


Figure 4.11 Schematic Diagram of a DC-DC Boost Converter with Switch S Closed [4.70]

computational complexity and realization through a larger hardware. A compromise is made by the observation of the precision of solutions.

The reference voltage for simulation purposes is assumed as 25 V. The membership functions are partitioned in the range of -1 to 1. These membership function can also be defined from $-V_{ref}$ to $+V_{ref}$ (-25 to +25) instead. However, in that scenario a total of 34 (17*2) parameters are required to be tuned and moreover, such a membership function would be valid only for this particular scenario. For instance, if two such devices are connected in series, membership function will not remain valid and a new membership function with $-V_{ref} = -50$ V to $+V_{ref} = +50$ V as universe of discourse has to be developed and again 34 parameters has to be tuned. To address this issue, the membership functions are partitioned with a universe of discourse as -1 to 1 and scaling factors are introduced to normalize the input and output variables. The scaling factors for error, change in error and change in duty cycle are assumed as K_e , K_{ce} and K_{dcu} . Thus, only 3 parameters need to be tuned with same rule-based and same membership function for all possible scenarios.

As mentioned earlier, tuning of the scaling factors is required to normalize the values of the variables. Various learning mechanism have been applied on different type of tuning application for Fuzzy Knowledge Base Controller (FKBC) exists in the literature [4.83]. For this application, a learning mechanism is required that can exploit all the possible values of the scaling factors so as to compute the accurate normalizing factor for the input and output variables. A fitness function, which guides the evolution process, has been defined as inverse of Integral Absolute Time Error, calculated as [4.87]:

$$IATE = \int_0^t |e| dt \quad (4.17)$$

and the fitness of the function will be calculated as [4.87]:

$$fitness = \frac{1}{IATE} \quad (4.18)$$

To obtain the optimum value of the objective function genetic algorithm is implemented so as to improve the fitness. Genetic algorithm's (GA) exploit objective functions to execute random search instead of relying on calculating local derivatives for the search process like classical control optimization methods. GA's are also more likely to arrive at the global optima because they work on a population of points as opposed to conventional optimization techniques, which utilize a point-by-point search approach. Figure 4.7 shows the bit-by-bit mechanism of a typical GA.

With the introduction of the scaling factors the input and output variables can be termed as; error ' $e^*(k) = k_e \times e(k)$ ', change in error ' $ce^*(k) = k_{ce} \times ce(k)$ ', and the change in duty cycle ' $d_{dcu}(k) = k_{dcu} \times d_{dcu}^*(k)$ '. Thus, the final control is a rule-base of IF $e^*(k)$ is...AND $ce^*(k)$ is...THEN dcu^* is...

For the premise part, Gaussian membership function is chosen which has continuous characteristics [4.78].

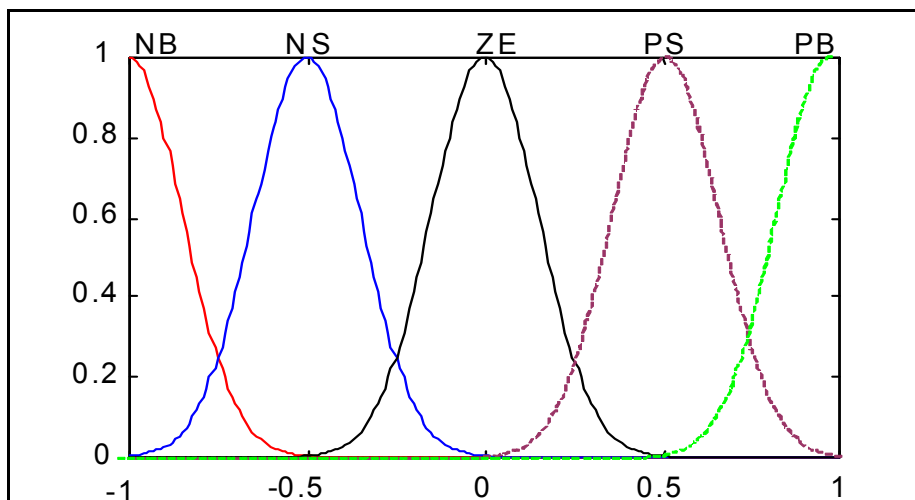


Figure 4.12 Gaussian Membership Functions for Inputs e^* & ce^*

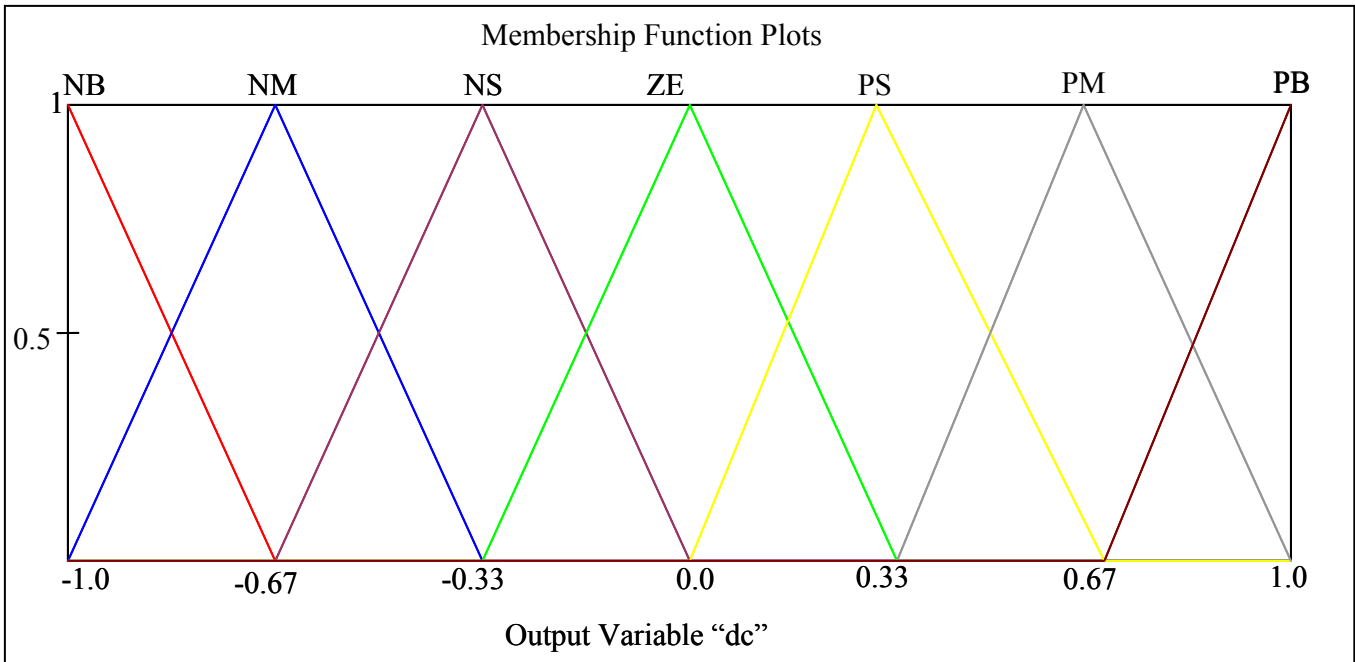


Figure 4.13 Triangular Membership Functions for Output dc^*

The output equation can be expressed in terms of membership function parameters, i.e. area and centroid of the membership function. To represent the control output equation in closed form, a perfect choice for the consequent part will be triangular membership function [4.78]. Hence, for output variable, triangular membership function has been taken with its universe of discourse normalized as $(-1 \leq dc \leq 1)$ as shown in Figure 4.13.

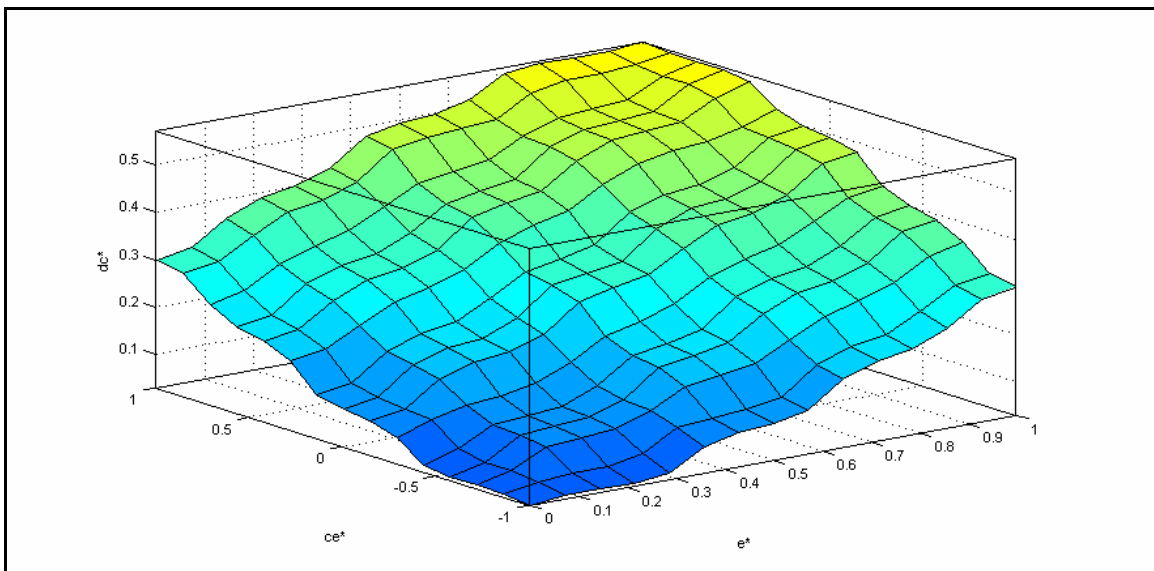


Figure 4.14 Surface of the Fuzzy Membership Function

Table 4.4 Rule-Base for FKBC

e^* ↓ ce^* →	NB	NS	ZE	PS	PB
NB	1. NB	2. NB	3. NM	4. NS	5. ZE
NS	6. NB	7. NM	8. NS	9. ZE	10. PS
ZE	11. NM	12. NS	13. ZE	14. PS	15. PM
PS	16. NS	17. ZE	18. PS	19. PM	20. PB
PB	21. ZE	22. PS	23. PM	24. PB	25. PB

An overall fuzzy surface for membership functions is shown in Figure 4.14

The rule-base (Table 4.3) for a controller works by monitoring error (e^*) and change in error (ce^*), which are the antecedent variables with NB, NS, ZE, PS, and PB as entries of fuzzy sets. Entries in the table are fuzzy sets associated with consequent variable dcu^* .

Thus, the rules can be read as

- R^1 : IF e^* is **NB** and ce^* is **NB** THEN dc^* is **NB**
 R^2 : IF e^* is **NB** and ce^* is **NS** THEN dc^* is **NB**
 R^3 : IF e^* is **NB** and ce^* is **ZE** THEN dc^* is **NM**
 R^4 : IF e^* is **NB** and ce^* is **PS** THEN dc^* is **NS**
 R^5 : IF e^* is **NB** and ce^* is **PB** THEN dc^* is **ZE**
 R^6 : IF e^* is **NS** and ce^* is **NB** THEN dc^* is **NB**
 R^7 : IF e^* is **NS** and ce^* is **NS** THEN dc^* is **NM**
 R^8 : IF e^* is **NS** and ce^* is **ZE** THEN dc^* is **NS**
 R^9 : IF e^* is **NS** and ce^* is **PS** THEN dc^* is **ZE**
 R^{10} : IF e^* is **NS** and ce^* is **PB** THEN dc^* is **PS**
 R^{11} : IF e^* is **ZE** and ce^* is **NB** THEN dc^* is **NM**
 R^{12} : IF e^* is **ZE** and ce^* is **NS** THEN dc^* is **NS**
 R^{13} : IF e^* is **ZE** and ce^* is **ZE** THEN dc^* is **ZE**
 R^{14} : IF e^* is **ZE** and ce^* is **PS** THEN dc^* is **PS**
 R^{15} : IF e^* is **ZE** and ce^* is **PB** THEN dc^* is **PM**
 R^{16} : IF e^* is **PS** and ce^* is **NB** THEN dc^* is **NS**
 R^{17} : IF e^* is **PS** and ce^* is **NS** THEN dc^* is **ZE**
 R^{18} : IF e^* is **PS** and ce^* is **ZE** THEN dc^* is **PS**
 R^{19} : IF e^* is **PS** and ce^* is **PS** THEN dc^* is **PM**
 R^{20} : IF e^* is **PS** and ce^* is **PB** THEN dc^* is **PB**
 R^{21} : IF e^* is **PB** and ce^* is **NB** THEN dc^* is **ZE**
 R^{22} : IF e^* is **PB** and ce^* is **NS** THEN dc^* is **PS**
 R^{23} : IF e^* is **PB** and ce^* is **ZE** THEN dc^* is **PM**
 R^{24} : IF e^* is **PB** and ce^* is **PS** THEN dc^* is **PB**
 R^{25} : IF e^* is **PB** and ce^* is **PB** THEN dc^* is **PB**

The “product-sum” inference mechanism is used for mapping the rule-base to the fuzzy set. The center-of-sums method is used for the defuzzification of the controller output.

4.3.2. Modeling of AGABFLC

In this dissertation, FLC and GAs are combined. GA is adopted for the tuning of FLC gain parameters K_e , K_{ce} , and K_{dc} . The function of K_e and K_{ce} is to scale down the value of error (e) and change of error (ce) within the range of Universe of Discourse for fuzzy partitioning of premise (antecedent) variables i.e. e and ce . K_{dc} is FLC controller output gain (since the universe of discourse for FLC output is -1 to $+1$, the defuzzified output will be within the range of -1 to $+1$) amplifies this range up to required level of process operation.

4.3.2.1. Initialization and learning. The reference voltage considered for simulation purpose as 25 V. The possible variation of output voltage could be from 0 to 25 V. Thus, the possible variation of error in voltage would be negative 25 to positive 25 which when normalized for universe of discourse of -1 to 1 will result in the range of -0.04 to 0.04 . A practically possible range of change in error in close proximity to the calculated range is thus considered for the error. Thus the possible order of the variation of the error is -10^{-3} to $+10^{-3}$. In a similar pattern, the variation of error is observed, normalized and a possible range is calculated for initializing the learning of GA for the change of error parameter. The output control parameter of the controller is based on the variation of the input duty cycle of the dc-dc converter. Theoretically, the input duty cycle can be varied from 0 to 1 but practical variation is from 0 to $2/3$ [4.90-4.91]. This fact

Table 4.5 Values of GA Parameters [4.87]

Parameters	Values
Crossover Probability (p_c)	0.8
Normal Mutation Probability (p_m)	0.01
Population Size	15x9=135
Individual Bit Length	10
Normal Mutation Rate (ξ)	0.6
Strong Mutation Probability (p'_m)	0.4
Maximum Number of Pools	9

is analyzed and explained in Appendix H. A smaller value of change in duty cycle will result in a slow response while a larger value will results in a very fast response which might not be desirable in order to avoid transient problems. This to be noted that these ranges are just to initialize the learning of the values of these parameters and the optimal value will be obtained through the learning of GA. Considering these facts, a range considered which is in close proximity of the possible limits. Thus, the range of gain parameters, for GA, to be tuned considered are $-0.001 \leq K_e \leq 0.001$, $10 \leq K_{ce} \leq 200$, and $0.01 \leq K_{dc} \leq 0.6$.

The optimal values for GA parameters for the tuning of FLC control parameters obtained through learning are tabulated in Table 4.5 [4.87].

The learning patterns for tuning the rules of the FKBC using the modified queen bee-based genetic algorithm is shown in Figure 4.15.

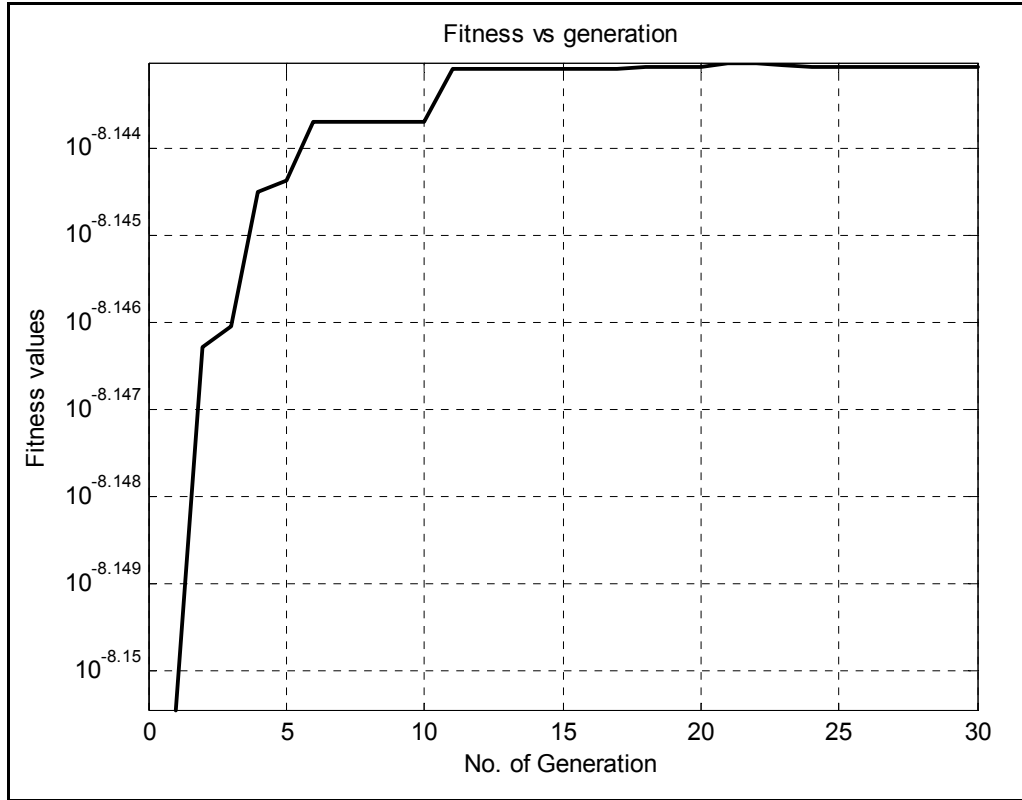


Figure 4.15 GA Based Learning Patterns for K_e , K_{ce} , and K_{dc}

The values of parameters $K_e=0.0479$, $K_{ce}=199.8045$, and $K_{dc}=0.0749$ are achieved in 21 generation with modified queen bee evolution with fitness value = 7.1941×10^{-9} and corresponding IATE = 1.3901×10^8 .

Once these parameters are tuned for the FKBC, the designed rule-base has the ability to take into account the changing weather condition. All other controllers like PI, PID, H_∞ control, VSC, etc., have failed due to the variation in the operating conditions; however, this is the beauty of the FKBC, it will never fail because of the heuristic knowledge base, though it may not necessarily perform optimally.

Table 4.6 Values of Tuned AGABFLC Parameters

Ke	0.04777126099706745
Kce	199.80449657869013
Kdc	0.07483870967741935
Fitness	$7.1940667600623175 \times 10^{-9}$
IATE	$1.3900343621378037 \times 10^8$

4.3.3 Simulation Results and Discussion

PV model developed earlier in Chapter 3 is implemented in this model. The specification of this PV module is given in Table 3.1. The pattern of variation of solar irradiance, ambient and cell temperature is shown in Figure 3.8 and Figure 3.9, respectively. Two scenarios are considered for simulation purpose. In the first case the load is considered as fixed and assumed a value of 30 ohm for simulation purpose and in the second scenario, the load is considered as variable and an optimum value of the load is being calculated on a real-time basis for achieving the instantaneous maximum power. The pattern of output current from PV array at MPP $I_{pvpanel}$ (indicated by black line) and load current I_{out} (indicated by blue line) for fixed and variable load are shown in Figure 4.16 and Figure 4.17 respectively. As it can be inferred from Figure 4.17 that the load current increases as the irradiance increases that lead to larger amount of power loss in the PV array and subsequently there is an increase in cell temperature. It can be further noticed that $I_{pvpanel}$ and I_{out} are different due to difference in the output voltage of the PV and the output voltage of the dc-dc converter (boost voltage) for approximately the same maximum power as shown in Figure 4.22.

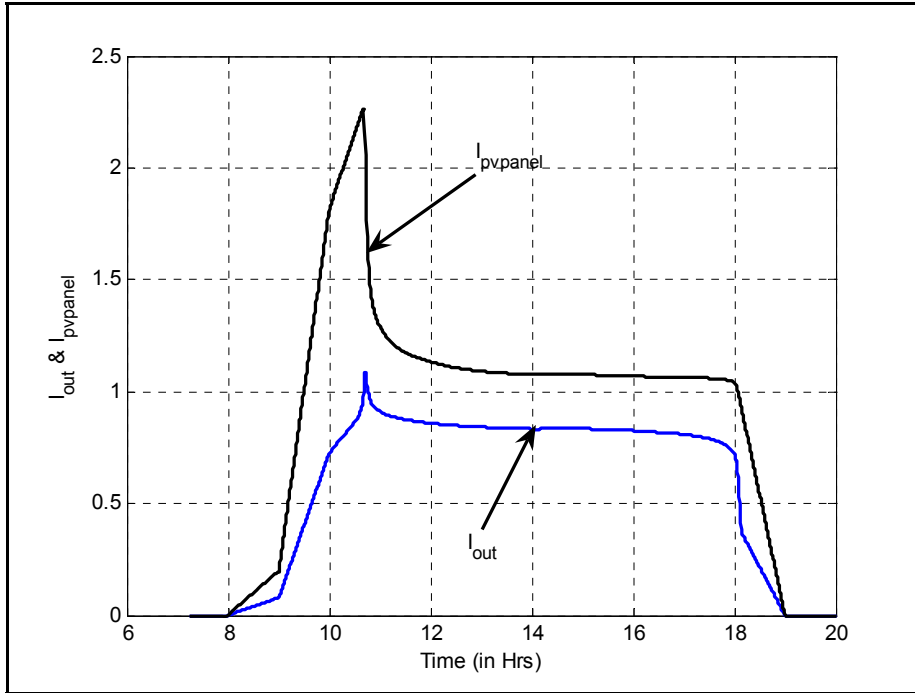


Figure 4.16 Pattern of the PV Panel Current and Actual Load Current with Fixed Load in a Day

The pattern of reference load voltage V_{ref} (indicated by red line), output voltage of PV array at MPP $V_{pvpanel}$ (indicated by black line) and load voltage V_{boost} (indicated by blue line) are shown in Figure 4.18 and Figure 4.19 for fixed and variable load respectively.

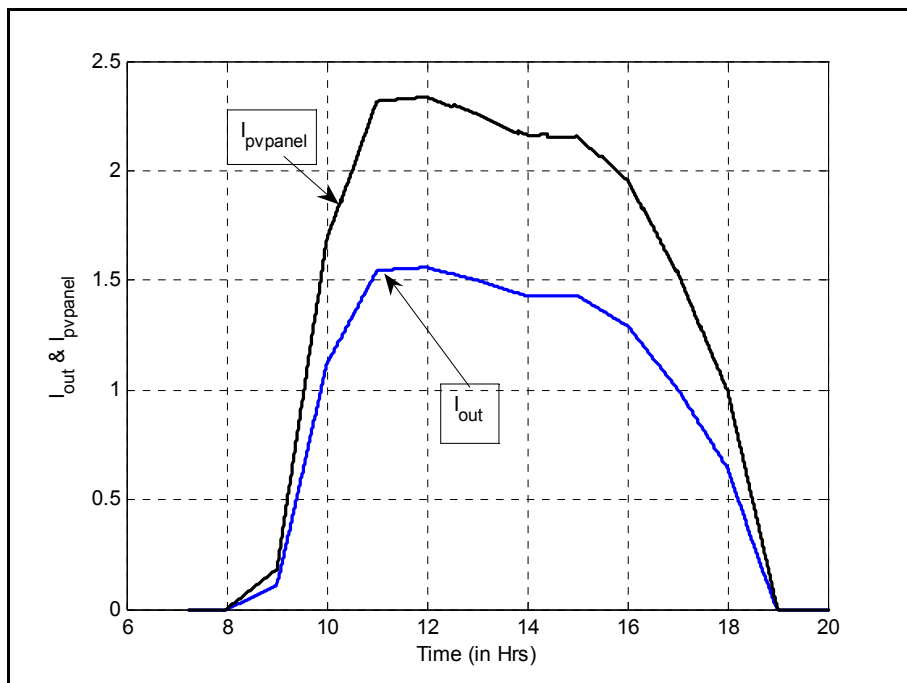


Figure 4.17 Pattern of the PV Panel Current and Actual Load Current with Variable Load in a Day

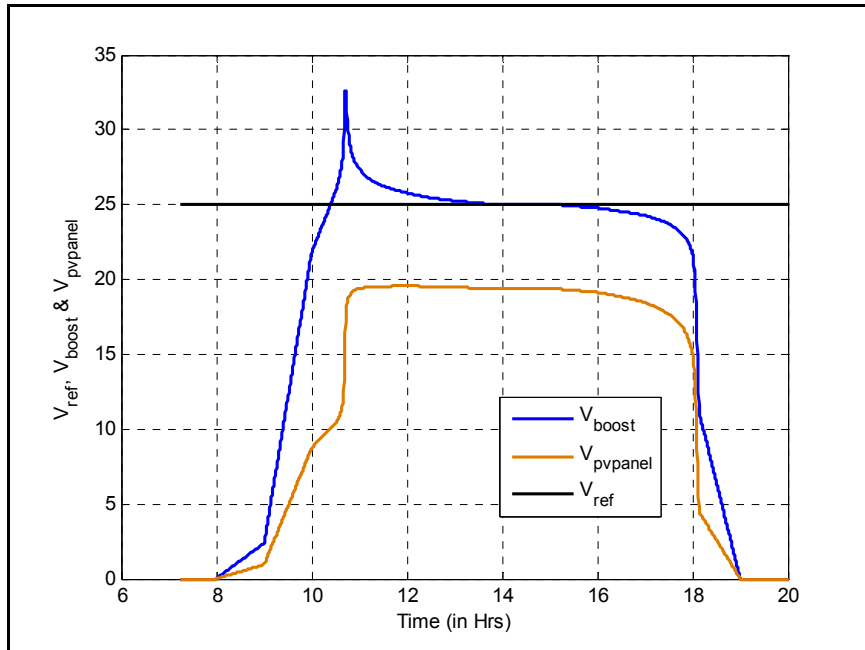


Figure 4.18 Ref. Load Voltage, Pattern of the PV Array Voltage, and the Boost Converter Voltage for Constant Load

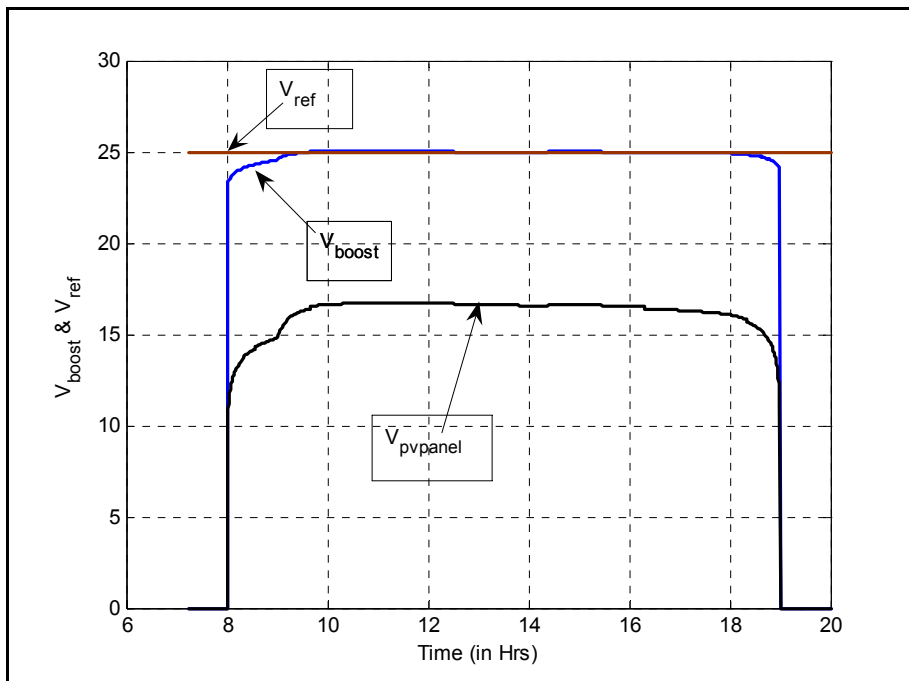


Figure 4.19 Ref. Load Voltage, Pattern of the PV Array Voltage, and the Boost Converter Voltage for Variable Load

As evident from Figures 4.18 and 4.19 that the error between V_{boost} and V_{ref} is quite significant, specially, during morning and evening, in case of fixed load scenario. The pattern of error for the fixed load condition can be observed in Figure 4.20. This is due to the reason that during these hours, MPPT need to match the relevant load according to available maximum power and thus, the PV is incapable to match the assumed fix load because of insufficient available power. This issue has been addressed by implementing the MPPT with the relevant variable load and thus the error is minimized as shown in Figure 4.21

4.3.3.1 AGABFLC simulation results. The pattern of error in voltage, with constant and variable loads is shown in Figures 4.20 and 4.21, respectively.

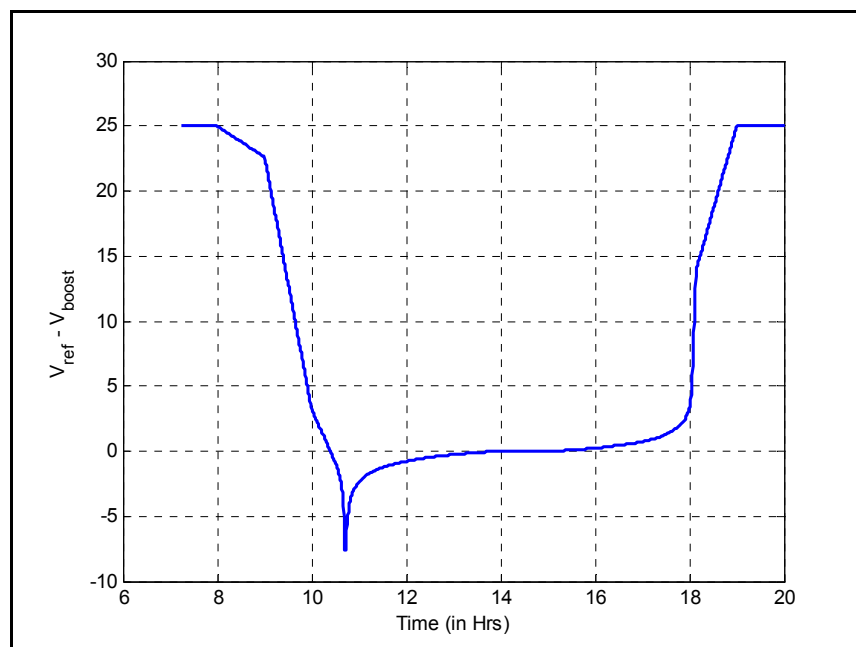


Figure 4. 20 Pattern of First Input of FLC Error Voltage with Fixed Load in a Day

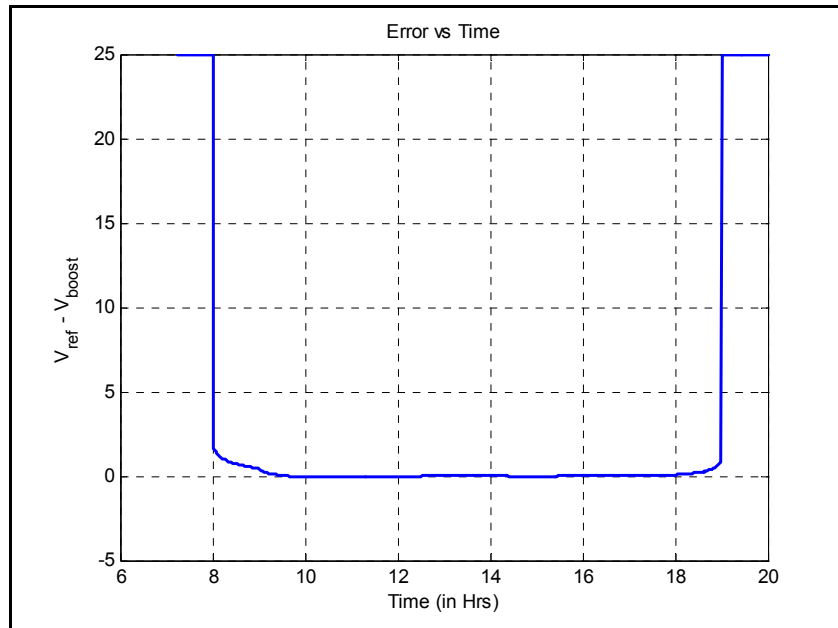


Figure 4. 21 Pattern of First Input of FLC Error Voltage with Variable Load in a Day

The pattern of change in error in voltage is shown in Figure 4.22. The output of the FLC is the change in duty cycle of DC-DC boost converter, integral of which is duty cycle. The pattern of duty cycle for fixed and variable loads is shown in Figure 4.23 and 4.24, respectively.

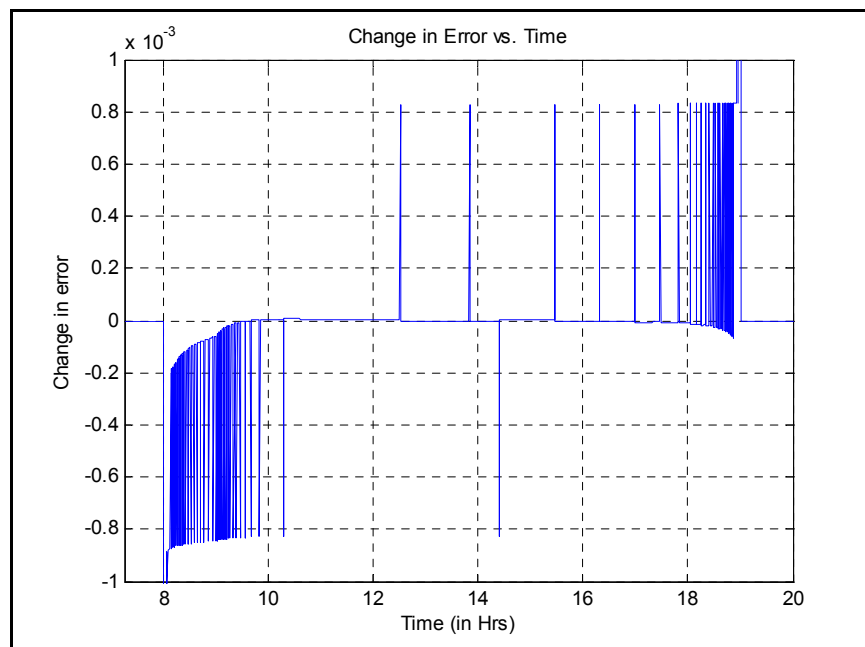


Figure 4. 22 Pattern of Second Input of FLC Change in Error Voltage for Variable Load in a Day

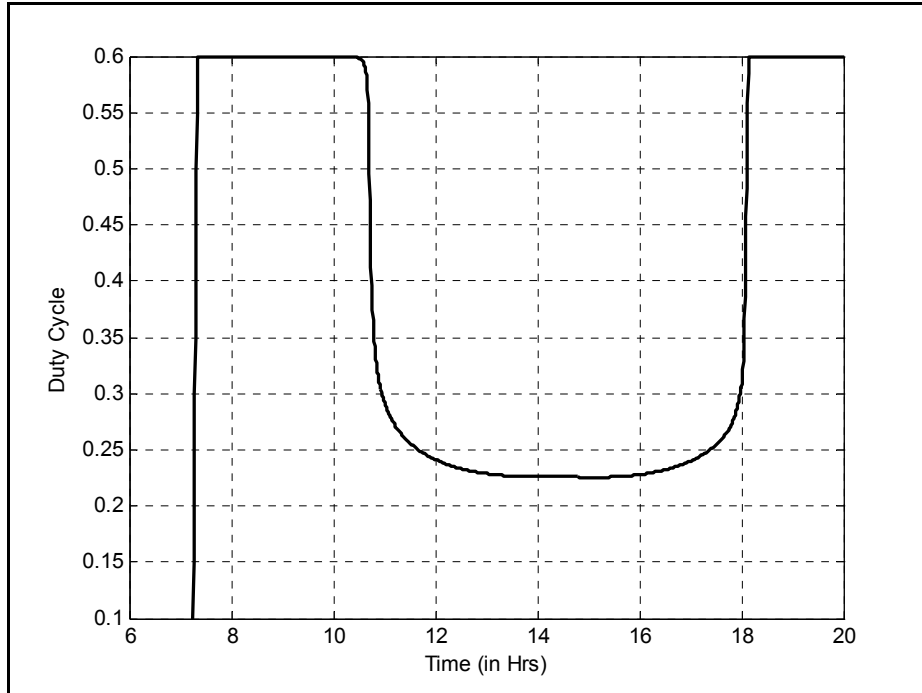


Figure 4.23 Pattern of the Duty Cycle for Fixed Load in a Day

The resulting pattern of resistive load R_{MPP} and R_{load} for fixed and variable load are shown in Figures 4.25 and 4.26, respectively.

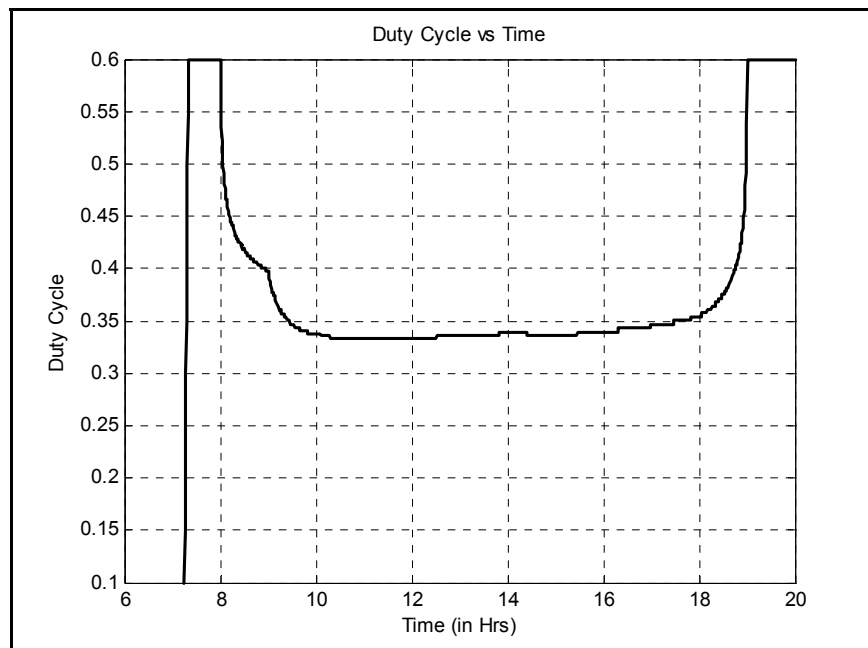


Figure 4.24 Pattern of the Duty cycle for Variable Load in a Day

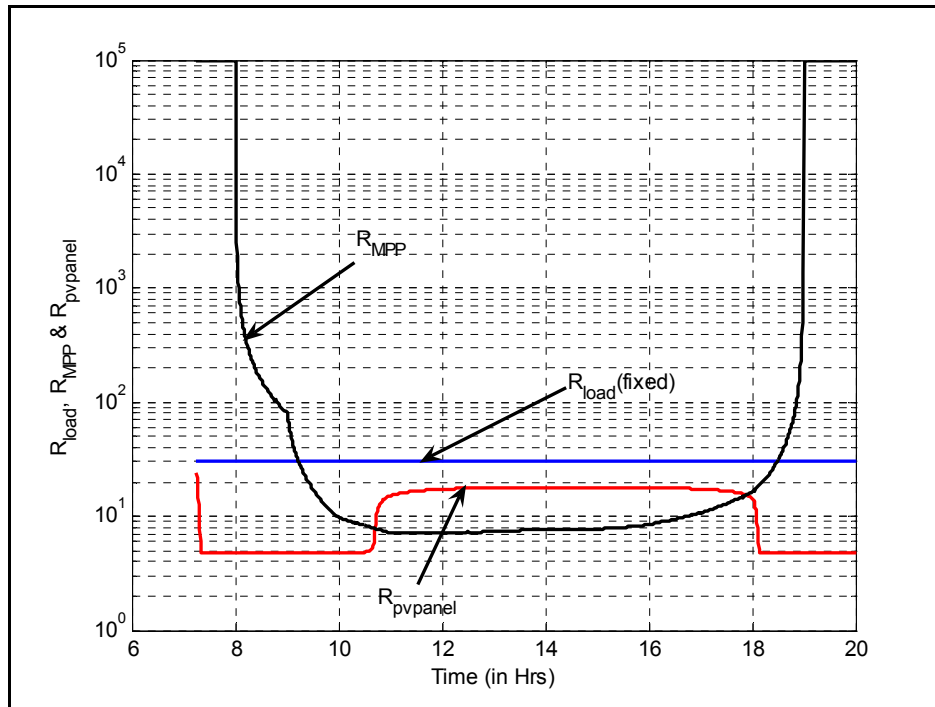


Figure 4.25 Patterns of the R_{MPP} and Fixed R_{load} in a Day

The pattern of MPP power obtained from MPPT model P_{max} (indicated by black dotted line) and output power at load from PV array with MPP tracking P_{load} (indicated by blue line) are shown in Figure 4.27 and 4.28 for fixed and variable loads respectively. As evident from Figure 4.27 that

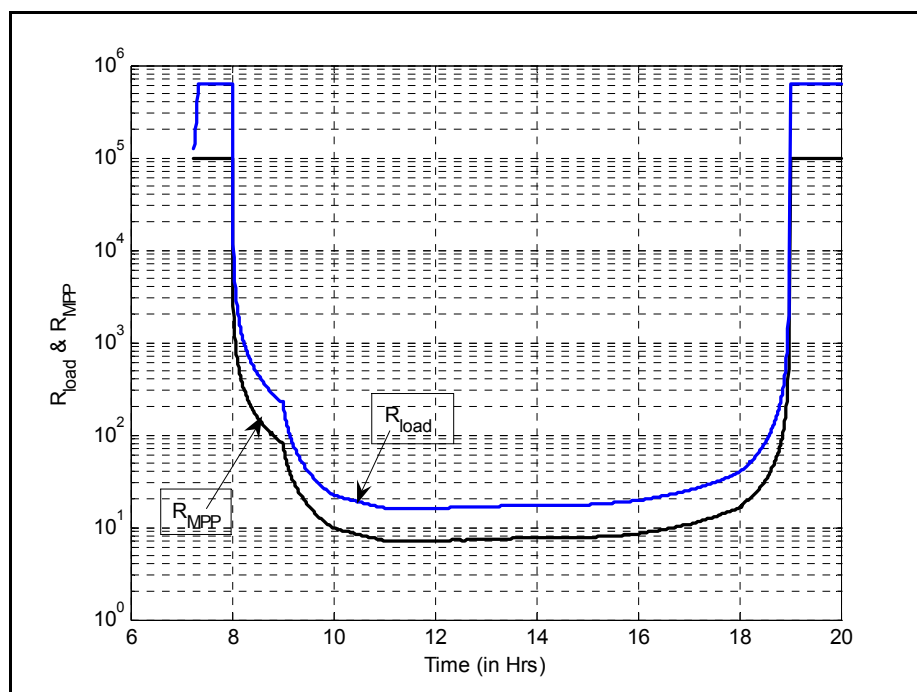


Figure 4.26 Patterns of the R_{MPP} and Variable R_{load} in a Day

with fixed load scenario, the controller has not transfer the instantaneous available maximum power to the load from the PV module.

A difference between R_{load} and R_{MPP} is observed in Figure 4.25 while P_{max} is same in Figure 4.27 because the R_{MPP} is the load seen by the PV array for MPPT and is evaluated by MPPT model of the PV array. The R_{load} is the actual load condition for maximum power point tracking under variable environmental conditions. This is a cumulative effect of duty cycle for DC-DC boost converter evaluated by FLC and R_{MPP} obtained from MPPT model as described earlier in equation 4.3.

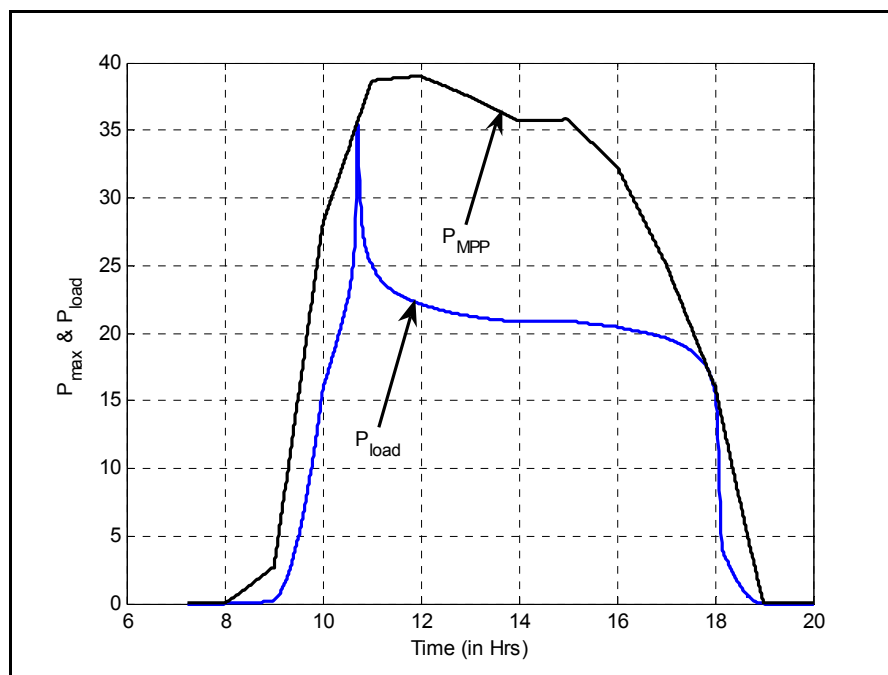


Figure 4. 27 Pattern of the MPPT Model Power and Power Harvested by the Load from PV Array for Fixed Load in a Day

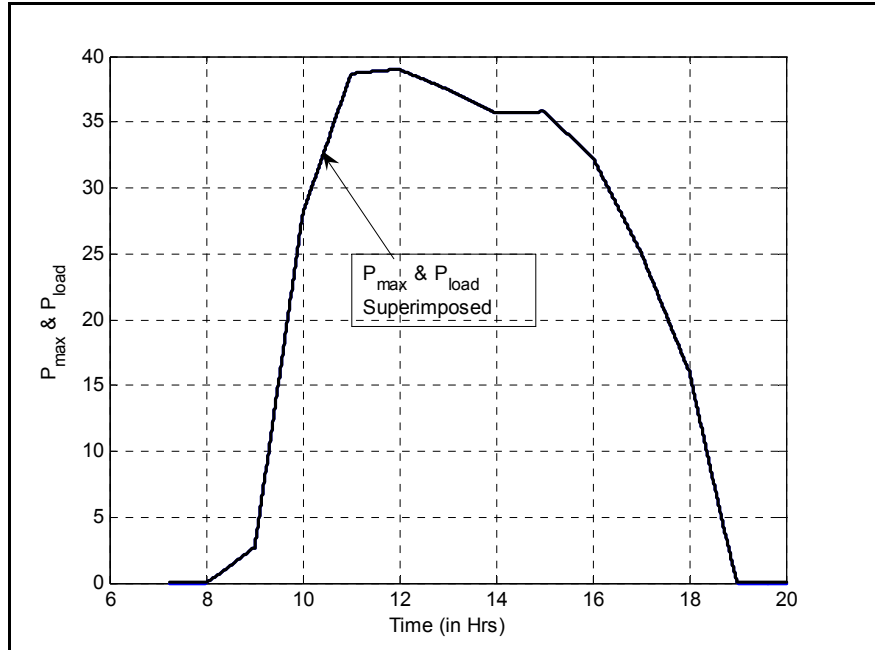


Figure 4.28 Pattern of the MPPT Model Power and Power Harvested by the Load from PV Array (Both are Super Imposed) for Variable Load in a Day

Both patterns of P_{max} and P_{load} are superimposed and this curve is indicating that the proposed scheme is efficiently tracking the maximum power harvesting maintaining the load voltage at reference level. Although both the powers are drawn with different legends (- and *, respectively) but this not prominent in the curves of Figure 4.28 as the calculation of dynamics is done every second.

The pattern of P_{max} and P_{load} are similar to the pattern of irradiance shown in Figure 3.8 (irradiance vs. time). Investigating Figures 4.17 and 4.19, it can be noticed that the rated load voltage is higher than the PV array output voltage and subsequently the load current is less than the PV array current. So that the input and output power to the DC-DC converter remains the same.

It can be further noticed that with the change in irradiance, both output voltage and output current of PV array are varying. But with the use of adaptive FLC for adapting the duty cycle of DC-DC converter, instantaneous value of load is achieved along with tracking the maximum power point of PV array. Thus a desirable performance of AGABFLC is observed for the optimal matching of the load at the MPP of a PV module for stand-alone applications.

4.4 Strategy for a Potential Hardware Development of AGBFLC

The hardware for AGBFLC-based controller developed in MATLAB/ Simulink environment, can be developed for the implementation of various PV applications. The strategy for the hardware development of the modeled controller is described in Figure 4.29. The Simulink model of the AGBFLC and the M file script for genetic algorithm are used by the Real-time work shop to generate the C code. This C code will then be compiled in the target specific microprocessor compiler and the compiled code will then be allocated to specific physical memory addresses followed by the calibration in terms of the required constraints. This calibrated and compiled code will then be implemented to obtain the microprocessor-based controller circuitry.

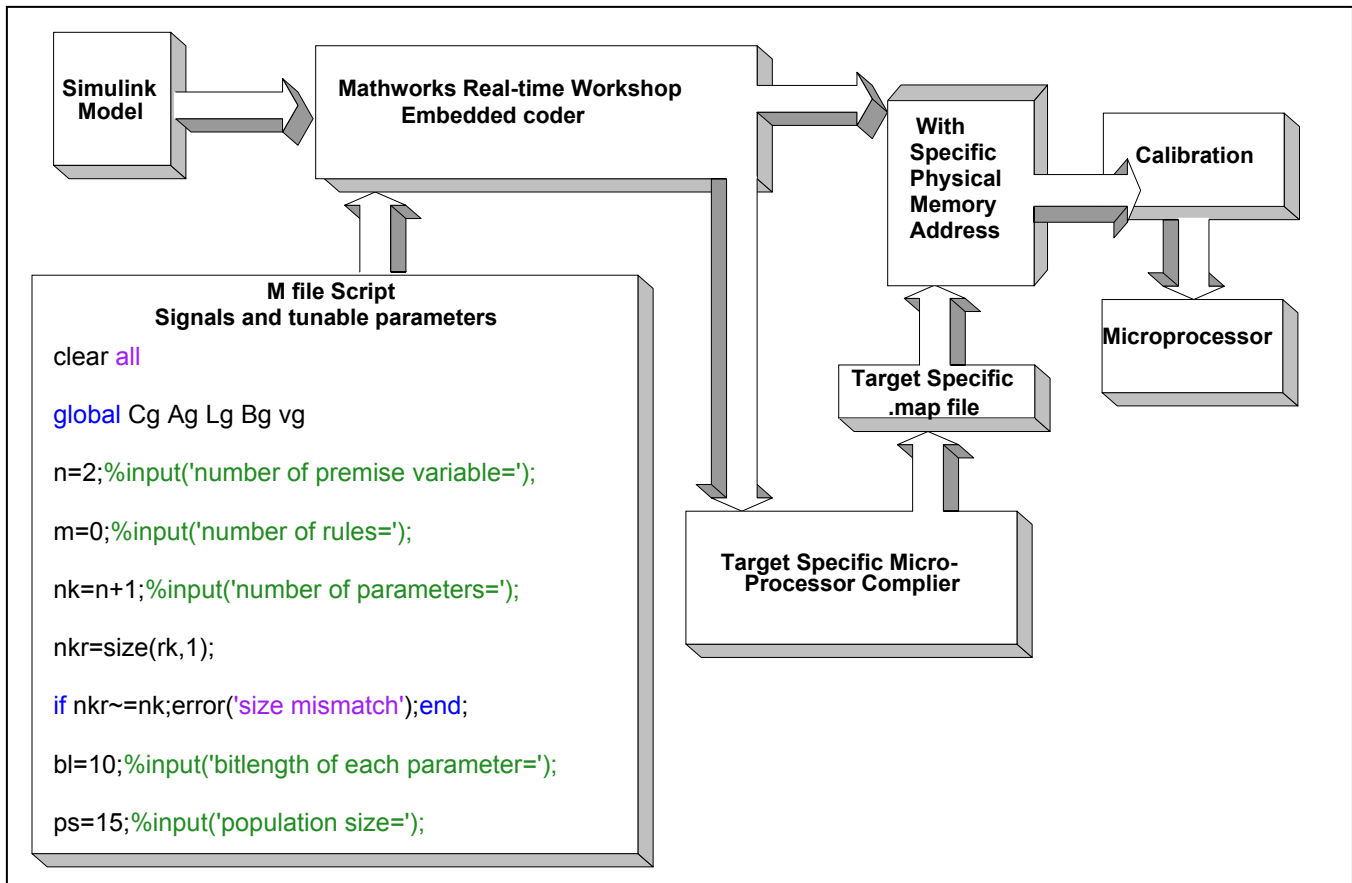


Figure 4.29 Strategy for the Hardware Development of the Controller [4. 89]

REFERENCES

- [4.1] T. Esum, P. L. Chapman, "Comparison of Photovoltaic Array Maximum Power Point Tracking Techniques," IEEE, 2006.
- [4.2] M.A.S. Masoum, H. Dehbonei and E.F. Fuchs, "Theoretical and experimental analyses of photovoltaic systems with voltage and current-based maximum power-point tracking," IEEE Transactions on Energy Conversion, Vol. 17, No. 4, pp. 514 – 522, Dec. 2002.
- [4.3] E. N. Costogue and S. Lindena, "Comparison of candidate solar array maximum power utilization approaches," in Intersociety Energy Conversion Eng. Conf., 1976, pp. 1449–1456.
- [4.4] W. J. A. Teulings, J. C. Marpinard, A. Capel, and D. O'Sullivan, "A new maximum power point tracking system," in Proc. 24th Annu. IEEE Power Electron. Spec. Conf., 1993, pp. 833–838.
- [4.5] Y. Kim, H. Jo, and D. Kim, "A new peak power tracker for cost-effective photovoltaic power system," in Proc. 31st Intersociety Energy Convers. Eng. Conf., 1996, pp. 1673–1678.
- [4.6] M.Veerachary, T. Senjyu, and K.Uezato, "Maximum power point tracking control of IDB converter supplied PV system," in IEE Proc. Elect. Power Applicat., 2001, pp. 494–502.
- [4.7] W. Xiao and W. G. Dunford, "A modified adaptive hill climbing MPPT method for photovoltaic power systems," in Proc. 35th Annu. IEEE Power Electron. Spec. Conf., 2004, pp. 1957–1963.
- [4.8] M. A. Slonim and L. M. Rahovich, "Maximum power point regulator for 4 kW solar cell array connected through inverter to the AC grid," in Proc. 31st Intersociety Energy Conver. Eng. Conf., 1996, pp. 1669–1672.
- [4.9] A. Al-Amoudi and L. Zhang, "Optimal control of a grid-connected PV system for maximum power point tracking and unity power factor," in Proc. Seventh Int. Conf. Power Electron. Variable Speed Drives, 1998, pp. 80–85.
- [4.10] Y. Jung, G. Yu, J. Choi, and J. Choi, "High-frequency DC link inverter for grid-connected photovoltaic system," in Conf. Record Twenty-Ninth IEEE Photovoltaic Spec. Conf., 2002, pp. 1410–1413.
- [4.11] S. Jain and V. Agarwal, "A new algorithm for rapid tracking of approximate maximum power point in photovoltaic systems," IEEE Power Electron. Lett., vol. 2, no. 1, pp. 16–19, Mar. 2004.
- [4.12] N. Femia, G. Petrone, G. Spagnuolo, and M. Vitelli, "Optimization of perturb and observe maximum power point tracking method," IEEE Trans. Power Electron., vol. 20, no. 4, pp. 963–973, Jul. 2005.
- [4.13] K. H. Hussein and I. Mota, "Maximum photovoltaic power tracking: An algorithm for rapidly changing atmospheric conditions," in IEE Proc. Generation Transmiss. Distrib., 1995, pp. 59–64.
- [4.14] K. Irisawa, T. Saito, I. Takano, and Y. Sawada, "Maximum power point tracking control of photovoltaic generation system under non-uniform insolation by means of monitoring cells," in Conf. Record Twenty-Eight IEEE Photovoltaic Spec. Conf., 2000, pp. 1707–1710.
- [4.15] Y.-C. Kuo, T.-J. Liang, and J.-F. Chen, "Novel maximum-power-point tracking controller for photovoltaic energy conversion system," IEEE Trans. Ind. Electron., vol. 48, no. 3, pp. 594–601, Jun. 2001.
- [4.16] K. Kobayashi, I. Takano, and Y. Sawada, "A study on a two stage maximum power point tracking control of a photovoltaic system under partially shaded insolation conditions," in IEEE Power Eng. Soc. Gen. Meet., 2003, pp. 2612–2617.
- [4.17] G. W. Hart, H. M. Branz, and C. H. Cox, "Experimental tests of open loop maximum-power-point tracking techniques," Solar Cells, vol. 13, pp. 185–195, 1984.
- [4.18] D. J. Patterson, "Electrical system design for a solar powered vehicle," in Proc. 21st Annu. IEEE Power Electron. Spec. Conf., 1990, pp. 618–622.
- [4.19] M. A. S. Masoum, H. Dehbonei, and E. F. Fuchs, "Theoretical and experimental analyses of photovoltaic systems with voltage and current-based maximum power-point tracking," IEEE Trans. Energy Convers., vol. 17, no. 4, pp. 514–522, Dec. 2002.

- [4.20] B. Bekker and H. J. Beukes, "Finding an optimal PV panel maximum power point tracking method," in Proc. 7th AFRICON Conf. Africa, 2004, pp. 1125–1129.
- [4.21] N. Mutoh, T. Matuo, K. Okada, and M. Sakai, "Prediction-data-based maximum-power-point-tracking method for photovoltaic power generation systems," in Proc. 33rd Annu. IEEE Power Electron. Spec. Conf., 2002, pp. 1489–1494
- [4.22] S. Yuvarajan and S. Xu, "Photo-voltaic power converter with a simple maximum-power-point-tracker," in Proc. 2003 Int. Symp. Circuits Syst., 2003, pp. III-399–III-402
- [4.23] R. M. Hilloowala and A. M. Sharaf, "A rule-based fuzzy logic controller for a PWM inverter in photo-voltaic energy conversion scheme," in Proc. IEEE Ind. Appl. Soc. Annu. Meet., 1992, pp. 762–769.
- [4.24] A. M. A. Mahmoud, H. M. Mashaly, S. A. Kandil, H. El Khashab, and M. N. F. Nashed, "Fuzzy logic implementation for photovoltaic maximum power tracking," in Proc. 9th IEEE Int. Workshop Robot Human Interactive Commun., 2000, pp. 155–160
- [4.25] B. M. Wilamowski and X. Li, "Fuzzy system based maximum power point tracking for PV system," in Proc. 28th Annu. Conf. IEEE Ind. Electron. Soc., 2002, pp. 3280–3284.
- [4.26] M. Veerachary, T. Senjyu, and K. Uezato, "Neural-network-based maximum-power-point tracking of coupled-inductor interleaved-boost-converter-supplied PV system using fuzzy controller," IEEE Trans. Ind. Electron., vol. 50, no. 4, pp. 749–758, Aug. 2003.
- [4.27] A. Hussein, K. Hirasawa, J. Hu, and J. Murata, "The dynamic performance of photovoltaic supplied dc motor fed from DC–DC converter and controlled by neural networks," in Proc. Int. Joint Conf. Neural Netw., 2002, pp. 607–612.
- [4.28] X. Sun, W. Wu, X. Li, and Q. Zhao, "A research on photovoltaic energy controlling system with maximum power point tracking," in Proc. Power Convers. Conf., 2002, pp. 822–826
- [4.29] L. Zhang, Y. Bai, and A. Al-Amoudi, "GA-RBF neural network based maximum power point tracking for grid-connected photovoltaic systems," in Proc. Int. Conf. Power Electron., Machines and Drives, 2002, pp. 18–23
- [4.30] Y. H. Lim and D. C. Hamill, "Simple maximum power point tracker for photovoltaic arrays," Electron. Lett., vol. 36, pp. 997–999, May 2000.
- [4.31] H. J. Beukes and J. H. R. Enslin, "Analysis of a new compound converter as MPPT, battery regulator and bus regulator for satellite power systems," in Proc. 24th Annu. IEEE Power Electron. Spec. Conf., 1993, pp. 846–852.
- [4.32] A. S. Kislovski and R. Redl, "Maximum-power-tracking using positive feedback," in Proc. 25th Annu. IEEE Power Electron. Spec. Conf., 1994, pp. 1065–1068.
- [4.33] J. Arias, F. F. Linera, J. Martin-Ramos, A. M. Pernia, and J. Cambroner, "A modular PV regulator based on microcontroller with maximum power point tracking," in Proc. IEEE Ind. Appl. Conf., 2004, pp. 1178–1184.
- [4.34] C.-T. Pan, J.-Y. Chen, C.-P. Chu, and Y.-S. Huang, "A fast maximum power point tracker for photovoltaic power systems," in Proc. 25th Annu. Conf. IEEE Ind. Electron. Soc., 1999, pp. 390–393.
- [4.35] R. Bhide and S. R. Bhat, "Modular power conditioning unit for photovoltaic applications," in Proc. 23rd Annu. IEEE Power Electron. Spec. Conf., 1992, pp. 708–713.
- [4.36] H. Sugimoto and H. Dong, "A new scheme for maximum photovoltaic power tracking control," in Proc. Power Convers. Conf., 1997, pp. 691–696.
- [4.37] S. J. Chiang, K. T. Chang, and C. Y. Yen, "Residential photovoltaic energy storage system," IEEE Trans. Ind. Electron., vol. 45, no. 3, pp. 385–394, Jun. 1998.
- [4.38] J. A. M. Bleijs and A. Gow, "Fast maximum power point control of current-fed DC DC converter for photovoltaic arrays," Electron. Lett., vol. 37, pp. 5–6, Jan. 2001.
- [4.39] M. Bodur and M. Ermis, "Maximum power point tracking for low power photovoltaic solar panels," in Proc. 7th Mediterranean Electrotechnical Conf., 1994, pp. 758–761.
- [4.40] T. Kitano, M. Matsui, and D.-h. Xu, "Power sensor-less MPPT control scheme utilizing power balance at DC link-system design to ensure stability and response," in Proc. 27th Annu. Conf. IEEE Ind. Electron. Soc., 2001, pp. 1309–1314.

- [4.41] N. Patcharaprakiti and S. Premrudeepreechacharn, "Maximum power point tracking using adaptive fuzzy logic control for grid-connected photovoltaic system," in IEEE Power Eng. Soc. Winter Meet., 2002, pp. 372–377.
- [4.42] B. M. Wilamowski and X. Li, "Fuzzy system based maximum power point tracking for PV system," in Proc. 28th Annu. Conf. IEEE Ind. Electron. Soc., 2002, pp. 3280–3284.
- [4.43] N. Khaehintung, K. Pramotung, B. Tuvirat, and P. Sirisuk, "RISC microcontroller built-in fuzzy logic controller of maximum power point tracking for solar-powered light-flasher applications," in Proc. 30th Annu. Conf. IEEE Ind. Electron. Soc., 2004, pp. 2673–2678.
- [4.44] M. Veerachary, T. Senjyu, and K. Uezato, "Neural-network-based maximum-power point tracking of coupled-inductor interleaved-boost-converter-supplied PV system using fuzzy controller," IEEE Trans. Ind. Electron., vol. 50, no. 4, pp. 749–758, Aug. 2003.
- [4.45] T. Hiyama, S. Kouzuma, and T. Imakubo, "Identification of optimal operating point of PV modules using neural network for real-time maximum power tracking control," IEEE Trans. Energy Convers., vol. 10, no. 2, pp. 360–367, Jun. 1995.
- [4.46] Y. Chen and K. M. Smedley, "A cost-effective single-stage inverter with maximum power point tracking," IEEE Trans. Power Electron., vol. 19, no. 5, pp. 1289–1294, Sep. 2004.
- [4.47] J.H.R. Enslin, M.S. Wolf, D.B. Snyman, and W. Swiegers, "Integrated Photovoltaic Maximum Power Point Tracking Converter," IEEE Transactions on Industrial Electronics, Vol. 44, No. 6, December 1997.
- [4.48] S.S. Sastry, "Introductory methods of Numerical Analysis," 4th edition, PHI .
- [4.49] C. J. Zarowski, "An Introduction to Numerical Analysis for Electrical and Computer Engineers, Wiley Interscience Publications
- [4.50] K. M. Passino, "Bridging the Gap Between Conventional and Intelligent Control," ,IEEE, 1993
- [4.51] T. Ray Chaudhuri, L. G. C. Hamey, R. D. Bell, "From Conventional Control to Autonomous Intelligent Methods," Oct. 1996.
- [4.52] K. M. Passino, "Fuzzy Vs. Conventional Control," IEEE, 1993.
- [4.53] M.B. Ghalia, "Modeling and Robust feedback Control of Uncertain Nonlinear Dynamical Systems Using Fuzzy Set Theory," PhD Dissertation, TTU, 1995
- [4.54] J.A. Duffie, W.A. Beckman, "Solar Engineering of Thermal Processes"; John Wiley & Sons Inc. 1991
- [4.55] T. Townsend, et al, "A New Performance Index for PV System Analysis," 24th IEEE PVSC, Dec. 1994
- [4.56] Ø. Ulleberg and S. O. MØRNER, "TRNSYS simulation models for solar-hydrogen systems," Solar Energy, Vol. 59, No. 4-6, pp. 271-279, 1997.
- [4.57] F.A. Farret and M.G. Simões, Integration of Alternative Sources of Energy, John Wiley & Sons, Inc., 2006.
- [4.58] M. R. Patel, Wind and Solar Power Systems, CRC Press LLC, 1999.
- [4.59] C. Palaniappan et al, "Renewable Energy Technologies", Narosa Publishing House.
- [4.60] G. N. Tiwari, "Solar energy", Narosa Publishing House, 2002
- [4.61] T. Bhattacharya, "Terrestrial solar photovoltaics", Narosa Publishing House, 1998
- [4.62] R. Messenger and J. Ventre, "Photovoltaic systems engineering", CRC Press 2000
- [4.63] E. H. Mamdani, "Application of fuzzy algorithms for control of simple dynamic plant," Proc. Inst. Elect. Eng., vol. 121, no. 12, pp. 1585–1588, Dec. 1974.
- [4.64] L.A. Zadeh, "A theory of approximate reasoning," Machine Intelligence, Halstead press, NY, Vol.9, pp:149-194
- [4.65] Zadeh L. A., "Outline of a new Approach to the Analysis of complex systems and decision process", IEEE Trans. Syst. Man. Cybern., vol. 3, no. 1, pp.28-44, 1973 & vol 15, pp. 15-30, 1979
- [4.66] D. Driankov, H. Hellendoorn, M. Reinfrank, "An Introduction to Fuzzy Control," Springer Verlag, 1992
- [4.67] A. Kandel, G. Langholz, "Fuzzy Control Systems," CRC Press, Sept. 1993.

- [4.68] J. Munda, S. Asato, H. Miyagi, "Fuzzy Logic Control in Hybrid Power Systems," Springer-Verlag Berlin Heidelberg, 2005.
- [4.69] Z. Kovacic, S. Bogdan, "Fuzzy Controller Design Theory and Applications," Taylor & Francis Group, LLC, 2006.
- [4.70] B Tomescu, "On the Use of Fuzzy Logic to Control Paralleled DC-DC Converters," *PhD Thesis* , Virginia Tech, 2001
- [4.71] Holland J.H, "Adaptation in neural and artificial systems", Univ. of Michigan press, Ann Arbor, 1975.
- [4.72] Davis, L, "A handbook of Genetic Algorithms", Van Nostrand Reinhold, New York 1990.
- [4.73] G. Caste llano, G. Attolico, and A. Distant, "Automatic generation of fuzzy rules for reactive robot controllers", *Robot. Auton. Syst.*, vol.22, pp. 133–149, 1997.
- [4.74] L. X. Wang and J. M. Mendel, "Generating fuzzy rules by learning from examples", *IEEE Trans. Syst., Man, Cybern.*, vol. 22, pp 1414–1427, Feb. 1992.
- [4.75] D. Park, A. Kandel, and G. Langholz, "Genetic-based new fuzzy reasoning models with application to fuzzy control", *IEEE Trans. Syst., Man, Cybern.*, vol. 24, pp. 39–47, Jan. 1994
- [4.76] F. Hoffmann and G. Pfister, "Learning of a fuzzy control rule-baseusing messy genetic algorithms", in *Genetic Algorithms and Soft Computing. Ser. Studies in Fuzziness and Soft Computing*, F. Herrera and J. L. Verde gay, Eds. Heidelberg, Germany: Physica-Verlag, "1996, vol. 8, pp. 279–305.
- [4.77] C.L. Karr and E.J. Gentry, "Genetic algorithm for fuzzy logic controller", *AI Expert Vol 2* pp. 26-33, 1991.
- [4.78] M.F. Azeem, M. Hanmandlu, N. Ahmad, "Structure Identification of Generalized Adaptive Neuro-Fuzzy Inference Systems", *IEEE Trans. On Fuzzy Systems*, vol 11, No. 5, October 2003, pp. 666-681.
- [4.79] Chokri, Djemel, Nabil, Adel, "Design of optimal FLC with GA", *IEEE Intern. sym. on intelligent control*. pp.98-103, 2002.
- [4.80] M.F. Azeem, Masood Anzar, "Effect of Normalization of Membership Functions in Premise Region of Generalized Adaptive Neuro-Fuzzy Inference System", *Proceedings of the IEEE Indian Annual Meet (INDICON'2004)*, IIT Kharaghpur, Kharagpur , INDIA, 20-22 December, 2004, pp. 294-298.
- [4.81] M.F. Azeem, "A Novel Parent Selection Operator in GA for Tuning of Scaling Factors of FKBC", *IEEE World Congress on Computational Intelligence (WCCI2006)- Vancouver, BC, Canada, 16-21 July 2006*, pp. 8153-8158.
- [4.82] D.E. Goldberg, "Genetic Algorithm in search, optimization and Machine learning", Addison-Wesley 1989.
- [4.83] Bhuvaneswari MC and Sivavandam SN, "Genetic Algorithm based Test Generation: An Analysis of Crossover Operators", *The Journal of The Computer Society of India*, vol. 32, No.1, pp10-17.
- [4.84] DF. Jong KA and SpearsWM, "An Analysis of the interacting roles of population size & crossover in genetic Algorithms", in *Proc. of the first workshop on parallel problem solving from nature*, Schwefel HP and Manner R (Eds), Dotmund, West Germany (Springer-verlag, Berlin, 1990), pp.39-47.
- [4.85] Syswerda G, "Uniform crossover in Genetic Algorithms", in *Proc of the third international conference on Genetic Algorithms*, Schaffer, J (Ed); (Morgan Kauffman Publishers, Cambridge, MA, 1989), pp. 2-9.
- [4.86] Sung Hoon Jung, "Queen bee evolution for genetic algorithms", *Electronics letters*, 20th March 2003, Vol. 36 No. 6 pp. 575-576. Online No.20030383, DOI: 10.1049/el: 20030383,IEEE 2003.
- [4.87] M. S. Alam, M.F. Azeem, "Modified Queen-Bee Based Evolution of GA for the tuning of scaling factors of FKBC", *IEEE India Annual Conference "INDICON 2004,IIT Kharagpur, India , "*, December 2004
- [4.88] Official Website of Mathworks <http://www.mathworks.com/> accessed on 04/10/2009
- [4.89] E.Estamos "Application of Mathworks model for Hybrid Vehicle Development," Battery group meeting minutes, Chrysler LLC, 2009
- [4.90] V. Ramanarayanan, "Course Material on Switched Mode Power Conversion," Indian Institute of Science, Sept. 2006.
- [4.91] Glasner, J. Appelbaum, "Advantage of Boost Vs. Buck Topology for Maximum Power Point Tracker in Photovoltaic Systems," *IEEE*, 1996

CHAPTER 5

CONCLUSIONS, RECOMMENDATIONS, AND FURTHER SCOPE OF RESEARCH

5.1 Conclusion

This dissertation dealt with modeling and control of stand-alone photovoltaic power generation systems *to extract and track the maximum power deliverable by the PV*.

A dynamic model of PV has been developed and validated experimentally. The model takes varying weather conditions into consideration. The performances of static and dynamic models are compared and significantly accurate and increased performance is achieved by the consideration of varying temperature and solar irradiance. The developed model is valid for any PV panel. The model can also be utilized to expedite research and development in the PV-based distributed generation system. Studies related to transient conditions and large scale performance can be performed through the developed model.

Design of experiment has been developed and performed for the validation of the developed model.. This experiment was performed over a span of 20 days with varying weather conditions. The modeling, experimentation, and verification of the developed model have portrayed a strong correlation between the simulated and the measured data values. R-squared value of 0.9996 is achieved through the design of the experiment. The predicted solar wattage through the model has an accuracy of 99.996 % which is almost pure normal error.

Maximum power generated by the PV has been obtained real-time using the proposed PV model. Then fuzzy logic control was used to control the duty cycle of the DC/DC booster used to provide constant output voltage and output power equal to the PV maximum power.

A novel method entitled as “Modified queen bee algorithm” which is an applied genetic algorithm method is also proposed and an algorithm is developed and implemented to tune the parameters of the fuzzy logic controller on a real-time basis.

An optimal performance of the AGABFLC controller has been observed through simulation for varying resistive loads.

Knowing the available power real-time allows for true maximum power tracking. This ability did not exist before this research was accomplished. The use of fuzzy logic control allows for robust maximum power tracking. The practical impact of this research is in knowing the true available maximum power and tracking it properly. This research work allows one to extract more power out of the PV and perform load matching than what is currently the case.

5.2 Recommendations for Further Work

5.2.1 Modeling and simulation of photovoltaic (PV) systems. The dynamic modeling of the PV module has been carried out, the uncertainties and the parametric variations have been taken into account. However, the aging factor of the PV panel has not been considered. Performance evaluation related to the study of the materials of the PV panel is required to include the aging factor of PV modules in the developed model. This study will help in the prediction of long-term performance of the stand-alone PV systems.

5.2.2 Design of experiment. When the model's aging factor is taken into account, design of experiment will be next step to validate the model. These experiments have to be performed on different PV modules with different life span expectancies.

5.2.3 Modeling and simulation of control system and model validation. The e AGBFLC performance needs to be analyzed by considering a variety of loads including inductive and capacitive loads. Precise tuned values of gain parameters of FLC can be determined by considering double crossover and multi crossover points

5.2.4 Design and development of hardware for control system. The hardware implementation of the AGBFLC controller may follow the proposed strategy described in Chapter 4.

APPENDIX A

NOMENCLATURE

T_a : Ambient temperature (°C)

T_c : Temperature of the cell/ collector surface (°C)

T_p : Temperature of the plate (bottom) (°C)

$$T = T_c - T_p$$

C_i : Overall heat capacity per unit area of the PV cell /thermal capacitance [J/(°C. m²)]

$\tau\alpha$: Transmittance – absorptance product of PV cell.

G_T : Irradiance (W/m² = Joule-Second//m²)

η_c : Efficiency of the PV cell

η : Empirical constant; $\eta=1$ for Ge & =2 for Si

U_L : Overall heat loss coefficient (J/m²)

V_d : Voltage across the diode (V_d)

V_{G_o} : Equivalent voltage of the prohibited band; $V_{G_o} = 0.785$ V for Ge & = 1.21 V for Si

V_T : Equivalent voltage to the Junction temperature; $V_T = kT / q = T / 11$

m : =2 for Ge &=2 for Si

k : Boltzman constant: $k = 1.38047 \times 10^{-23}$

q : Electron charge; $q = 1.60210 \times 10^{-19}$

I_s : Reverse saturated current of the diode, (~100pA)

I_d : Temperature-dependent diode current

I_p : PV cell leakage current

I_L, I_λ : Photon current; depends on insulation and wavelength of photons (light

$h_{c,p-c}$: Convection coefficient between the plate and the cover W/m².C

$h_{r,p-c}$: Radiation coefficient between the plate and the cover W/m².K

$h_{r,c-a}$: Radiation coefficient for the cover to ambient temperature W/m².C

h_w : Wind heat loss coefficient W/m².C

N_u : Nusselt number (dimensionless)

k_1 : Thermal conductivity

L : Plate to cover spacing

β : Collector Tilt angle

R_a : Rayleigh number

g : Gravitational constant

ν : kinematic viscosity

α : Thermal diffusivity

β' : Volumetric coefficient of expansion (for an ideal gas $\beta' = 1/T$)

ε_p : Plate effective emittance

ε_c : Collector surface effective emittance

APPENDIX B

SIMULINK MODELS FOR PV MODULE

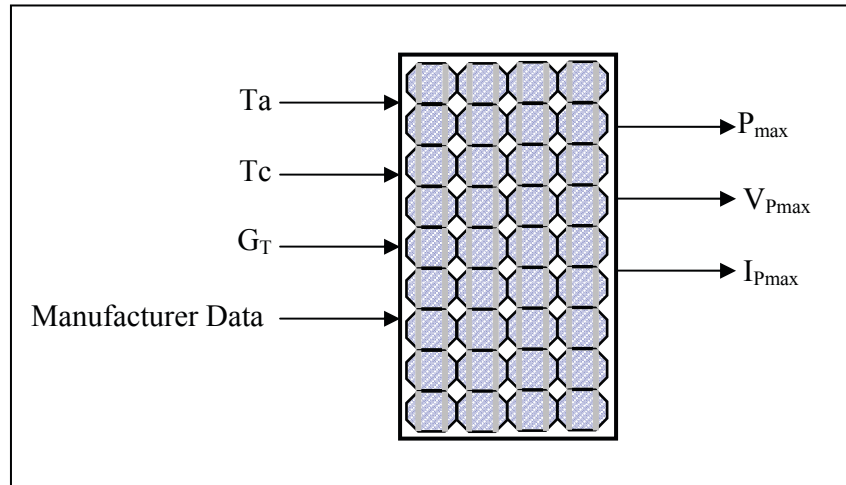


Figure B. 1 Simulink Model of PV Cell (Static Model)

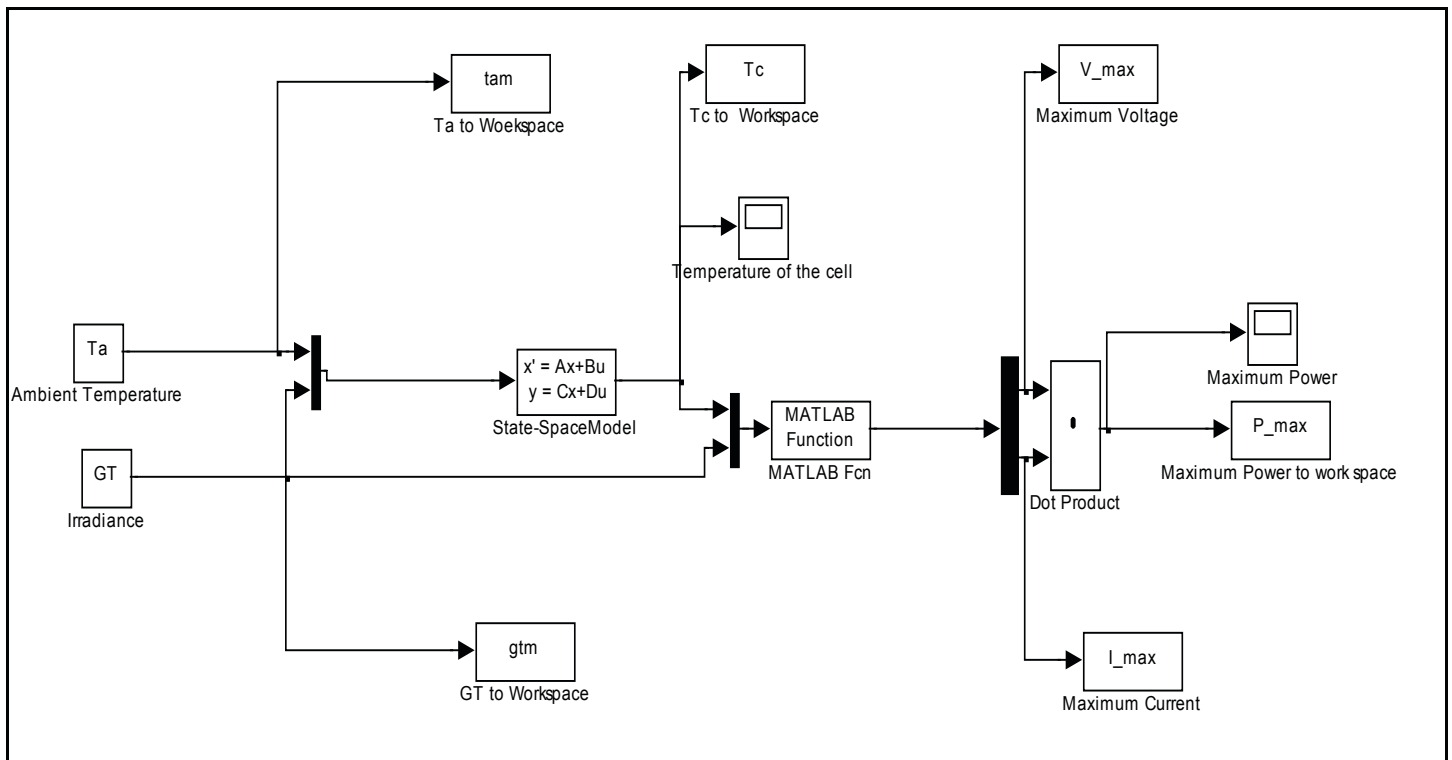


Figure B. 2 Simulink Model of PV Cell (Dynamic Model)

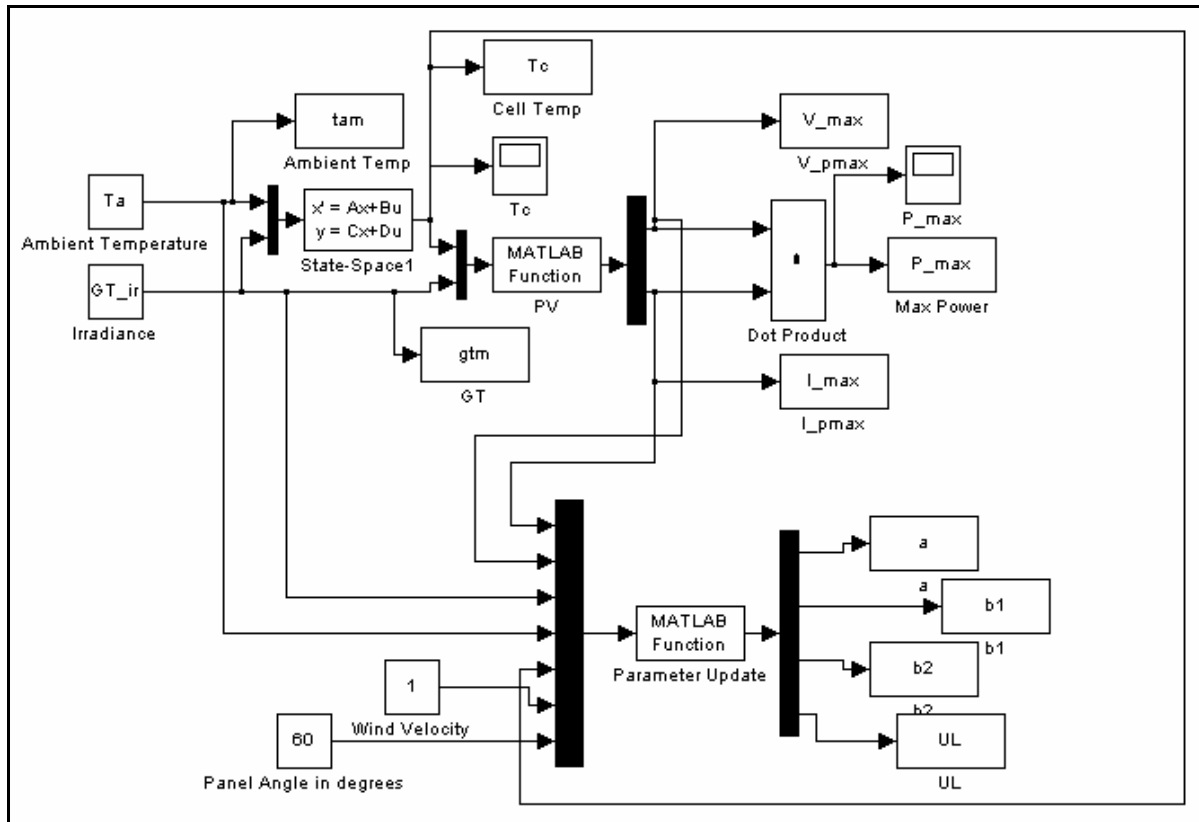


Figure B. 3 Simulink Model of PV Cell with Calculation of Parameters

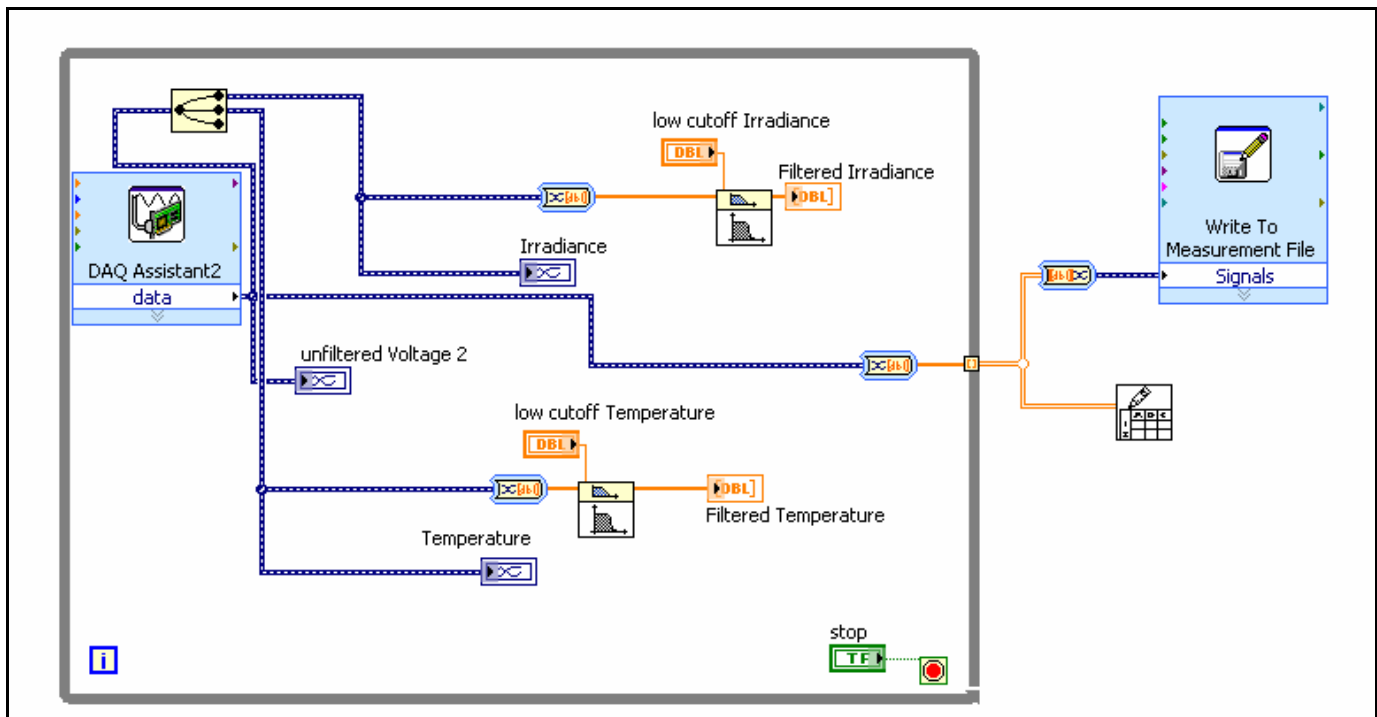


Figure B. 4 Data Collection through DAQ

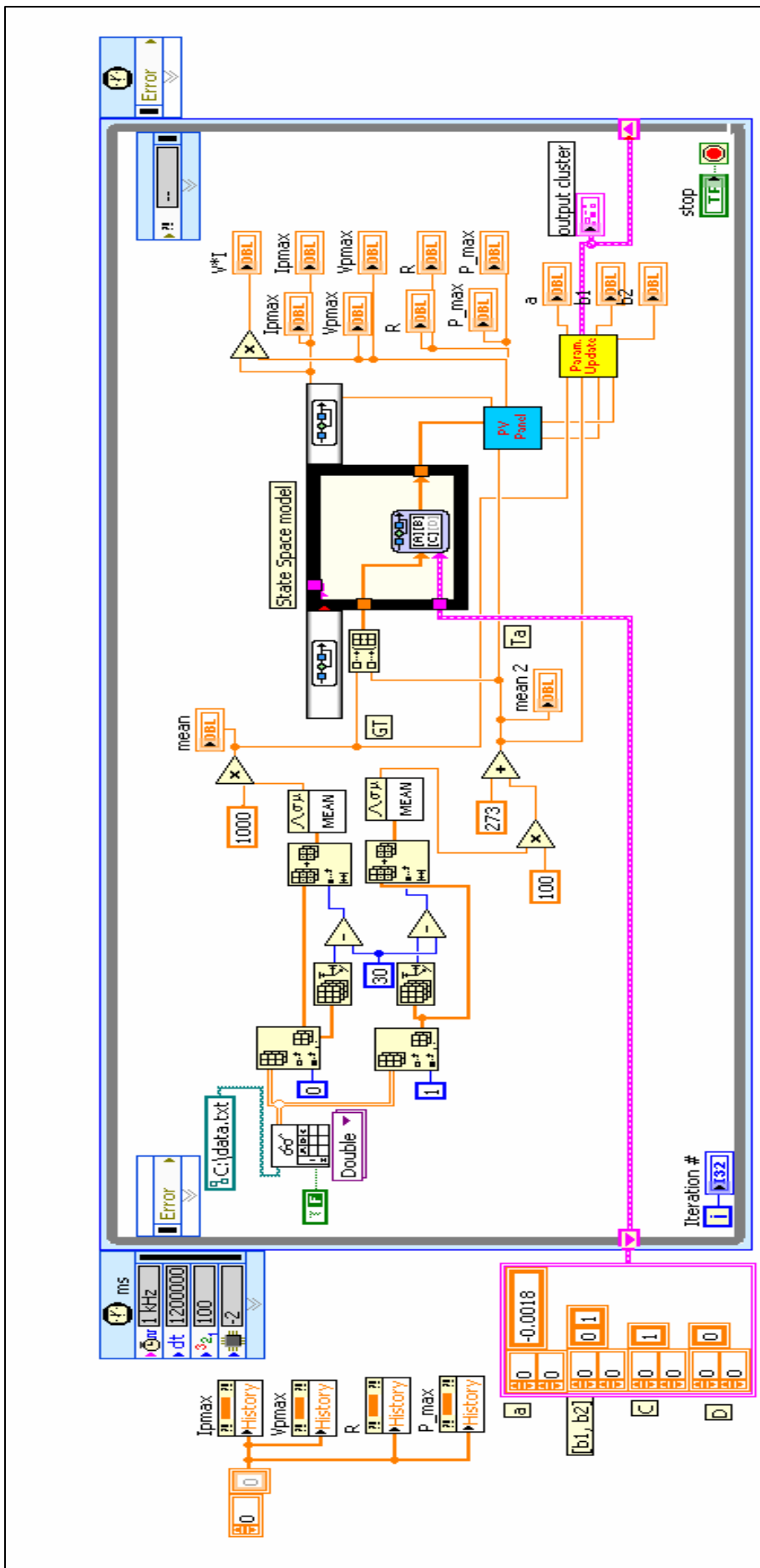


Figure B. 5 Lab View Model of PV Module

APPENDIX C

SPECIFICATIONS OF THE INSTRUMENT USED IN THE EXPERIMENT

C.1 PV Module [3.48]

Intelligent module design

- All cells are electrically matched to assure the greatest power output possible.
- Ultra-clear tempered glass provides excellent light transmission and protects from wind, hail, and impact.
- Torsion and corrosion resistant anodized aluminum module frame assures dependable performance, even through harsh weather conditions and in marine environments.
- Built-in bypass diodes (12V configuration) help system performance during partial shadowing.

High quality

- Every module is subject to final factory review, inspection and testing to assure compliance with electrical, mechanical and visual criteria.
- 36 PowerMax® single-crystalline solar cells deliver excellent performance even in reduced-light or poor weather conditions.
- Cell surfaces are treated with the Texture Optimized Pyramidal Surface (TOPS™) process to generate more energy from available light.
- Fault tolerant multi-redundant contacts on front and back of each cell provide superior reliability.
- Solar cells are laminated between a multi-layered polymer backsheet and layers of ethylene vinyl acetate (EVA) for environmental protection, moisture resistance, and electrical isolation.
- Durable back sheet provides the module underside with protection from scratching, cuts, breakage, and most environmental conditions.
- Laboratory tested and certified for a wide range of operating conditions.
- Ground continuity of ≤ 1 ohm for all metallic surfaces.
- Manufactured to exacting Siemens quality standards.

Easy installation

- ProCharger™-CR junction box accepts conduit, cable or wire and is designed for easy field wiring.
- Lightweight aluminum frame and pre-drilled mounting holes for easy installation.
- Factory configured for 12V operation and may be reconfigured in the field for 6V operation.
- Modules may be wired together in series or parallel to attain required power levels.

Performance warranty

- 25 Year limited warranty on power output.

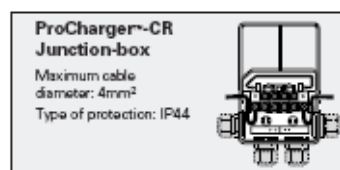
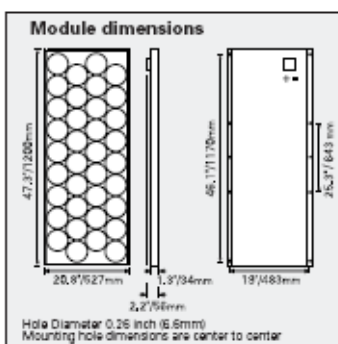
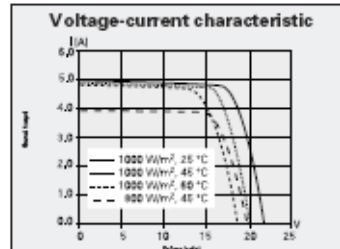
Further information on solar products, systems, principles and applications is available in the Siemens Solar product catalog.

Siemens modules are recyclable.

Siemens Solar GmbH
A joint venture of
Siemens AG and Bayernwerk AG
Postfach 46 07 05

Solar module SP75	
Electrical parameters	
Maximum power rating P_{max} [Wp] ¹⁾	75
Rated current I_{MPP} [A]	4.4/8.8
Rated voltage V_{MPP} [V]	17.0/8.5
Short circuit current I_{SC} [A]	4.8/9.6
Open circuit voltage V_{OC} [V]	21.7/10.9
Thermal parameters	
NOCT ²⁾ [°C]	45 ±2
Temp. coefficient: short-circuit current	2.06 mA / °C
Temp. coefficient: open-circuit voltage	-0.77 V / °C
Qualification test parameters ⁴⁾	
Temperature cycling range [°C]	-40 to +85
Humidity freeze, Damp heat [%RH]	85
Maximum system voltage [V]	600 V per UL (1000 V per ISPR)
Wind Loading PSF [N/m ²]	50 [2400]
Maximum distortion ³⁾ [°]	1.2
Hailstone impact Inches [mm]	1.0 [25]
MPH [m/s]	52 [v=23]
Weight Pounds [kg]	16.7 [7.6]

- 1) Wp (Watt peak) = Peak power (Minimum Wp = 70 Watts)
Air Mass AM = 1.5
Irradiance $E = 1000 \text{ W/m}^2$
Cell temperature $T_c = 25^\circ\text{C}$
- 2) Normal Operating Cell Temperature at:
Irradiance $E = 800 \text{ W/m}^2$
Ambient temperature $T_a = 20^\circ\text{C}$
Wind Speed $v_w = 1 \text{ m/s}$
- 3) Diagonal lifting of module plane
- 4) Per IEC 61215 test requirements
- 5) 12 volt configuration



Your address for photovoltaics from Siemens Solar



© Siemens Solar 1998 Status 11/98 - Subject to modification.

Siemens Solar Industries
P.O.Box 6032
Camarillo, CA 93011, U.S.A.
Web site: www.siemens.com

Siemens Showa Solar Pte. Ltd.
166 Kallang Way
Singapore 349249
Tel: 65 676 3999

C.2 Handheld Solar Meters Model 776E [3.50]

As given on the product webpage: <http://www.dataeng.com/776.htm> accessed on 11/11/08

“The models 776 solar meters are hand held solar intensity meters used to measure direct plus diffuse solar radiation. The meter is a rugged two bearing micro ammeter. The sensor is a space grade silicon cell carefully loaded to insure good linearity of response versus intensity. The scale is calibrated in both heat units (BTUH/ft²) and electrical units (Watts/m²). The mean calibration error over a wide range of intensities is 3%. Dimensions are 2.3 in. X 3.6 in. X 1.2 in. Weight is 3 oz [3.50].”



Solar Meter Model 776E [picture copied from 3.50]

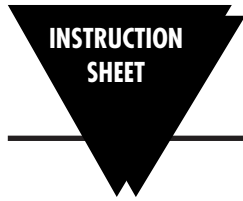
As given on the product webpage: <http://www.dataeng.com/776.htm> accessed on 11/11/08

“Model 776E: The model 776E is generally suited for measuring the transmission loss through transparent materials or filter materials such as window films and screens. It has the sensor located on the top end of the meter body so the meter can be pointed at a solar source and “before” and “after” measurements can be made”.

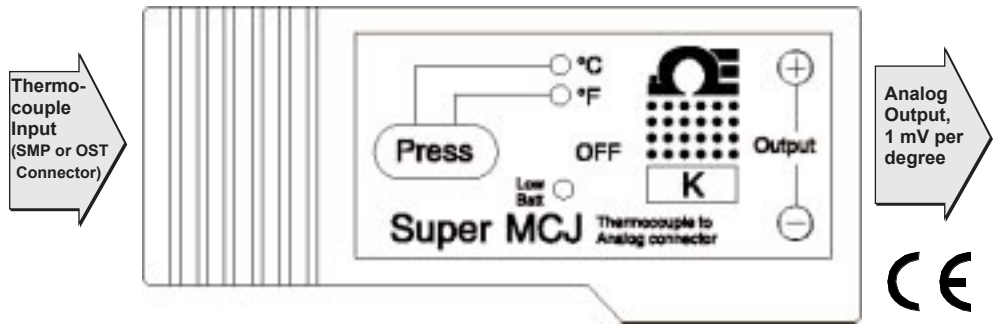


Super MCJ

SMCJ-J, SMCJ-K, SMCJ-T



M-2813



Thermocouple-to-Analog Connector

GENERAL DESCRIPTION

This is a Thermocouple to Analog Connector. It converts a thermocouple input signal (Type J, K, or T) to a linear, compensated, amplified analog output. The unit provides 1mV/°F or 1mV/°C analog output. The analog output can go to a strip chart recorder or a digital voltmeter for temperature monitoring.

The unit is powered by a single AA size lithium battery. In order to install the battery, remove the back cover and place the battery on the PC board. The battery polarity is indicated on the PC board. If the battery is installed reverse, the unit will not power up. The back cover is mounted to the front cover via two mounting holes.

The input connection can be SMP or OST type connections. The output connection is standard banana plug or jack. The plastic case and the rubber gasket Bumper Band® provides a rugged and sealed connector design. Figure 1 provides a functional flow chart of how the unit operates. This unit is operated using a single tactile feedback button (Press).

There are 3 LEDs built into the connector. The °C green LED flashes once every 2 seconds when the output provides 1mV/°C. The °F green LED flashes once every 2 seconds when the output provides 1mV/°F. If the input is open the °C and °F green LEDs both flash alternately once a second.

When the battery voltage drops below a certain level, a red LED starts to flash once a second. This is a low battery indication. The battery must be replaced with a fresh battery immediately.

Field Adjustments

The unit is field adjustable by removing the back cover and accessing the three potentiometers. R17 provides offset adjustment when the unit is in mV/°F mode. R42 provides offset adjustment when the unit is in mV/°C mode. R32 provides span (gain) adjustment either in mV/°F or mV/°C mode.

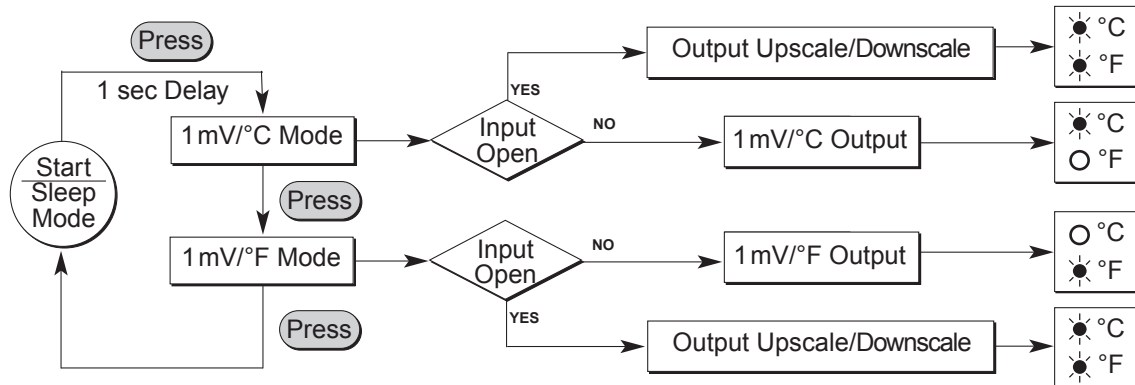


Figure 1, Functional Flow Chart

SPECIFICATIONS

Measuring Temperature Range:

Type J: -100 to +750°C (-148 to +1382°F)
 Type K: -100 to +1250°C (-148 to +2282°F)
 Type T: -100 to +350°C (-148 to +662°F)

Accuracy @ 75°F ambient temperature across the range:

Type J: ±1.4°C (±2.5°F)
 Type K: ±3°C (±5°F)
 Type T: ±2°C (±3°F)

Input Connection: SMP or OST connector

Output Connection: Standard Banana Plug or Jack

Thermocouple Break Protection:

Output goes Upscale (std.)
 °F & °C Green LEDs flash once a second

Output: 1mV/°F or 1mV/°C
 °F or °C Green LEDs flash once every 2 seconds

Output Load: 1K-Ohms min.

Power: One AA size Lithium Battery, 3.3 to 3.6 VDC 1900 mA/H

Battery Life @ 75°F Ambient Temperature: 1440 hours (60 Days), continuous operation, no load

Low Battery Indication:
 Red LED flashes once a second

Response Time (0 to 63% of Final value): 150 msec

Operating Temperature: 0 to 50°C (32 to 122°F)

Thermal Zero Drift: 0.05 mV/°C (0.05 mV/°F) ambient temperature change

Operating Relative Humidity: 95% or less, without condensation

Dimensions: 4"L x 2" W x 1"H (10L x 5W x 2.5H cm)

Weight: 147 lbs (67g)

Accessories

Model No.	Description
OM-NOMAD-BATT	Replacement Battery
TAC80B-BJ	In-line banana plug (red and black)

Low-Cost, Bus-Powered Multifunction DAQ for USB – 12- or 14-Bit, up to 48 kS/s, 8 Analog Inputs

Specifications

Typical at 25 °C unless otherwise noted.

Analog Input

Absolute accuracy, single-ended

Range	Typical at 25 °C (mV)	Maximum (0 to 55 °C) (mV)
±10	14.7	138

Absolute accuracy at full scale, differential¹

Range	Typical at 25 °C (mV)	Maximum (0 to 55 °C) (mV)
±20	14.7	138
±10	7.73	84.8
±5	4.28	58.4
±4	3.59	53.1
±2.5	2.56	45.1
±2	2.21	42.5
±1.25	1.70	38.9
±1	1.53	37.5

Number of channels..... 8 single-ended/4 differential
 Type of ADC Successive approximation

ADC resolution (bits)

Module	Differential	Single-Ended
USB-6008	12	11
USB-6009	14	13

Maximum sampling rate (system dependent)

Module	Maximum Sampling Rate (kS/s)
USB-6008	10
USB-6009	48

Input range, single-ended ±10 V
 Input range, differential ±20, ±10, ±5, ±4, ±2.5, ±2, ±1.25, ±1 V
 Maximum working voltage ±10 V
 Overvoltage protection ±35 V
 FIFO buffer size 512 B
 Timing resolution 41.67 ns (24 MHz timebase)
 Timing accuracy 100 ppm of actual sample rate
 Input impedance 144 kΩ
 Trigger source..... Software or external digital trigger
 System noise..... 5 m V_{rms} (±10 V range)

Analog Output

Absolute accuracy (no load) 7 mV typical, 36.4 mV maximum at full scale
 Number of channels..... 2
 Type of DAC Successive approximation
 DAC resolution..... 12 bits
 Maximum update rate 150 Hz, software-timed

Output range 0 to +5 V
 Output impedance..... 50 Ω
 Output current drive 5 mA
 Power-on state..... 0 V
 Slew rate..... 1 V/μs
 Short-circuit current 50 mA

Digital I/O

Number of channels..... 12 total
 8 (P0.<0..7>)
 4 (P1.<0..3>)
 Direction control Each channel individually programmable as input or output
 Output driver type
 USB-6008 Open-drain
 USB-6009 Each channel individually programmable as push-pull or open-drain
 Compatibility CMOS, TTL, LVTTTL
 Internal pull-up resistor 4.7 kΩ to +5 V
 Power-on state..... Input (high impedance)
 Absolute maximum voltage range..... -0.5 to +5.8 V

Digital logic levels

Level	Min	Max	Units
Input low voltage	-0.3	0.8	V
Input high voltage	2.0	5.8	V
Input leakage current	–	50	μA
Output low voltage (I = 8.5 mA)	–	0.8	V
Output high voltage (push-pull, I = -8.5 mA)	2.0	3.5	V
Output high voltage (open-drain, I = -0.6 mA, nominal)	2.0	5.0	V
Output high voltage (open-drain, I = -8.5 mA, with external pull-up resistor)	2.0	–	V

Counter

Number of counters 1
 Resolution 32 bits
 Counter measurements..... Edge counting (falling edge)
 Pull-up resistor..... 4.7 kΩ to 5 V
 Maximum input frequency 5 MHz
 Minimum high pulse width..... 100 ns
 Minimum low pulse width..... 100 ns
 Input high voltage 2.0 V
 Input low voltage 0.8 V

Power available at I/O connector

+5 V output (200 mA maximum) +5 V typical
 +4.85 V minimum
 +2.5 V output (1 mA maximum) +2.5 V typical
 +2.5 V output accuracy 0.25% max
 Voltage reference temperature drift... 50 ppm/°C max

¹Input voltages may not exceed the working voltage range.

PEL-300 Programmable D.C. Electronic Load



SPECIFICATIONS	
RATING	
Operating Voltage	DC 3 ~ 60V
Current	6mA ~ 60A
Power	1 ~ 300W
Minimum Operation	3V
CV MODE	
Operating Range	3 ~ 60V
Setting Accuracy	$\pm (0.1\% + 40\text{mV})$
Setting Resolution	20mV
CC MODE	
Operating Range	6mA ~ 60A
Setting Accuracy	6.02A ~ 60A Range $\pm (0.5\% + 100\text{mA})$
	0.602A ~ 6A Range $\pm (0.1\% + 10\text{mA})$
	6mA ~ 0.6A Range $\pm (0.1\% + 1\text{mA})$
Setting Resolution	6.02A ~ 60A Range 20mA
	0.602A ~ 6A Range 2mA
	6mA ~ 0.6A Range 0.2mA

Appendix D

A Report on Design of Experiment

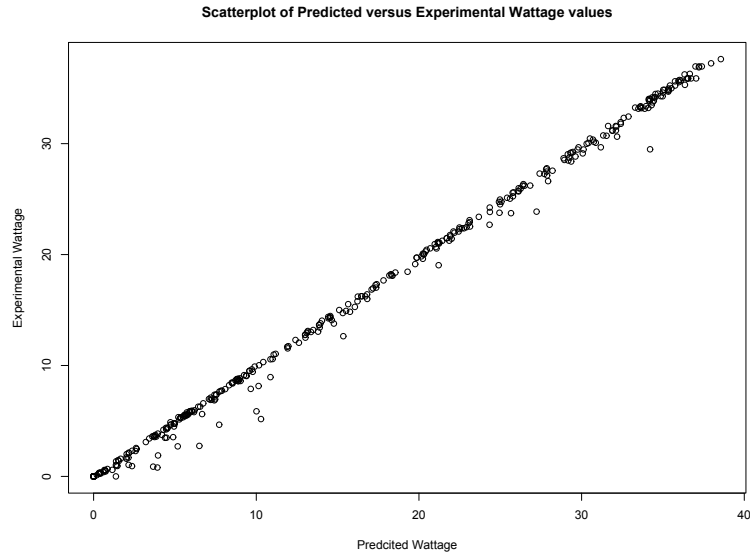
Consulting Report for Mr. Saad Alam
Micheal R. Allen, Assistant Professor
Department of Mathematics
Tennessee Technological University, TN

Overview

Recently, because of worldwide energy concerns, solar cell use has been on the rise, almost exponentially. One use is the placement of a solar cell array next to or on a house as a resource for electric power. Of course, at night the array is basically incapable of producing any wattage and hence is backed up by a set of rechargeable batteries. During the day the array produces electricity which is either stored in the batteries or is used by the occupants of the house. In the event the demand is too great for either the solar array and or the batteries, the control system of the house for the electric power will grab power from the utility grid. One proble, though, is the accurate prediction of kilowatt usage and how much wattage the solar cell array will produce. When it is cloudy or cold, solar cells do not produce as much electricity as they would on a sunny, warm day. Unfortunately, the routine manufacturing specifications of a solar cell do not include the wattage produced based on any environmental factors but simply give the average maximum wattage the cell can produce.

Problem

Hence, the problem presented here concerns the prediction of the wattage produced by a solar cell based on its environment. Mr. Saad Alam presented a mathematical model which included the amount of light seen by the solar cell as well as its temperature. Using a feedback loop, Mr. Alam then predicted the wattage of said solar cell. The following is a plot of the predicted versus the experimental wattage values obtained from a solar cell on various days and at various temperatures.



Solution

As can be seen from the graph, the predicted and experimental values are linearly related. This indicates that Mr. Alam's feedback predictive model appears to be doing its job. But, we now concern ourselves with how good this prediction is. Consider the following model:

$$W_{exp} = \beta_0 + \beta_1 W_{pred} + \epsilon$$

where W_{exp} is the wattage obtained from the solar cell, W_{pred} is the predicted wattage of the solar cell, β_0 is the intercept (and should be zero unless W_{pred} is a biased), β_1 is the slope (and should be 1 unless W_{pred} is not consistent) and ϵ is the error of prediction and is assumed to independent and identically distributed from a normal distribution for each wattage value. The following is a regression analysis obtained in R of all the data applied to this linear model.

Coefficients:

```
Estimate Std. Error t value Pr(>|t|)
(Intercept) -0.302210 0.056471 -5.352 1.54e-07 ***
pred_new 0.992952 0.002756 360.256 < 2e-16 ***
```

—
Signif. codes: 0 '***' 0.001 '**' 0.01 '*' 0.05 '.' 0.1 ' ' 1

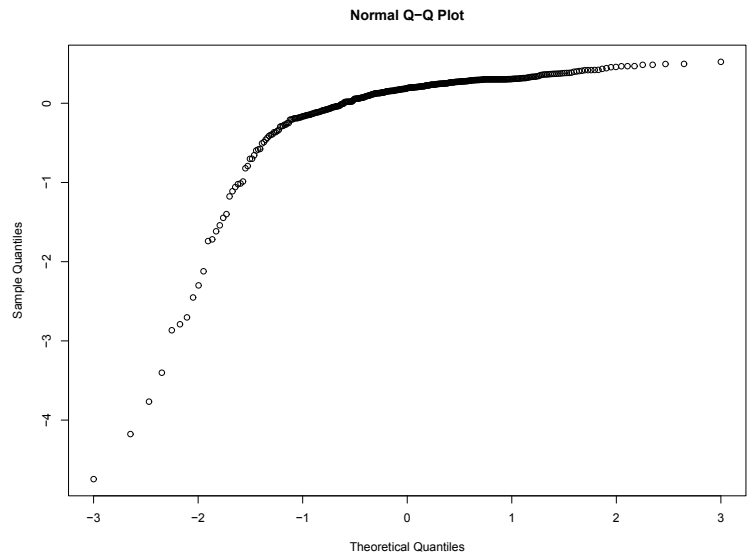
Residual standard error: 0.6433 on 368 degrees of freedom

Multiple R-Squared: 0.9972, Adjusted R-squared: 0.9972

F-statistic: 1.298e+05 on 1 and 368 DF, p-value: < 2.2e-16

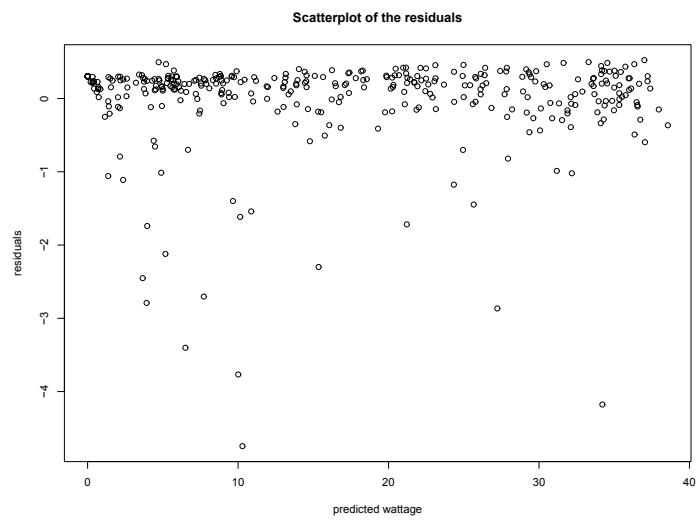
Because the final p-value is so close to zero, the linear model more than adequately fits the data. In basic terms, the Mr Alam's prediction procedure is

predicting the experimental wattage of a solar based on its environmental factors with 99.72% accuracy. Next, diagnostics were applied to the linear model to check the validity of the model. First, the residuals were analyzed to check the assumptions of normality and constant variance.



As can be seen from the quantile-quantile plot, the quantiles of the residuals do not follow a diagonal line which indicates a deviation from normality. There appears to be a group of data that causes this deviation from normality.

Next is a plot of the residuals versus the predicted wattage.



The residuals show a tendency for the predicted wattage to under predict the experimental wattage in about 50 of the cases. This can also be seen in the first plot where a majority of the data falls on the diagonal line but just a few data points are below the line and in the regression analysis with a significantly negative intercept.

Third, cross validation was used to check the validity of the linear model. The data was separated into two groups, either by date, temp perature, or amount of sunlight and separate regression models were found for each group.. If the original linear model is valid then the two models found should have statistically equivalent slopes and intercepts. In all the cross validation attempts, most of the slopes were not statistically equivalent. Below is an example calculation when the cross validation sets were separated by date.

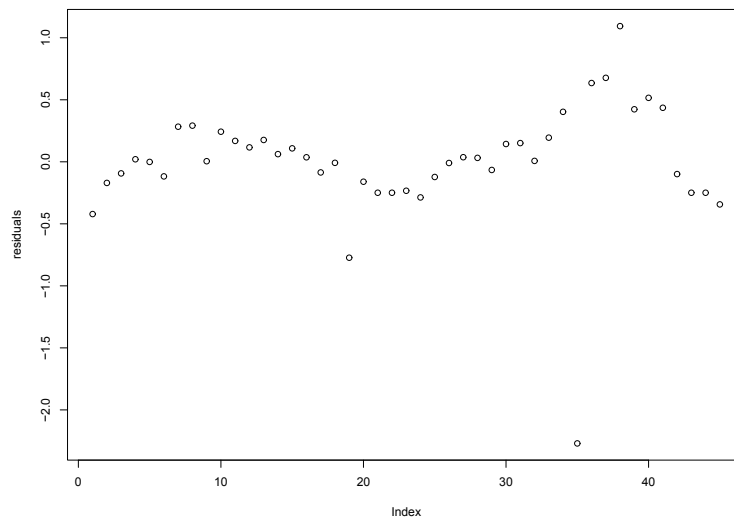
H_o : The slopes are equivalent

H_1 : The slopes are different

$$\text{Test Statistic: } t = \frac{\text{Slope 2} - \text{Slope 1}}{\text{Standard error of slope 1}} = \frac{1.000536 - 0.986024}{0.002564} = 5.66$$

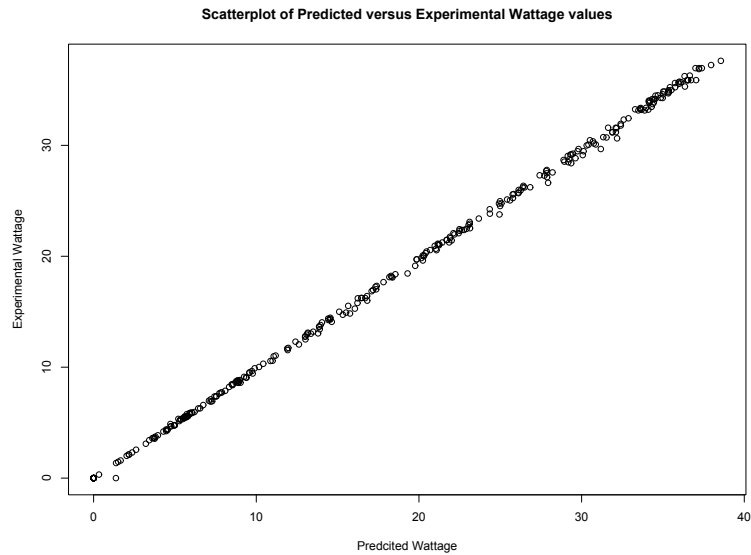
$$\text{p-value: } 2P(T_{df=141} > 5.66) \approx 0$$

Because of these three problems, the original model was deemed invalid. To remedy the situation, further investigation was done to look for outliers and influential points. After using multiple tests for influential cases, it was found that the morning and dusk wattage predcitions had too much error and were causing the invalidity and nonnormality. Here is a plot of the first 45 residuals which shows an almost cyclic pattern in the amount of error, although it is not repeated in the hwole data set.



The extreme values correspond to the moring and dusk. Hence, the linear

model fitted again to all the data points with the morning and dusk data points that caused the most extreme errors removed. The following is a scatterplot of the new data set.



Notice the linear fit looks even better than before. The summary of the regression analysis is shown below.

Coefficients:

	Estimate	Std. Error	t value	Pr(> t)
(Intercept)	-0.058737	0.024773	-2.371	0.0183 *
new_pred	0.987602	0.001135	870.506	<2e-16 ***

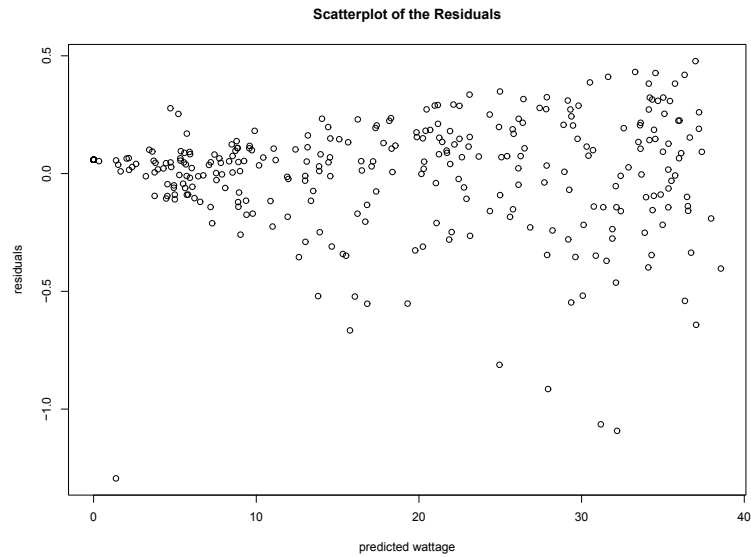
Signif. codes: 0 '***' 0.001 '**' 0.01 '*' 0.05 '.' 0.1 ' ' 1

Residual standard error: 0.2384 on 313 degrees of freedom

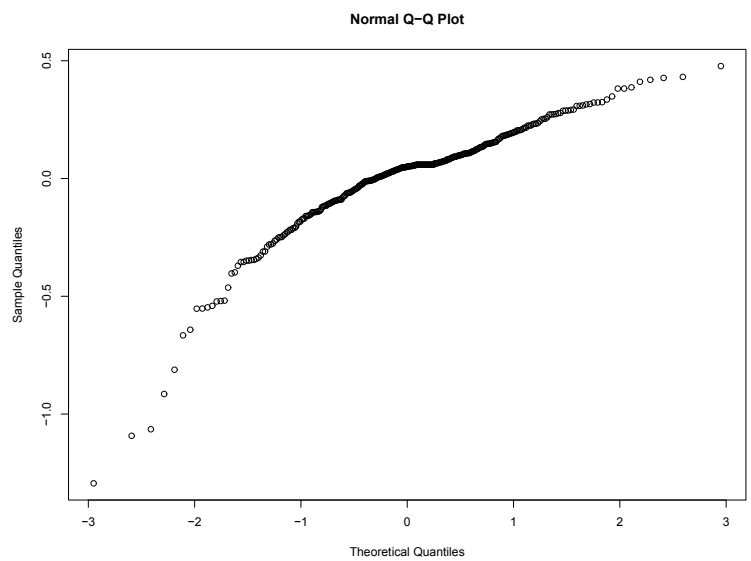
Multiple R-Squared: 0.9996, Adjusted R-squared: 0.9996

F-statistic: 7.578e+05 on 1 and 313 DF, p-value: < 2.2e-16

Notice the adjusted R-squared value has gone up significantly and the p-value for the intercept is not as strong. Likewise, the scatterplot of the residuals has improved.



Although there is a slight megaphone effect seen in the residuals, it is a much better fit than before. The quantile-quantile plot verifies this.



This quantiles here are much more linear than before although there appears to be just a few more outliers in the data set pulling the quantiles away from normality. Finally, with regards to validity, only one cross validation procedure, by date, gave any indication of invalidity. All the rest showed statistically

equivalent slopes.

Conclusion

The predictive procedure designed by Mr. Alam is valid. It predicts, with only slight bias, the true wattage produced by a solar cell using environmental factors with 99.96% accuracy taking into account morning and dusk error. With a little more diagnostics, the linear fit could probably be improved to an accuracy of 99.99% with almost pure normal error.

11/8/2008	14:30	113	13.1	286.25	286.27	13.27	5.814	16.61	0.350	47.452	-0.003	0.003	1.26E-05	1.30	4.3	5.59	3.851	44.07	13.192	12.684	0.003	0.006
11/8/2008	15:00	97	12.9	286.05	286.3	13.3	4.945	16.46	0.300	54.792	-0.003	0.003	1.26E-05	1.64	2.91	4.77	3.486	37.83	13.071	12.615	0.002	0.005
11/8/2008	15:30	45	12.4	285.55	286.22	13.22	2.184	15.71	0.139	113.022	-0.003	0.003	1.27E-05	1.18	1.79	2.11	3.274	17.55	12.443	12.035	0.001	0.002
11/8/2008	16:00	9	11.8	284.95	286.03	13.03	0.388	14.07	0.028	510.327	-0.003	0.003	1.28E-05	0.35	0.9	0.32	18.800	3.51	11.052	8.974	0.000	0.000
11/8/2008	16:30	0	11.5	284.65	285.81	12.81	0.000	0	0.000	0.000	-0.003	0.003	1.30E-05	0.00	0	0.00	0.000	0	0.000	0.000	0.000	0.000
Day 19																						
11/9/2008	6:00	5	4.4	277.55	289.63	16.63	0.201	13.17	0.015	863.288	-0.002	0.002	1.50E-05	0.18	0.67	0.12	39.970	1.95	10.303	6.185	0.000	0.000
11/9/2008	6:30	77	4.2	277.35	287.77	14.77	3.845	16.14	0.238	67.749	-0.003	0.003	1.32E-05	1.89	1.9	3.59	6.606	30.03	12.804	11.958	0.002	0.004
11/9/2008	7:00	184	3.8	276.95	286.22	13.22	9.726	17.04	0.571	29.853	-0.003	0.003	1.27E-05	2.48	3.89	9.65	0.814	71.76	13.554	13.444	0.005	0.010
11/9/2008	7:30	273	3.9	277.05	285	12	14.769	17.43	0.847	20.570	-0.003	0.003	1.26E-05	2.80	4.92	13.78	6.724	106.47	13.872	12.939	0.007	0.014
11/9/2008	8:00	298	4.1	277.25	284.02	11.02	16.239	17.55	0.925	18.967	-0.003	0.003	1.25E-05	2.80	5.79	16.21	0.166	116.22	13.973	13.949	0.008	0.016
11/9/2008	8:30	243	4.5	277.65	283.22	10.22	13.168	17.46	0.754	23.151	-0.003	0.003	1.25E-05	2.30	5.7	13.11	0.440	94.77	13.895	13.833	0.007	0.013
11/9/2008	9:00	301	4.8	277.95	282.63	9.63	16.493	17.65	0.934	18.887	-0.003	0.003	1.25E-05	2.80	5.8	16.24	1.534	117.39	14.050	13.834	0.008	0.016
11/9/2008	9:30	276	5	278.15	282.14	9.14	15.098	17.62	0.857	20.562	-0.003	0.003	1.25E-05	2.60	5.77	15.00	0.636	107.64	14.026	13.937	0.008	0.015
11/9/2008	10:00	167	5.2	278.35	281.68	8.68	8.942	17.26	0.518	33.317	-0.003	0.003	1.25E-05	1.80	4.83	8.69	2.768	65.13	13.729	13.349	0.004	0.009
11/9/2008	10:30	142	5.5	278.65	281.32	8.32	7.550	17.15	0.440	38.957	-0.003	0.003	1.25E-05	1.89	3.9	7.37	2.367	55.38	13.633	13.310	0.004	0.007
11/9/2008	11:00	102	5.6	278.75	281.01	8.01	5.331	16.87	0.316	53.381	-0.003	0.003	1.26E-05	1.44	3.66	5.27	1.144	39.78	13.402	13.249	0.003	0.005
11/9/2008	11:30	105	5.6	278.75	280.74	7.74	5.503	16.92	0.325	52.019	-0.003	0.003	1.26E-05	1.44	3.7	5.33	3.185	40.95	13.439	13.011	0.003	0.005
11/9/2008	12:00	108	5.6	278.75	280.52	7.52	5.675	16.96	0.335	50.687	-0.003	0.003	1.26E-05	1.48	3.77	5.58	1.678	42.12	13.473	13.247	0.003	0.006
11/9/2008	12:30	127	5.7	278.85	280.36	7.36	6.738	17.11	0.394	43.450	-0.003	0.003	1.26E-05	1.69	3.9	6.59	2.179	49.53	13.603	13.307	0.003	0.007
11/9/2008	13:00	159	6.2	279.35	280.32	7.32	8.537	17.31	0.493	35.098	-0.003	0.003	1.26E-05	2.06	4.07	8.38	1.794	62.01	13.768	13.521	0.004	0.008
11/9/2008	13:30	159	5.9	279.05	280.24	7.24	8.540	17.32	0.493	35.127	-0.003	0.003	1.25E-05	2.06	4.1	8.45	1.101	62.01	13.772	13.620	0.004	0.008
11/9/2008	14:00	158	5.6	278.75	280.12	7.12	8.487	17.32	0.490	35.345	-0.003	0.003	1.25E-05	2.06	4.1	8.45	0.487	61.62	13.774	13.707	0.004	0.008
11/9/2008	14:30	146	5.3	278.45	279.97	6.97	7.815	17.26	0.453	38.119	-0.003	0.003	1.25E-05	1.90	4.06	7.71	1.297	56.94	13.726	13.548	0.004	0.008
11/9/2008	15:00	139	5.1	278.25	279.81	6.81	7.426	17.23	0.431	39.975	-0.003	0.003	1.25E-05	1.84	4	7.36	0.891	54.21	13.699	13.577	0.004	0.007
11/9/2008	15:30	87	4.9	278.05	279.61	6.61	4.532	16.82	0.269	62.428	-0.003	0.003	1.25E-05	1.10	3.93	4.32	4.607	33.93	13.356	12.741	0.002	0.004
11/9/2008	16:00	15	4.9	278.05	279.39	6.39	0.697	15.1	0.046	327.344	-0.003	0.003	1.26E-05	0.48	1.08	0.52	25.576	5.85	11.907	8.862	0.000	0.001
11/9/2008	16:30	0	4.7	277.85	279.04	6.04	0.000	0	0.000		-0.003	0.003	1.29E-05	0.00	0	0.00	0.000	0	0.000	0.000	0.000	0.000
Day 20																						
11/12/2008																						
Rain/Sprinkling/Cloudy																						
Day 21																						
11/13/2008																						
Rain																						
Day 22																						
11/14/2008																						
Rain																						
Day 23																						
11/15/2008																						
Rain																						

APPENDIX F

SOLUTION OF TRANSCENDENTAL EQUATION FOR TRACKING THE MPP OF PV

Recalling equation 3.6, it is observable that the exact solution of this transcendental equation can not be found for output current of Photovoltaic using combination of elementary functions.

$$I_0 = I_\lambda - I_s \left[e^{\frac{V+I_0 R_s}{\alpha}} - 1 \right] \quad (\text{F.1})$$

The above equation is of the form $x = f(x); \quad x = I_0$ (F.2)

To describe the method for finding the roots of the equation

$$f(x) = 0 \quad (\text{F.3})$$

Equation F.3 can be re written as $x = \theta(x)$ (F.4)

This equation can be written in different ways. As an example an algebraic equation F.5 can be expressed as equation F.6

$$y^3 + y^2 - 1 = 0 \quad (\text{F.5})$$

$$y = (1 + y)^{-1/2}, \quad y = (1 - y^3)^{1/2}, \quad y = (1 - y^2)^{1/3}, \dots \quad (\text{F.6})$$

Assuming x_0 is an approximate value of the desired root ξ . Substituting x_0 for x in equation (F.4) on RHS, the first approximation would be

$$x_1 = \theta(x_0) \tag{F.7}$$

Consecutive approximations will give

$$x_2 = \theta(x_1), x_3 = \theta(x_2), x_n = \theta(x_{n-1}) \tag{F.8}$$

The sequence of approximations x_0, x_1, \dots, x_n will not always converge to some number ξ .

Theorem F.1 states the conditions which are sufficient for the convergence of the sequence [4.48].

However, if it does converge, ξ is a solution of the equation $x = \theta(x)$. Consider the equation

$$x_{n+1} = \theta(x_n) \tag{F.9}$$

The approximations at the n th and the $(n+1)$ th stages are related as in equation F.9. As n increases, LHS of equation F.9 converges to the solution ξ , and if θ is continuous RHS converges to $\theta(\xi)$. Hence, $\xi = \theta(\xi)$, which shows that ξ is a root of the equation $x = \theta(x)$.

Theorem F.1 [4.48]: “Let $x = \xi$ be a root of $f(x) = 0$ and let I be an interval containing the point $x = \xi$. Let $\theta(x)$ and $\theta'(x)$ be continuous in I , where $\theta(x)$ is defined by the equation $x = \theta(x)$ which is equivalent to $f(x) = 0$. Then if $|\theta'(x)| < 1$ for all x in I , the sequence of approximations $x_0, x_1, x_2, \dots, x_n$ defined by (F.9) converges to the root ξ , provided that the initial approximation x_0 is chosen in I .”

Proof [4.48]: Since ξ is a root of the equation $x = \theta(x)$, it can be written as:

$$\xi = \theta(\xi) \quad (\text{F.10})$$

and equation F.9 is

$$x_1 = \theta(x_0) \quad (\text{F.11})$$

Subtracting F.11 from F.10 gives

$$\xi - x_1 = \theta(\xi) - \theta(x_0) \quad (\text{F.12})$$

According to the mean value theorem [4.48], RHS of equation F.12 can be expressed as $(\xi - x_0)\theta'(\xi_0)$, $x_0 < \xi_0 < \xi$ which gives equation F.12 as

$$\xi - x_1 = (\xi - x_0)\theta'(\xi_0), \quad x_0 < \xi_0 < \xi \quad (\text{F.13})$$

Similarly,

$$\xi - x_2 = (\xi - x_1)\theta'(\xi_1), \quad x_1 < \xi_1 < \xi \quad (\text{F.14})$$

$$\dots \xi - x_{n+1} = (\xi - x_n)\theta'(\xi_n), \quad x_n < \xi_n < \xi \quad (\text{F.15})$$

Assuming

$$|\theta'(\xi_i)| \leq k < 1 \text{ for all } i \quad (\text{F.16})$$

and observing (F.12)-(F.15) gives

$$|\xi - x_1| \leq k|\xi - x_0|, \quad |\xi - x_2| \leq k|\xi - x_1|, \dots \quad (\text{F.17})$$

This can be concluded from equation F.17 that every consecutive approximation remains in I, subject to the initial approximation chosen from I. Multiplication of equation F.12 and F.15 gives:

$$\xi - x_{n+1} = (\xi - x_0)\theta'(\xi_0)\theta'(\xi_1) \dots \theta'(\xi_n) \quad (\text{F.18})$$

As $|\theta'(\xi_t)| < k$, equation F.18 can be written as

$$|\xi - x_{n+1}| \leq k^{n+1} |\xi - x_0| \quad (\text{F.19})$$

As evident from equation F.19 that as on LHS $n \rightarrow \infty$, RHS of the equation will tend to zero and thus the successive approximations of x_0, x_1, \dots , converges to the root ξ if $k < 1$. The graphical representation of this method is given in Figure F.1. By sketching the line $y = x$ and the curve $y = \theta(x)$ and considering the way in which the approximations x_i are obtained, a geometrical significance of the method is obtained and this is shown in Figure F.1.

F.1. Uniqueness of the roots [4.48]

The value of root ξ calculated in the above analysis is also unique. This statement can be justified through the following analysis.

Assuming ξ_1 and ξ_2 be the two roots of equation F.4.; which implies that $\xi_1 = \theta(\xi_1)$ and $\xi_2 = \theta(\xi_2)$. Hence, $|\xi_1 - \xi_2| [1 - |\theta'(n)|] = 0$. Since $|\theta'(n)| < 1$, it follows that $\xi_1 = \xi_2$, and hence the root is unique [4.48].

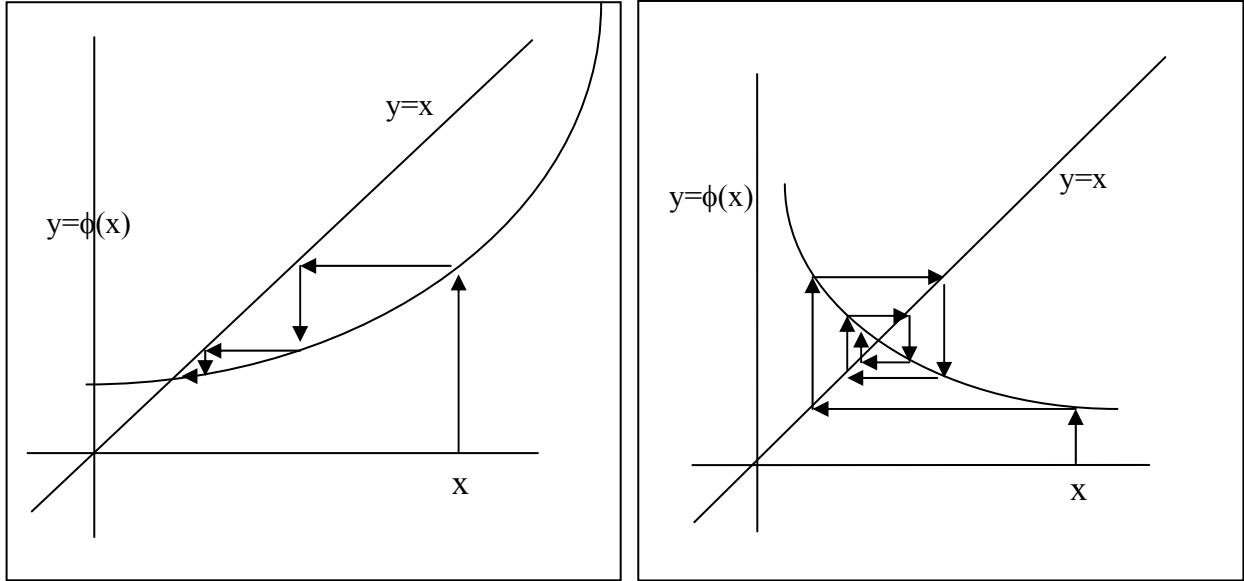


Figure F.1 Convergence of $x_{n+1} = \theta'(x_n)$

F.2. Error Analysis [4.48]

To calculate the error in the above method, equations F.13 to F.19 will be used. It can be inferred that

$$|\xi - x_n| = |\theta(\xi) - \theta(x_{n-1})| \leq k|\xi - x_{n-1}| = k|\xi - x_n + x_n - x_{n-1}| = k|\xi - x_n| + k|x_n - x_{n-1}|.$$

So that

$$|\xi - x_n| \leq \frac{k}{1-k}|x_n - x_{n-1}| \leq \frac{k^n}{1-k}|x_1 - x_0| \quad (\text{F.20})$$

Mathematically, the speed of the convergence would be faster if the value of k is smaller and vice versa [4.48]. If Λ is the specified accuracy, i.e. if $|\xi - x_n| \leq \Lambda$ then equation F.20 will give

$$|x_n - x_{n-1}| \leq \frac{1-k}{k} \Lambda \quad (\text{F.21})$$

The desired precision can be obtained through equation F.20 by calculating the difference between two consecutive iterations [4. 48].

F. 3. Newton-Raphson method [4.48]

Let x_0 be an approximate root of $f(x) = 0$ and let $x_1 = x_0 + h$ be the accurate value of root so that $f(x_1) = 0$. Expanding $f(x_0 + h)$ by Taylor's series:

$$f(x_0) + hf'(x_0) + \frac{h^2}{2!} f''(x_0) + \dots = 0 \quad (\text{F.22})$$

Neglecting the second and higher order derivatives:

$$f(x_0) + hf'(x_0) = 0 \quad (\text{F.23})$$

so that

$$h = -\frac{f(x_0)}{f'(x_0)} \quad (\text{F.24})$$

To get more accuracy, x_1 will be calculated instead of x_0 , so that

$$x_1 = x_0 - \frac{f(x_0)}{f'(x_0)} \quad (\text{F.25})$$

This can be generalized for successive values of x as

$$x_{n+1} = x_n - \frac{f(x_n)}{f'(x_n)} \quad (\text{F.26})$$

This is the Newton-Raphson formula.

Comparing equation F.26 with equation F.9

$$x_{n+1} = \varphi(x_n) \quad (\text{F.27})$$

which gives

$$\varphi(x) = x - \frac{f(x)}{f'(x)} \quad (\text{F.28})$$

which can further gives

$$\varphi'(x) = \frac{f(x)f''(x)}{[f'(x)]^2} \quad (\text{F.29})$$

Assuming $f(x), f'(x), f''(x)$ are continuous and bounded on any interval having root $x = \zeta$; $f(x) \neq 0$ if ζ is a simple root. Also, $|f'(x)| \geq \varepsilon$ for some $\varepsilon > 0$ in a proper neighborhood of ζ as $f'(x)$ is assumed as continuous. In the above neighborhood of ζ , the interval $|f(x)f''(x)| < \varepsilon^2$ as $f(\zeta) = 0$ and $f(x)$ is continuously twice differentiable. Thus, in this interval,

$$\varphi'(x) < 1 \quad (\text{F.30})$$

Therefore by Theorem F.1, equation F.28 describing Newton Raphson formula will converge, if the initial value x_0 is assumed in the close vicinity of ζ . For ζ having multiple roots, the rate of convergence of Newton-Raphson method will be slow [4.48]. The rate of the convergence of Newton Raphson method for $f(\zeta) = 0$ can be obtained by Taylor's expansion series as

$$f(x_n) + (\zeta - x_n)f'(x_n) + \frac{1}{2}(\zeta - x_n)^2 f''(x_n) = 0 \quad (\text{F.31})$$

which gives

$$-\frac{f(x_n)}{f'(x_n)} = (\zeta - x_n) + \frac{1}{2}(\zeta - x_n)^2 \frac{f''(x_n)}{f'(x_n)} \quad (\text{F.32})$$

Comparing equations F.28 and F.34 give [4.48]

$$x_{n+1} - \zeta = \frac{1}{2}(x_n - \zeta)^2 \frac{f''(x_n)}{f'(x_n)} \quad (\text{F.33})$$

Substituting $\varepsilon_n = x_n - \zeta$ in equation F.35 gives [4.48]

$$\varepsilon_{n+1} = \frac{1}{2} \varepsilon_n^2 \frac{f''(x_n)}{f'(x_n)} \quad (\text{F.34})$$

Thus, it can be inferred from equation F.35 that the Newton-Raphson process has a *second-order* or *quadratic* convergence. This methodology can be implemented for algebraic as well as transcendental equations and is valid even if the roots of the equation are complex [4.48]. Graphically, the portion of the curve $y = f(x)$ between the point $(x_0, f(x_0))$ and the x axis in Figure F.2 is replaced by the tangent to the curve at the point x_1 .

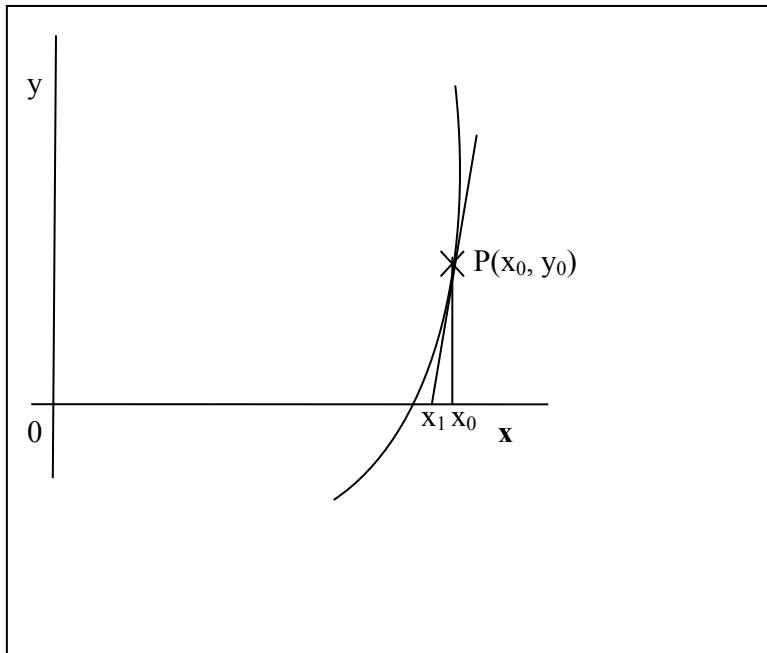


Figure F. 2 Newton Raphson Methods [4.48]

A MATLAB code is written and embedded in the MMPT model of the PV module (Appendix B) for the implementation of Newton Raphson method for achieving the maximum power point (MPP) of the PV module.

APPENDIX G

FUZZY LOGIC FUNDAMENTALS

Basic concepts of fuzzy theory are described briefly in this appendix. Detailed explanation of Zadeh's Fuzzy theory can be viewed at [4.64-4.66].

G.1 Fuzzy Sets and membership Functions

Let C be a set of all integers greater than 5

$$C = \{x : x \in \mathbb{N}, x > 5\} \quad (\text{G.1})$$

and F be a set of all integers much greater than 5. So

$$F = \{x : x \in \mathbb{N}, x \gg 5\} \quad (\text{G.2})$$

As evident from above two relations that the set C is precisely defined while the set F is not defined precisely because of the imprecision in the term “much greater”.

To determine an element with certain criteria from sets C and F, one can follow the approach as discussed in [4.66]. According to conventional set theory, a set can be defined by its characteristic function by defining element as 1 or 0 depending upon membership or non membership of the element. If I is the universal set of all integers then, the characteristic function of the set C will have values $\mu_C(x) = 1$ if $x \in I$ and $\mu_C(x) = 0$ if $x \notin I$, $\mu: I \rightarrow \{0,1\}$. Thus, Equation G.1 defines a crisp set with a definite element values while the elements of set F are difficult to define as crisp values

and could be defined with different membership degree. Such a set is called Fuzzy set. The membership function $\mu_F(x)$ of fuzzy set F can be defined as :

$$\mu_F(x) = \left\{ \begin{array}{ll} 0 & \text{for } x < 5 \\ \frac{x-5}{100} & \text{for } 5 \leq x \leq 105 \\ 1 & \text{for } x > 105 \end{array} \right\} \quad (G.3)$$

Thus, Integers less than 5 has membership degree 0 and does not belong to fuzzy set F and $\mu_F(6)$ has membership degree 0.1 and $\mu_F(95)$ has membership degree 0.9. Crisp set C and Fuzzy set F are shown in Figure G.1.

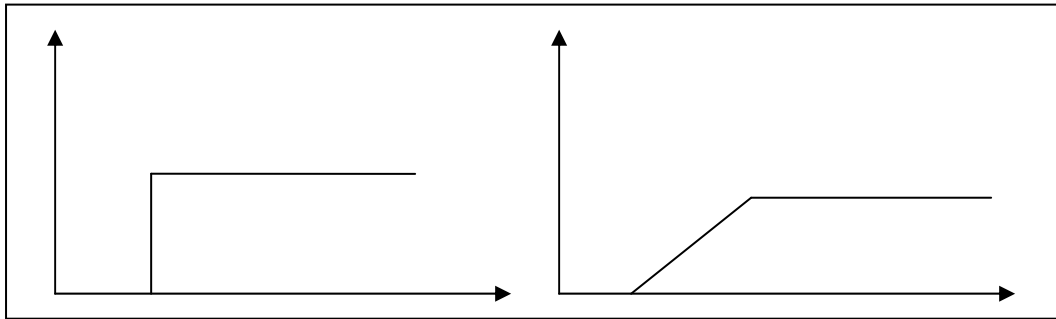


Figure G.1 Graphical Representation of Crisp and Fuzzy Set [4.70]

Thus, in fuzzy set theory, membership function defines how every point of the input space is represented by a degree of membership between 0 and 1. Hence, fuzzy set F in the universe of discourse U is defined by a membership function μ_F with values in $[0, 1]$.

$$F = \{x, \mu_F(x) \mid \forall x \in U\} \quad (G.4)$$

Fuzzy set membership function can be defined through various shapes depending upon the suitability, simplicity and efficiency of fuzzifying and defuzzifying strategy [4.70].

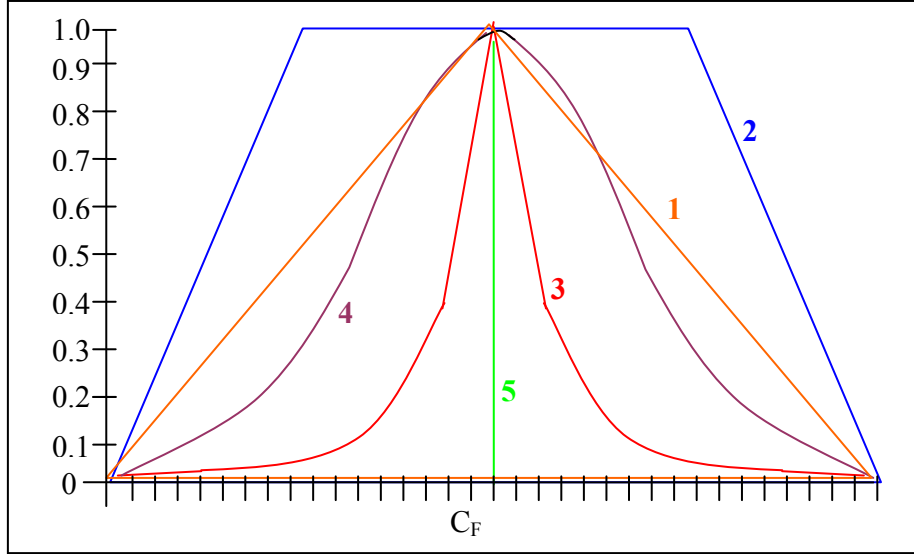


Figure G. 2 Typical Shapes of Membership Functions: 1- Triangular, 2- Trapezoidal, 3- Gaussian, 4- Bell-Shaped, 5- Singleton [4.70]

Popular membership functions are triangular, trapezoidal and Gaussian membership functions. Typical shapes of membership functions is shown in Figure G.2

G.2. Basic Operations on Fuzzy Sets

Let F_1 and F_2 are two fuzzy sets with same universe of discourse U . The equality, complement, union and intersection of fuzzy sets F_1 and F_2 can be expressed as

$$F_1 = F_2 \quad \text{iff} \quad \mu_{F_1}(x) = \mu_{F_2}(x), \forall x \in U \quad (\text{G.5})$$

$$F_1 \subset F_2 \quad \text{iff} \quad \mu_{F_1}(x) \leq \mu_{F_2}(x), \forall x \in U \quad (\text{G.6})$$

$\overline{F_1}$ is a fuzzy set in U , compliment to F_1 , with membership function expressed as

$$\mu_{\overline{F_1}}(x) = 1 - \mu_{F_1}(x), \forall x \in U \quad (\text{G.7})$$

The Union and intersection of F_1 and F_2 are also fuzzy sets in U with their membership function is expressed as

$$\mu_{F_1 \cup F_2}(x) = \max[\mu_{F_1}(x), \mu_{F_2}(x)] \quad \forall x \in U \quad (\text{G.8})$$

$$\mu_{F_1 \cap F_2}(x) = \min[\mu_{F_1}(x), \mu_{F_2}(x)] \quad \forall x \in U \quad (\text{G.9})$$

G.3. Fuzzy IF-THEN Statements

The conventional binary logic is expressed either as true or false with values 1 and 0, respectively. Contrary to this fuzzy logic input space is represented by a degree of membership between 0 and 1, often referred as degree of truth or degree of membership. Detailed information is available in [4.66, 4.69] Fuzzy rules are expressed as linguistic variables [4.66]. Symbolically they are expressed as [4.66]:

$$\mathbf{If} \langle \text{fuzzy proposition} \rangle \mathbf{then} \langle \text{fuzzy proposition} \rangle \quad (\text{G.10})$$

Then the fuzzy expression defined on $X \times Y$ where X and Y are the universe of discourse of linguistic variables x and y can be expressed as

$$\mathbf{If} \langle x \text{ is } A \rangle \mathbf{then} \langle y \text{ is } B \rangle \quad (\text{G.11})$$

The Fuzzy statement in G.11 can be explained as [4.66]

i. The statement is called fuzzy rule

ii. “ $\langle x \text{ is } A \rangle$,” is called the antecedent of the rule represented by fuzzy set $\overline{F_1} = \int_x \mu_{F_1}(x) / x$

and “ $\langle y \text{ is } B \rangle$,” is called as the consequent of the rule and represented by fuzzy set

$$\overline{F_2} = \int_y \mu_{F_2}(y) / y \quad .$$

iii. The fuzzy condition will be a fuzzy relation μ_F such that

$$\forall x \in X \forall y \in Y: \mu_F(x, y) = \mu_{F_1}(x) * \mu_{F_2}(y) \quad (\text{G.12})$$

APPENDIX H

DC-DC BOOST CONVERTER

DC- DC converters convert electrical power from one voltage to a different voltage level. For example, power from a 12 V battery fed to an electronic load at 5 V through a DC-DC converter. A stable output dc voltage with minimal output impedance for a broad range of frequency is a desirable feature of a DC-DC converter [4.89- 4.90]. Depending upon the output voltage DC-DC converter can be categorized as Buck (step down), Boost (step up) and buck –boost converters.

A schematic diagram of DC-DC boost converter is represented in Figure H.1. This converter operates in two configurations ON and OFF depending on the switching state of switch S.

Considering an ideal DC –DC boost converter, i.e., assuming the components with an ideal behavior, operating in a steady state for a continuous operational mode of DC-DC boost converter, the switch S is closed during the ON state as shown in Figure H.1. The change in inductor current during the closing time period (t) of the switch is determined as in equation H.1 [4.70] and the increment in the inductor current at the end of ON time (T) is calculated as in equation H.3. The fraction of time period of ON state (T) or the commutation period is represented by duty cycle D which varies from 0 to 1.

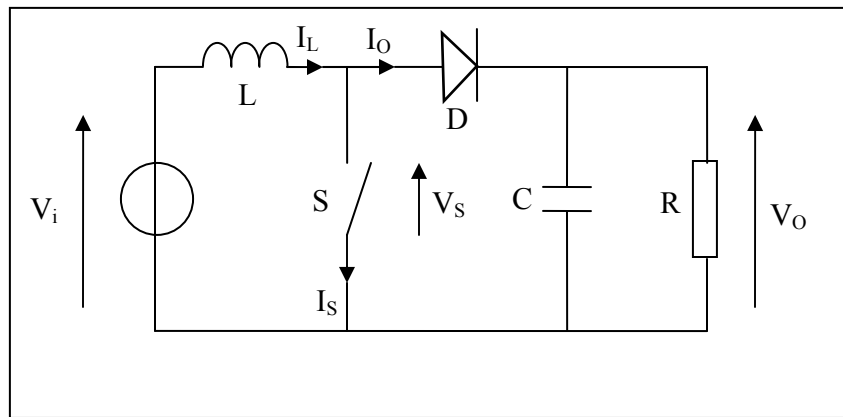


Figure H.1 Schematic Diagram of a DC-DC Boost Converter with Switch S Open [4.70]

$$\frac{\Delta I_{LON}}{\Delta t} = \frac{V_i}{L} \quad (H.1)$$

$$\Delta I_{LON} = \int_0^{D*T} \frac{V_i}{L} dt \quad (H.2)$$

So,

$$\Delta I_{LON} = \frac{V_i}{L} D*T \quad (H.3)$$

where

L : Inductance

V_i: Input voltage

I_L : Inductor Current

D: Duty cycle of the converter

T: Time for switch was closed; also known as commutation period of converter.

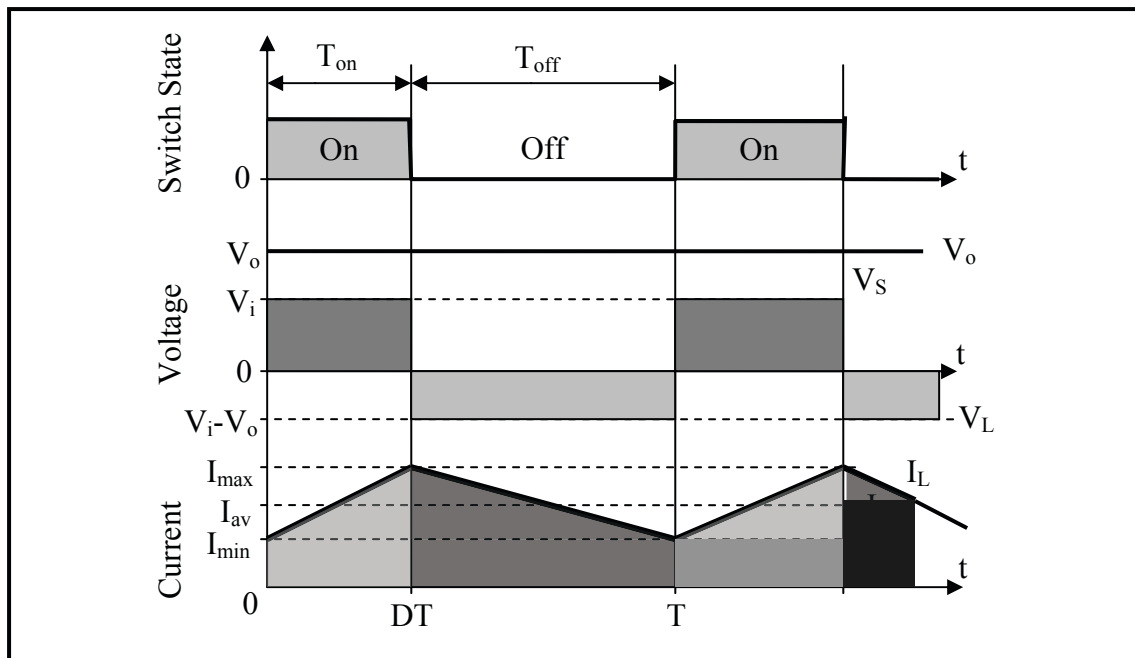


Figure H. 2 Pattern of the Variation of Different Variables of DC-DC Converter in a Duty Cycle [4.70]

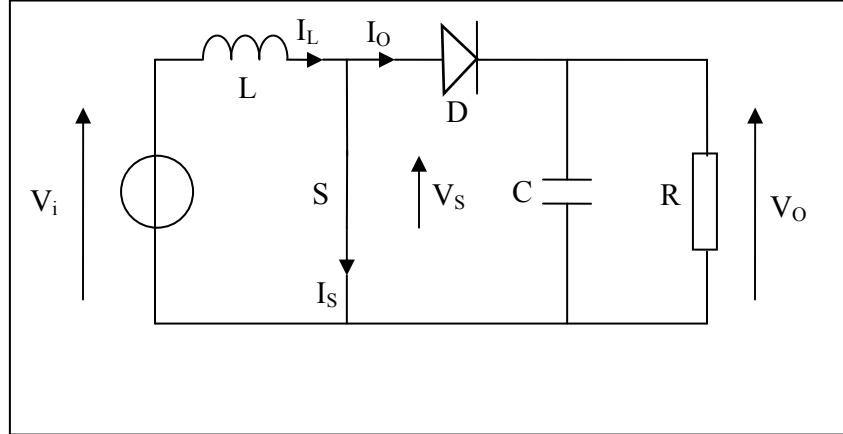


Figure H. 3 Schematic Diagram of a DC-DC Boost Converter with Switch S Closed [4.70]

During the OFF state the switch S is open as shown in Figure H.3 and the variation of different variables involved in duty cycle is shown in Figure H.2. The change in inductor current during the opening time period (t) of switch is determined as in Equation H.4 and the increment in the inductor current at the end of OFF time $((1-D)T)$ is calculated as in Equation H.6 [4.70].

$$\frac{\Delta I_{LOFF}}{\Delta t} = \frac{V_i - V_o}{L} \quad (H.4)$$

where

V_o : voltage at the output of DC-DC converter.

$$\Delta I_{LOFF} = \int_0^{(1-D)*T} \frac{(V_i - V_o)}{L} dt \quad (H.5)$$

So,

$$\Delta I_{LOFF} = \frac{(V_i - V_o)}{L} * (1 - D)T \quad (H.6)$$

For a DC-DC boost converter operating in a steady state, the energy stored in the inductor at the opening or closing of switch S or vice versa will be equal [4.89].

$$E_L = \frac{1}{2} * L * \Delta I_{L_{ON}}^2 = \frac{1}{2} * L * \Delta I_{L_{OFF}}^2 \quad (\text{H.7})$$

So, with the consideration of the direction of the flow of current, the total amount of current flows in the circuit during one duty cycle will be mathematically zero.

$$\Delta I_{L_{OFF}} + \Delta I_{L_{ON}} = 0 \quad (\text{H.8})$$

Substituting Equations H.3 and H.6 in H.8 we have:

$$\frac{V_i}{L} D * T + \frac{(V_i - V_o)}{L} * (1 - D) T = 0 \quad (\text{H.9})$$

or,

$$V_o = \frac{V_i}{(1 - D)} \quad (\text{H.10})$$

So, the duty cycle of a DC –DC boost converter is

$$D = 1 - \frac{V_i}{V_o} \quad (\text{H.11})$$

As can be inferred from Equation H.11 that as the duty cycle D varies from 0 to 1, the output voltage is always greater than the input voltage and theoretically come close to infinity when duty cycle value approaches to 1.

APPENDIX I

SIMULINK MODEL FOR AGABFLC

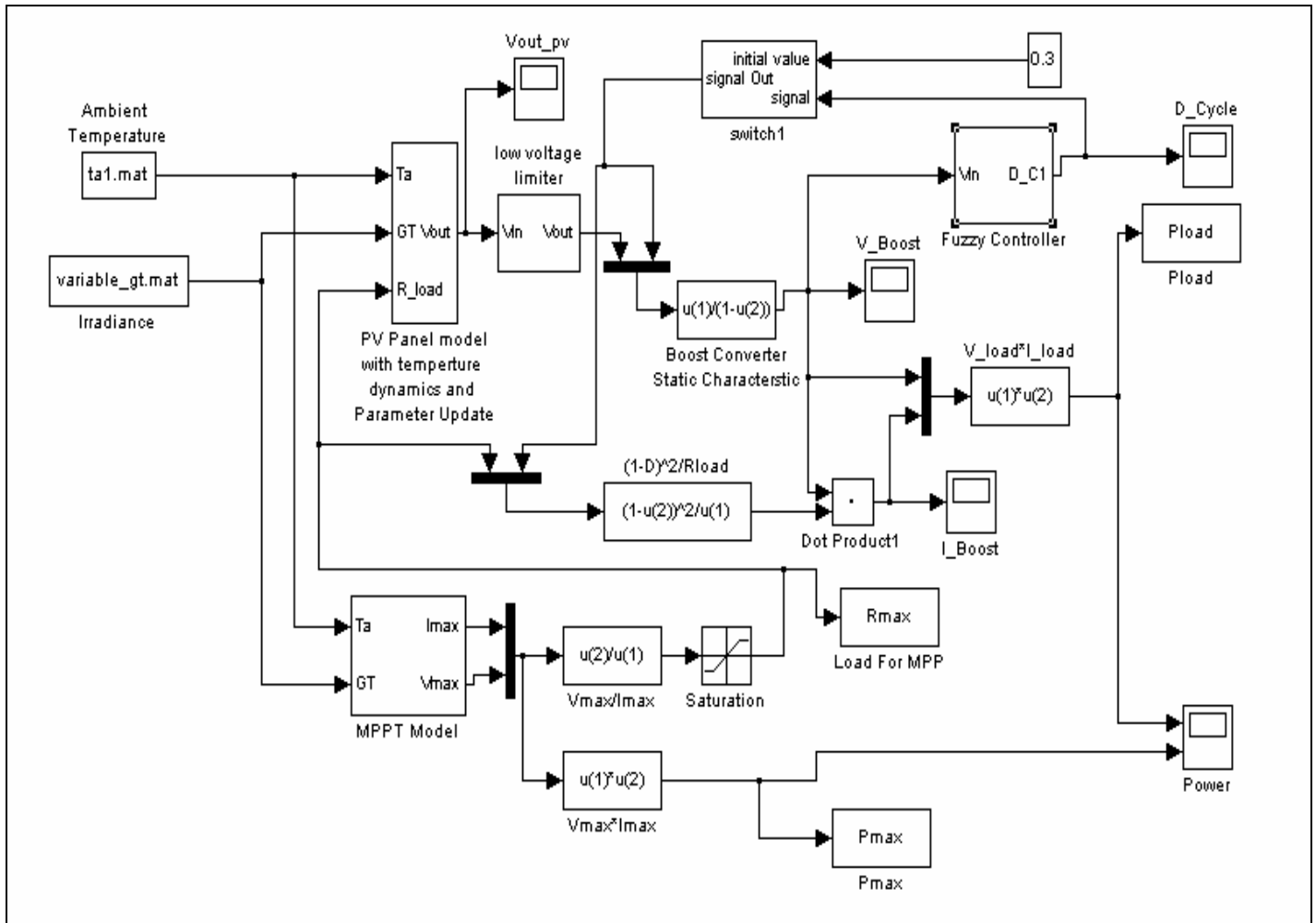


Figure I.1 Simulink Model of the Whole System with AGABFLC Controller

VITA

Mohammad Saad Alam was born on December 8, 1981 in Aligarh, Uttar Pradesh, India to the (Late) Dr. Shah Alam and Mrs. R. Alam. He graduated with a bachelor's degree in Electrical Engineering in summer 2003 from Aligarh Muslim University in Aligarh, India. For pursuing higher education, he relocated to the United States in fall of 2004 and joined a master's degree program in Electrical and Computer Engineering with specialization in Energy, Environment and Economics at Illinois Institute of Technology, Chicago, IL. During his masters, he worked on the development of a hybrid fuel cell lithium-ion battery based vehicle at the center of electro chemical engineering of Illinois Institute of Technology, Chicago. He graduated from his masters program in fall 2005. He continued his education at Mississippi State University by joining the doctoral degree program for Electrical Engineering in spring of 2006. During his enrollment at Mississippi state university, he worked on the development of hybrid fuel cell – battery based distributed generation system for electric ship application, sponsored by the Office of Naval Research of United States. In fall of 2006 he transferred to Tennessee Tech University to complete his doctoral degree program. Currently he is working in the hybrid vehicle development division of Chrysler LLC as Product and Development Engineer in Auburn Hills, MI.